University of Southampton

Faculty of Engineering & the Environment

Energy Technology Group

High Temperature Secondary Lithium-ion Batteries Operating Between 25 ^{o}C and 150 ^{o}C

DOI: https://doi.org/10.5258/SOTON/D1057

by

Daniel Richard Wright

BSc (Hons.), MSc, MCSM

Thesis for the degree of Doctor of Philosophy

August 2019

University of Southampton

Abstract

Development of lithium-ion batteries suitable for high temperature applications requires a holistic approach to battery design because degradation of some of the battery components can produce a serious deterioration of the other components, and the products of degradation are often more reactive than the starting materials. Therefore, a careful selection and systematic characterisation of the components of lithium ion batteries is required in order to identify a number of materials and protocols for battery assembly that give promising performance at high temperatures.

This project investigates the high temperature operation of secondary lithium-ion batteries, giving an understanding of the temperature limitation of binders, electrolytes, positive electrode materials, negative electrode materials and current collectors. This thesis has successfully demonstrated the high temperature operation of lithium ion batteries up to a temperature of 150 ^{o}C. Results have shown that the main factors which are responsible for capacity fade are the electrolyte, electrode binder and the current collector. It has been effectively demonstrated that lithium iron phosphate cells can be operated up to a temperature of 150 ^{o}C by replacing $LiPF_6$, with an alternative electrolyte LiODFB (Chapter 4). However, capacity fade was rapid at this temperature due to failure of the binder, causing first cycle irreversible capacity and long-term capacity loss (Chapter 5). It was also demonstrated in Chapter 6 that aluminium current collector corrosion was occurring during high temperature operation, as described in chapter 6.

Suggestions for further work are made in the following areas:

1. Electrolyte: the investigation of electrolytes suitable for high temperature operation could be expanded to electrolyte additives in order to allow effective stabilisation of the SEI at higher temperatures. It should also include alternative electrolyte systems such as polymers and solid-state electrolytes since it is likely that the limit of what can be achieved in liquid carbonate systems has been reached.
2. Binder: Further work should look at optimising the electrode binders, further evaluating the use of PAI as a binder for use at high temperatures, evaluating in a full Li-ion cell configuration.
3. Current Collector: alternative current collectors should be investigated for use at high temperatures that don't corrode when operated at 150 ^{o}C. The protection of the current

collector could also be investigated using either coatings for the aluminium current collector or by electrolyte additives that allow effective passivation of the surface which do not fail at high temperatures.

Faculty of Engineering & the Environment

Energy Technology Group

Thesis for the degree of Doctor of Philosophy

High Temperature Secondary Lithium-ion Batteries Operating Between 25 ^{o}C and 150 ^{o}C

by

Daniel Richard Wright

Table of Contents

Table of Tables

Table of Figures

Table of Figures

Table of Figures

Table of Figures

Research Thesis: Declaration of Authorship

Print name:	Daniel Richard Wright

Title of thesis:	High Temperature Secondary Lithium-ion Batteries Operating Between 25 ^{o}C and 150 ^{o}C

I declare that this thesis and the work presented in it are my own and has been generated by me as the result of my own original research.

I confirm that:

1. This work was done wholly or mainly while in candidature for a research degree at this University;
2. Where any part of this thesis has previously been submitted for a degree or any other qualification at this University or any other institution, this has been clearly stated;
3. Where I have consulted the published work of others, this is always clearly attributed;
4. Where I have quoted from the work of others, the source is always given. With the exception of such quotations, this thesis is entirely my own work;
5. I have acknowledged all main sources of help;
6. Where the thesis is based on work done by myself jointly with others, I have made clear exactly what was done by others and what I have contributed myself;
7. Parts of this work have been published as:

D. R. Wright, N. Garcia-Araez, J. R. Owen, Energy Procedia 151 (2018) 174-181

Signature:		Date:	

Important note:

The completed signed and dated copy of this form should be included in your print thesis.

A completed and dated but unsigned copy should be included in your e-thesis

Acknowledgements

I dedicate this thesis to Holly my (very nearly) wife for all of her support and love she has given me throughout one of the biggest challenges in my life. I will always be grateful that I met you during my PhD and I can't wait to spend the rest of our lives together.

I would like to thank everyone who has supported me throughout this PhD in particular my family. My mum, dad and sister Jenn have supported me throughout my PhD and have always supported me through all my mad plans and schemes my whole life and I thank you for this always.

Lets not forget my supervisors John, Nuria and Andrew and also Girts at QinetiQ for all their help and expertise who made this thesis possible. Another thanks needs to go to the members of the Owen/Garcia-Araez group of past and present: Jimmy, Mike, James, Tom, Nina, Liam, Sam, Rinaldo, Vivek, Nimah, Ben and Sara. Thank you for all putting up with me and helping me throughout my PhD.

Chapter 1 Introduction

1.1 Lithium-ion Batteries

The 20th century saw the invention and the commercialisation of the modern lithium-ion battery with Sony introducing the first commercially available rechargeable lithium ion battery in 1991.[1,2] This design utilised the "rocking-chair" design using lithium insertion electrodes of lithium cobalt oxide and graphite.[3] In 1996 Goodenough discovered phospho-olivines as positive electrode materials for lithium ion batteries, introducing lithium iron phosphate (LFP) as a safer and more stable electrode material.[4] Todays commercial batteries mostly still utilise a system similar to Sony's lithium cobalt oxide and graphite insertion electrodes with an electrolyte based on organic carbonate solvents and lithium hexafluorophosphate.[3]

Lithium-ion batteries have revolutionised the energy storage market and applications for batteries are rapidly expanding, with demands for high performance batteries required in many technological fields. In applications such as portable devices or electric vehicles, lithium-ion batteries have currently no contender in terms of energy density or durability. However, the restricted temperature range of -25 °C to 60 °C is a problem for a number of applications that require high energy rechargeable batteries that operate at a high temperature (>100 °C).[5] One such application is the oil and gas industry which requires batteries to operate at temperatures of up to 150 °C.[6] Going above the maximum operating temperature risks degradation and irrecoverable damage often resulting in reduced cell capacity, reduced cell lifetime, cell failure and in some cases fires and explosions. High temperature batteries used in the oil and gas industry are typically Li-ion primary batteries, however there is a drive to replace this with secondary lithium ion technology. [7] Currently the options for high temperature lithium-ion secondary batteries are limited due to the instability of the interface between the lithiated carbon negative electrode and the organic electrolyte. Development of lithium-ion batteries suitable for high temperature applications requires a holistic approach to battery design because degradation of some of the battery components can produce a serious deterioration of the other components, and the products of degradation are often more reactive than the starting materials.[8]

1.2 Principle of Lithium-ion Batteries

A Li-ion battery consists of two lithium insertion electrodes (a positive electrode e.g. $LiFePO_4$ on an Al current collector and a negative electrode e.g. graphite on a Cu current collector), with a Li^+ conducting separator and an electrolyte (e.g. $LiPF_6$ dissolved in organic carbonate solvents). On charge lithium ions are extracted from the LFP positive electrode, into the electrolyte, through the separator and insert into the graphite negative electrode. On discharge the process is reversed by where the lithium ions are extracted from the graphite negative electrode, into the electrolyte, through the separator and insert into the LFP positive electrode. Figure 1-1 shows a diagram of a lithium-ion battery, equation 1-1 to equation 1-3 show the reactions occurring. [9]

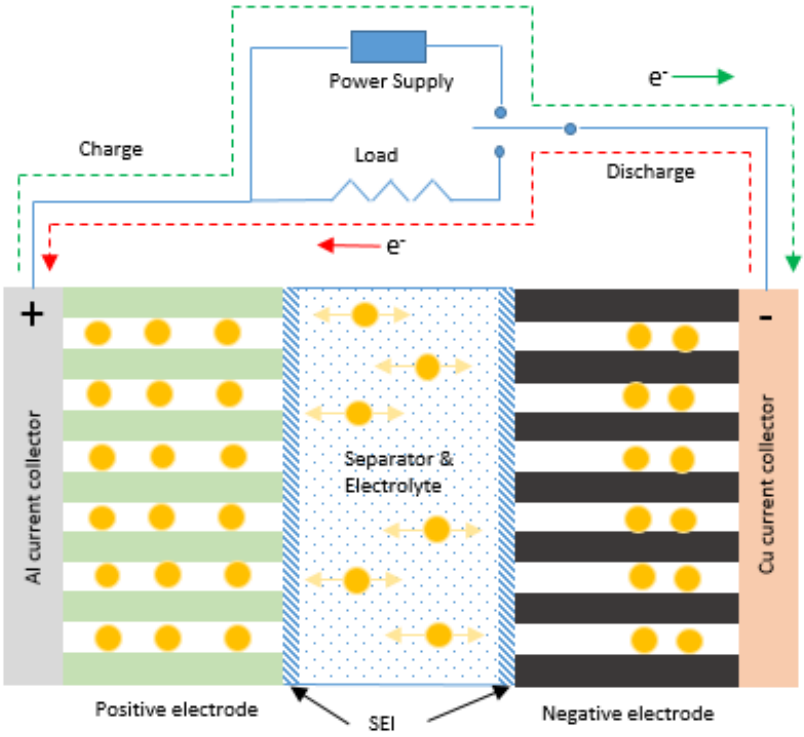

Figure 1-1 Diagram of a lithium-ion battery adapted from Aravindan et al [10]

$$LiFePO_4 \underset{Li\ insertion}{\overset{Li\ extraction}{\rightleftarrows}} FePO_4 + Li \qquad \text{Equation 1-1}$$

$$6C + Li \underset{Li\ extraction}{\overset{Li\ insertion}{\rightleftarrows}} LiC_6 \qquad \text{Equation 1-2}$$

$$LiFePO_4 + 6C \underset{discharge}{\overset{charge}{\rightleftarrows}} FePO_4 + LiC_6 \qquad \text{Equation 1-3}$$

1.3 Degradation of Lithium-ion Batteries

Electrolyte decomposition has been identified as the main cause of degradation in lithium ion cells, particularly the reactions that occur at the negative electrode/ electrolyte interface, typically causing 10% loss of capacity on the first cycle.[11,12] On charge of the graphite negative electrode, electrolyte breakdown occurs at 0.8 V[13], these reactions produce products which form the solid electrolyte interphase (SEI), a diagram of which can be seen in Figure 1-2. The SEI is composed of a variety of inorganic and organic species, such as semi-carbonates, polyolephines, alkoxides, polymers, Li_2O, LiCl, LiF, $LiCO_2$-R and Li_2CO_3.[14] The production of an SEI is essential since it protects the electrolyte from further breakdown once formed but allows ion conductivity. Electrolyte breakdown occurs because the operating potential of the negative electrode and positive electrodes are outside of thermodynamic potential stability window of the electrolyte illustrated in Figure 1-3.[15]

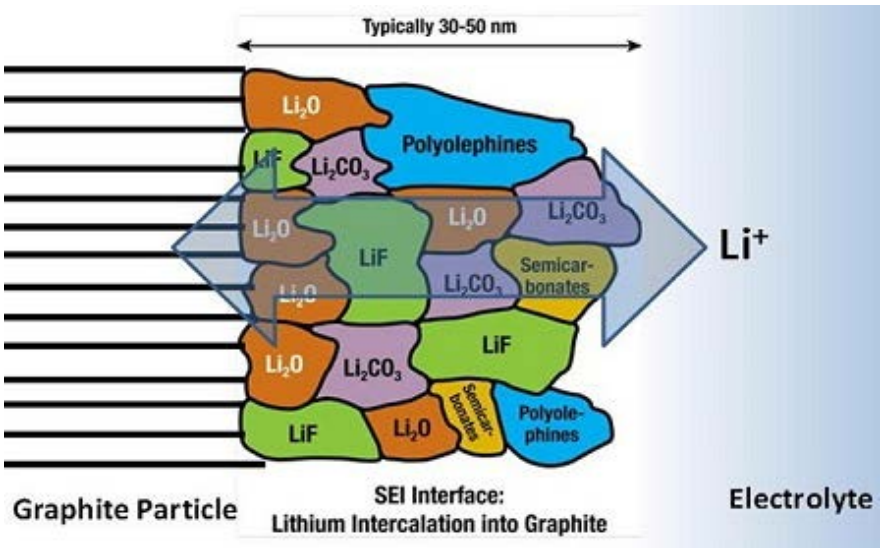

Figure 1-2 Diagram of an SEI layer on a graphite surface showing the variety of compounds which form the SEI. Reproduced with permission from L. Hardwick from *University of Liverpool Department of Chemistry- Hardwick Group* [16] Image adapted by L. Hardwick from *Peled et al*[14]

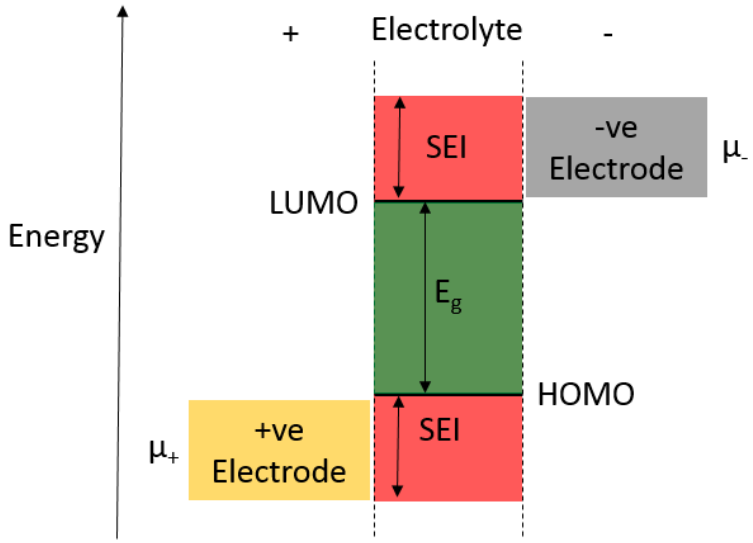

Figure 1-3 Diagram showing the energy differences between the positive electrode (cathode) and negative electrode (anode) and the electrolyte stability window. Adapted from *Goodenough et al*[15]

As described by *Goodenough et al*[15], if the negative electrode electrochemical potential (μ_-) is above the lowest unoccupied molecular orbital (LUMO) of the electrolyte then electrolyte breakdown occurs. The electrolyte breakdown occurs until a passivation layer is formed on the negative electrode surface, blocking electron transfer from the negative electrode to the electrolyte LUMO. Conversely if the positive electrode electrochemical potential (μ_+) is below the highest unoccupied molecular orbital (HOMO) then electrolyte breakdown occurs. The electrolyte breakdown occurs until a passivation layer is formed on the positive electrode surface, which blocks the electron transfer from the electrolyte HOMO to the positive electrode. To achieve thermodynamic stability of the electrolyte μ_- and μ_+ should be within the energy gap between the HOMO and LUMO (E_g) however this restricts the open circuit potential, V_{oc}, shown in equation 1-4, where e denotes the magnitude of the electron charge. Producing an SEI can give additional kinetic stability of the electrode/electrolyte interface, allowing a larger V_{oc}, however $eV_{oc} - E_g$ should not be too large otherwise further electrolyte breakdown will occur. Higher temperatures will increase the kinetics and therefore electrolyte breakdown will occur more easily[11,15]

$$eV_{OC} = \mu_- - \mu_+ \leq E_g \qquad \text{Equation 1-4}$$

Where:

e = magnitude of electron charge

V_{OC} = open circuit potential

μ_- = negative electrode electrochemical potential

μ_+ = positive electrode electrochemical potential

E_g = energy gap between the HOMO and LUMO of the electrolyte

There are many factors that affect the formation of the SEI namely electrode composition, electrolyte composition, temperature and cycling conditions. The SEI has a large impact on the first cycle capacity loss, cell impedance, rate capability, cell safety and cycle life. Figure 1-4 shows the electrode/ electrolyte processes which can occur[11,15]:

1. **Electrolyte decomposition/ SEI formation-** As detailed above electrolyte decomposition occurs which forms the SEI. In addition to the breakdown products which form the SEI, the electrolyte also reacts to produce un-wanted side products. These not only consume electrolyte but can form detrimental products which can react with other cell components. This can have a severe impact on the cell performance and often results in degradation of the cell.
2. **SEI growth and stabilisation-** The SEI surface takes time to grow on the surface of the electrode, requiring several charge discharge cycles to fully mature. During this process the SEI continues to grow and stabilise.
3. **SEI dissolution and precipitation-** During cycling the SEI can be broken or dissolve and precipitate, further consuming electrolyte to repair the SEI.

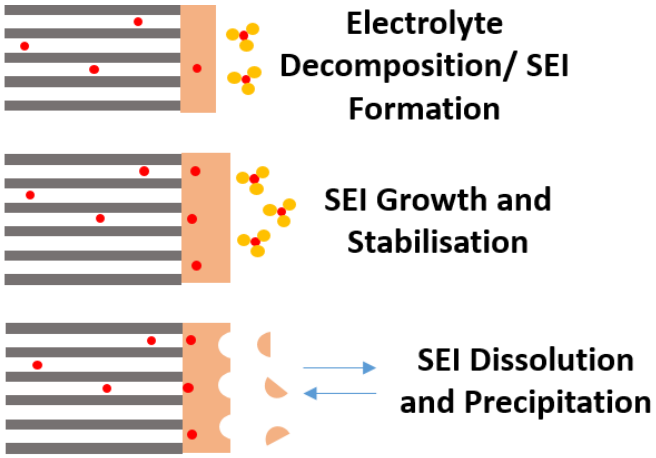

Figure 1-4 Diagram showing electrolyte breakdown, SEI formation, destruction and stabilisation on a graphite electrode surface. Adapted from *Vetter et al*[17]

At elevated temperatures the electrolyte breakdown reactions occur at an increased rate and result in greater consumption of electrolyte and unwanted side products. It has been identified that several processes can occur at the electrode/ electrolyte interface, which are depicted in Figure 1-5:

a) **SEI destruction-** Higher temperatures can result in the breakdown of the SEI which consumes further electrolyte to repair SEI damage. The cycle of SEI breakdown and electrolyte breakdown to reform the SEI causes the consumption of electrolyte leading to capacity fade.[7]

b) **SEI thickening-** It has also been reported in the literature that higher temperatures can cause the SEI to grow thicker and more resistive, increasing the cell impedance. It has been reported that impedance rise can be as high as 50% greater for cells aged at 70 ^{o}C.[18] Vetter *et al* have reported that electrolyte decomposition and decrease of electrode surface area due to continuous SEI growth are two major causes of cell degradation at higher temperatures.[17]

c) **Reactions of the SEI with metal cations-** The SEI can change composition from reactions with metal cations, it has been reported that the Mn^{2+} ions can react with SEI components and produce products such as $MnCO_3$ and MnF_2, which leads to the change in passivation properties of the SEI and can result in further electrolyte breakdown.[19] Song *et al*[20] and Lewandowski *et al*[21] have reported that one of the causes of degradation in a lithium iron phosphate/ graphite full cell is caused by the dissolution of iron into the electrolyte causing it to deposit on the graphite electrode. This iron then causes accelerated decomposition of

the electrolyte resulting in a thick SEI layer. Hsieh *et al*[22] have also reported similar findings and has found trace quantities of iron contained in the electrolyte solutions.

d) SEI composition changes- It has been reported that the organic content of the SEI can be reduced at higher temperatures, which can result in a brittle SEI, decreasing the mechanical stability of the SEI.[7] Other authors have also observed similar findings commenting that that the ratio of carbonates on the surface of the SEI change with temperature.[23] It has also been reported that structural changes such as phase transitions and disordering of the positive electrode materials can occur with materials such as NMC.[24] It has also been reported in the literature that that the reaction at a charged positive electrode/electrolyte interface is of most importance when the cell is stored at high temperatures. Some small changes can occur in the active material over time, for example structural changes that cause mechanical stress and over time can cause cracking and structural damage. Broussely *et al* have reported that at elevated temperatures side reactions at the positive electrode/ electrolyte interface occur, involving the oxidation of electrolyte.[12]

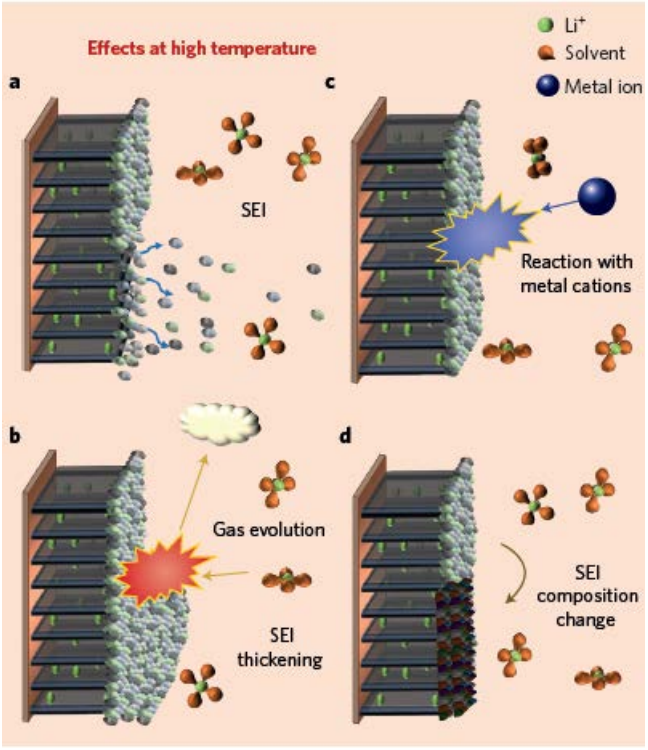

Figure 1-5 Processes occurring at the electrode/ electrolyte interface during high temperature operation of Li-ion batteries reproduced with permission from Nature from *Rodrigues et al*[25]

1.4 High Temperature Battery Technology

1.4.1 Lithium-copper Oxide/ Lithium-copper Oxyphosphate battery

The Li/CuO battery has a broad range of temperature operation and is capable of operation from -40 to 150 ^{o}C. It has a high energy density of 300 Wh/kg with an open circuit potential of 2.25 V with an operating voltage of 1.2 V to 1.5 V. The Li/$Cu_4O(PO_4)_2$ battery is capable of operation up to 175 ^{o}C has voltage of range of 2 to 2.7 V.[5,26] The Li/CuO and Li/$Cu_4O(PO_4)_2$ primary cells are composed of a lithium negative electrode and a copper oxide or copper oxyphosphate positive electrode, with an electrolyte composed of lithium perchlorate and dioxolane. The discharge process for both types of cell can be seen below in equation 1-5 and equation 1-6.[5,26] However both systems have disadvantages; firstly they are both primary cells which is undesirable. The other big drawback of this system is the safety issues associated with the use of lithium perchlorate and dioxolane electrolyte which has shown to be explosive.[26]

$2\,Li + CuO \rightarrow Li_2O + Cu$ Equation 1-5

$8Li + Cu_4O(PO_4)_2 \rightarrow 4Cu + Li_2O + 2Li_3PO_4$ Equation 1-6

1.4.2 Lithium Thionyl Chloride Battery

Still in use today is the lithium thionyl chloride primary battery which is capable of a wide temperature operation of -55 ^{o}C to +130 ^{o}C, with a working voltage range of 3 V to 3.6 V. Unlike conventional Li-ion systems which have the active materials in the positive and negative electrodes, the active material in a lithium thionyl chloride battery is contained in the electrolyte. The lithium thionyl chloride battery consists of a lithium metal negative electrode, glass fibre separator, a carbon positive electrode and an electrolyte composed of lithium tetrachloroaluminate ($LiAlCl_4$) dissolved in thionyl chloride ($SOCl_2$). The $SOCl_2$ acts as both an electrolyte and active material in the battery, with the discharge process as seen in equation 1-7. Much like the Li/CuO and Li/$Cu_4O(PO_4)_2$ batteries the lithium thionyl chloride battery is also a primary cell, which is undesirable. The other disadvantage of this system is that for safety of the battery operation should not be exceeded over 150 ^{o}C. However, this type of cell has a very long shelf life as very little self-discharge occurs (1-2%

capacity loss per year). This type of battery also has a flat voltage profile which means it can deliver a constant voltage.[5,27]

$4Li + 2SOCl_2 \rightarrow 4LiCl + S + SO_2$ Equation 1-7

1.4.3 Sodium-sulphur Batteries

The most famous of high temperature batteries dates back to the 1960's, the sodium-sulphur battery which operates between 270 and 350 ^{o}C. The cell is composed of a positive electrode of molten sulphur, a negative electrode of molten sodium, separated by a Na^+ conducting β″-alumina solid electrolyte ($NaAl_{11}O_{17}$), as seen in Figure 1-6. On discharge the sodium is oxidised, the Na^+ ions migrate through the electrolyte to the sulphur electrode where the sulphur is reduced and combines with the sodium to produce Na_2S_5. On charge the process is reversed by where the Na_2S_5 is oxidised to produce S and Na^+, the Na^+ then migrates back through the solid electrolyte to the negative electrode. This system firstly requires a high temperature to be maintained to ensure the sodium and sulphur remains molten and to ensure the solid electrolyte remains wetted and conductive of the Na^+ ions. Lower temperature systems have been researched utilising a Na-Cs alloy electrode that operates as low as 95 ^{o}C. Perhaps the largest issue with these batteries is the unsafe nature of molten sodium and sulphur and the large physical size which restricts them to stationary grid storage applications.[28,29]

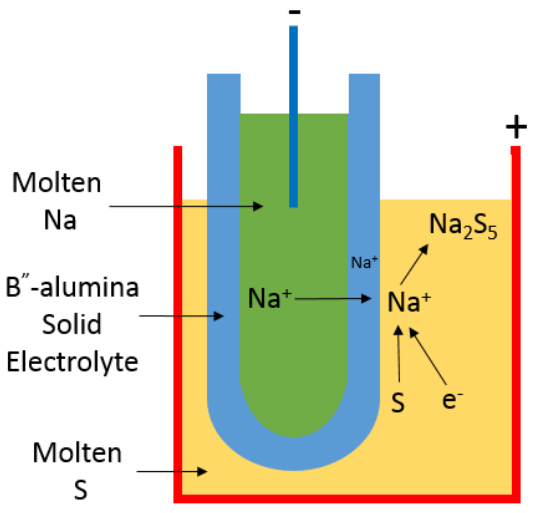

Figure 1-6 Schematic of a sodium sulphur battery adapted from *Dunn et al*[28]

1.4.4 Solid State Batteries

Solid state batteries have been researched as the replacement to organic liquid-based lithium-ion batteries due to being intrinsically safer. However, their complexity to manufacture and low power and capacity at ambient temperatures has limited their application. However solid state lithium batteries for use at high temperatures have been researched since the conductivity and kinetics are improved at higher temperatures.[30] Ilika, a solid state battery research company has reported a production of a solid state battery (Stereax P180) capable of operation between -40 ^{o}C and +150 ^{o}C.[31] It utilises a solid state electrolyte and a silicon negative electrode, the details of which can be seen in Table 1-1.

Table 1-1 The properties of the Stereax P180 battery at 150 ^{o}C. Data obtained from *Ilika*[32]

Capacity	180 µAh at 1C
Operating Voltage	3 - 3.8 V
Maximum Continuous Current	50C
Cycle Life	4000 cycles at 5% DoD 200 cycles at 100% DoD
Cell Resistance	15 Ω on Charge cycle 1 100% SoC

1.5 Lithium-ion Battery Electrolytes

It was introduced in section 1.3 that the reactions at the electrode/electrolyte interface are the primary source of degradation in lithium-ion batteries. This is due to reactions of the electrolyte with the electrode surface which form the SEI, however the SEI can become degraded by higher temperatures which causes further breakdown of electrolyte leading to capacity fade. One of the key factors to high temperature lithium-ion batteries is therefore the electrolyte. The term electrolyte can either refer to the lithium salt itself or the solution of a lithium salt in a mixture of solvents, this thesis will refer to the latter. Typically, the electrolyte used in lithium ion cells is lithium hexafluorophosphate ($LiPF_6$) in a combination of organic carbonate solvents. The study of a more stable electrolyte system for lithium ion batteries can be divided into three categories the electrolyte solvent, electrolyte salt and electrolyte additives. The research of all of these aims to improve the stability of the electrode/ electrolyte interface and to improve the thermal stability of these components to make a safer battery that is capable of a greater number of cycles. Goodenough identified a number of requirements that electrolytes must satisfy[15]:

1. Large electrochemical stability window.
2. Electrochemically stable with the electrodes, forming an SEI to improve kinetic stability if the electrode is operating outside the electrochemical stability window.
3. The electrode/ electrolyte interface must be stable to volume changes of the electrodes during cycling.
4. The Li^+ conductivity (σ_{Li^+}) must be greater than 10^{-4} S cm^{-1}.
5. The electronic conductivity (σ_e) must be less than 10^{-10} S cm^{-1}.
6. Be made from non-flammable materials.
7. Have a low toxicity.
8. Have a low cost.

In reality meeting all these requirements is a big challenge, therefore there needs to be compromises made, which is the case for currently used lithium ion battery electrolytes. Liquid organic electrolytes have been the industry standard for lithium-ion battery production since Sony started production in 1991 and have been in use ever since.[3] Although liquid organic electrolytes do not satisfy all of the requirements which are set-out above, they are relatively inexpensive, easy to manufacture and dissolve lithium salts readily.[33] The major advantage however is that liquid

organic electrolytes have a suitable ionic conductivity (>10^{-4} S cm^{-1}) at room temperature, something which alternative systems lack.[34] However their flammability is an issue which has meant that much work has been undertaken to find alternative systems with improved thermal and electrochemical stability, Table 1-2 shows a summary of the types of electrolyte systems available. A majority of the work has focussed on the use of ionic liquids and polymers to replace conventional carbonate solvents, however polymers and ionic liquids have a major disadvantage that their ionic conductivities are much lower than those of organic carbonate solvents. Hybrid systems, using mixtures of liquid organic electrolytes with polymers and ionic liquids can increase the conductivity of the electrolyte while extending the operating temperature of the electrolyte, examples of this can be seen in Table 1-2. However, such systems add complexity and changes to manufacturing methods, this is something which is not desired by the lithium-ion battery industry. Literature has stated that changing a manufacturing method in a lithium-ion battery production is more difficult than changing a material providing that the same production methods can be used.[35] Therefore improvements to the current technology using existing methods is more preferential over those which use new methods is much preferred by the industry and are much more likely to reach commercialisation.

Table 1-2 Summary of different types of electrolyte solvents used in lithium ion batteries adapted from *Goodenough et al*[15]

Electrolyte	**Example**	**Ionic conductivity at RT (x 10^{-3} S/cm)**	**Electrochemical window vs Li/Li^+ (V)**	**Flammable?**
Liquid organics	1M $LiPF_6$ in EC:DEC (1:1)	7	1.3 V to 4.5 V	✓
Polymers	LiTFSI-P(EO/MEEGE)	0.1	<0.0 V to 4.7 V	✓
Liquid organics + Polymers	0.04$LiPF_6$ + 0.2EC + 0.62DMC + 0.14 PAN	4.2	Up to 4.4 V	✓
Ionic Liquids + Polymers	1M LiTFSI + P_{13}TFSI + PVDF-HFP	0.18	<0.0 V to 5.8 V	✓
Ionic Liquids + Liquid Organics + Polymers	56% LiTFSI-Py_{24}TFSI + 30% PVDF-HFP + 14% EC/PC	0.81	1.5 V to 4.2 V	✓
Inorganic Solids	$Li_{4-x}Ge_{1-x}P_xS_4$ (x=0.75)	2.2	<0.0 V to 5.0 V	×
Inorganic Liquids	$LiAlCl_4$ + SO_2	70	Up to 4.4 V	×
Ionic Liquids	1M LiTFSI in EMI-TFSI	2	1.0 V to 5.3 V	×

1.5.1 Carbonate Solvents

As was discussed above organic carbonate solvents are the industry standard for lithium ion battery electrolytes. Typically, a combination of carbonate solvents are used for example ethylene carbonate (EC), propylene carbonate (PC) and dimethyl carbonate (DMC), pictured in Figure 1-7. Ethylene carbonate is an important component in the electrolyte as literature has shown that EC plays an important role in the formation of the SEI. The SEI forms a passivation layer which prevents further electrolyte decomposition from occurring and consuming electrolyte which leads to capacity fade.[36,37] Since EC is a viscous liquid and is not liquid at room temperature other carbonate solvents are also added into the electrolyte e.g. PC, EMC, DEC. These components reduce the viscosity of the electrolyte which is important for a low activation energy for lithium-ion diffusion into the electrolyte and a lower charge transfer resistance of the electrolyte, allowing the battery to be operated at a faster rate of charge and discharge without effecting the capacity.[15] Other carbonate solvents are also believed to form other products on the electrode surfaces as well since reactions occur between the lithium ions and the carbonate molecules to produce lithium carbonates. The exact mechanisms are widely debated in the literature.[11] However the major drawback of carbonate based electrolytes is the flammability of them, a reason why research has aimed to replace them with alternative systems.

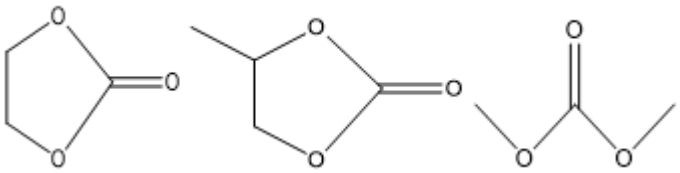

Figure 1-7 Structures of EC (left), PC (centre) and DMC (right).

Electrolyte components need to be carefully chosen that are not only thermally stable on their own i.e. that do not breakdown or vaporise at higher temperatures, but thermally stable during electrochemical operation. The thermal properties of typical lithium-ion battery carbonate solvents can be seen in Table 1-3. As can be seen from the table most of these solvents have relatively low boiling points with only EC and PC only suitable at 150 °C. However it has been reported in the literature that PC-based electrolytes with no EC cause graphite exfoliation.[11,38]

Table 1-3 Properties of a range of battery electrolyte carbonate solvents. Data from BASF[39]

Solvent	Boiling Point ˚C	Flash Point ˚C
Diethyl Carbonate (DEC)	125-129	33
Dimethyl Carbonate (DMC)	90	15
Ethylene Carbonate (EC)	247-249	150
Ethyl Methyl Carbonate (EMC)	108	23
Propylene Carbonate (PC)	242	135

Figure 1-8 shows a graphical representation of graphite exfoliation and the differences between an SEI formed using PC and EC. It can be observed that with PC there is poor SEI coverage with substantial graphite exfoliation and cracking occurring. It has also been reported in the literature that electrolytes containing a higher content of PC lead to an SEI which is thicker and of a higher resistance. The cause of the thicker SEI is due to PC causing exfoliation of the graphite, this in turn causes further breakdown of the electrolyte forming a thick SEI with high resistance.[38] Whereas with EC it is observed that the SEI coverage is good with no graphite exfoliation occurring. It has been shown in the literature that EC can be used successfully as the electrolyte solvent in high temperature batteries up to a temperature of 115 °C.[11,40]

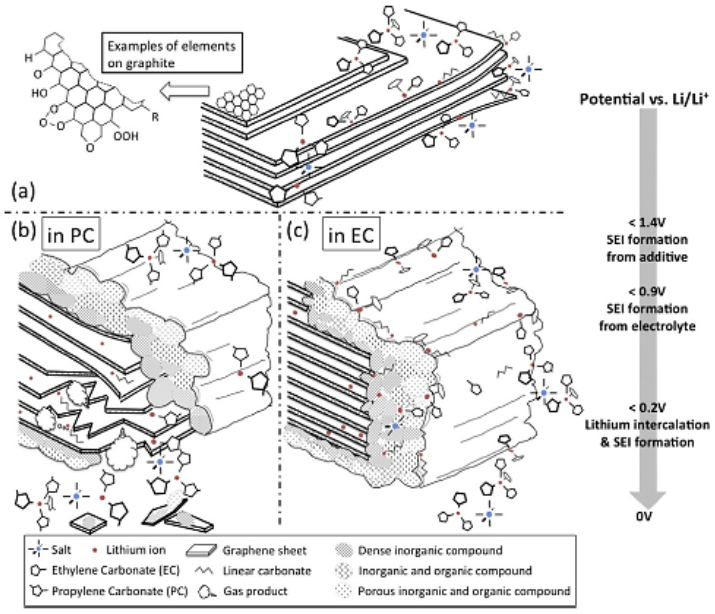

Figure 1-8 Diagram showing graphite exfoliation and the formation of the SEI using PC and EC electrolyte solvents. Reproduced with permission (CC BY 4.0) from An et al[11]

Another class of promising carbonate solvents is fluorinated carbonate solvents, these have a higher thermal and voltage stability than conventional carbonate solvents, due to the strong carbon-fluorine bond. Hu *et al* demonstrated the use of a fluorinated solvent combination of fluroroethylene carbonate (FEC), methyl 2,2,2-trifluoroethyl carbonate (F-EMC) and 1,1,2,2-tetrafluroethyl 2,2,2,2-tetrafluropropyl ether (F-EPE) 3:5:2 V:V with 1M lithium hexafluorophosphate ($LiPF_6$). This type of electrolyte has shown to achieve better capacities and coulombic efficiencies than $LiPF_6$ in EC/EMC electrolytes in $LiNi_{0.5}Mn_{1.5}O_4$/graphite cells cycled between 3.9 V and 4.9 V at 55 ˚C.[41] Dahn *et al* have also investigated fluorinated solvents and have showed that fluoroethylene carbonate (FEC) and di-2,2,2-trifluroethyl carbonate (TFEC) (3:7) show better performance than EC:EMC at 40 ˚C up to 4.6 V.[42]

1.5.2 Ionic Liquids

For higher temperature batteries ionic liquids have been researched. Ionic liquids have received considerable attention since they have an extremely high boiling point and extremely low vapour pressure. This is due to the very strong ion-ion interactions of the cations and anions in the ionic liquid; however this results in a high viscosity of the ionic liquid. This is an issue with ionic liquid-based electrolytes at room temperature, as the viscosity increases on addition of a lithium salt. This makes the rate of wettability of the electrodes more difficult since the electrolyte has to fill in the pores of the electrodes, this process is much slower with a high viscosity electrolyte. There are several issues with ionic liquids that have plagued the application into batteries. Firstly, the purity of ionic liquids has been issue, the purification process is difficult, since they cannot be distilled like other solvents. The purity of ionic liquids has improved over the years to the extent that they are viable for battery applications. Water is also an issue in ionic liquids and they require extensive drying to ensure that water levels are minimal. The other issue that has been reported with ionic liquids is that the potential stability window is largely reduced at high temperatures.[43–45] Jeff Dahn has also reported[46] that not all ionic liquids are more stable than carbonate solvents, in fact it was shown that some ionic liquids are much less stable than carbonate solvents. Out of six different ionic liquids tested only three of the ionic liquids showed to be more stable than carbonate solvents:

- 1-butyl-2,3-dimethylimidazolium bis(trifluoromethanesulfonyl)imide (BMMI-TFSI).
- 1-butyl-1-methylpiperidinium bis(trifluoromethanesulfonyl)imide (Pp14-TFSI).
- *N*-trimethyl-*N*-butylammonium bis(trifluoromethanesulfonyl)imide (TMBA-TFSI).

Two ionic liquids had similar reactivity to carbonate solvents:

- 1-Ethyl-methylimidazolium bis(trifluoromethanesulfonyl)imide (EMI-TFSI).
- 1-propyl-1-methylpyrrolidinium bis(fluorosulfonyl)imide (Py13-FSI).

One of the ionic liquids was much less stable than carbonates:

- 1-ethyl-3-methylimidazolium bis(fluorosulfonyl)imide (EMI-FSI).

Lin *et al*[47] has shown that a phosphonium ionic liquid with LiTFSI to operate at 100 ^{o}C with capacity dropping to 50% of the initial capacity after 70 cycles. Marczewski *et al*[48] proposed an ionic liquids-in-salt electrolyte where the salt content is higher than the ionic liquid content reporting high ionic conductivities, however this work was a proof of concept study and didn't test the electrolytes in a working cell. Ionic liquids have also been used in combination with carbonate solvents to give both the advantages of an ionic liquid (high temperature stability) and carbonate solvents (good conductivity). Ababtain *et al*[49] showed that a mixture of 80% 1-methyl-1-propylpiperidinium bis(trifluromethanesulfonyl)-imide (pip) ionic liquid to 20% propylene carbonate (PC) capable of operation between 25 ^{o}C to 100 ^{o}C using a 3D nano silicon negative electrode.

1.6 Lithium-ion Battery Electrolyte Salts

1.6.1 Lithium hexafluorophosphate ($LiPF_6$)

Typically, the electrolyte used in lithium ion cells is lithium hexafluorophosphate ($LiPF_6$), seen in Figure 1-9, in a combination of organic carbonate solvents. $LiPF_6$ has unique set of properties which make it a suitable its use in commercial cells. $LiPF_6$ is used because it improves the corrosion resistance of the aluminum current collector, literature shows that $LiPF_6$ forms both Al_2O_3 and AlF_3 layers on aluminum current collectors to passivate them. $LiPF_6$ also has good solubility in a range of solvents and has a good conductivity at room temperature.[50–55] Literature has shown that $LiPF_6$ is an essential component in the electrolyte helping to form a stable SEI to stop further electrolyte breakdown from occurring. A study by Zhou *et al* used DSC analysis to compare an exothermic peak relating to the reaction between lithiated graphite and the electrolyte solvent (EC/DMC). Results showed that the electrolyte solvent without any $LiPF_6$ in the electrolyte had a much higher heat value than that of the electrolyte containing $LiPF_6$. Results also showed that higher concentrations of $LiPF_6$ in the electrolyte resulted in much less heat compared to lower concentrations, the authors concluded that $LiPF_6$ is an essential component in the electrolyte in order to form a stable SEI layer resulting in less electrolyte reactions. [56] *Sato et al* stated that low levels of HF in the electrolyte, associated with the reaction of $LiPF_6$ with trace water help with the formation of the SEI.[57]

$LiPF_6$ is a thermally stable salt with a decomposition temperature of >175°C.[10] However $LiPF_6$ reacts with water even at room temperature, as shown in equation 1-8 and equation 1-9 this severely lowers the decomposition temperature.[57–59] It has been reported that the breakdown process of $LiPF_6$ when in an electrolyte solution can be as low as 80°C.[43] Electrochemically initiated reactions of $LiPF_6$ with solvents have also been demonstrated, as shown in equation 1-10 to equation 1-12. The rate of these reactions is accelerated at higher temperatures, the products of which react with the cell components[43]. Literature has shown that $LiPF_6$ is unstable for use at elevated temperatures in lithium ion batteries[11,59,68–70,60–67].

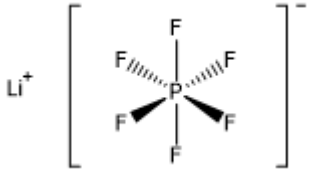

Figure 1-9 Structure of $LiPF_6$.

$$LiPF_6 \rightleftharpoons LiF + PF_5$$ Equation 1-8

$$PF_5 + H_2O \rightarrow POF_3 + 2HF$$ Equation 1-9

$$LiPF_5 + ROH \rightarrow POF_3 + RF + HF$$ Equation 1-10

$$POF_3 + ROH \rightarrow POF_2OR + HF$$ Equation 1-11

$$POF_3 + RCO_3R \rightarrow POF_2OR + RF + CO_2$$ Equation 1-12

1.6.2 Lithium [bis(oxalate)borate] (LiBOB)

LiBOB, shown in Figure 1-10, has been researched as a replacement to $LiPF_6$ due to being more thermally stable, having a decomposition temperature of over 290 °C[71]. In addition, LiBOB does not undergo decomposition like those seen in Equation 1-8 to Equation 1-12. It has also been demonstrated that LiBOB facilitates the passivation of the aluminium current collector.[13,40,71–74] However work by *Xu et al*[75] showed that LiBOB has some disadvantages compared to $LiPF_6$. Firstly, LiBOB has issues with solubility in solvents such as EC and PC, which limits the concentration of LiBOB that can be used (typically <1M depending on solvents used). However *Xu et al*[75] showed that that γ-butyrolactone can be used as a co-solvent to allow higher concentrations to be used. The same work also showed that the SEI on both positive and negative electrodes can be of high resistance, increasing the overall cell impedance. The authors however reported that the γ-butyrolactone used to increase the solubility of the LiBOB into the electrolyte results in a lower cell impedance. It has been reported LiBOB is less conductive than $LiPF_6$ when dissolved in the same carbonate solvents.[71]

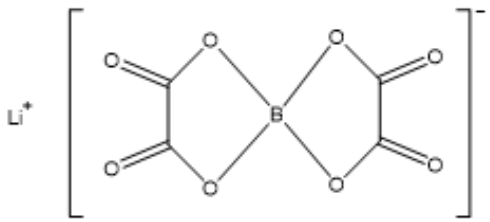

Figure 1-10 Structure of Lithium [bis(oxalato)borate] (LiBOB).

Work by Kurita *et al*[40] has demonstrated that LiBOB can be used successfully as an electrolyte salt up to a temperature of 115°C, the results of which can be seen in Figure 1-11. Half cells of LFP vs Li were constructed with an electrolyte of 1M LiBOB in EC and a glass fibre separator. The cells were then charged and discharged using galvanostatic cycling for 50 cycles at a range of C-rates (0.5C-200C) and a range of temperatures (60-115°C). It was observed that capacity was not temperature dependent at low C-rates but was however dependant at higher C-rates. This is due to the fact that at high C-rates the reaction is limited by lithium diffusion and so temperature increases the rate at which lithium diffusion occurs. At 115 ˚C the capacity observed was 160 mAh g^{-1} showing an 86% capacity retention after 50 cycles.[40] These results represent a benchmark of what can be achieved in a high temperature lithium ion battery which utilises a carbonate based electrolyte.

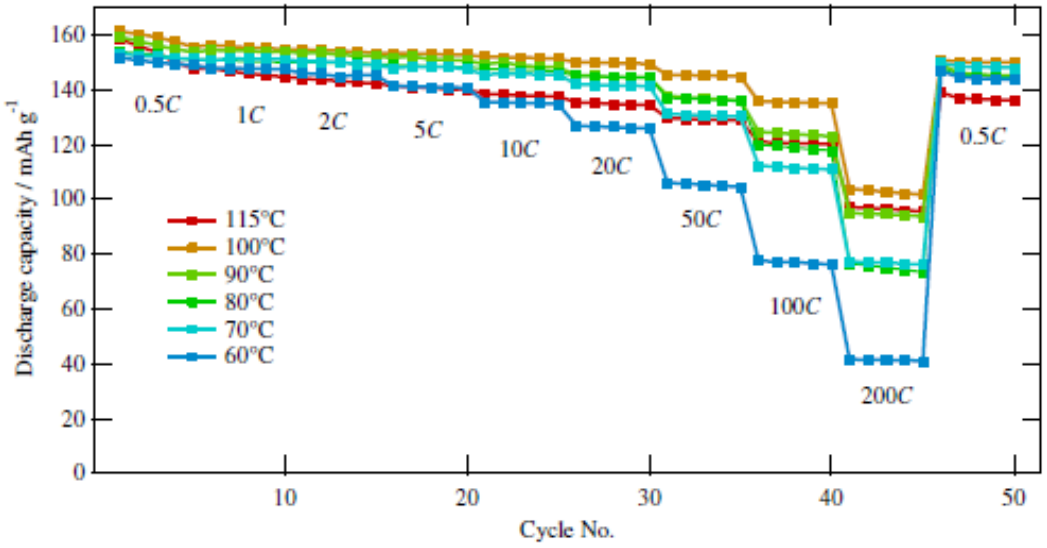

Figure 1-11 Graph showing the effect of temperature and C-rate on the discharge capacity of a $LiFePO_4$ half-cell with LiBOB/EC electrolyte. Reproduced with permission from Elsevier from Kurita et al[40]

1.6.3 Lithium oxalyldifluroborate (LiODFB)

Another lithium salt which has been researched as a replacement for $LiPF_6$ is lithium oxalyldifluoroborate (LiODFB).[10,76–78] Introduced by *Zhang*[76] in 2006, LiODFB was found to possess the advantages of LiBOB, whilst having some distinct advantages over it. The structure of LiODFB, seen in Figure 1-12, is a variation of LiBOB, where one of the oxalato groups has been replaced with two fluorine groups. Studies by *Zhang*[76] showed that LiODFB has a higher solubility in carbonate

solvents compared to LiBOB allowing higher concentrations of the salt. The same author showed that LiODFB has a higher conductivity compared to LiBOB, attributed to the lower viscosity of the electrolyte solution and higher salt dissociation compared to LiBOB. The same work reported that LiODFB produces a much more stable SEI due to the degradation products that make up the SEI, with the breakdown of the LiODFB shown in Figure 1-13. The LiODFB can either break one of the F bonds (product I) leaving the oxalato group intact or break one of the O-B bonds leaving the fluorine groups intact (product II). The products I and II can then go on to react with SEI components to produce oligomers, which produces a much more stable SEI.

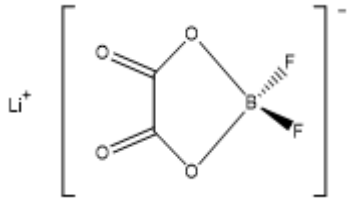

Figure 1-12 Structure of LiODFB.

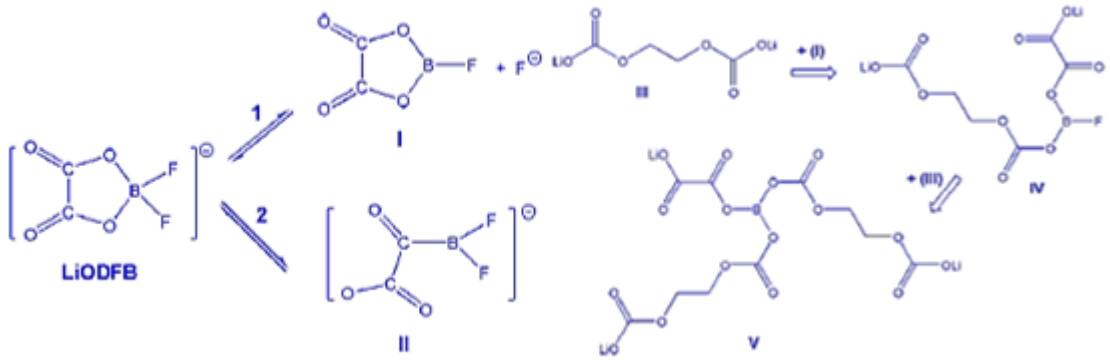

Figure 1-13 Scheme showing the degradation reactions of LiODFB producing SEI components. Reproduced with permission from Elsevier from Zhang[76]

Li et al[77] has demonstrated the use of LiODFB as replacement for $LiPF_6$ at 65 ^oC, using $LiFePO_4$/ graphite full cells. Results showed that an electrolyte of 1M LiODFB in EC/PC/DMC (1:1:3 v/v) had a relatively high conductivity of 8.25 mS cm^{-1} at 25 ^oC. The full cells composed of $LiFePO_4$ and artificial graphite cells showed a good capacity retention over 100 cycles of 92% at 25 ^oC and 88% at 65 ^oC. In comparison to 1M $LiPF_6$ in EC/PC/DMC (1:1:3 v/v) the full cells only achieved a 50% capacity

retention after 100 cycles at 65 ^{o}C. The discharge capacities of the full cells with the LiODFB electrolyte at both room temperature and 65 ^{o}C were higher than that of $LiPF_6$.

1.6.4 Mixed Salt Electrolytes

Lithium Bis(trifluoromethane)sulfonimide (LiTFSI), seen in Figure 1-14, is a lithium salt that is commonly used in lithium air and lithium sulphur research as the lithium salt. LiTFSI is not currently in use as a salt in lithium ion batteries due to the inability to form a protective passivation layer on the aluminium current collector, which results in the corrosion of the aluminium current collector. This is problematic for lithium ion batteries that operate at higher potentials than lithium air and lithium sulphur.[53,79–82] It does however have a high decomposition temperature of 360 ^{o}C which makes it a very attractive choice as a high temperature lithium electrolyte salt.

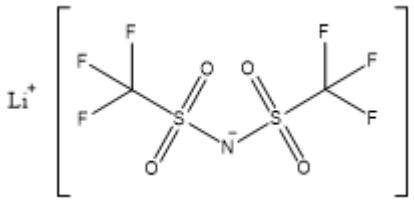

Figure 1-14 Structure of LiTFSI.

It has been documented in the literature that LiTFSI can be used in lithium ion batteries when used in combination with other lithium salts. It has been reported by Chen *et al*[83] that using a combination of LiTFSI and LiBOB at a ratio of $LiTFSI_{0.6}$-$LiBOB_{0.4}$ shows a better capacity retention on cycling than $LiPF_6$ when cycled at 60 ^{o}C in $LiFePO_4$ half cells. Results showed that after cycling for 1000 cycles there was only a 5.4% capacity loss at 1C with the $LiTFSI_{0.6}$-$LiBOB_{0.4}$ electrolyte. This performance has been attributed to the LiBOB decomposing to form a passivation layer on the Al. *Li et al*[84] have also shown LiODFB to be effective when combined with LiTFSI in supressing Al corrosion, however this report does not test high temperature cycling stability. This aluminium corrosion can be seen in the SEM images in Figure 1-15. Image (a) shows the fresh Al with (b) showing Al subjected to 4.2V for two weeks with 1M $LiPF_6$ electrolyte which shows that corrosion of Al doesn't occur since a passivation layer has occurred with $LiPF_6$. Images (c) and (d) showing when the Al has been subjected to a 1M LiTFSI electrolyte for two weeks at 4.2V, severe corrosion

has occurred to the Al surface. Images (e) and (f) showing a 1M LiTFSI solution with a 2% weight of LiODFB added, this time no corrosion has occurred and looks similar to that of $LiPF_6$.

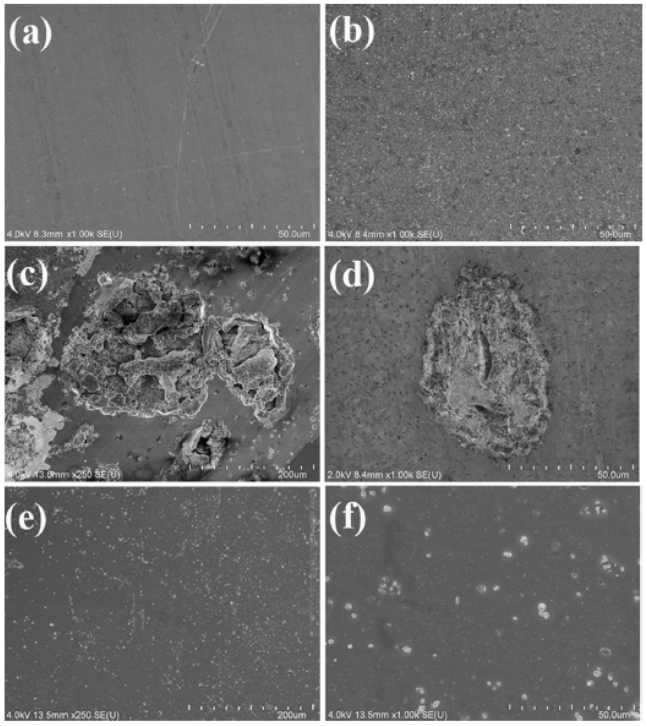

Figure 1-15 SEM images of fresh Al foil (a), Al exposed to 1M $LiPF_6$ for two weeks at 4.2V (b), Al exposed to 1M LiTFSI for two weeks at 4.2V (c&d) and Al exposed to 1M LiTFSI + 2% wt of LiODFB for two weeks at 4.2V (e&f). Reproduced with permission from Elsevier from *Li et al*[84]

Another recent publication by *Zheng et al*[85] has taken this concept a step further by adding in a small quantity of $LiPF_6$ (0.05M) into an electrolyte of 0.4M LiBOB/ 0.6M LiTFSI in EC/ EMC (4:6 w/w), the results of which can be seen in Figure 1-16. The results show that the electrolyte is stable for 400 cycles in NMC half cells showing a 90% capacity retention at 60 ˚C. Compared to 1M $LiPF_6$ in EC/ EMC (4:6 w/w) which has a rapid capacity fade by 45 cycles and 0.4M LiBOB/ 0.6M LiTFSI in EC/ EMC (4:6 w/w) without the addition of the $LiPF_6$ which fades to cell failure by 275 cycles. The improved cycling stability at 60 ˚C has been attributed to the passivation properties of $LiPF_6$ helping to form a more stable SEI, as it is documented in the literature that $LiPF_6$ helps in forming the SEI layer.[56,57]

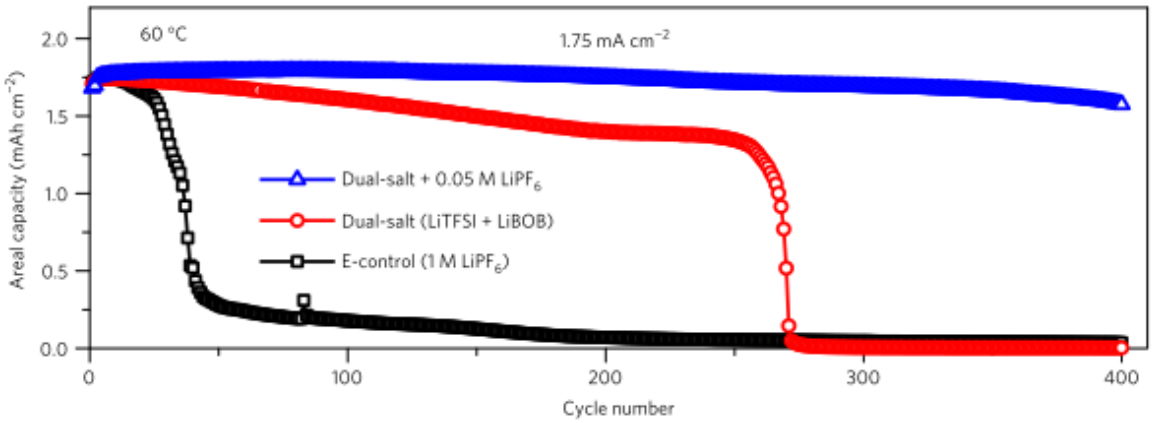

Figure 1-16 Cycling of NCM half cells with 1M $LiPF_6$ (black), 0.6M LiTFSI + 0.4M LiBOB (red) and 0.6M LiTFSI + 0.4M LiBOB + 0.05M $LiPF_6$ (blue) in EC/ EMC (4:6 w/w) at 60 ^{o}C. Reproduced with permission from Nature from *Zheng at al*[85].

1.7 Lithium-ion Battery Electrolyte Additives

There are several electrolyte additives that have been investigated in the literature that aim to stabilise the SEI layer and allow higher temperature operation. The idea behind an additive is that they are easier to oxidise and reduce than the other electrolyte components, in the process forming a passivation layer on the electrodes preventing the breakdown of the other electrolyte components. Herstedt *et al* investigated a range of common additives using electrochemical and DSC measurements.[86] The results showed the use of additives increased the first cycle irreversible capacity, with improvement in the coulombic efficiency after 25 cycles over those without any additive. The addition of ethyltriacetoxysilane (ETAS) and vinylene carbonate (VC) proved to be the most suitable additives. The onset temperature for the first thermally activated reaction with the additives is higher than without, suggesting that there is better stabilisation with the addition of the additive, VC showing the highest onset temperature. In the literature VC has received much attention[87,88] for improving the stability of the SEI, improving Coulombic efficiency and rate performance. However Deshpande *et al* has reported that it shows no significant impact on the capacity fade of cells.[89]

Another additive tris(Pentafluorophenyl) Borane (TPFPB) has been reported in the literature with results showing that the onset temperature for the first thermally activated reaction is shifted to 140-160 ^{o}C in an electrolyte formulation of $LiBF_4$ in EC: DEC 2:1.[90]

Another additive 2-(triphenylphosphoranylidene) succinic anhydride (TPSA) has been reported by Ryou *et al* and has shown an increase of 43% capacity retention at 55 ^{o}C for 100 cycles at C/2 in a $LiMn_2O_4$ / graphite cell.[91] As was detailed in section 1.5.1 fluorinated carbonates have shown to be good replacements to conventional carbonate solvents. *Myung-Hyun Ryou et al* have used a 2% weight addition of FEC to an electrolyte solution of 1M $LiPF_6$ in EC/PC/DEC in a graphite/ $LiMn_2O_4$ cell and showed that capacity retention at 60 ^{o}C after 130 cycles was 20% higher that without the additive.[92]

Another group has investigated fluorosilane additive 1,2-bis(difluromethylsilyl) ethane (FSE) and has shown it to be an effective additive at 0.5% w/w into a 1M $LiPF_6$ in EC/DMC (3:7 v/v) with a $LiMn_2O_4$/ graphite cell. Results showed that capacity retention and coulombic efficiency were much better with the addition of the additive than without for operation at 60 ^{o}C, seen in Figure 1-17. However concentrations over 0.5% resulted in detrimental capacity loss, which is due to the breakdown of the FSE, which contributes to increased impedance on the electrode surfaces.[93]

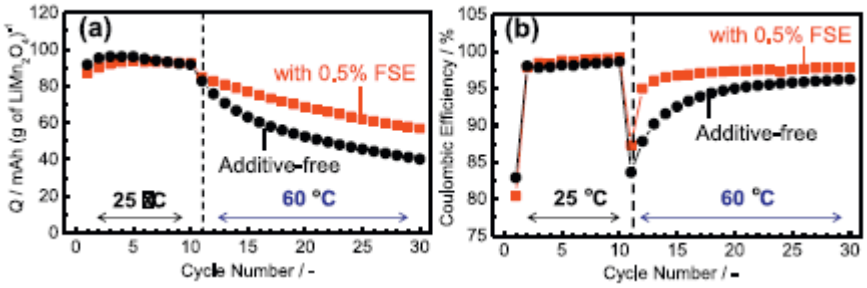

Figure 1-17 Galvanostatic cycling of $LiMn_2O_4$/ graphite cells with an electrolyte of 1M $LiPF_6$ in EC/DMC (3:7 v/v) with and without the addition of 0.5% FSE. Reproduced with permission from Elsevier from *Yamagiwa et al*[93]

Haibo Rong et al have shown an imidazole electrolyte additive to be effective at both high voltages and high temperatures. A 0.25% addition of 1,10-sulfonyldiimidazole (SDM) was added to a 1M $LiPF_6$ in EC/EMC/DEC 3:5:2 w/w in a $Li/LiNi_{0.5}Mn_{1.5}O_4$ cell. Results showed that the addition of SDM is effective for operating up to 4.9V at a temperature of 55 ^oC showing much higher coulombic efficiencies and capacity over 100 cycles, compared without. Impedance spectroscopy showed that the addition of the SDM results in a much lower impedance compared to the electrolyte without. Results also showed lower concentrations of Mn and Ni on the lithium metal negative electrode with the addition of SDM, due to less metal dissolution at the positive electrode. This is confirmed by the analysis of the positive electrode showing higher levels of Mn and Ni with the added SDM, the analysis of the positive electrode also shows less C, O and P levels on the positive electrode (which shows that less carbonate breakdown has occurred). HOMO energy calculations have showed that the reasons for this is that SDM has a less negative HOMO energy level than the carbonate solvents and so oxidises more readily, meaning much less oxidation of the carbonate solvents.[94]

Yanbo Liu et al have shown that tris(trimethylsilyl) borate (TMSB) to be an effective additive for operation at 55 ^oC when 0.5% w/w is added to an electrolyte of 1M $LiPF_6$ in EC/DMC in a $Li/ LiMn_2O_4$ cell. Cycling results showed that the electrolyte containing TMSB has much higher capacity over 180 cycles, with higher columbic efficiencies observed. Impedance spectroscopy shows that the impedance is much lower for cells with added TMSB. These results have been attributed due to the TMSB forming a stable passivation on the electrodes with a low impedance and the ability of TMSB to effectively co-ordinate with F which removes the LiF from the SEI (which is known to reduce cell life).[95]

1.8 Lithium-ion Battery Electrode Materials

Before the introduction of lithium insertion materials metal lithium was used in early rechargeable batteries in the 1970's, since the use of metal lithium as a negative electrode gives the highest energy density.[9] However the use of lithium is problematic due to lithium dendrite formation which causes cell shorting and side reactions of the metal lithium with the electrolyte. This results in reduced cell lifetimes and serious safety issues.[2] However the replacement of metal lithium with lithium insertion electrodes reduces cell voltage, specific energy (Wh kg^{-1}), energy density (Wh L^{-1}), cell capacity (mAh g^{-1}) and rate capability. Insertion electrode materials are used since the insertion of lithium into solid state materials is simple and reversible. Research has focussed on improving electrode insertion materials to further progress on these desirable properties. There are two fundamental requirements for electrode materials[9,96]:

a) A high specific charge (Ah kg^{-1}) and charge density (Ah L^{-1}).[9]
b) A high positive electrode redox potential for the positive electrode and a low negative electrode redox potential for the negative electrode to give a high cell voltage.[9]

1.8.1 Negative Electrode Materials

Numerous materials have been proposed for lithium ion battery negative electrodes such as transition- metal oxides, lithium alloys and polymers. Carbons and more specifically graphite are still the greatest choice for lithium ion batteries due to being inexpensive and possessing unique properties which make it well suited for lithium intercalation/de-insertion. Carbons have higher specific redox potentials, have better stability and show better cycling performance than other negative electrodes. Lithium alloys and silicon, for example, have large volume changes (typically >100% expansion for Li alloys[9] and >600% for Si[97]) on lithium insertion/ de-insertion which make them poorly suited to battery applications. This has consequences on the formed solid electrolyte interphase (SEI) layer often being broken/destroyed each cycle, which consumes electrolyte and causes rapid capacity fade. The reaction of carbon negative electrode materials proceeds via the generalised reaction that can be seen in equation 1-13.[96]

$$x\,Li^+ + x\,e^- + C_n \underset{Li\,extraction}{\overset{Li\,insertion}{\rightleftharpoons}} Li_xC_n \qquad \text{Equation 1-13}$$

There are two main categories of lithium insertion negative carbon electrodes graphitic and non-graphitic carbons. Graphitic carbons are the most widely used negative electrode material for lithium-ion batteries since they have the following advantages[98]:

- Relatively high capacity.
- Can operate down to a low voltage (close to 0 V vs Li/Li^+)
- Has a flat voltage profile.
- Low volumetric expansion and contraction on cycling (~10%).
- Low cost.
- Its ability to form a stable SEI under normal operating conditions.

Graphitic carbons are characterised as carbons with a layered structure with a perfect stacking order of graphene layers. These stacking layers can either be hexagonal graphite (AB) or rhombohedral graphite (ABC), however due to the small transformation energy required to transition between the two forms "perfect" graphite is not easily available. The term graphite is therefore used irrespective of the stacking order.[9,96] The insertion of lithium into graphite occurs between the graphene layers, this is depicted in Figure 1-18.

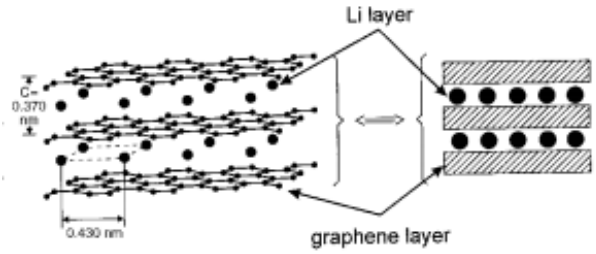

Figure 1-18 Diagram of graphite, showing the insertion of lithium between the graphene layers. Reproduced with permission from John Wiley and Sons from *Winter et al*[9]

It has been shown that there are several defined stages of insertion of lithium into graphite, this is depicted in Figure 1-19. The first stage which occurs at around 0.8 V vs Li/Li^+, is the decomposition

of electrolyte forming the SEI layer on the graphite electrode surface. The decomposition of the electrolyte to form the SEI layer results in an irreversible capacity loss which can be seen in Figure 1-20, this irreversible capacity loss is greatest in the first cycle with subsequent cycles having lower irreversible capacities.[99] The SEI provides a passivation layer which minimises the breakdown of the electrolyte on subsequent cycles. Typically for the first charge/ discharge cycle of graphite the discharge capacity of the graphite exceeds that of the theoretical capacity and this is due to the extra charge passed to allow the electrolyte breakdown to form the SEI. Once the SEI formation has taken place the lithium then goes through the stages of insertion, as shown in Figure 1-19:

- Stage 3: LiC_{24} occurring at 0.2 V.
- Stage 2L: LiC_{18} and Stage 2: LiC_{12} occurring at 0.14 V.
- Stage 1: LiC_6 occurring at 0.09 V.

Figure 1-19 shows that there are plateaus at the voltages associated with the transitions between the stages of lithium insertion. The final form LiC_6, gives a theoretical capacity of 372 mAh g^{-1}. [9,96,100,101]

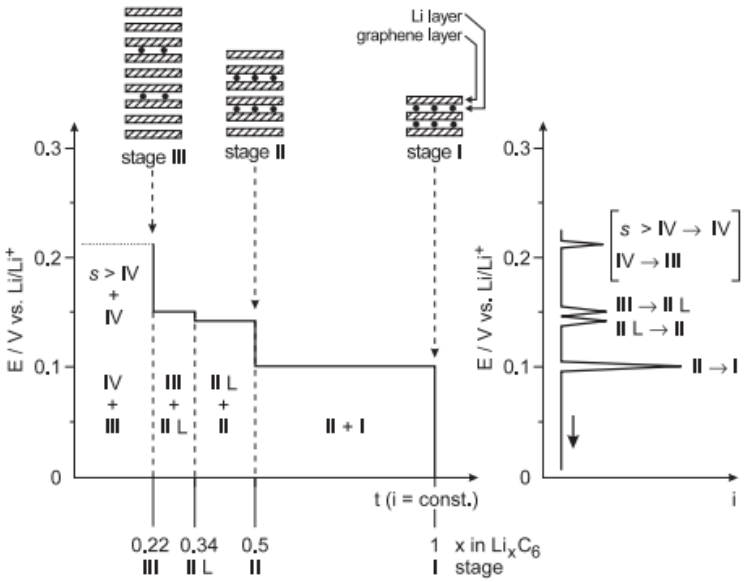

Figure 1-19 Diagram showing the insertion of lithium into graphite. Reproduced with permission from John Wiley and Sons from *Winter et al*[9]

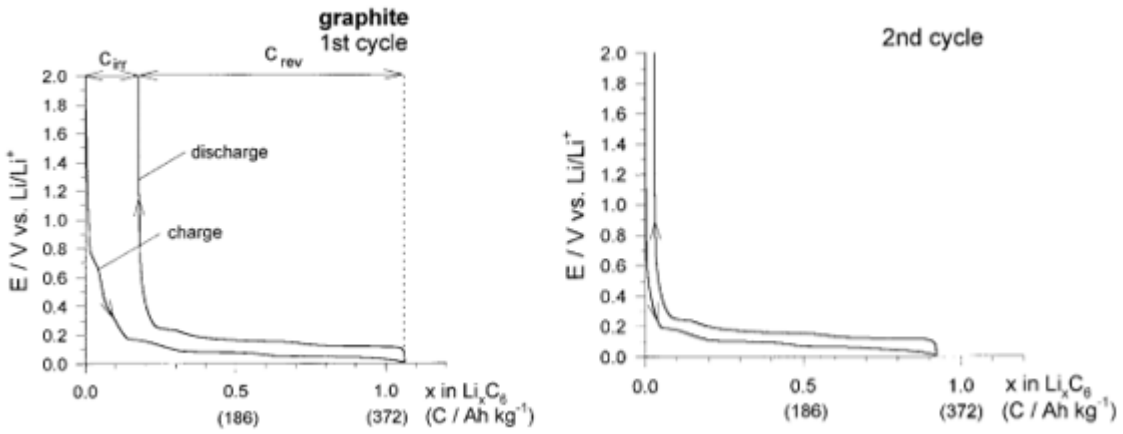

Figure 1-20 Diagram showing the first two charge/ discharge profiles of graphite insertion/ de-insertion. Reproduced with permission from John Wiley and Sons from *Winter et al*[9]

Many high temperature studies on graphite have mainly focussed on assessing the effect of temperature on the SEI and the subsequent ageing mechanisms that occur. It has been shown that the negative electrode/ electrolyte interface is unstable at elevated temperatures due to the electrolyte breakdown reactions occurring at an increased rate and resulting in greater consumption of electrolyte and unwanted side products.[7,12,102,17–24]

Markevich et al[103] assessed the cycling performance of half cells of electrodes of natural graphite flakes (KS15) and electrodes with a mixture of graphitised meso carbon micro beads (MCMB) and meso carbon fibres (MCF) (4:6). Coin cells were fabricated and cycled at 60 and 80 ˚C with an electrolyte of 1M $LiPF_6$ in EC/EMC (1:2) with a c-rate of C/4 for the KS15 graphite and C/8 for the MCMB-MCF.[103] Results showed that the synthetic graphite (KS15) had a 95 % capacity retention after cycling at 80 ˚C for 120 cycles, the MCMB-MCF electrodes showed much greater rate of decline in capacity with only a 7 % capacity retention at 60 ˚C and a 1 % capacity retention at 80 ˚C after 120 cycles. The poor capacity retention on cycling the MCMB-MCF electrodes has been attributed not to the degradation of the materials but rather the formation of a thick SEI layer, increasing the impedance of the electrodes, leading to capacity fade. This is attributed to the fact that the MCMB-MCF particles mostly have edge planes compared to graphite which is composed mostly of basal planes, the former is much more reactive with the electrolyte. The authors commented that the round shape of the particles lead to continuous surface reactions causing the formation of a thick SEI layer. Similar observations have been made in the literature with regards to thicker SEI layers being formed on graphite. *Andersson et al*[102] observed an additional layer which they termed a macroscopic layer forming on the SEI surface of synthetic graphite of graphite half cells stored at

60 ^{o}C with an electrolytes of 1M $LiPF_6$ in EC/DMC (2:1) and 1M $LiBF_4$ in EC/DMC (2:1). *Andersson et al*[104] found that the macroscopic layer is mainly composed from LiF, with studies showing that LiF content increases with increasing temperature. The other component which was found to be predominant on the graphite surface was polymeric carbon which was attributed to the increased decomposition of the electrolyte on the graphite. *Edstrom et al* also observed the formation of LiF on graphite surfaces with 1M $LiPF_6$ in EC/DEC.[13]

Markevich et al[103] also investigated the effect of a full cell configuration compared to that of half cells for both the positive and negative electrodes. A full cell configuration of a $LiCoO_2$ positive electrode and an MCMB-MCF negative electrode with a 1M $LiPF_6$ in EC/DMC (2:1) electrolyte. Half cells of $LiCoO_2$/ Li and MCMB-MCF/ Li were also fabricated with the same electrolyte. Results showed that the half cells of MCMB-MCF declined quickly only retaining 23 % of the original capacity over 65 cycles at 60 ˚C whereas the $LiCoO_2$ half cells retained 85 % of the original capacity over 65 cycles at 60 ˚C. The full cell configuration was then cycled for 100 cycles at 60 ˚C, results showed a capacity retention of 38 % after 100 cycles at 60 ˚C. The electrodes were then taken from the full cells and half cells were fabricated with each electrode, assembling with fresh electrolyte, then cycled again at 60 ˚C. The results showed that the MCMB-MCF half-cell worked only for a few cycles whereas the $LiCoO_2$ still continued to function for the 20 cycles that the half cells were cycled for.

The effect of temperature on graphite has also been studied in full cell configurations with *Song et al*[20] showing the effect of temperature on lithium iron phosphate/ synthetic graphite full cells with an electrolyte composed of 1M $LiPF_6$ in EC/DMC/EMC (1:1:1). Cells were cycled at 55 ˚C using galvanostatic cycling between 2 and 3.85 V using a charge current of 1C and discharge current of 3C. Results showed that the cells retained 70% capacity retention over 600 cycles when cycled at 55 ˚C. The reason for the capacity fade was discovered to be the dissolution of the iron into the electrolyte which then deposits on the graphite electrode surface causing accelerated decomposition of the electrolyte leading to a thicker SEI layer on the graphite.

A similar study of full cell configuration of lithium iron phosphate and graphite cell was done by *Liu et al*[105]. The authors commented that the primary source of capacity loss is due to the loss of active lithium due to instability of the negative electrode/ electrolyte interface. The volume changes on cycling giving rise to damage of the SEI, which causes consumption of electrolyte which consumes active lithium. The authors also commented that graphite exfoliation, cracking and delamination from the current collector could also be causes of the capacity fade.

Non-graphitic carbons are carbons which have a planar hexagonal arrangement of carbons but with no order in the c direction like is the case with graphite, this leads to a disordered carbon. The

structure consists of amorphous regions, embedding and crosslinking more graphitic regions. This is depicted in Figure 1-21. Unlike graphite insertion, the mode of lithium-ion storage for non-graphitic carbons is less understood and is widely debated amongst the literature.[106] The charge/ discharge curves differ considerably to that of graphite with no distinguishable plateaus observed. This is due to the disordered nature of non-graphitic carbons which produces non-equivalent sites, unlike graphite where the sites are equivalent. Non-graphitic carbons can store more or less lithium compared to graphite, termed high specific charge ($x > 1$ in Li_xC_6 where $x = 1$ for graphite) or low specific charge ($x < 1$ in Li_xC_6 where $x = 1$ for graphite).[9,96]

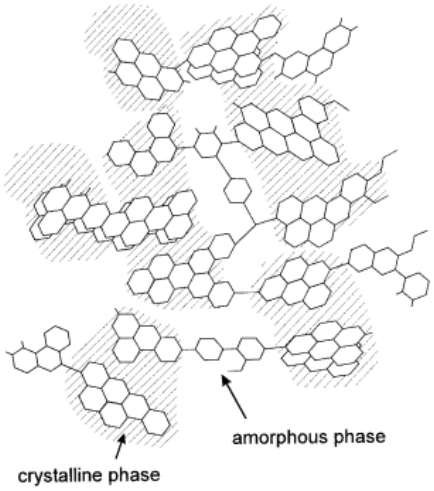

Figure 1-21 Diagram of a non-graphitic carbon. Reproduced with permission from John Wiley and Sons from *Winter et al*[9]

Despite high specific charge carbons being able to store more lithium compared to graphite, surface areas of these carbons are higher than graphite and some studies have shown that the irreversible capacity is high in high surface area carbons such as hard carbons.[107–115] However Work by *MacNeil et al*[116] showed that the surface area isn't an indicator of a higher irreversible capacity, the work showed that surface area doesn't correlate with irreversible capacity i.e. a higher surface area carbon does not necessarily mean a higher irreversible capacity. In the same study *MacNeil et al*[116] compared the reactivity of various carbon electrode materials with electrolytes at elevated temperatures using accelerating rate calorimeter (ARC) and also compared the irreversible capacities as a function of their surface area. It was shown that the higher the surface area of the carbon the higher the temperature rise shown in the ARC, however there was one result which did not fit with the results and that was for a high surface area petroleum coke. Results showed much lower than expected heat rise, suggesting that surface area isn't the only factor for reaction at high

temperature. The authors attributed the processes occurring were an initial activation process of the decomposition of the SEI followed by the reaction between the lithium and the electrolyte.

Literature has shown that hard carbons could be a promising replacement for graphite at elevated temperatures due to having a higher resistance to solvent co-intercalation than graphite.[25] *Zheng et al*[117] investigated hard carbons as a negative electrode material for elevated temperatures up to a temperature of 80 ^{o}C using an ionic liquid electrolyte. Hard carbon electrodes were produced from phenolic resin and half cells were prepared with an electrolyte of 1M LiTFSI in an ionic liquid of trimethylhexylammonium bistrifluoro-methane sulfonylimide (TMHA-TFSI). Results showed that at room temperature the discharge capacity is low due to the lithiation of the hard carbon being slow and a large voltage hysteresis is observed for the charge/ discharge cycle. The other reason is that the conductivity of the ionic liquid is increased at 80 ^{o}C. The capacity of the hard carbon at 80 ^{o}C was 675.0 mAh g^{-1} with a first cycle coulombic efficiency of 73.6% was achieved which is much higher capacity than that of graphite. The reason for the improved performance of the hard carbon compared to graphite is that hard carbon with ionic liquid electrolyte works well without the need for an SEI due to the increased stability of the ionic liquid preventing electrolyte breakdown.

1.8.2 Positive Electrode Materials

While graphite remains an industry standard for the negative electrode materials research has focused on finding new positive electrode materials for lithium ion batteries in order to increase the specific energy (Wh kg^{-1}), energy density (Wh L^{-1}) and operating voltage of lithium-ion batteries. There are three categories of positive electrode material[9]:

1. Inorganic transition-metal oxide materials.
2. Organic molecules.
3. Polymers.

Inorganic transition-metal oxide materials are the most widely adopted in Li-ion technology. The reaction of inorganic transition-metal oxide materials proceeds via the generalised reaction that can be seen in equation 1-14.[9]

$$Li_{x+\Delta x}MX \underset{discharge}{\overset{charge}{\rightleftharpoons}} \Delta x\, Li^{+} + \Delta x\, e^{-} + Li_{x}MX \qquad \text{Equation 1-14}$$

There are three main classes of inorganic transition-metal oxide materials that currently exist within lithium ion batteries:

1. Layered structure.
2. Spinel structure.
3. Olivine structure.

Layered oxides have the general formula $LiMO_2$ (where M = Co, Cr, V, or Ni), the structure can be seen in Figure 1-22. This type of structure has Li^+ and M^{3+} ions occupying alternate (111) planes of the rock salt structure which gives rise to an arrangement of O-Li-O-M-O along the c axis. The oxygen stacking sequence is ABC along the c axis with Li^+ and M^{3+} ions occupying the octahedral interstitial sites of the cubic close-packed oxygen array. This is an O3 layer structure (Li^+ ions occupying octahedral sites with three MO_2 sheets per unit cell). The lithium insertion is two dimensional and is capable of high lithium conductivity and high electronic conductivity. $LiCoO_2$ is capable of operation up to 4 V with a stable voltage throughout discharge, making it an attractive choice for Li-ion batteries. Although the theoretical capacity of $LiCoO_2$ is 272 mAh g^{-1} its useable capacity is limited to 140 mAh g^{-1}. This is due to oxygen evolution occurring above insertion of 0.8Li and electrolyte degradation occurring at potentials greater than 4.2 V vs Li/Li^+.[9,96,118–120]

Layered compounds such as NMC (lithium-nickel-manganese-cobalt-oxide $LiNi_xMn_yCo_zO_2$) and LNMO (lithium-nickel-manganese-oxide $LiNi_{0.5}Mn_{1.5}O_4$) have shown be promising as electrode materials. However they have been shown to be unstable at elevated temperatures producing gases such as O_2, CO_2 and CO and have large capacity fading on cycling.[121,122] This has restricted such materials to be used only high as 60 ˚C, seen in Table 1-6. However, good performance has been observed at 60 ˚C with these materials, it has been reported that a 90% capacity retention after 400 cycles at 60 ˚C for NMC 442 vs Li using an electrolyte of 0.6M LiTFSI + 0.4M LiBOB + 0.05M $LiPF_6$ in EC/EMC (4:6 w/w).[85]

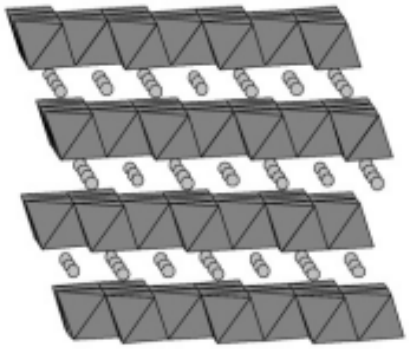

Figure 1-22 Diagram showing layered structure ($LiCoO_2$). Reproduced with permission from Elsevier from Ohzuku et al[120]

Spinel oxides have the general formula LiM_2O_4 (where M = Mn, V, Ti), the structure can be seen in Figure 1-23. In this structure the Li^+ and $M^{3+/4+}$ ions occupy the 8a tetrahedral and 16d octahedral sites of the cubic close-packed oxygen array, giving the structure $(Li)_{8a}(M_2)_{16d}O_4$. The strong edge-shared octahedral $[M_2]O_4$ array allows the insertion and de-insertion of lithium ions from the tetrahedral sites without the change in the spinel structure. Lithium insertion is three dimensional with high lithium conductivity and high electronic conductivity observed. It is possible to insert a second lithium into the empty 16c octahedral sites in LiM_2O_4 to give $Li_2M_2O_4$. However, this causes repulsion of the Li^+ ions in the 8a tetrahedral and 16c octahedral sites causing the Li^+ ions in the tetrahedral sites to be displaced to the octahedral sites making an ordered rock salt structure of $(Li_2)_{16c}(M_2)_{16d}O_2$. The theoretical capacity of the material 148 mAh g^{-1}, but in practice, capacities of only around 120 mAh g^{-1} are obtained.[9,96,120,123]

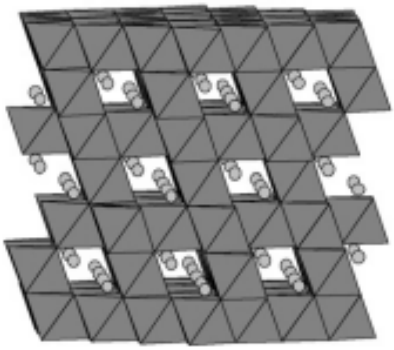

Figure 1-23 Diagram showing spinel structure ($LiMn_2O_4$). Reproduced with permission from Elsevier from *Ohzuku et al*[120]

Lithium iron phosphate (LFP), seen in Figure 1-24, was introduced by Goodenough [4] in 1997 as a safer, non-toxic, more stable positive electrode material. This is due to structural stability from the covalent bonded PO_4 units and the chemical stability of having $Fe^{2+/3+}$ rather than $M^{3+/4+}$ in $LiMO_2$ materials. The olivine structure composes of FeO_6 octahedra and PO_4 tetrahedra units. Lithium iron phosphate transitions between two phases $FePO_4$ (fully charged) and $LiFePO_4$ (fully discharged), with a two-phase region on the plateaux ($Li_{1-x}FePO_4$), this results in a flat voltage profile at 3.5 V. Typically the voltage range used is between 2.5 V to 4.5 V giving a specific discharge capacity of 160 mAh g^{-1}. However $LiFePO_4$ has poor electronic conductivity and requires carbon coating to increase the conductivity.[4,9,96,120] Lithium iron phosphate is a well-established positive electrode material which has been shown in the literature to possess high thermal stability, electrochemical stability and good cycle life.[45,124] The majority of high temperature studies >100 ˚C utilise $LiFePO_4$ as the electrode choice, due to its higher thermal stability than other positive electrode materials. The performance of lithium iron phosphate is improved at higher temperatures with the increase in rate capability and increase in capacity.[125,126] LFP has shown to be effective as a stable positive electrode material up to 250 ˚C. *Muñoz-Rojas et* al [45] investigated half cells of lithium iron phosphate with no binder with a molten LiTFSI electrolyte cycled at 230 and 250 ˚C, results showed that capacity was 84% after 5 cycles at 250 ˚C.

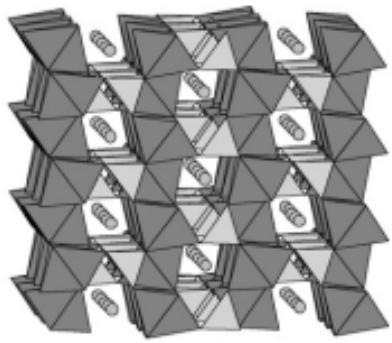

Figure 1-24 Diagram showing olivine structure ($LiFePO_4$). Reproduced with permission from Elsevier from Ohzuku et al[120]

Yiqing Huang et al[127] studied the thermal stability of a range of electrode materials using TGA and DSC analysis. The materials investigated were $Li_{0.1}Ni_{0.8}Co_{0.15}Al_{0.05}O_2$ (NCA), $FePO_4$ (FP), $Mn_{0.8}Fe_{0.2}PO_4$ (MFP) and $VOPO_4$. TGA was performed on the electrode materials in the absence of any electrolyte and DSC was performed on the electrode materials with and without the presence of 1 M $LiPF_6$ in EC/DMC 1:1 electrolyte, the results of which are summarised in Table 1-4. The most thermally stable material was shown to be $FePO_4$ which has a thermal stability up to a temperature of 600 ˚C

and does not generate heat during DSC without the presence of electrolyte and showed a low heat rise with electrolyte. The least stable material was shown to be NCA decomposing between 200-300 ˚C and shows significantly higher heat rise compared to the other positive electrode materials (674 J g^{-1} without electrolyte and 793 J g^{-1} with electrolyte). The thermal stability was found to be in the order of FP > MFP > $VOPO_4$ > NCA.

Table 1-4 Table showing the thermal stability of positive electrode materials. Adapted from *Huang et al*[127]

Material	**Thermal Stability/ ˚C**	**Heat Rise without electrolyte/ J g^{-1}**	**Heat Rise with electrolyte/ J g^{-1}**
$FePO_4$	600	0	251
$Mn_{0.8}Fe_{0.2}PO_4$	300-350	73	476
$VOPO_4$	200-300	0	407
$Li_{0.1}Ni_{0.8}Co_{0.15}Al_{0.05}O_2$	200-300	674	793

1.9 Lithium-ion Battery Electrode Binders

As well as the active material in an electrode, a binder is used to adhere all the particles of the active material and conductive carbon to the electrode substrate. The purpose of this is to allow even conduction of electrons and ions throughout the entire electrode and the binder must maintain mechanical stability and be chemically/electrochemically stable. The requirements for a lithium-ion battery electrode binder are as follows[128,129] :

1. It must have high adhesion properties in order to hold the active battery material and conductive carbon together and to the surface of the electrode current collector foil. Figure 1-25 shows the possible ways which binders could take, (a) represents the perfect scenario by where particles are held together by the binder and to the current collector. (b) and (c) represent a poor binder where the distribution is poor between particles and current collector.
2. It must be chemically inert with the electrolyte not being plasticised by the solvents or reacting with the electrode active materials.
3. It must be physically stable on any expansion and contraction of the electrode volumes due to the insertion and de-insertion of lithium ions.
4. It must be thermally stable, not melting or decomposing at the operational temperature of the battery.
5. It must be electrochemically stable, i.e. not oxidising or reducing on charging and discharging of the battery.

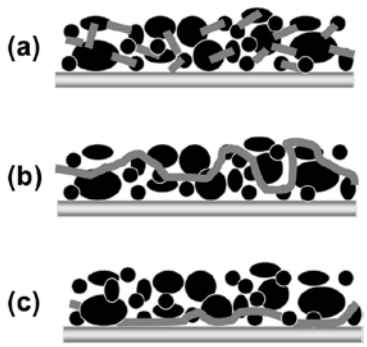

Figure 1-25 Diagram showing the possible binding of electrode binder with active electrode material and carbon to the current collector. Reproduced with permission (CC BY-NC 3.0) from *Choi et al*[129]

1.9.1 Polyvinylidene Fluoride (PVDF)

The binder used in commercial lithium-ion batteries is polyvinylidene fluoride (PVDF), pictured in Figure 1-26, typically PVDF 5130 is used since it is a specially designed polymer for battery binder applications having a large electrochemical stability window[130,131], with a melting point of 158-166 ^{o}C. Despite polymers having the important role of ensuring the mechanical stability and the conductivity of the particles between each other and the current collector the research into the active materials and electrolyte are much more studied. Binders can either soften/ melt or decompose at high temperatures, resulting in a loss of mechanical stability in the electrode. Contact losses between the active material, carbon and binder in composite electrodes can occur; which can either be mechanical or electrical contact losses.[17,132]

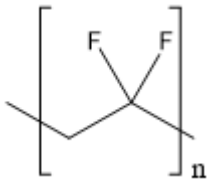

Figure 1-26 Structure of PVDF.

Bodenes et al[7] has reported that the main mechanism of degradation for a $LiNi_{1/3}Mn_{1/3}Co_{1/3}O_2$ (NMC) / carbon cylindrical cell cycled at 120 ^{o}C was the ageing of the PVDF binder in the NMC positive electrode. The authors showed that by using XPS the PVDF migrates from the NMC electrode to form a PVDF layer on the surface of the NMC electrode. This leads to poor lithium insertion into the electrode which was shown by the authors using ^{7}Li NMR. In addition to this PVDF was also detected on the surface of the negative carbon electrode. This is attributed to the fact that the PVDF dissolves into the electrolyte and is deposited on the negative electrode, making Li insertion and de-insertion more difficult. The results showed that 71% of the total PVDF was on the surface of the positive electrode after the cells were cycled at 120 ^{o}C. *Bodenes et al*[133] also detected dissolution of the PVDF binder for cells of NMC/ graphite cycled at 85 ^{o}C, evidenced by XPS of the negative electrode surface.

1.9.2 Polyamide-imide (PAI)

Polyamide-imide (PAI), pictured in Figure 1-27, has been identified as an alternative binder to PVDF. Studies of PAI have shown that PAI possess high thermal stability (>300 ˚C) and high mechanical stability due to the chemical interactions between the amide and imide units in the polymer. Hydrogen bonding occurs between the amide groups and intermolecular interactions occur between the imide groups in the polymer increasing the mechanical stability.[131,134]

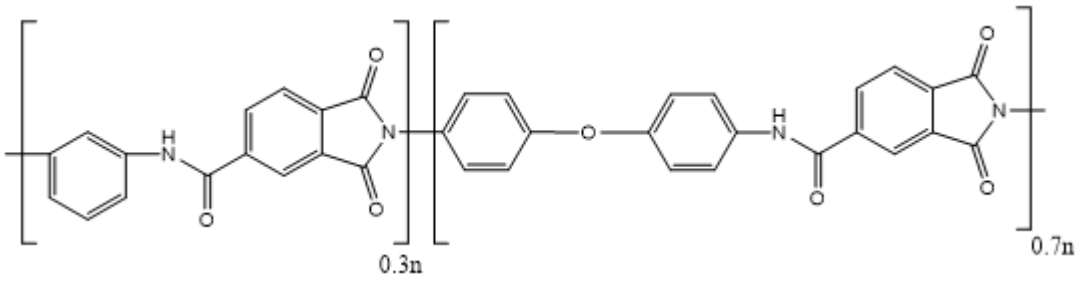

Figure 1-27 Structure of Torlon 4000 T PAI. Adapted from *Choi et al*[135]

The high mechanical stability of PAI has been used to increase the stability of silicon electrodes which have an expansion of >600%[97] on insertion/de-insertion. Work by *Choi et al*[135] has shown that PAI is much more stable on cycling than PVDF with silicon, achieving a capacity of 1700 mAh g^{-1} and a coulombic efficiency of 99.5% over 20 cycles for silicon with PAI binder vs Li. This is due to the fact that the PAI is able to maintain the mechanical stability of the electrode which PVDF is unable to achieve. The silicon PVDF electrode on the other hand had a very poor coulombic efficiency on the first cycle (28.9%) compared to that of silicon PAI (74.9%) and after the first cycle the PVDF electrodes failed to cycle after the first cycle due to failure of the electrical contacts of the silicon and the current collector.

PAI has also been researched as an alternative binder to PVDF in high temperature applications. *Morishita et al*[131] showed that NMC with PAI binder performed much better than that of NMC with PVDF binder when cycled at 60 ˚C. Initially the discharge capacity for NMC(PAI) vs SiO cell was similar to that of NMC (PVDF) vs SiO cell at 60 ˚C, the performance after 500 cycles was somewhat different for NMC(PAI) vs SiO the capacity was 88 mAh g^{-1} and for NMC (PVDF) vs SiO was 25 mAh g^{-1}. The mechanical properties of the PAI and PVDF were compared and it was shown that the

tensile strength, elongation and elastic modulus were all higher for PAI compared for PVDF at 100 ˚C for 10 hours, the results of which can be seen in Table 1-5.

Table 1-5 Table showing the mechanical properties of PVDF and PAI. Data from *Morishita et al*[131].

	PVDF	**PAI**
Tensile Strength (N mm^{-2})	29	207
Elongation (%)	3.6	102.4
Elastic modulus (N mm^{-2})	1339	3500

1.9.3 Polyacrylnitrile (PAN)

Polyacrylnitrile, seen in Figure 1-28, has also been investigated as a binder for lithium-ion batteries due to the fact PAN has a much higher melting temperature (>300 ˚C[136]) and because of the chemical properties of PAN. The CN groups in PAN mean that PAN is highly polar and the CN bonds can form strong hydrogen bonding and dipole-dipole interactions which give it good adhesion properties.[136] The strong adhesion properties have meant that PAN has been used as a binder in silicon negative electrodes where PVDF is poor performing due to poor mechanical properties.[131,137] PAN has also been used in $LiNi_{0.5}Mn_{1.5}O_4$ (LNMO) electrodes[138] to coat the surface of the electrode surface in order to minimise the direct electrolyte contact with the LNMO particles minimising the metal dissolution into the electrolyte. Results showed that half cells of LMNO with a 1M $LiPF_6$ in DMC/ DEC/ EC (1:1:1 v/v) cycled for 100 cycles at 55 ˚C exhibited a higher capacity and higher capacity retention with PAN coated LNMO than uncoated LMNO. The PAN LMNO showed a discharge capacity of 112.9 mAh g^{-1} and a 95.2 % capacity retention compared to uncoated which had a discharge capacity of 104.7 mAh g^{-1} and an 87.8 % capacity retention. However, the LMNO electrode only used PAN as the electrode coating and not for the adhesion of the electrode to the current collector (PVDF was still used).

PAN has also been investigated for a range of negative electrode materials by *Gong et al*[136] who investigated the effect of PAN on the performance of graphite and silicon/graphite compared to PVDF binder. Results showed that the PVDF electrodes performed the least well of the two binders with the PVDF silicon/graphite electrode reaching zero capacity after 5 cycles due to failure of the mechanical properties of the PVDF. The initial coulombic efficiency for the electrodes made with

PAN binder for graphite were 81 % for graphite and 84 % for silicon/graphite, much higher than that of PVDF binder for graphite 79 % and 11 % for silicon/graphite at room temperature. The cycling performance gives a higher capacity over 50 cycles compared to PVDF electrodes however the high temperature performance isn't investigated.

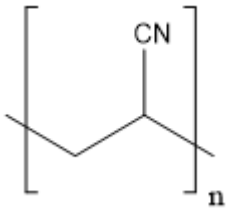

Figure 1-28 Structure of PAN.

1.10 Summary of High Temperature Studies

Table 1-6 shows a summary table of key results in the literature of high temperature studies of lithium ion batteries. What is apparent from the literature is that higher temperature studies of lithium ion batteries operating above 60 ^{o}C is limited in the literature, mainly due to the thermal instability of the materials. As mentioned in section 1.9 layered oxides such as NMC have been shown to be unstable at elevated temperatures producing gases such as O_2, CO_2 and CO. This results in large capacity fading on cycling and has restricted their use to 60 ˚C, with materials such as LFP being used at temperatures >60 ^{o}C.[121,122] What is also apparent from the table is that electrode materials are dependent on the electrolyte for example $LiFePO_4$ can be operated up to 250 ^{o}C with a molten salt of LiTFSI[45] and other studies have shown that LFP can operated up to 120 ^{o}C using an EC/ LiBOB electrolyte[40]. Therefore, the best high temperature performance is achieved with the use of a stable electrode material such as LFP and LTO with high temperature stable lithium salts such as LiBOB and higher thermally stable solvent such as EC. Despite polymers having the important role of ensuring the mechanical stability and the conductivity of the particles between each other and the current collector there is a lack of research into binders suitable for use at elevated temperatures.[17,132]

Table 1-6 Summary table of key high temperature studies of Li-ion batteries

Temp. ˚C	Electrolyte	Electrode(s) and binder	Separator	Capacity and retention	Reference
40	1M $LiPF_6$ in FEC:TFEC + 2% PES and 0.5% MMDS	NMC 442 (PVDF) vs Graphite (CMC/ SBR)	Not specified	240 mAh g^{-1} 75% after 800 cycles	[42]
60	0.6M LiTFSI + 0.4M LiBOB + 0.05M $LiPF_6$ in EC/EMC (4:6 w/w)	NMC 442 vs Li	Celgard 2500	163 mAh g^{-1} 90% after 400 cycles	[85]
55	1M $LiPF_6$ in FEC/ F-EMC/ E-EPE (3:5:2)	LMNO (PVDF 5130) vs Graphite (PVDF 9300)	Celgard 2325	130 mAh g^{-1} 50% after 250 cycles	[41]
55	1M $LiPF_6$ + 0.25 wt% SDM in EC/EMC/DEC (3:5:2 wt%)	$LiNi_{0.5}Mn_{1.5}O_4$ (PVDF) vs Li	Celgard 2400	120 mAh g^{-1} 96% after 100 cycles	[94]
55	1.2M $LiPF_6$ in F-AEC/F-EMC/F-EPE (2:6:2)	$LiNi_{0.5}Mn_{1.5}O_4$ vs $Li_4Ti_5O_{12}$	Celgard 3501	125 mAh g^{-1} 96% after 80 cycles	[139]

55	0.4M $Li_2B_{12}F_9H_3$ + 2% LiODFB in EC/EMC (3:7, w/w)	Graphite / $Li_{1.1}[Ni_{1}/_{3}Mn_{1}/_{3}Co_{1/3}]_{0.9}O_2$ pouch cells	Not Stated	250 mAh g^{-1} 70% after 1200 cycles	[140]
55	1M $LiPF_6$ + 5 wt% di-(2,2,2 trifluoroethyl)carbonate (DFDEC)) alone and 3 wt% VC in EC/EMC (3:7 v/v)	$Li_{1.13}Mn_{0.463}Ni_{0.203}Co_{0.203}O_2$ (PVDF) vs graphite (PVDF)	Celgard C210	227 mAh g^{-1} 77% after 50 cycles	[141]
55	1.2M $LiPF_6$ + 1 wt% LTFOP in EC/EMC (3:7 w/w)	$LiNi_{0.33}Co_{0.33}Mn_{0.33}O_2$ (PVDF) vs MCMB (PVDF)	Celgard 3501	120 mAh g^{-1} 88% after 200 cycles	[142]
60	1.15M $LiPF_6$ in EC/EMC (3:7 v/v) With the following additives for separate tests: 2% vinylene carbonate (VC) 2% succinonitrile (SN) 2% propene sulfone (PST) 2% propane sulfone (PS)	$Li[Ni_xCo_yMn_z]O_2$ (NCM) (PVDF) vs graphite (CMC/SBR)	Not stated	VC = 90% after 50 cycles SN = 95% after 50 cycles PST = 97% after 50 cycles PS = 99% after 50 cycles	[143]
60	1M $LiPF_6$ in EC/DEC (1:1 w/w)	$LiNi_{0.33}Co_{0.33}Mn_{0.33}$ (PVDF) vs $Li_4Ti_5O_{12}$ (LTO) (PVDF)	Celgard 2325	175 mAh g^{-1} 95% after 100 cycles	[144]
55	1M $LiPF_6$ + 0.1wt% TPSA in EC/DEC (1:1 v/v)	$LiMn_2O_4$ (PVDF) vs graphite (PVDF)	Not stated	120 mAh g^{-1} 75% after 100 cycles	[91]
60	1M $LiPF_6$ + 2 wt% FEC in EC/DEC/PC (30:65:5 wt%)	$LiMn_2O_4$ vs graphite	Not stated	116 mAh g^{-1} 88% after 130 cycles	[92]
60	1M $LiPF_6$ + 0.5 wt% FSE in EC/DMC (3:7 v/v)	$LiMn_2O_4$ (PVDF) vs graphite (SBR/CMC)	Polyolefin porous membrane (layered Polypropylene-polyethylene)	90 mAh g^{-1} 62% after 20 cycles	[93]

60	1M $LiPF_6$ in (EC/DMC/DEC) (1:1:1 v/v/v)	LTO-coated $LiMn_2O_4$ (PVDF) vs Li	Celgard 2400	132 mAh g^{-1} 97% after 100 cycles	[145]
60	1M LiFNFSI in EC / EMC (3:7 v/v)	$LiCoO_2$ vs Graphite	Celgard 2325	120 mAh g^{-1} 63% after 100 cycles	[146]
60	1.05M $LiPF_6$ in EC/DMC (1:1 v%)	$AlPO_4$ coated $LiCoO_2$ (PVDF) vs Li	15 µm microporous poly- ethylene separator	180 mAh g^{-1} 79% after 30 cycles	[147]
100	1.6 M LiTFSI mono-$(C_6)_3PC_{10}$-TFSI	$LiCoO_2$ vs Li	Celgard 480	135 mAh g^{-1} 52% after 70 cycles	[47]
100 200	LiPON	$LiCoO_2$ vs Sn_xN_y No Binder sputtered onto glass substrate with Pt currently collectors	LiPON	193 µAh 5 cycles 140 µAh 1 Cycle	[148]
60	0.6M LiTFSI + 0.4M LiBOB in EC/EMC (4:6 w/w)	$LiFePO_4$ (PVDF 5130) vs Li	Not stated	155 mAh g^{-1} 94 % after 1000 cycles	[83]
65	1M LiODFB EC/PC/DMC (1:1:3, v/v)	$LiFePO_4$ (PVDF) vs graphite (PVDF)	Celgard 2400	375 mAh 88% after 100 cycles	[77]
80	polymeric lithium tartaric acid borate poly(vinylidene fluoride-co-hexafluoroprope (PLTB@PVDF-HFP) swollen with PC	$LiFePO_4$ (PVDF) vs Li	Electrolyte is separator	159.6 mAh g^{-1} 89.8% after 60 cycles	[149]
115	1M LiBOB in EC	$LiFePO_4$ PVDF vs Li	Glass Fibre	160 mAh g^{-1} 86% after 50 cycles	[40]
120	poly(oxyethylene) methacrylate-g-poly(dimethyl siloxane) (POEM-g-PDMS) doped with lithium triflate (1:20)	$LiFePO_4$ (electrolyte is binder) vs Li	Electrolyte is separator	160 mAh g^{-1} 63% after 30 cycles	[150]
120	1M LiBOB in PC	$LiFePO_4$ (PVDF) vs Li	FCCN- flame retardant thermal resistant cellulose based composite nonwoven separator (cellulose,	160 mAh g^{-1} 90% after 20 cycles	[151]

			sodium alginate, flame retardant, silica 2:1:1:0.5)		
250	Molten LiTFSI	$LiFePO_4$ (no binder) vs Li	Glass fibre	84% after 5 cycles	[45]

1.11 Aims and Objectives of Project

Currently the options for high temperature lithium-ion secondary batteries is limited due to the instability of the interface between the lithiated carbon negative electrode and the organic electrolyte. Development of lithium-ion batteries suitable for high temperature applications requires a holistic approach to battery design because degradation of some of the battery components can produce a serious deterioration of the other components, and the products of degradation are often more reactive than the starting materials. Therefore, a careful selection and systematic characterisation of the components of lithium ion batteries is required in order to identify a number of materials and protocols for battery assembly that give promising performance at high temperatures. At the start of the project it was decided to use well characterised industry standard materials such as $LiFePO_4$ and graphite. The decision to use well characterised industry standard materials was made for the following reasons:

1. An understanding of the temperature limitations of binders, separators, electrolytes, positive electrode materials, negative electrode materials and current collectors was required. Therefore, an understanding of the materials used in current Li-ion technology can be made in order to focus the efforts on the most important components.
2. Changing a manufacturing method in a lithium-ion battery production is more difficult than changing a material providing that the same production methods can be used.[35] Therefore improvements to the current technology using existing methods is more preferential over those which use new methods is much preferred by the industry and are much more likely to reach commercialisation.

The aims of the project were:

1. To investigate the performance of lithium ion cells operating between 25 ^{o}C and 150 ^{o}C.
2. To predict what temperature range over which useful performance can be achieved.

The objectives were:

To understand the temperature limitations of binders, electrolytes, positive electrode materials, negative electrode materials and current collectors.

Chapter 2 Experimental

2.1 List of Chemicals

Component	Material	Manufacturer	Supplier
Positive electrode active material	Lithium Iron Phosphate ($LiFePO_4$)	Tatung	QinetiQ
Negative electrode active material	Mesophase Graphite Powder Anode (MGPA) graphite powder		QinetiQ
	Biocarbotron Hard Carbon Type 1	Kuraray	QinetiQ
Electrode Binder	Solef 5130 Polyvinylidene fluoride (PVDF)	Solvay	QinetiQ
	Polyamide-Imide 4000T-HV (PAI)		QinetiQ
	Polyacrylonitrile (PAN)	Sigma Aldrich	QinetiQ
Electrode Ink solvent	1-Methyl-2-pyrrolidinone (NMP)	Sigma Aldrich	
Negative electrode foil	Copper foil 10µm (pouch cells)		QinetiQ
	Copper Foil 0.125mm (Swagelok Cells)	Advent Materials	
Positive electrode foil	Aluminium foil 20µm (pouch cells)		QinetiQ
	Aluminium Foil 0.125mm (Swagelok Cells)	Advent Materials	
Electrode conductive carbon	Acetylene Black 100% compressed powder Shawinigan Black	Chevron Phillips Chemical Company LP	Cairn International
Electrolytes	BASF Electrolyte LP30- 1M $LiPF_6$ in EC:DMC (1:1 w/w)	BASF	
	BASF Electrolyte LP57- 1M $LiPF_6$ in EC:EMC (1:1 w/w)		
	1M $LiPF_6$ in EC:EMC (1:3 w/w)		
Electrolyte Solvent	Ethylene Carbonate	Sigma Aldrich	
Electrolyte Salts	Lithium hexafluorophosphate ($LiPF_6$)		
	Lithium bis(oxalato)borate (LiBOB)		

	Lithium difluoro(oxalato)borate (LiODFB)		
Cell Separator	Glass microfibre filter (Swagelok Cells)	Whatman	VWR
	Celgard Polypropylene 2500	Celgard	QinetiQ
Lithium foil	Metal lithium foil	Rockwood Lithium	

2.2 Preparation of Swagelok Cells

2.2.1 Preparation of Electrodes

1. Active material, acetylene black, binder (dissolved in NMP) and NMP were weighed and added into a vial.
2. Active material, acetylene black, binder and NMP were magnetically stirred for a minimum of 2 hours to fully incorporate all the components to make an ink.
3. The stirrer bar was removed and the ink homogenised (IKA T25 homogeniser equipped with an 8mm diameter stator), starting at 10,000 RPM for 5 minutes, 15,000 RPM for a further 5 minutes, 20,000 RPM for 2 minutes and finally 25,000 RPM for 2 minutes to give a fully uniform suspension.
4. Electrode foil was rubbed down with fine grit paper to remove surface impurities and is cleaned using acetone.
5. The foil was coated with the ink using a K bar and rubber coating mat and dried on a hotplate at 80°C in a fume hood until the solvent was evaporated. The electrodes were then dried at 100°C for 1 hour to dry.
6. Electrode disks were then cut from the coated foil (11 mm diameter, Nogami handheld electrode cutter) and compressed in a hydraulic press (Graseby Specac Press Carver Lab Press) at 10 tonnes to compress the electrode surface to result in a thinner film and improved particle connectivity.
7. The electrode disks were then dried overnight at 120 °C using a Büchi® drying tube under vacuum (4 x 10^{-1} mBar) before being transferred to an argon filled glovebox (MBraun, <1ppm water and oxygen).

2.2.2 Preparation of Electrolytes

For the experiments not utilising commercial electrolytes (chapters 4-6), electrolytes were made in house. The electrolyte salts (LiBOB and LiODFB) were dried at 120 °C for a minimum of 2 days using a Büchi® drying tube under vacuum (4 x 10^{-1} mBar). The electrolyte solvent ethylene carbonate (EC) were used as bought. Electrolytes were prepared in an argon filled glove box (MBraun, <1ppm water and oxygen). The EC was melted on a hotplate at 50 ^{o}C until liquid, the

electrolyte salt was added to the vial, the EC added to the vial and the stirrer bar added, the electrolyte was then left to stir on the hotplate at 50 ^{o}C overnight.

2.2.3 Assembly of Test Cells

Swagelok test cells composed of a working electrode ($LiFePO_4$ positive electrode or graphite negative electrode), two glass fibre separators (13mm diameter), electrolyte (8 drops or 120 µL), and a counter/reference electrode (lithium foil or $Li_{0.5}FePO_4$ electrode) were assembled in an argon filled glove box (MBraun, <1ppm water and oxygen). Figure 2-1 shows an inflated picture of the components of the test cell.

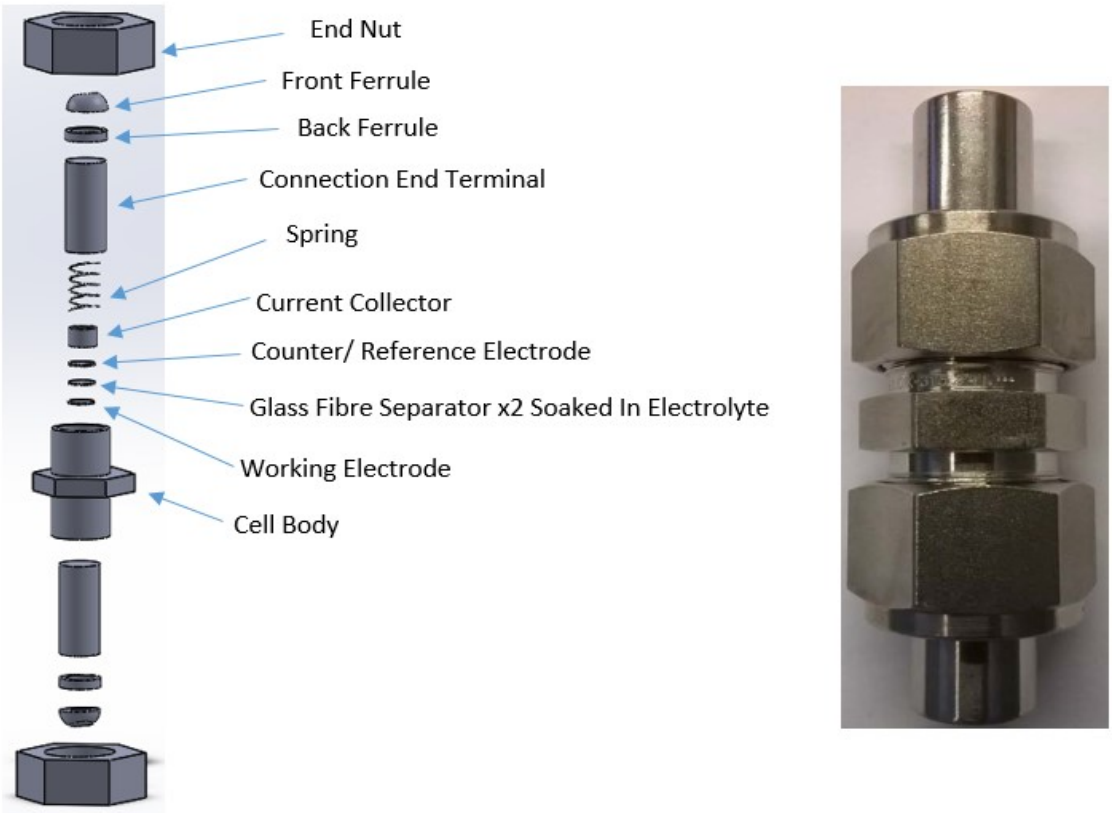

Figure 2-1 Assembly of a test cell, showing components (left) and assembled cell (right).

2.3 Preparation of Pouch Cells

The manufacturing of the pouch cell electrodes and pouch cells was conducted in a dry room using QinetiQ's facilities.

2.3.1 Preparation of Electrodes

1. Active material, Acetylene black and binder (dissolved in NMP) were weighed in a fume hood into a container and stirred until mixed thoroughly.
2. NMP (if needed) was added and the ink homogenised (IKA homogeniser) until a fully uniform suspension achieved.
3. The foil was coated with the ink using a doctor blade coating machine and allowed to dry on a hotplate at 80°C to evaporate the NMP and then 100 °C for 1 hour.
4. The electrodes were then calendard using a roll mill to achieve required film density.
5. The electrodes were then cut for use pouch cells using a hydraulic press with a specially designed electrode cutter die (electrode area of 26.5 cm^2).
6. The electrodes were then dried overnight at 120 °C in a vacuum oven.

2.3.2 Assembly of Test Cells

Full lithium ion pouch cells were assembled in a dry room composed of a lithium iron phosphate positive electrode, polypropylene separator, negative (graphite or hard carbon negative electrode) and LP57 electrolyte. The cell was enclosed in a heat-sealed polymer coated aluminium pouch cell casing, with the electrolyte injected into the pouch before being vacuum sealed. Figure 2-2 shows a diagram of the components of a pouch cell next to an assembled cell.

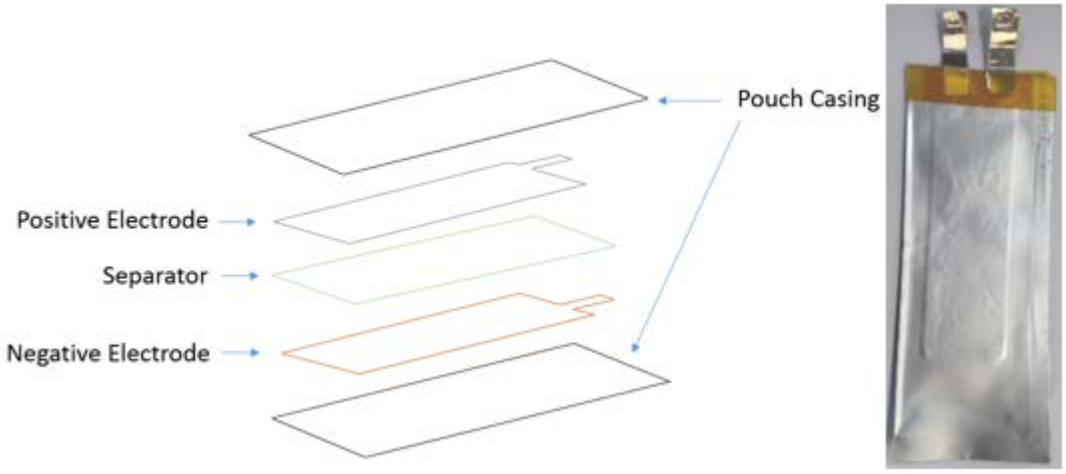

Figure 2-2 Diagram of the components of a Li-ion pouch cell (left) and an assembled pouch cell (right).

2.4 Characterisation Techniques

2.4.1 Galvanostatic Cycling

Galvanostatic cycling was conducted on a VMP2 potentiostat running EC lab software. Galvanostatic cycling is an electrochemical technique used to assess the charge/ discharge performance of a battery. Galvanostatic cycling yields information about the batteries performance namely charge/discharge capacity, reversible/irreversible capacity and coulombic efficiency. The technique involves applying a constant current to the cell whilst recording the change in the potential of the cell to set limits of potential. The current is switched between positive and negative values to assess the charge/discharge process of the cell. Figure 2-3 shows a representation of the current during galvanostatic cycling.

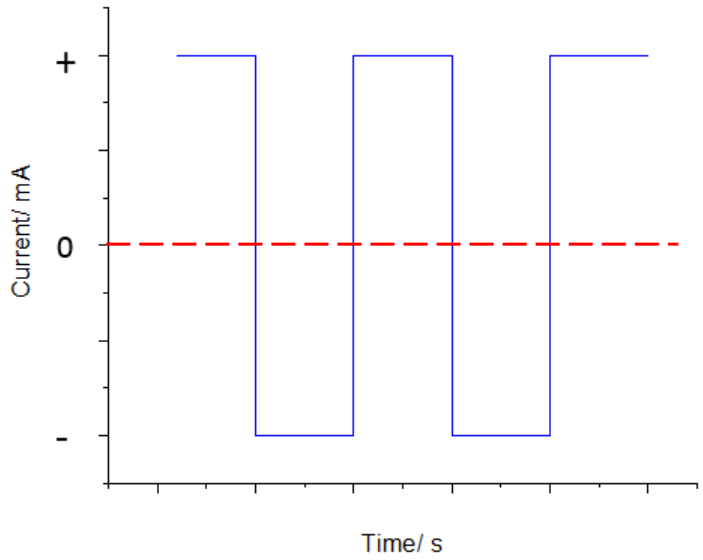

Figure 2-3 Representation of current during galvanostatic cycling.

The rate at which a cell is charged and discharged relative to its capacity is termed C-rate. Where 1C corresponds to charging or discharging to the theoretical capacity in 1 hour. It is calculated by equation 2-1, to calculate the current applied, equation 2-1 is re-arranged to give equation 2-2.

$$C_{rate}\ (h^{-1}) = \frac{Current\ (mA)}{Theoretical\ capacity\ (mAh\ g^{-1})\ x\ Weight\ of\ active\ material\ (g)} \qquad \text{Equation 2-1}$$

$$Current\ (mA) = Weight\ of\ active\ material\ (g)\ x\ Theoretical\ capacity\ (mAh\ g^{-1})\ x\ C_{rate}\ (h^{-1})$$ Equation 2-2

C-rate can have a dramatic effect on the cell performance, in particular, the capacity of the cell. This is due to the fact that lithium ion diffusion into solid state materials is a relatively slow process and so the C-rate limits the capacity of cell. Usually C-rate is something which is investigated for lithium ion batteries since it is desirable to have a battery that is capable of operation from low to high C-rates. The performance of the battery at different C-rates is determined by the electrode materials (insertion and de-insertion of lithium) and the electrolyte (lithium transport through the electrolyte) and the separator (lithium transport through the separator).

2.4.1 Powder X-ray Diffraction (XRD)

PXRD is a rapid, non-destructive, bulk analytical technique used for the identification of powdered crystalline materials. It can give the following information:

- Phase Identification: For identifying a sample, this is done by matching the pattern with a data base (D2 Phaser uses PDXL2 Rigaku database).
- Peak positions: Unit cell size/shape and symmetry.
- Peak widths: sample crystallinity.

A PXRD machine is composed of an X-ray source, a sample holder and an X-ray detector. The X-rays are generated by the bombardment of electrons (produced by heating a filament) at a source (typically Cu) by applying a voltage. The X-rays are directed at the powdered sample, the X-rays then interact with the sample and the scattered x-rays are detected at the receiving slit and detected. This is done for a range of angles of 2θ, depending on the sample being investigated. The principle of X-ray diffraction is that the X-ray hits the sample and produces constructive interference. The sample diffracts a proportion of the X-rays which are then detected, these diffracted rays are due to the d-spacing in the sample and because each chemical has a different set of d-spacing values the sample can be identified from a data base. PXRD was used for identifying samples of lithium iron phosphate and iron phosphate samples during de-lithiation.

2.4.1 Thermogravimetric Analysis (TGA)

Thermogravimetric analysis (TGA) is a destructive technique designed to look at thermal stability and thermal decomposition of chemicals. It consists of a sample holder, a heater and a highly accurate microbalance. A sample of known weight is placed in a crucible (either Aluminium metal or Aluminium oxide) and heated at a constant heating rate, the sample is continually weighed to determine the weight loss due to thermal degradation. The results are typically represented as either % weight loss or mass weight loss and temperature vs time. TGA is a good indicator of thermal stability of a material.

2.4.1 Differential Scanning Calorimetry (DSC)

Differential scanning calorimetry (DSC) is a destructive technique to look at the thermal properties of materials, in particular polymers for determining the glass transition temperature, T_m. It consists of a sample holder, a heater, and a cooling system. A sample of known weight is placed in an aluminium crucible with a lid and a blank aluminium crucible with a lid are heated to maintain a constant temperature between the sample and reference sample, with the temperature being raised linearly with time. DSC is particularly used to measure phase transitions in materials for example melting processes are endothermic processes requiring more heat to raise the temperature, whereas crystallisation for example are exothermic processes release heat and so less heat is required to raise the temperature.

2.4.1 Scanning Electron Microscopy (SEM) and Energy-dispersive X-ray Spectroscopy (EDX)

SEM coupled with EDX allows the surface of materials to be visually studied (SEM) along with elemental analysis (EDX). These powerful techniques can allow a detailed analysis of a surface down to an nm level, meaning individual particles can be imaged and elementally analysed. The SEM works by emitting electrons on to the surface of the material under investigation, the electrons are then emitted by the sample and detected which then produce a digital image of the surface.

Secondary electrons emitted give information on the first few nm of the surface and is the usually of the most interest, backscattered electrons on the other-hand give information deeper into the sample typically a few µm and give a lower resolution image. In EDX, the user can select areas of interest from the SEM image to elementally analyse, once the area has been selected an x-ray is focussed onto the sample. The x-ray then excites an electron from an inner shell which ejects the electron from the shell, this creates an electron hole which is filled from an outer shell. The energy difference between the two shells releases an x-ray which is detected, each element has characteristic energies (KeV) and so elemental composition of a surface is possible.

For the study of the aluminium current collectors the cells were disassembled and the aluminium foils were washed using ethanol to remove the electrolyte and dried at 80 ˚C prior to mounting onto SEM stubs, the samples were then mounted into the Phillips XL30 ESEM coupled with EDX.

2.5 Temperature Control

Reliable and accurate temperature control was an important consideration in this work, in particular during electrochemical measurements. There are two methods of temperature control that can be adopted to test the effect of temperature on cell performance, constant temperature cycling and ramped temperature cycling. The first gives information on a cells performance at a set temperature over its lifetime, which is compared with other cells cycled at different set temperatures. The second method where the temperature is ramped up every few cycles gives information on the cells performance over a temperature range. This method is more representative of what conditions a battery may be subjected to over its lifetime. However, this method is often difficult to execute i.e. timing the temperature control with the number of cycles, given that the amount of time for a cycle changes. Automation of this process would require electronics to control the oven with the potentiostat in order to match up with the cycling of the cells. The other disadvantage of this method is that as a cell cycles it is continually ageing, so by the time that the cell gets to the higher temperatures it has already been subjected to a certain degree of cell ageing. This means that the effect of temperature on the cell at that point is a function of the number of previous cycles and temperatures it was subjected to. The interpretation of results is therefore difficult as there are a number of variables. Therefore, the former method of cell temperature control was used. To test the effect of different temperatures a number of ovens can be set to different temperatures and cells cycled at the set temperatures. This means that effect of temperature on cell performance can be compared like for like with no other factors influencing the result.

When working at higher temperatures this can be particularly challenging since most cables for electrochemical measurements are designed to work at room temperature. Specially designed cables were made in-house to work at higher temperatures. Coaxial cable which has a coating of FEP polymer as the insulating outer-casing which can be operated in conditions up to 200 ^{o}C was used to make the cables. 2mm banana plugs were soldered to these coaxial cables to act as connectors to the potentiostat, these were secured with a layer of epoxy resin and a plastic cover, on top of this heat shrink to completely cover the connection and to label the cables. The cable assembly can be seen in Figure 2-4.

Figure 2-4 Photographs of the specially designed cables showing the banana plug (left), FEP coated coaxial cables with banana plugs connected (middle) and the completed cable assembly (right).

In order to allow connection of the cables to the VMP a specially designed connection box was made which had a series of 2mm female banana plugs 3 connections from the VMP (WE, CE, RE) and three connections to the coaxial cables (WE, CE, RE). A diagram and a picture of the control box can be seen on the in Figure 2-5.

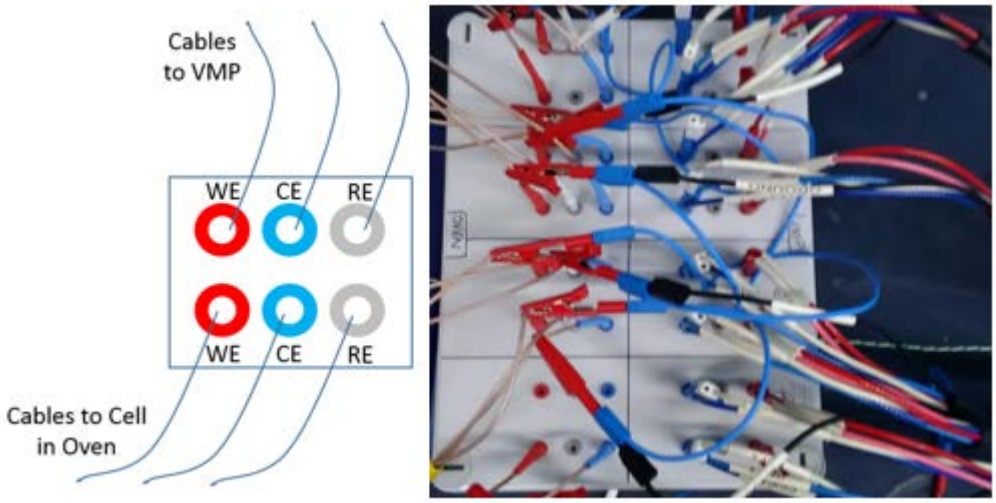

Figure 2-5 Cable connection box for connecting cables to VMP diagram (left) and connection box photograph (right).

In order to monitor the temperature of the ovens whilst in use a multichannel data logger (picolog) with k type thermocouple probes were used to monitor the temperature of the ovens in real time to a computer. This was essential for checking and monitoring the temperature of the bank of ovens, which were set to four temperatures (60 ^{o}C, 90 ^{o}C, 120 ^{o}C and 150 ^{o}C). The cables and thermocouple are fed into the ovens through a top access hole and sealed with glass fibre wool to

maintain temperature. The electrochemical cell can then be connected inside the oven, seen in Figure 2-6. The resulting complete temperature-controlled battery cycling set-up can be seen in Figure 2-7.

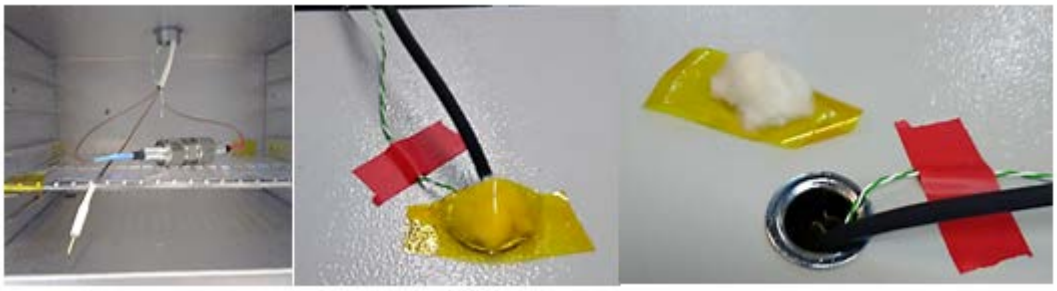

Figure 2-6 Photographs showing a Swagelok cell connected in the oven (left) and the cables coming into the top of the oven access hole (middle and right).

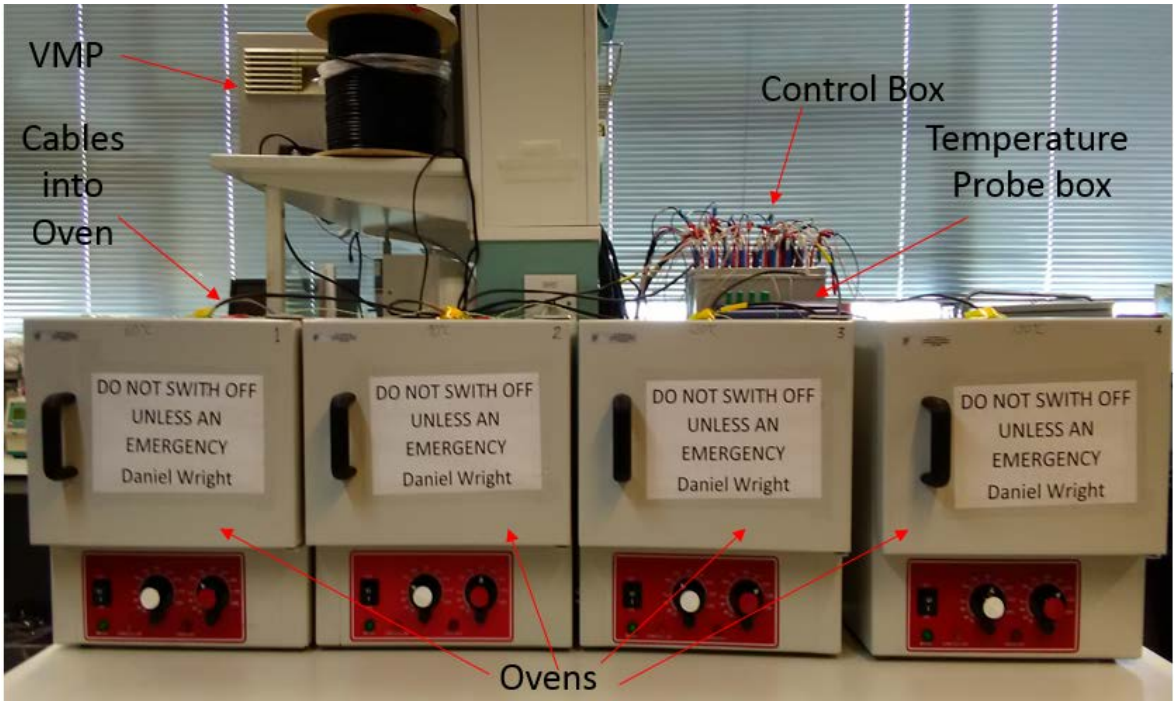

Figure 2-7 Photograph showing the whole temperature-controlled battery cycling set-up.

Chapter 3 Effect of Temperature on Negative Electrodes

3.1 Introduction

It was understood from the literature review in chapter 1 that the most important degradation reactions occur at the charged negative electrode because of its high reactivity as a reducing agent. Therefore, it was important to study graphite negative electrodes at elevated temperatures, this allowed a benchmark in terms of performance that the rest of the studies could be compared against. Once this benchmark was established the effect of negative electrode materials was then studied. For this study it was chosen to examine the effect of the negative electrode active materials and the binders on the galvanostatic cycling of half cells and full pouch cells from room temperature up to 80 ^{o}C. It will aim to identify a stable electrode formulation for use at elevated temperatures.

3.2 Aims and Objectives

The aims of this chapter were:

1. To understand the cycling behaviour of graphite half cells between 25 ^{o}C and 80 ^{o}C.
2. To investigate the cycling behaviour of graphite and hard carbon electrodes between 25 ^{o}C and 80 ^{o}C.
3. To investigate the effect of electrode binders on the cycling behaviour of graphite and hard carbon electrodes between 25 ^{o}C and 80 ^{o}C.

The objectives of this chapter were:

To understand the temperature limitations of negative electrode materials and binders and to find a more stable negative electrode at elevated temperatures.

3.3 Experimental Details

For this study graphite electrodes were fabricated and test cells assembled according to the methods given in section 2.2, chapter 2. The first study that was conducted was the effect of temperature on the cycling of graphite half cells, utilising a graphite ink working electrode (90% graphite, 3% acetylene black, 7% PVDF binder coated on a copper current collector), metal lithium foil counter/reference electrode, two glass fibre separators and 8 drops of LP30 electrolyte. Cells were tested using galvanostatic cycling at range of temperatures using temperature-controlled ovens, the details of which can be seen in section 2.5, chapter 2. In order to evaluate the effect of temperature on the performance of graphite galvanostatic cycling is used, as described in chapter 2. This yields several key pieces of information which are vital to evaluating the performance of a cell. Following the nomenclature that is used for full cell studies, charge is defined here as the process of lithiation of graphite, and discharge refers to the process of de-lithiation. The following terms can be defined

- **Discharge capacity (Q_{disch}):** This is the amount of useable charge a battery (or a battery material) can store, this is usually quoted in Ah.
- **Charge capacity: (Q_{ch}):** This is the amount of charge a battery required to charge a battery (or a battery material), this is usually quoted in Ah.
- **Specific Capacity (Q/mass):** This is the capacity of the battery relative to its weight, quoted in Ah/kg. However, in battery science it is more commonly quoted as the capacity relative to the active material weight.
- **Reversible capacity (Q_{rev}):** This is the useable capacity of the cell i.e. the charge that is passed during the discharge cycle, seen in Figure 3-1.
- **Irreversible capacity (Q_{irr}):** This is the capacity that is lost in a particular charge/discharge cycle due to electrolyte breakdown and SEI formation i.e. the difference between the charges passed on the charge and discharge cycle, seen in Figure 3-1.
- **Coulombic efficiency (CE):** This is the percentage of the charge that is given up on the discharge cycle, seen in Equation 3-1.

$$Coulombic\ Efficiency\ \% = \frac{Qdisch}{Qch}\ x\ 100 \qquad \text{Equation 3-1}$$

For the study of negative electrode materials, graphite (MGPA) and hard carbon (HCT1) were chosen along with the electrode binders polyvinylidene fluoride (PVDF 5130), polyamide imide (PAI) and polyacrylonitrile (PAN). The electrodes were fabricated and Swagelok half cells and pouch cells were assembled according to the methods given in section 2.3, chapter 2. The electrodes were all subjected to the same drying techniques, except PAI where half of the electrodes were subjected to the same drying as the other electrodes and half of electrodes had an additional heating step at 240 ^{o}C. Literature has previously used higher temperatures in order to heat treat electrodes with PAI binder[131,152] , it was decided to compare both the standard drying technique and the additional heating step with the PAI to see it has an effect on the performance.

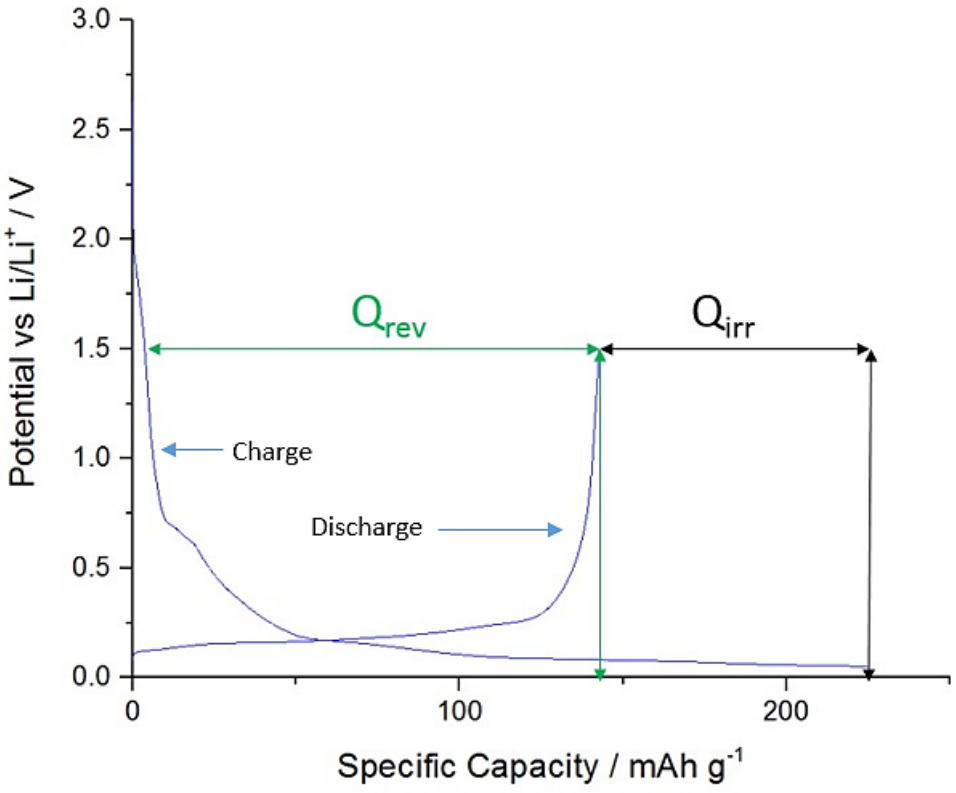

Figure 3-1 Graph showing potential vs specific capacity for the first cycle galvanostatic cycling of MGPA graphite electrodes using C/10 C-rate charged to a capacity limit of 250 mAh g^{-1} and discharged to 1.5V. Reversible and irreversible capacities annotated.

3.4 Effect of Elevated Temperature on Graphite

As was discussed in section 1.8.1, the insertion of lithium into the graphite structure has been shown to occur over several stages of insertion of the lithium into the graphite structure (Figure 1-18 and Figure 1-19). Figure 3-2 shows the insertion and extraction of lithium into graphite for the first cycle. As can be seen from this graph the results obtained for this graphite agree with those observed in the literature[9,96,99–101].

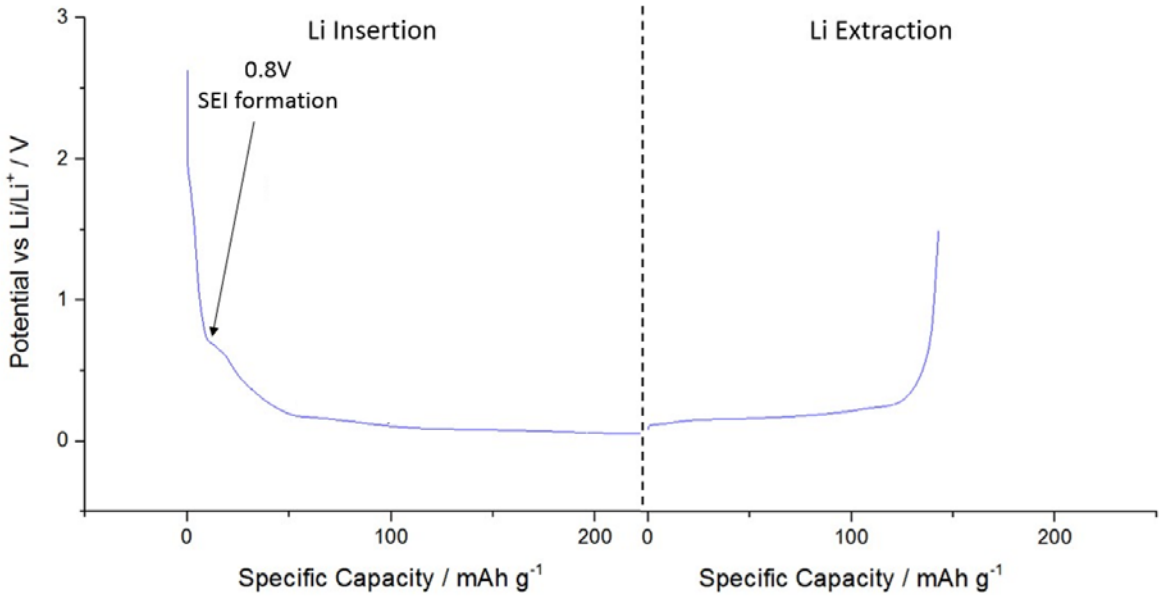

Figure 3-2 Graph showing potential vs specific capacity for the first cycle galvanostatic cycling of graphite electrodes vs Li metal with LP30 electrolyte using C/10 C-rate, charged to a capacity limit of 250 mAh g^{-1} and discharged to 1.5V, showing the Li Insertion and extraction in graphite.

To evaluate the effect of temperature on cell performance irreversible capacity (Q_{irr}), the loss of capacity on each charge/ discharge cycle is used. On the first charge/ discharge cycle Q_{irr} is high due to the side reactions used to form the SEI layer, with Q_{irr} stabilising after the first few cycles. Since Q_{irr} is a measure of the side reactions occurring in the cell and it is known that these side reactions are increased at higher temperatures, Q_{irr} should therefore increase with temperature. [7,12,102,17–24]

To test this graphite half cells were charged and discharged using galvanostatic cycling at a rate of C/10, to a set charge capacity of 250 mAh g^{-1} and then discharged to a voltage of 1.5 V at 25, 40, 60

and 80 ˚C. The irreversible capacities were then calculated for the first charge/ discharge cycle seen in Figure 3-3. The results show that as temperature is increased the irreversible capacity increases, this can be attributed to the increasing temperature causing a greater degree of electrolyte breakdown. There are two processes of electrolyte breakdown which occur in lithium ion cells SEI formation and undesirable electrolyte side reactions. As temperature is increased these side reactions increase due to the increased kinetics and so the irreversible capacity increases with temperature.[13,102–104]

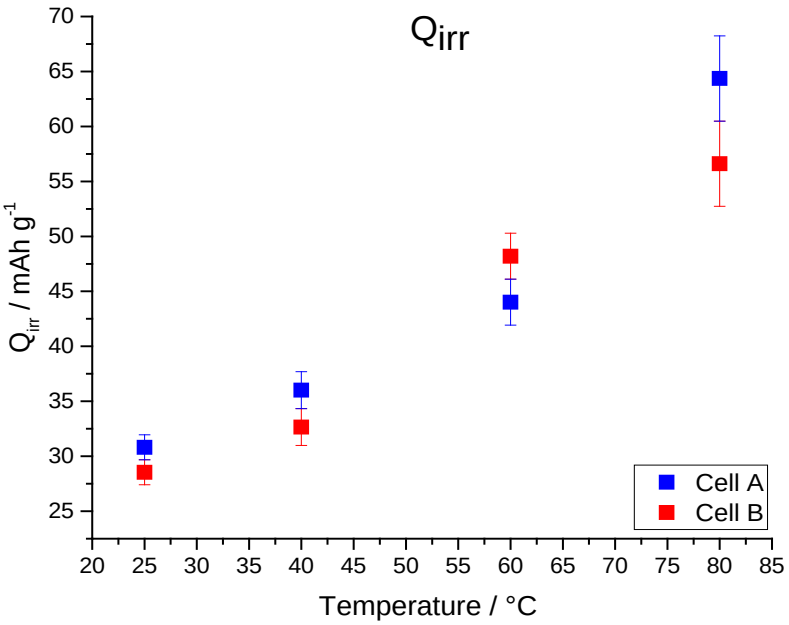

Figure 3-3 Graph showing Q_{irr} values obtained from the first cycle galvanostatic cycling of graphite electrodes using C/10 C-rate, charged to a capacity limit of 250 mAh g^{-1} and discharged to 1.5V.

Q_{irr} can be used to evaluate the effective activation energy of the electrolyte breakdown occurring since the average current associated with reversible reactions can be defined as follows

$$I_{irr} = \frac{Q_{irr}}{t} \qquad \text{Equation 3-2}$$

Where:

I_{irr} = irreversible current (mA), averaged over the charge process

Q_{irr} = irreversible capacity (mAh g^{-1})

t = time (h)

The rate of irreversable reactions can be defined as the number of moles of electrons involved in the irreversable reactions per unit time.

$$\frac{d\,n}{d\,t} = \frac{Q_{irr}}{F\,t} \qquad \text{Equation 3-3}$$

Where:

F = faradays constant = 96485 C mol^{-1}

n = number of moles of electrons involved in irreversible reactions

Since this reaction occurs over the area of the electrode the rate should be normalised by the surface area of the electrode. This gives us the following rate equation, seen in Equation 3-4:

$$Normalised\ rate\ per\ area\ of\ electrode = \left(\frac{1}{A}\right)\left(\frac{d\,n}{d\,t}\right) = \frac{Q_{irr}}{F\,t\,A} \qquad \text{Equation 3-4}$$

Where:

A = area (cm^2)

In these experiments, the time is constant because the total charge capacity is limited to 250 mAh g^{-1} with the total charge current set to 372 mAh g^{-1}. The normalised rate per area of electrode is expected to follow a temperature dependence following the Arrhenius equation, shown in Equation 3-5. A plot of ln Q_{irr} vs 1/T is expected to be linear, with the gradient of the line equating to $-E_{Act}/R$.

$$k = Be^{-\frac{E_{Act}}{RT}} \qquad \text{Equation 3-5}$$

Where:

k= rate constant

B= pre-exponential factor

E_{Act} = Activation energy (kJ^{-1} mol^{-1})

R = Gas constant (8.3145 J K^{-1} mol^{-1})

T= Temperature (K)

A plot of ln Q_{irr} vs 1/T is presented in Figure 3-4, it is observed that the line is linear in relationship which is expected for Arrhenius. Using Equation 3-5 an estimate of 11.6 ± 0.4 kJ mol^{-1} for the effective activation energy of the irreversible reactions is obtained here for the MGPA graphite employed in the present experiments. *Zheng et al*[153] investigated the activation energy of the capacity loss of storage of MCMB graphite half cells with an electrolyte of 1M $LiPF_6$ in EC/DMC (2:1 v/v) at temperatures between 21 ˚C and 80 ˚C. Results showed that the capacity loss was less than 1.5 % after 4 days at 21 ˚C and 20 % after 4 days at 80 ˚C. This was attributed to the loss of intercalated lithium due to the reaction with the electrolyte. The authors estimated that the activation energy associated with this reaction using Arrhenius relationship was 39.7 kJ mol^{-1}. This value is higher than the effective activation energy obtained in the present study (ca. of 11.6 ± 0.4 kJ mol^{-1}). This difference could be ascribed to the different method of evaluation of the effective activation energy of irreversible reaction and/or to the difference in the materials employed.

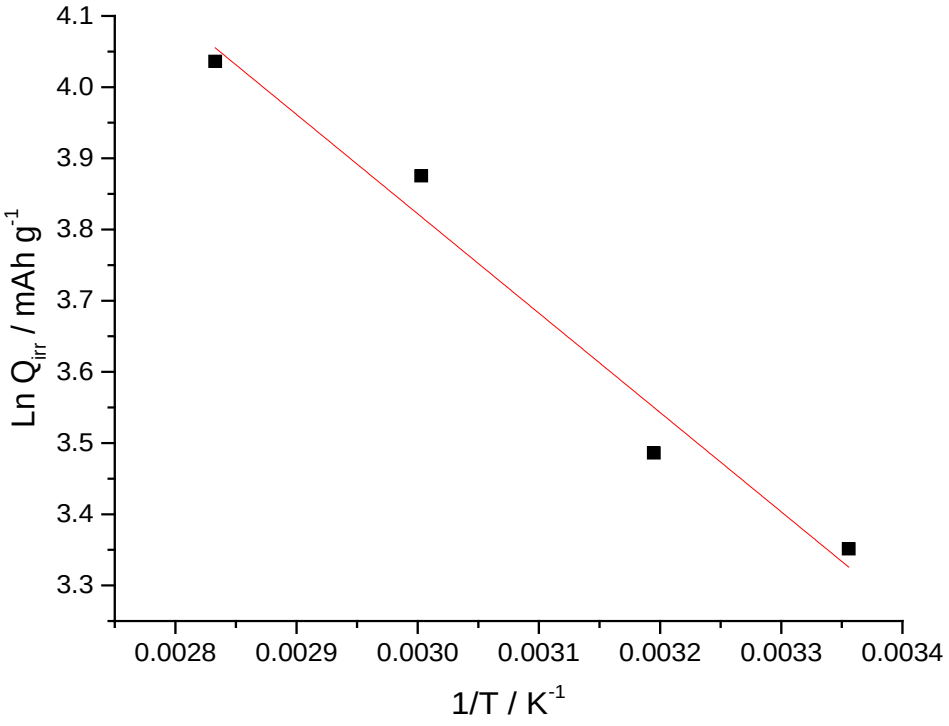

Figure 3-4 Arrhenius plot obtained from the first cycle galvanostatic cycling of graphite electrodes using C/10 C-rate, charged to a capacity limit of 250 mAh g^{-1} and discharged to 1.5V.

3.5 Effect of Negative Electrode Formulation at Elevated Temperatures

3.5.1 Comparison of Graphite and Hard Carbon at Elevated Temperatures

Figure 3-5 displays a plot comparing the cycling performance of graphite (MGPA) and hard carbon (HCT1) with PVDF 5130 electrodes at 25 and 60 ^{o}C. Cells were cycled at a rate of C/10 between 1.5 V and 0.05 V vs Li/Li^{+}, cycles 1 to 3 were cycled at 25 ^{o}C and cycles 4 to 6 were cycled at 60 ^{o}C. What is apparent from this graph is that there are clear differences between the graphite and hard carbon. It is observed that hard carbon has a much lower coulombic efficiency for cycle 1 (25 ^{o}C) compared to graphite. This is a consequence of the higher surface area of the hard carbon (4.00 m^{2} g^{-1})[154] compared to that of the graphite (0.71 m^{2} g^{-1})[155], i.e. more electrolyte breakdown that has to occur to form SEI. After cycle 1 at 25 ^{o}C the values for cycles 2 and 3 at 25^{o}C and for cycles 4-6 at 60 ^{o}C are very similar for both hard carbon and graphite with graphite having a slightly higher coulombic efficiency. Literature has shown that higher surface area carbons give rise to higher degrees of electrolyte breakdown to form the SEI.[107–115]. It seen that the first cycle at 60 ^{o}C (cycle 4) that there is a drop in the coulombic efficiency for both the graphite and hard carbon. This is most likely a consequence of further electrolyte breakdown occurring at the negative electrode/ electrolyte interface. It is also observed at 60 ^{o}C (cycles 4-6), the columbic efficiency observed is much lower than that of room temperature, with a columbic efficiency of less than 90 %. Literature has suggested that as the cycling temperature is increased, electrolyte breakdown and side reactions occur at an increased rate and give rise to higher irreversible capacities and greater capacity fade.[13,102–104]

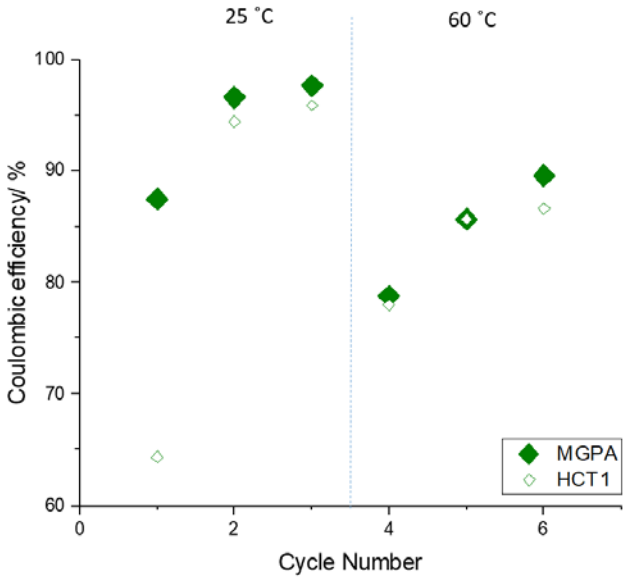

Figure 3-5 Coulombic efficiency graph comparing graphite (MGPA) with hard carbon (HCT1) using PVDF 5130 as the binder. Cycles 1-3 are 25 ^{o}C and 4-6 are 60 ^{o}C.

3.5.2 Comparison of PVDF, PAI and PAN at Elevated Temperatures

Figure 3-6 and Figure 3-7 display the effect of binders PAI, PVDF and PAN on the performance of graphite and hard carbon electrodes. Figure 3-6 shows the comparison of the binders with graphite, it is observed that the binder has a large influence on the coulombic efficiency. It is observed that for cycle 1 (25 ^{o}C) coulombic efficiency is less than 90 % for all the binders, this is most likely the breakdown of the electrolyte in order to form the SEI, this was seen in Figure 3-5 for graphite and hard carbon with PVDF binder.[99] It is also observed that for the first cycle at 60 ^{o}C (cycle 4) there is also a drop in coulombic efficiency, this was also observed in Figure 3-5 and was attributed to degradation reactions occurring at the electrode/ electrolyte interface.

It can be observed from the graph that there is a less than 90% coulombic efficiency for the graphite electrodes with the PVDF binder, this is something which was observed for the graphite in Figure 3-5. It can be seen from Figure 3-6 that PVDF has the lowest coulombic efficiency at 60 ^{o}C on cycle 6. *Bodenes et al*[7] have reported that at elevated temperatures PVDF migrates from the bulk electrode to form a PVDF layer on the surface of the electrode. This leads to poor lithium insertion into the electrode which was shown by the authors using ^{7}Li NMR. It is observed that the largest difference in the performance in terms of coulombic efficiency of the binders can be seen when the cells are cycled at 60 ^{o}C. It is observed that the only binder to not have a drop in capacity on cycle

4 (60 °C) is for the cured PAI, the coulombic efficiency is close to 100%. The other binders, including the uncured PAI have a dramatic decline in capacity at 60 °C, this can be attributed to additional breakdown of electrolyte on the surface.[13,102–104] After cycle 4 the coulombic efficiencies then increase again for the other binders, with the order of highest to lowest coulombic efficiencies being PAI cured > PAN > PVDF > PAI uncured.

It is observed for cycle 1 that the PAI has a much lower coulombic efficiency than that of the PVDF and PAN. At 25 °C (cycles 1 to 3) it can be observed that PAI and PAI cured at 240 °C have similar coulombic efficiencies, however at 60 °C (cycles 4-6), the uncured PAI has a lower coulombic efficiency compared to the cured PAI. Literature has suggested that PAI subjected to heat treatment has better capacity retention than that of lower temperature drying, due to stronger adhesion of PAI binder. This is due to interactions of the amide and imide chains in the PAI, which help to improve the contact of active material, conductive carbon and the current collector.[152] The better performance of electrodes with PAI as the binder compared to that of PVDF has been attributed to the PAI supressing electrolyte decomposition on the particle surface as the PAI helps to form a protective layer on the particles, which leads to less capacity loss on cycling.[131] It can be observed from Figure 3-6 that PAN also has good performance at room temperature with the highest cycle 1 coulombic efficiency of all the binders. It can be seen however that the coulombic efficiency drops dramatically on cycle 4 (60 °C) and is lower than all binders except uncured PAI, the performance improves on subsequent cycles and is close to that of the cured PAI by cycle 6.

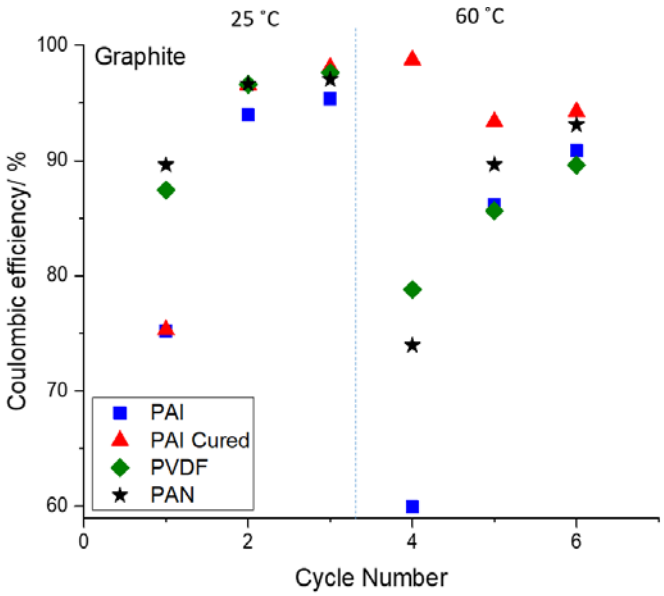

Figure 3-6 Coulombic efficiency graph comparing PAI, PAI cured, PVDF and PAN binders using graphite as the negative electrode material. Cycles 1-3 are 25 °C and 4-6 are 60 °C.

It can be observed from the coulombic efficiency graph pictured in Figure 3-7, that binder choice with hard carbon electrodes has a more pronounced effect than is the case with graphite (Figure 3-6). It can firstly be observed that the coulombic efficiencies are much lower than those that were seen with graphite, something which was observed in Figure 3-5. It is observed that at 25 ^{o}C there is not much differences in the coulombic efficiencies of the binders, cycle 1 shows that PVDF has a slightly better capacity than PAI, this is the same as is observed for graphite. At 60 ^{o}C however, PAI cured outperforms that of the PVDF and PAI uncured, achieving a coulombic efficiency of around 95% for cycles 4-6 (60 ^{o}C). It is observed that the curing of the PAI has the same effect with hard carbon as is seen with graphite, with the curing of the PAI improving the coulombic efficiency. However, the coulombic efficiencies are much lower for all binders for hard carbon than for graphite, this was observed in Figure 3-5, particularly for cycle 1. This is due to the fact that the high surface area of hard carbon compared to graphite gives rise to a higher degree of electrolyte breakdown that would have a detrimental effect of long-term performance of the cell.

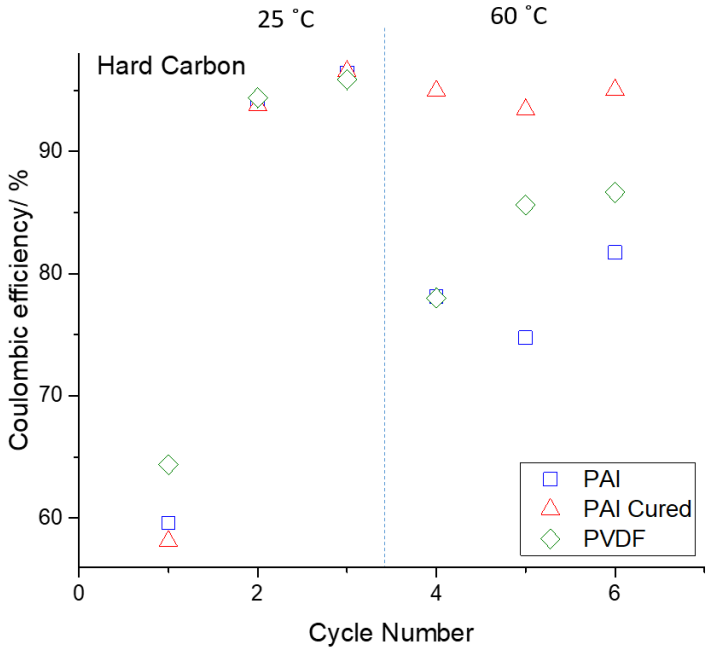

Figure 3-7 Coulombic efficiency graph comparing PAI, PAI cured, PVDF and PAN binders using hard carbon as the negative electrode material. Cycles 1-3 are 25 ^{o}C and 4-6 are 60 ^{o}C.

3.5.3 Overall Comparison of Effect of Active Material and Binder on Elevated Temperature Performance

Figure 3-8 shows a comparison of the reversible capacities for graphite and hard carbon with PAI, PAI cured, PVDF and PAN. It can be observed from the graph that the reversible capacity increases when the cells are cycled at 60 ^{o}C, this can be attributed to the increased rates of reaction for the lithium ion transport and improved conductivity of the electrolyte.[22] The biggest increase in reversible capacity is observed for hard carbon, at 25 ^{o}C the capacity is much lower than that of graphite despite having a higher theoretical capacity of 460 mAh g^{-1} than graphite. *Zheng et al*[117] investigated hard carbons as a negative electrode material for elevated temperatures up to a temperature of 80 ^{o}C. Results showed that at room temperature the discharge capacity is low due to the lithiation of the hard carbon being slow and a large voltage hysteresis is observed for the charge/ discharge cycle. The capacity of hard carbon with cured PAI binder is comparable to that of graphite with cured PAI binder, however the first cycle irreversible capacity is much higher for hard carbon compared to graphite, seen in Figure 3-9 and Figure 3-10. It can be observed that irreversible capacity is much higher for hard carbon than it is for graphite, this is particularly the case for cycle 1. It is observed that the irreversible capacity is in the region of 4 times as large for hard carbon as is observed with graphite (for PVDF and PAN binders).

Not all the electrodes show a capacity increase with temperature, graphite with uncured PAI shows a decrease in capacity at 60 ^{o}C. Literature has previously used higher temperatures in order to heat treat electrodes with PAI binder[131,152]. It can also be seen that graphite with PVDF binder shows an increase in reversible capacity on cycle 4 at 60 ^{o}C, however cycles 5 and 6 show a decrease in capacity suggesting degradation reactions occurring. However, for hard carbon with PVDF binder it is observed that the reversible capacities increase at 60 ^{o}C, showing a much lower decrease in reversible capacity over cycles 4-6 compared to that of graphite with PVDF binder. For all the electrodes the reversible capacity decreases with the number of cycles, except that of graphite with PAN binder. The reversible capacity for graphite with PAN increases with cycle number even increasing 60 ^{o}C, indicating that this binder looks to be more stable at higher temperatures. An indication that a graphite binder with PAN binder looks to also be a very promising combination for a negative electrode material at higher temperatures.

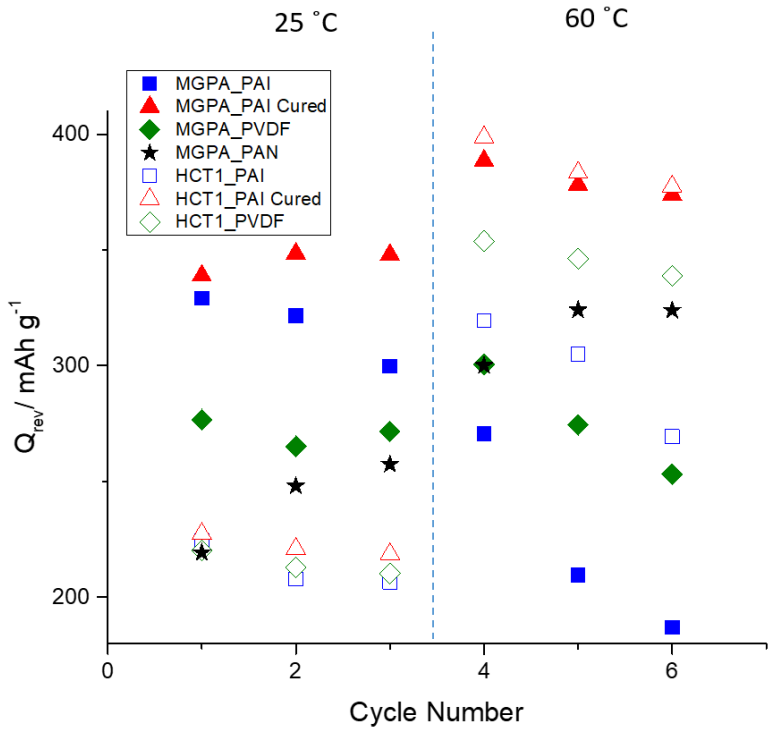

Figure 3-8 Graph showing the reversible capacity for MGPA and HCT1 with PAI, PAI cured at 240 ^{o}C, PVDF and PAN binders. Cycles 1-3 are 25 ^{o}C and 4-6 are 60 ^{o}C.

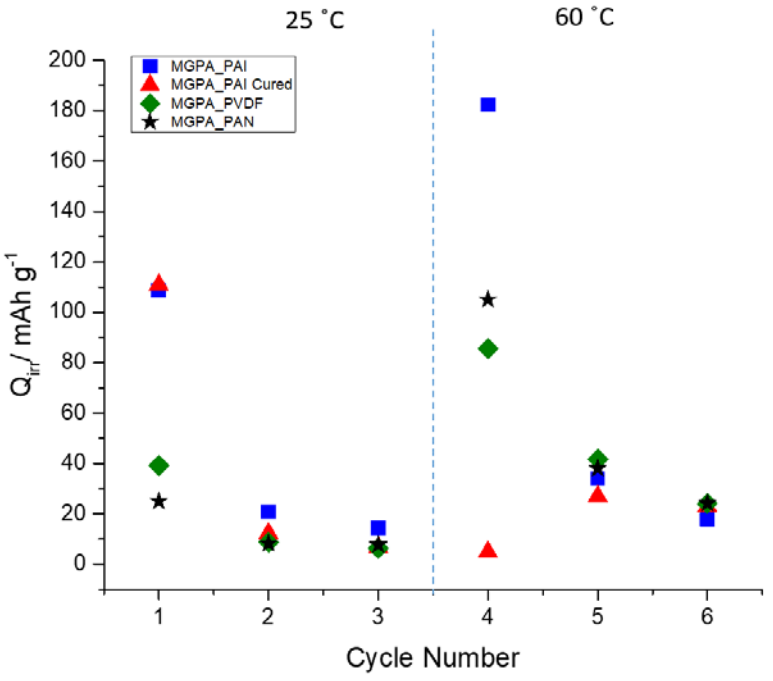

Figure 3-9 Graph showing the irreversible capacity for graphite with PAI, PAI cured at 240 ^{o}C, PVDF and PAN binders. Cycles 1-3 are 25 ^{o}C and 4-6 are 60 ^{o}C.

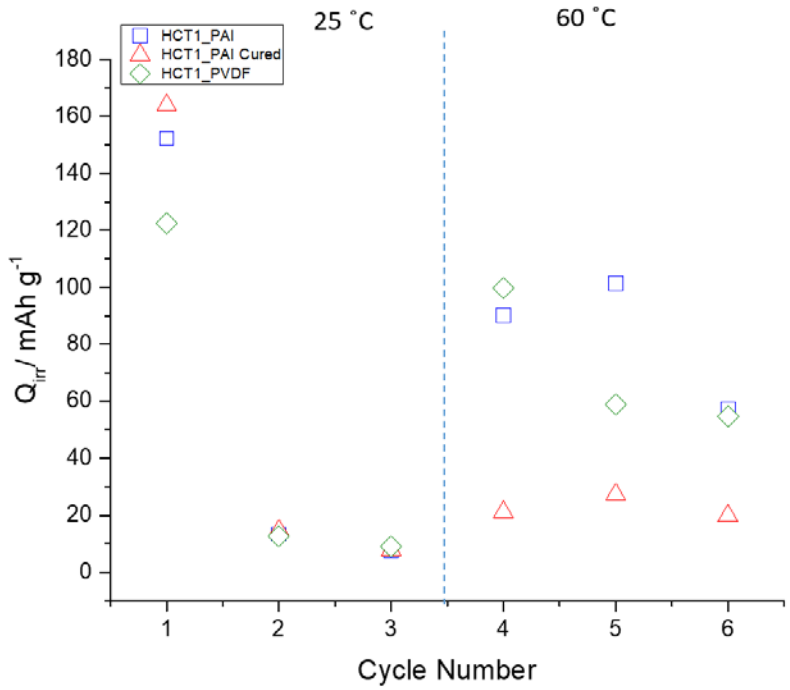

Figure 3-10 Graph showing the irreversible capacity for hard carbon with PAI, PAI cured at 240 ^{o}C, PVDF and PAN binders. Cycles 1-3 are 25 ^{o}C and 4-6 are 60 ^{o}C.

3.6 Investigation of Lithium-ion Pouch Cells Elevated Temperatures

Figure 3-11 shows the coulombic efficiency for pouch cells of graphite with PAI (uncured), hard carbon with PAI (uncured), and graphite with PAN with lithium iron phosphate positive electrode. Cells were charged to a potential of 4.5 V and discharged to a potential of 2.5 V vs Li/Li^+ using a C-rate of C/10 at 25 ^oC for cycles 1 to 3 and 60 ^oC for cycles 4 to 6.It was shown in section 3.5 that PAI which was not subjected to heat treatment had a low coulombic efficiency in comparison to PAI which was heat treated and also PVDF and PAN. This is also the case when PAI is used in pouch cells for both hard carbon and graphite, seen in Figure 3-11. It can be seen that graphite with PAN however performs well, initially showing an 85% coulombic efficiency on cycle 1, with a coulombic efficiency of over 95% on subsequent cycles. It is also observed that after cycle 1 all three pouch cells have very similar coulombic efficiencies suggesting that the binder is having the most influence on the first cycle capacity, where SEI formation takes place.

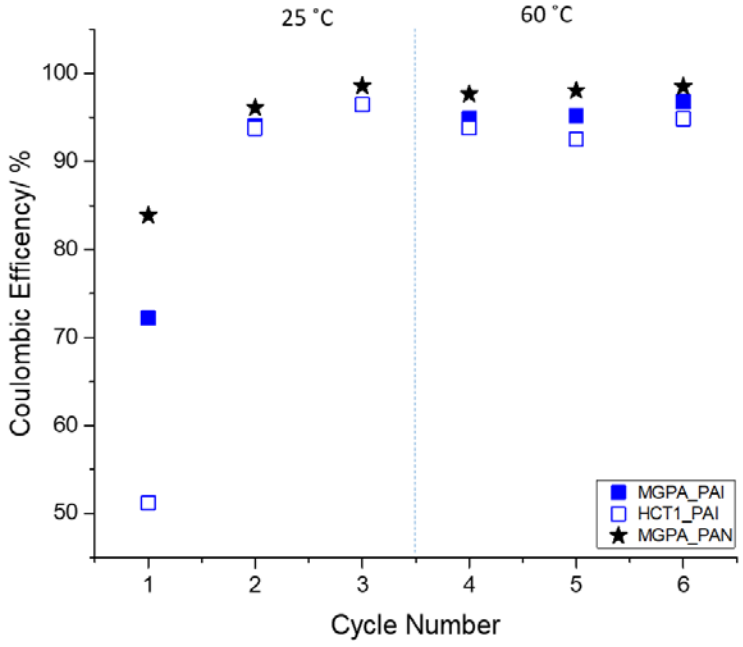

Figure 3-11 Coulombic efficiency graph comparing Li-ion pouch cells of MGPA and PAI, HCT1 and PAI and MGPA and PAN. Cycles 1-3 are 25 ^oC and 4-6 are 60 ^oC.

As the pouch cells of graphite and PAN binder responded well at 60 °C, showing the best coulombic efficiency of the pouch cells tested these cells were tested further at 80 °C. This is the temperature at which the electrolyte can be safely operated to. Figure 3-12 shows the results of the cycling of the graphite PAN pouch cells operating at 80 °C. It is observed that after 30 cycles the capacity has declined by 50%, reaching 10 mAh g^{-1} by 130 cycles. This is probably due to the continued degradation of the electrolyte on the electrode surface (continuous SEI destruction and formation).

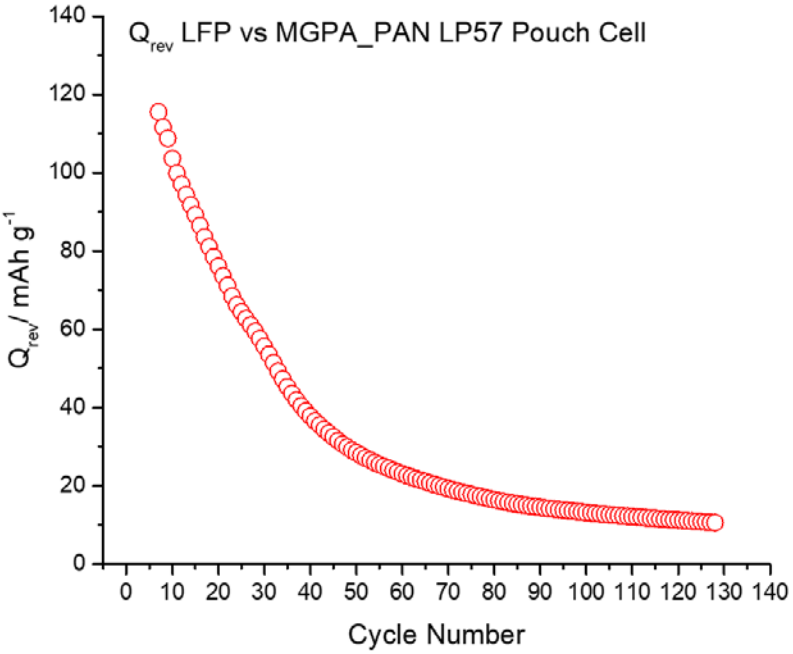

Figure 3-12 Graph showing the reversible capacity of a pouch cell of $LiFePO_4$ electrode using PVDF binder against graphite using PAN binder, LP57 electrolyte showing the reversible capacity of the cell cycled at 80 °C.

3.7 Conclusions

The effect of temperature on the galvanostatic cycling on graphite half cells was evaluated. The results showed that as temperature is increased the irreversible capacity increases, due to the formation of an increased growth of SEI with temperature. Using irreversible capacity to calculate the activation energy of the reactions at the electrode/ electrolyte interface using Arrhenius estimates a value of 11.6 kJ mol^{-1} ±0.4 kJ mol^{-1}.

Graphite and hard carbon were investigated as negative electrode materials and results showed that hard carbon has a large irreversible capacity loss on the first cycle. This effect was attributed to the high surface area of the hard carbon resulting in a higher amount of electrolyte breakdown resulting in SEI. The hard carbon also didn't perform to the expected capacity which is quoted in excess of 400 mAh g^{-1}, but the observed capacity improved on heating the cells at 60 ^{o}C.

A range of binders were investigated namely PVDF, PAI and PAN. Results showed that PAI was a poor performer giving rise to large irreversible capacity losses. However, when the electrodes were subjected to an additional drying stage of 240 ^{o}C to cure the polymer results showed good coulombic efficiencies and lower irreversible capacity losses. PVDF seemed to perform well with good coulombic efficiencies and reasonable $Q_{irr.}$ values obtained. PAN was only tested with graphite but results were very promising giving rise to good coulombic efficiency and $Q_{irr.}$ values, with good retention of capacity on heating at 60 ^{o}C. It should be noted that further work in electrode optimisation would be required in order for a careful comparison of binders is made, however results do show that PAN is a promising binder when used with graphite electrodes.

Pouch cells were assembled with lithium iron phosphate positive electrodes, and negative electrodes of graphite and PAI, hard carbon and PAI and graphite and PAN. The electrodes of graphite and hard carbon with PAI binder had low 1st cycle coulombic efficiency due to a high irreversible capacity loss. Graphite with PAN also has a first cycle inefficiency due to SEI formation but not to the same extent of the PAI. Extended cycling of the graphite PAN pouch cells showed that capacity retention at 80 ^{o}C was poor, leading to 50% capacity loss by 30 cycles.

Chapter 4 Effect of Electrolytes at Elevated Temperatures

4.1 Introduction

In chapter 3 the effect of negative electrode materials (graphite and hard carbon) and electrode binders (PVDF, PAI and PAN) on high temperature performance was evaluated. Results showed that hard carbon had a larger irreversible capacity compared to graphite, due to the larger surface area of hard carbon giving rise to a higher degree of electrolyte breakdown associated with the formation of the SEI. This results in higher degree of reduction of the electrolyte at the interface, which increases at elevated temperatures. Therefore, one of the most important requirements for high temperature operation is a thermally stable electrolyte. Chapter 1 showed that the instability of the graphite/ electrolyte interface is due to the breakdown of electrolyte, this is a consequence of the electrolyte going outside of its voltage stability window, causing reduction of electrolyte.

In chapter 1 it was shown that carbonate electrolyte solvents capable of operation to 150 ^{o}C was limited to ethylene carbonate (EC), due to the fact that that the rest of the commonly used carbonate solvents are thermally unstable at this temperature. [39] The only other carbonate solvent suitable at this temperature is propylene carbonate (PC) however it is well documented in the literature that PC-based electrolytes with no EC content causes graphite exfoliation.[11,38] It is well documented in literature that EC plays an important role in the formation of the SEI.[36,37]

The commonly used lithium salt $LiPF_6$ is unsuitable for operation at high temperatures because of the reactions which occur with the trace quantities of water in the electrolyte which severely lowers the decomposition temperature.[57–59] The rate of these reactions is accelerated at higher temperatures, the products of which react with the cell components[43]. Literature has shown that $LiPF_6$ is unstable for use at elevated temperatures in lithium ion batteries[11,59,68–70,60–67]. The literature review showed two promising lithium salts which are capable of high temperature operation LiBOB and LiODFB. Literature[40] has shown that LiBOB can be effectively used as a replacement for $LiPF_6$ up to a temperature of 115°C. Kurita *et al* prepared cells using an electrolyte of 1M LiBOB in EC, with an LFP electrode vs lithium metal using a glass fibre separator and cycled them using galvanostatic cycling for 50 cycles at a range of c-rates (0.5C-200C) and a range of temperatures (60-115°C). At 115 ˚C the capacity observed was 160 mAh g^{-1} showing an 86% capacity retention after 50 cycles.[40] These results represent a benchmark of what can be achieved in a high

temperature lithium ion battery which utilises a carbonate based electrolyte. *Li et al*[77] has demonstrated the use of LiODFB as replacement for $LiPF_6$ at 65 ^oC, using $LiFePO_4$/ graphite full cells. The full cells composed of $LiFePO_4$ and artificial graphite cells showed a good capacity retention over 100 cycles of 88% at 65 ^oC. In comparison 1M $LiPF_6$ in EC/PC/DMC (1:1:3 v/v) the full cells composed of $LiFePO_4$ and artificial graphite only achieved a 50% capacity retention after 100 cycles at 65 ^oC. Therefore, this electrolyte study will study the effect of two electrolyte formulations 1M LiBOB in EC and 1M LiODFB in EC at 60, 90, 120 and 150 ^oC.

In order to study the effect of temperature on the thermal stability of electrolytes an electrode that is stable at high temperatures should be used. Lithium iron phosphate is a thermally stable electrode material that has a flat voltage profile with a nominal voltage of 3.5 V. Cells which have lithium iron phosphate as both electrodes is an ideal system for studying this. In order to do this the reference and counter electrode must have an a 1:1 ratio of $LiFePO_4$ to $FePO_4$ in order for the electrode to be in the flat two phase 3.5 V potential region, seen in Figure 4-1. The electrode coating of the reference/ counter electrode must be in-excess compared to the $LiFePO_4$ working electrode in order to have an excess of lithium.

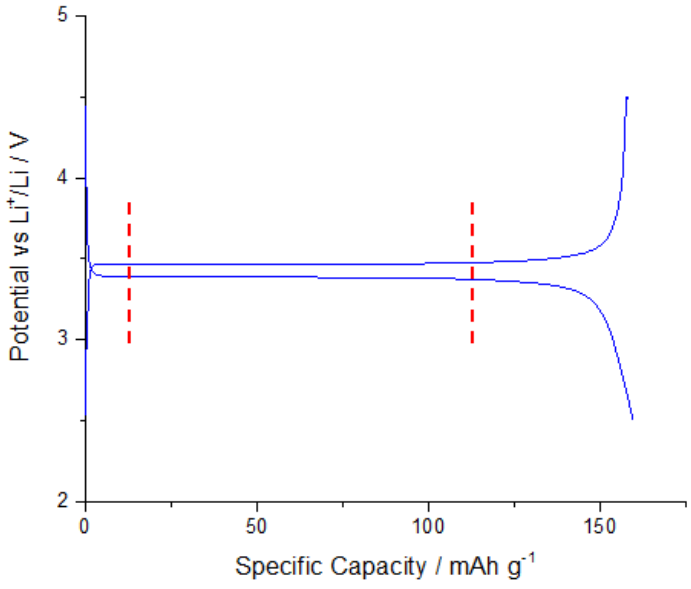

Figure 4-1 Potential vs specific capacity for a $LiFePO_4$ half-cell showing the two-phase plateau region. A PVDF binder was used, LP30 electrolyte and cell was cycled at a C-rate of C/10.

4.2 Aims and Objectives

The aims of this chapter were:

1. Investigation of $LiFePO_4$ as a reference and counter electrode in place of lithium metal.
2. To investigate the increase in the rate of electrolyte decomposition at elevated temperatures.
3. To investigate electrolyte salts that are capable of operating in the region of 60-150 ^{o}C.

The objectives of this chapter were:

To understand the temperature limitations of electrolytes and to find a more stable electrolyte at elevated temperatures.

4.3 Experimental Details

To produce $FePO_4$, $LiFePO_4$ was chemically de-lithiated using potassium persulphate according to the method used by *Ramana et al*[156,157]. 5.805g of potassium persulphate was dissolved in 184ml water and 5g of $LiFePO_4$ was added, the mixture was stirred on a magnetic stirrer plate for 24 hours, filtered, washed with distilled water and dried overnight at 80 ^oC. The powder was then characterised using PXRD to confirm that the sample had been de-lithiated. Figure 4-2 shows the spectrum for $FePO_4$ matched with the data base for $FePO_4$, confirming the de-lithiation of the $LiFePO_4$.

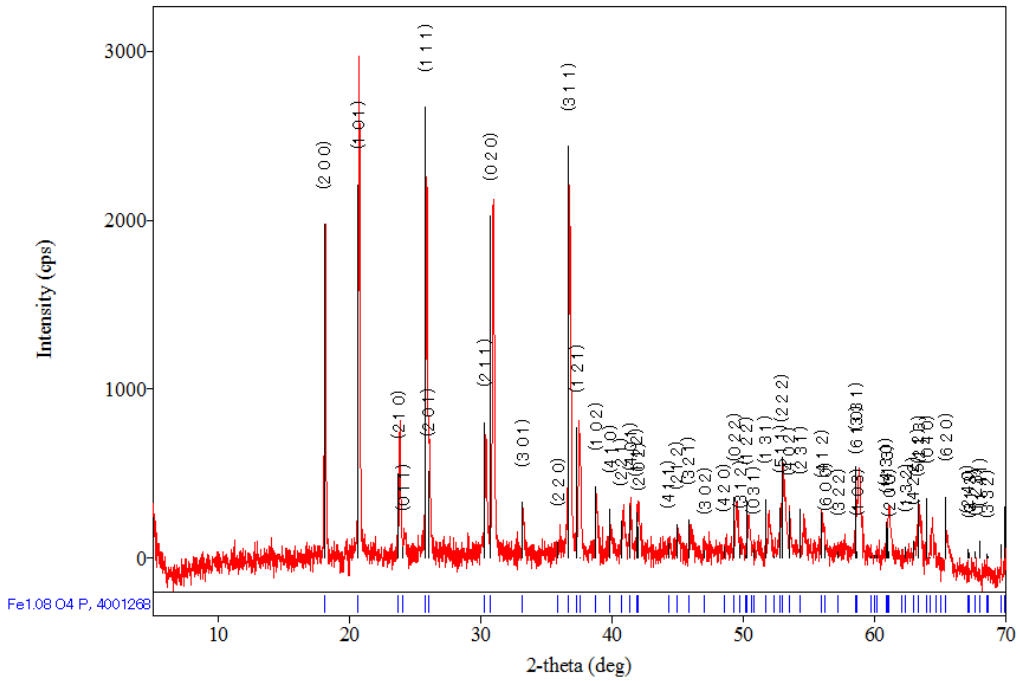

Figure 4-2 PXRD of $FePO_4$ powder showing the peak labelling compared with the database for $FePO_4$.

$LiFePO_4$ electrodes were made using 76 % $LiFePO_4$, 12 % PVDF binder and 12 % carbon black, $Li_{0.5}FePO_4$ electrodes were made using the same percentages but using a 1:1 ratio of $LiFePO_4$ and $FePO_4$. To produce the $Li_{0.5}FePO_4$ electrodes the electrode loading was 4 times in excess compared to that of the $LiFePO_4$ electrodes. To test the electrodes Swagelok cells were assembled using $Li_{0.5}FePO_4$ vs lithium metal as the CE/RE and LFP vs $Li_{0.5}FePO_4$ as the CE/RE the electrolyte used for testing was LP30. Figure 4-3 shows a graph of galvanostatic cycling of $Li_{0.5}FePO_4$ against lithium metal. The first cycle charge is around 80 mAh g^{-1} which shows that the electrode is 50% lithiated

as the practical capacity of $LiFePO_4$ is around 160 mAh g^{-1}. Figure 4-4 shows a plot of $LiFePO_4$ vs the $Li_{0.5}FePO_4$ and shows that the RE/CE is working well showing the expected capacities for lithium iron phosphate.

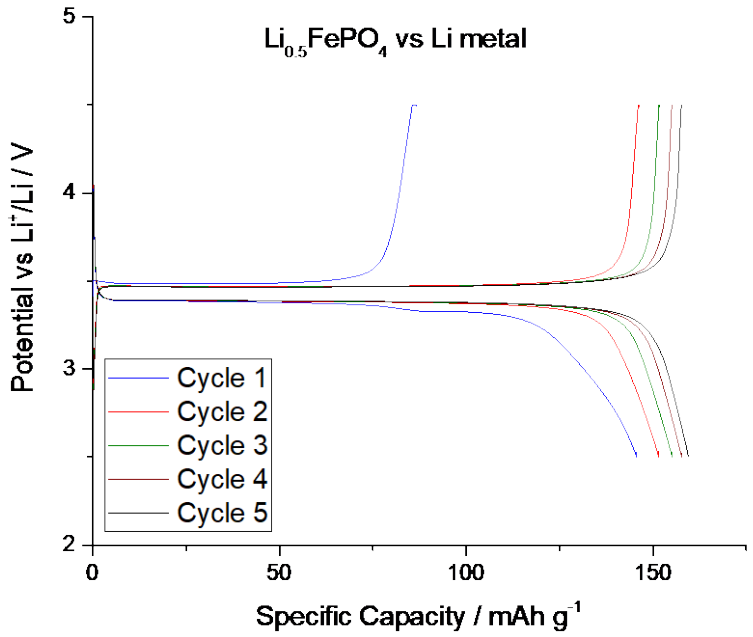

Figure 4-3 Capacity vs potential plot for $Li_{0.5}FePO_4$ vs Li metal at 25 ^{o}C. A PVDF binder was used, LP30 electrolyte and cell was cycled at a C-rate of C/10.

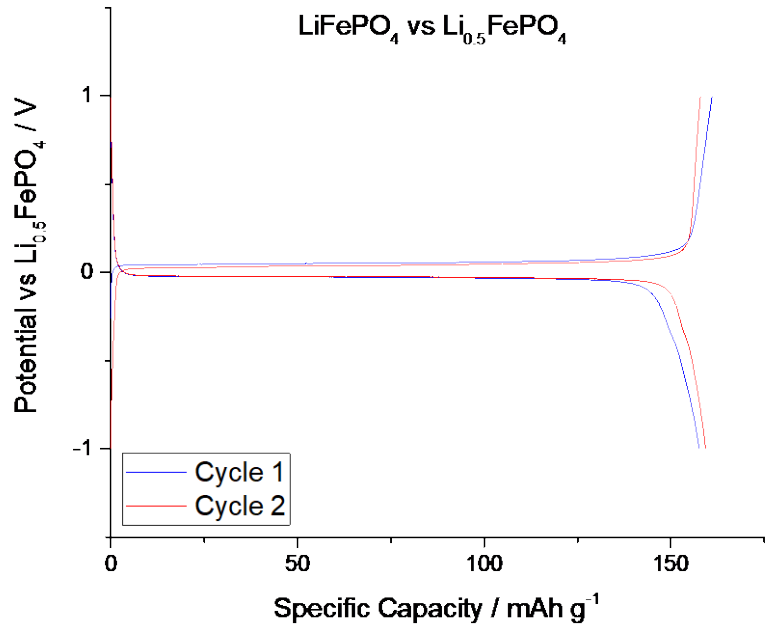

Figure 4-4 Capacity vs potential plot for $LiFePO_4$ vs $Li_{0.5}FePO_4$ RE/CE. A PVDF binder was used, LP30 electrolyte and cell was cycled at a C-rate of C/10.

Swagelok cells were built with $LiFePO_4$ as the working electrode, $Li_{0.5}FePO_4$ as the reference and counter electrode, two glass fibre separators, and 120 µl of electrolyte. Cells were then put into ovens and heated for 1 hour prior to cycling, the cells were then cycled for 1 cycle at C/10 as a formation cycle and then cycled at 1C for 101 cycles.

4.4 Results of TGA of Electrolyte Salts

It was decided to look at the thermal stability of the LiBOB and LiODFB using TGA, it was also decided to compare this with $LiPF_6$ as well, the results of which can be seen in Figure 4-5. It can be seen from this graph that $LiPF_6$ has the lowest thermal stability, showing a decomposition temperature starting at around 65 ^oC. This is probably down to the trace quantities of water contained in the electrolyte salt which catalyse the decomposition, confirming what is observed in the literature.[43,57–59] *Yang et al*[158] have shown that the presence of 300 ppm water in the carrier gas of the TGA results in a lowering of the decomposition temperature of $LiPF_6$ from 107 ^oC to 80 ^oC. The graph also shows that LiBOB appears to have a higher thermal stability starting to decompose at around 300 ^oC compared to LiODFB which starts to decompose at around 225 ^oC. These results confirm that LiODFB and LiBOB are suitable candidates for operation at 150 ^oC, with $LiPF_6$ being unsuitable at this temperature.

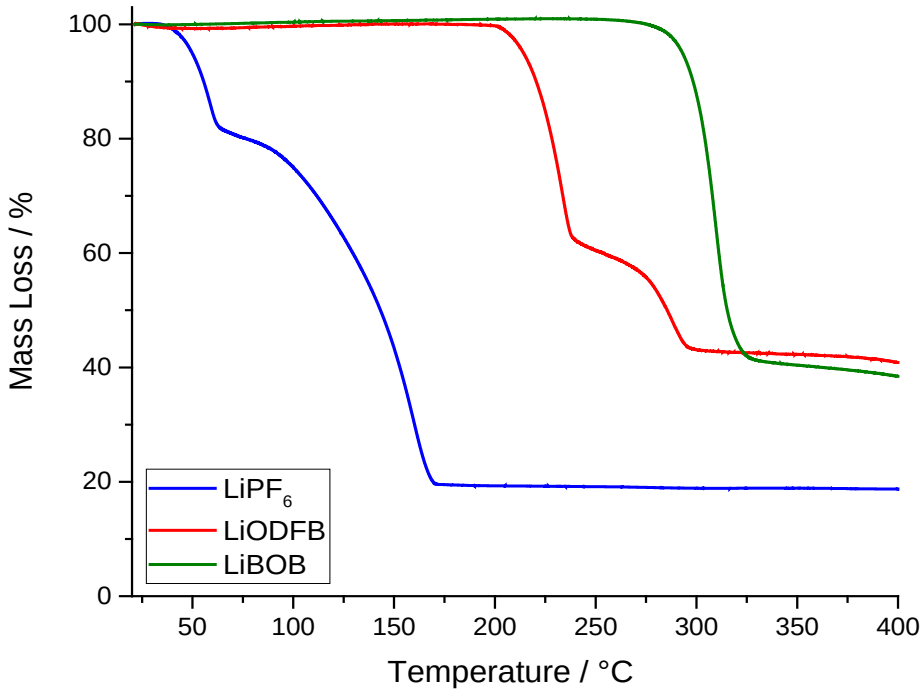

Figure 4-5 TGA plot showing mass loss % vs temperature for $LiPF_6$, LiODFB and LiBOB.

4.5 Results from Galvanostatic Cycling

4.5.1 LiBOB and LiODFB Galvanostatic Plots

Figure 4-6 to Figure 4-9 show the potential vs specific capacity plots for electrolytes of 1M LiBOB and LiODFB in EC at 60 ^{o}C, 90 ^{o}C, 120 ^{o}C and 150 ^{o}C. It is observed from Figure 4-6 that the capacity at 60 ^{o}C for LiBOB shows no deviation from the flat potential cut-off point expected with LFP, with a capacity of 160 mAh g^{-1} observed. The charge/ discharge is very flat, with very little reduction in capacity observed over 102 cycles. It can be seen for the LiODFB at 60 ^{o}C that there is a small deviation on the first cycle for the charge, which is larger than the comparable process for LiBOB, this is an irreversible process since this feature is not seen in subsequent cycles. The probable cause of this is the passivation of the electrode surface, either electrolyte breakdown to form SEI or passivation of the aluminium current collector.

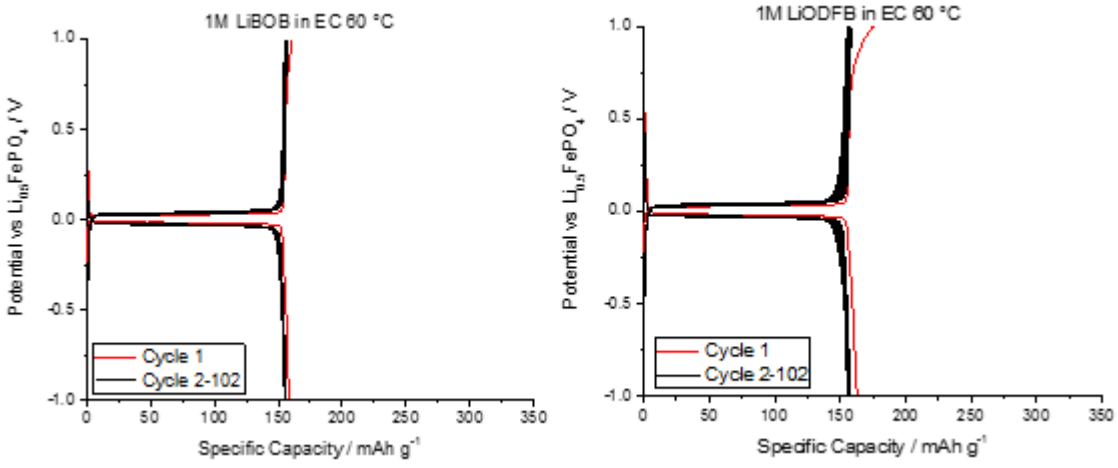

Figure 4-6 Potential vs specific capacity plots for LiBOB (left) and LiODFB (right) at 60 ^{o}C.

A similar observation can be observed for LiBOB at 90 ^{o}C, seen in Figure 4-7, where it is observed that there is deviation on first cycle charge curve. This feature can also be seen for LiODFB at 90 ^{o}C, except this time it is much more pronounced, with a “capacity” of around 325 mAh g^{-1} observed for the first cycle charge. The theoretical capacity of LFP is 170 mAh g^{-1}, therefore this extra charge passed is due to an irreversible process occurring on the first cycle charge. However, after the first cycle, both the cells with LiBOB and LiODFB electrolyte have a very stable cycling capacity over 102 cycles with minimal loss in capacity.

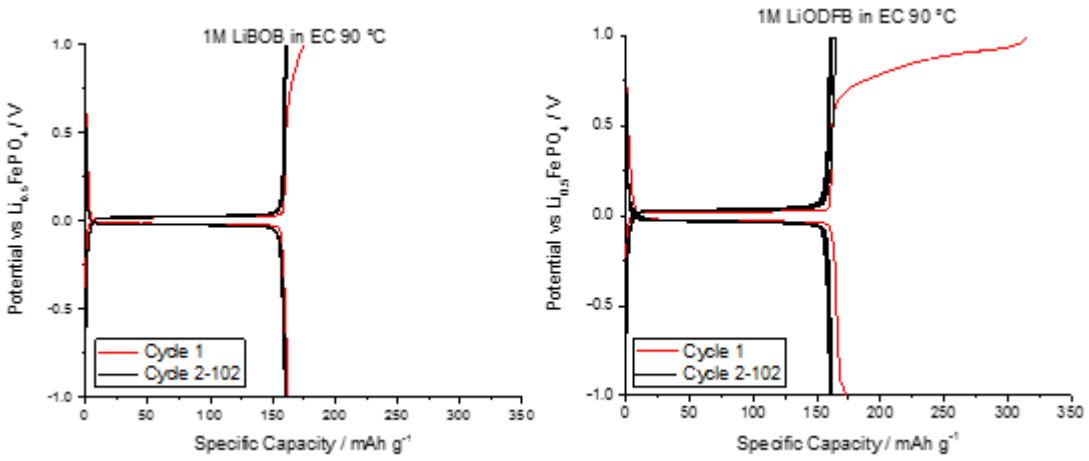

Figure 4-7 Potential vs specific capacity plots for LiBOB (left) and LiODFB (right) at 90 °C.

As the temperature is raised further to 120 °C and 150 °C, seen in Figure 4-8 and Figure 4-9, it is observed that the first cycle extra charge has increased further with the addition of an extra plateaux. The size of this plateaux is larger at 120 °C than at 150 °C, which is most likely due to the increased rate of reaction occurring. The effect of temperature on the first cycle capacity is summarised in Figure 4-10, where the first cycle charge/ discharge curves are plotted for LiBOB and LiODFB at all temperatures. It is witnessed that LiODFB exhibits a higher capacity than LiBOB, which could be due to reaction of the fluorine with the electrode surface contained the LiODFB which isn't present in LiBOB. What is also apparent at 120 °C and 150 °C is that significant capacity fade occurs with both electrolytes, with capacity faded to 130 mAh g^{-1} at 120 °C and 20 mAh g^{-1} at 150 °C after 102 cycles.

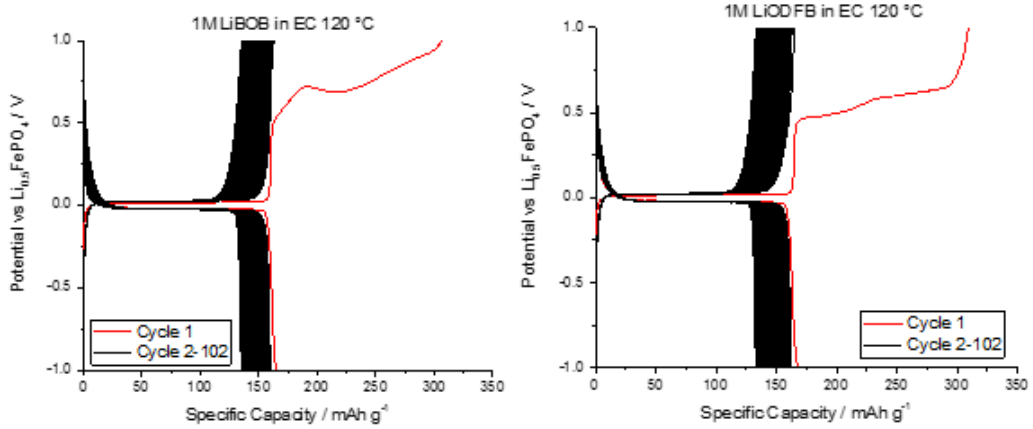

Figure 4-8 Potential vs specific capacity plots for LiBOB (left) and LiODFB (right) at 120 °C.

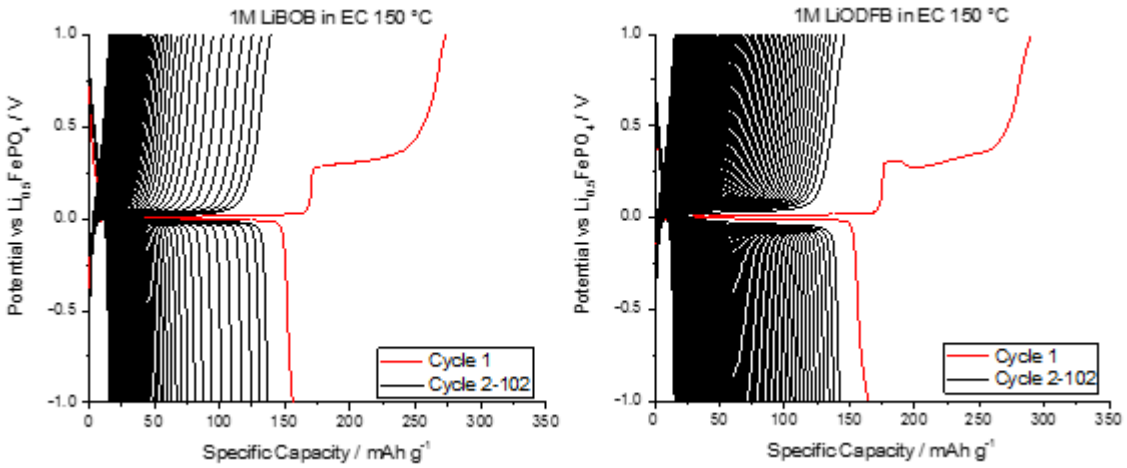

Figure 4-9 Potential vs specific capacity plots for LiBOB (left) and LiODFB (right) at 150 ^{o}C.

It is observed that when lithium iron phosphate is cycled at elevated temperatures the first cycle charge capacity exceeds that of the theoretical capacity i.e. a charge capacity of >170 mAh g^{-1}, this can be seen in Figure 4-10. For example, with LiODFB at 120 ^{o}C it can be seen that at 0.45 V vs $Li_{0.5}FePO_4$ the cell is already at the theoretical capacity of 170 mAh g^{-1}. It can be seen that there is the presence of an extra plateaux after 0.45 V vs $Li_{0.5}FePO_4$, the excess charge that is passed is not that of lithium de-insertion but of side reactions occurring at the electrode/ electrolyte interface. The source of this extra charge could be caused by several factors but could be:

- Electrolyte breakdown- at higher temperatures the kinetics of side reactions at the electrode/ electrolyte increase. These reactions consume electrolyte and form increasing resistive passivation layers which leads to capacity fade.
- Binder failure- at higher temperatures the binder which is a polymer can either melt or degrade which leads to contact losses of the electrode particles and the current collector. This can then lead to the exposure of the aluminium current collector, which the electrolyte and the lithium can react with causing corrosion of the aluminium current collector.

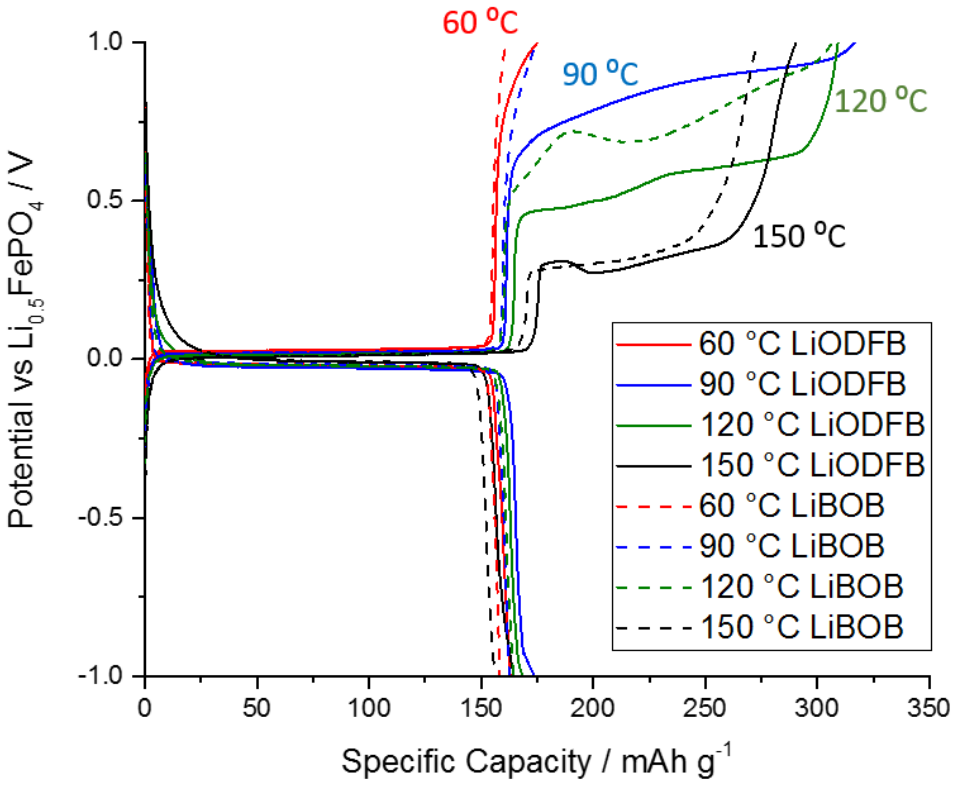

Figure 4-10 Potential vs specific capacity plots for the first cycle of LiBOB and LiODFB electrolytes at 60, 90, 120 and 150 °C.

4.5.2 LiBOB and LiODFB Specific Discharge Plots

Figure 4-11 shows plots of specific discharge capacity vs cycle number. It is observed that for both salts the discharge capacity is higher at 90 °C than 60 °C with no significant degrading of the capacity over 102 cycles. At 120 °C the same trend can be observed, nevertheless the capacity starts to decline at 30 cycles for LiODFB and 40 cycles for LiBOB. The capacity after 102 cycles at 120 °C is around 130 mAh g^{-1} which is good capacity retention for such a high temperature. At 150 °C for LiODFB capacity fade has reached 50 % at 20 cycles and for LiBOB it is reached by 10 cycles for LiBOB, with the cells at a capacity of 20 mAh g^{-1} after 102 cycles.

To compare this with literature *Kurita et al*[40] has shown that lithium iron phosphate half cells operating at 115 ˚C the capacity observed was 160 mAh g^{-1} showing an 86% capacity retention after 50 cycles. At 120 ˚C the capacity retention was shown to be 76% after 102 cycles which is a better performance than *Kurita et al*[40] who cycled them for half the time at a lower temperature. The performance at 150 ˚C is not comparable since it is much higher than was investigated during their

study. *Li et al*[77] demonstrated the use of LiODFB at 65 ^{o}C, using $LiFePO_4$/ graphite full cells. The full cells composed of $LiFePO_4$ and artificial graphite cells showed a good capacity retention over 100 cycles of 88% at 65 ^{o}C. Comparing with the results achieved in figure 4.11 the performance of the LiODFB performs better with a 97 % capacity retention at 60 ^{o}C and 91 % capacity retention at 90 ^{o}C both which are better capacity retention than achieved by *Li et al*[77]. This is the first time LiODFB has been demonstrated to operate above 65 ^{o}C.

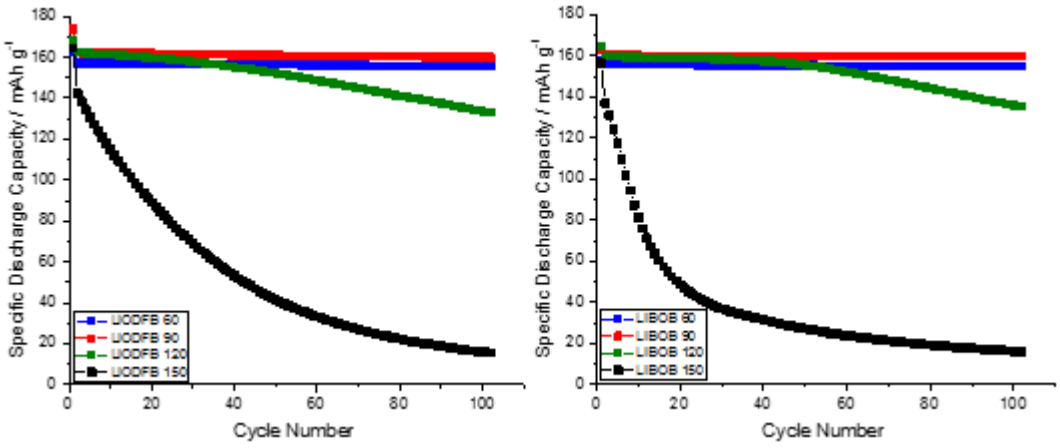

Figure 4-11 Specific discharge capacity vs cycle number plots for electrolytes of LiODFB (left) and LiBOB (right) in EC.

Figure 4-12 displays the specific discharge capacities compared by temperature for both electrolytes. It is observed that for 60, 90 ^{o}C and 150 ^{o}C the discharge capacity for LiODFB is higher than LiBOB. Although the discharge capacity at 120 ^{o}C is initially better for LiODFB, after 30 cycles the LiBOB performs better. This seems to be an anomaly however since the rest of the data suggests that LiODFB has a better higher temperature performance.

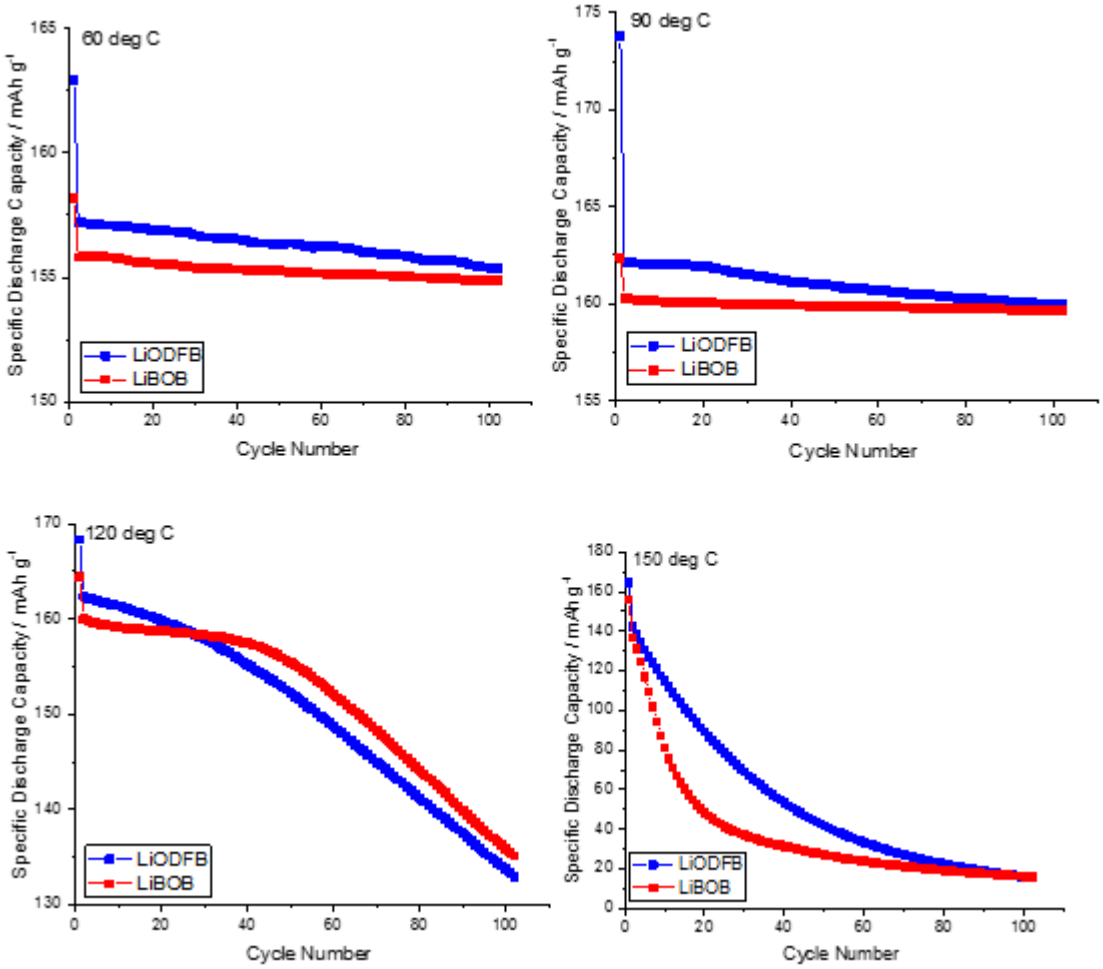

Figure 4-12 Specific discharge capacity vs cycle number plots for electrolytes of LiODFB (left) and LiBOB (right) in EC.

4.5.3 LiBOB and LiODFB Coulombic Efficiency Plots

Figure 4-13 displays a plot of the coulombic efficiency vs temperature for cycle 1 for LiBOB and LiODFB. Coulombic efficiency decreases with temperature with LiODFB having a lower coulombic efficiency at 60 ^{o}C and 90 ^{o}C compared to LiBOB. It is observed that there are large differences between the two salts at 90^{o}C, this is mainly due to the extra charge passed on the first charge cycle for LiODFB, seen in Figure 4-10. It is observed however that at 120 and 150 ^{o}C the coulombic efficiencies are similar for both electrolyte salts, with not much difference between the coulombic efficiency at 120 and 150 ^{o}C.

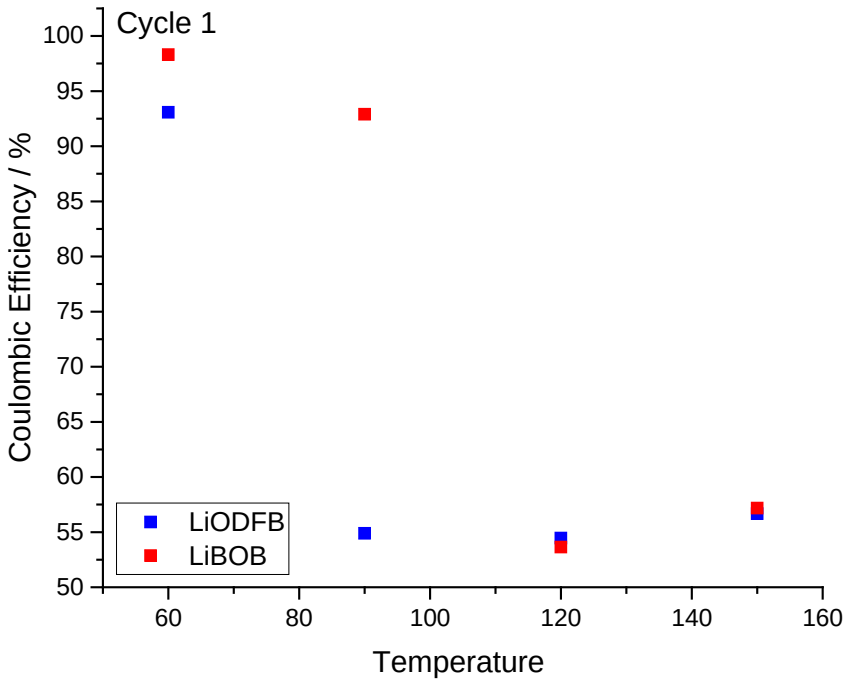

Figure 4-13 Coulombic efficiency vs temperature for cycle 1 for LiODFB and LiBOB.

Figure 4-14 presents the coulombic efficiency plots for cycles 2-102 for LiBOB and LiODFB, it can be seen the coulombic efficiency decreases with increasing temperature. Initially at 60 ^{o}C LiODFB has a higher coulombic efficiency than LiBOB, nonetheless after 4 cycles LiBOB has a better coulombic efficiency. A similar trend can be seen at 120 ^{o}C, where initially a better coulombic efficiency is seen for LiODFB, but after 25 cycles LiBOB has an improved coulombic efficiency. This is interesting as LiODFB performed better in terms of the specific discharge capacities and showed much better stability on cycling at high temperatures. At 90 ^{o}C however LiODFB has a greater coulombic efficiency than LiBOB. At 150 ^{o}C LiBOB again has an improved coulombic efficiency compared to LiODFB.

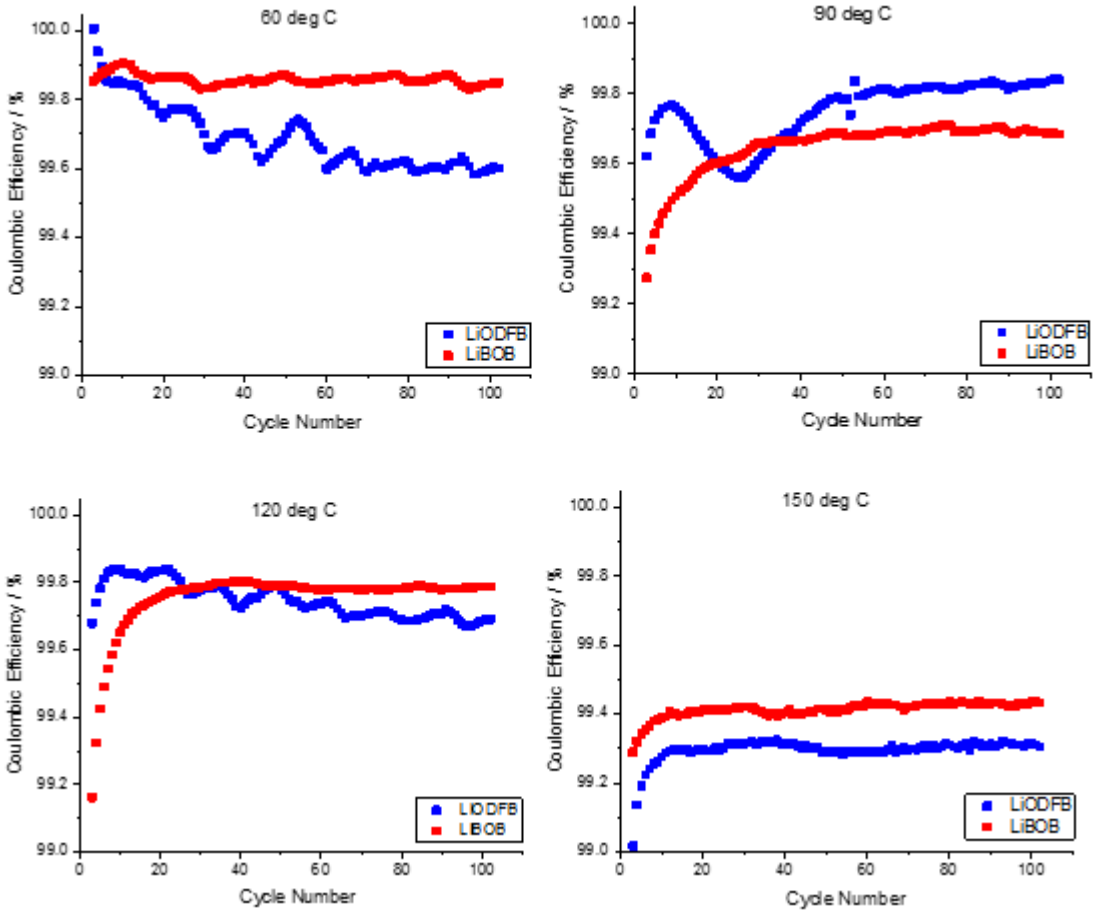

Figure 4-14 Coulombic efficiency vs cycle number plots for cycles 2-102 for LiODFB and LiBOB.

4.5.4 LiBOB and LiODFB Irreversible Capacity Plots

Figure 4-15 shows the irreversible capacity plots vs temperature for the first cycle for LiBOB and LiODFB. It can be seen that irreversible capacity increases with temperature since it was shown that during cycle 1 there is a significant reaction that occurs on the first cycle charge that consumes a significant proportion of charge. Figure 4-16 compares the irreversible capacity vs cycle number for cycles 2-102 for LiBOB and LiODFB, it is observed that at 60, 120 and 150 ^{o}C LiODFB has the higher irreversible capacities, however at 120 ^{o}C the irreversible capacity is lower than LiBOB. At 60 ^{o}C it observed that although initially LiODFB has a lower irreversible capacity, however after 5 cycles the irreversible capacity increases, this same trend is also seen at 120 ^{o}C by where after 25 cycles the LiODFB irreversible capacity increases. The reverse case can be seen for 90 ^{o}C by where LiODFB has a lower irreversible capacity than LiBOB over 102 cycles. At 150 ^{o}C it can be seen that LiODFB has a higher irreversible capacity by where after 102 cycles they reach the same values. From the

irreversible capacity plots it would appear that LiBOB would be the better choice over LiODFB, however looking at the reversible capacity data LiODFB has higher capacities and a slower decline in capacity over 102 cycles.

It is also observed that at 150 ^{o}C that the irreversible capacity values don't match with the change in specific discharge capacity seen in Figure 4-11. It is observed for irreversible capacity, seen in Figure 4-16, that irreversible capacity goes from around 1 mAh g^{-1} to around 0.2 mAh g^{-1} at 150 ^{o}C. On the other hand looking at Figure 4-11 it is observed that capacity loss per charge/ discharge cycle is around 5 mAh g^{-1} per cycle. This mismatch suggests that it is not just electrolyte breakdown but other reactions in the cell since if it was electrolyte breakdown the decline in discharge capacities would be very similar to those of irreversible capacity values.

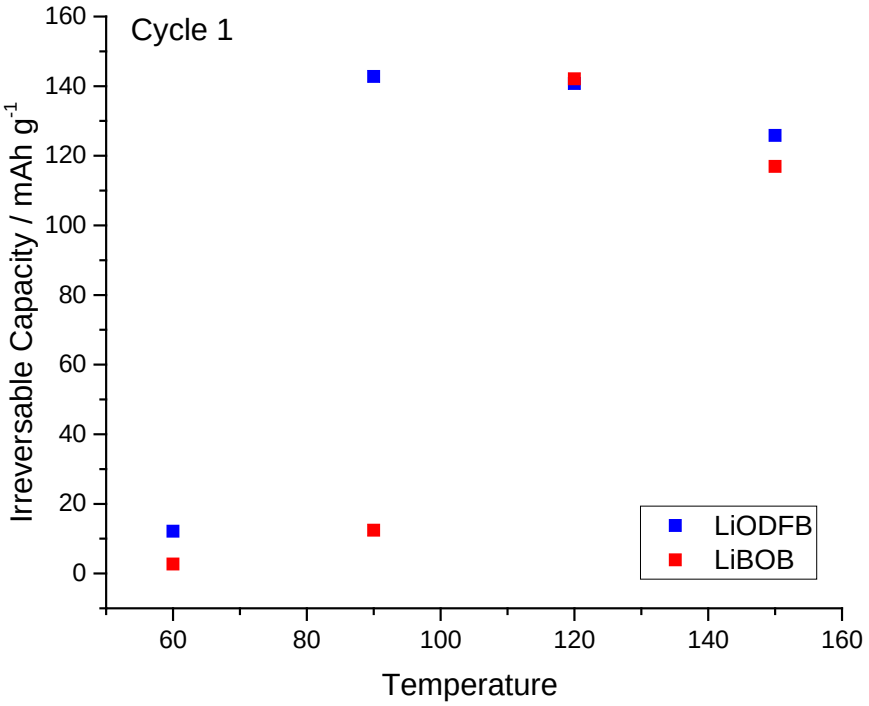

Figure 4-15 Irreversible capacity vs temperature for cycle 1 for LiODFB and LiBOB.

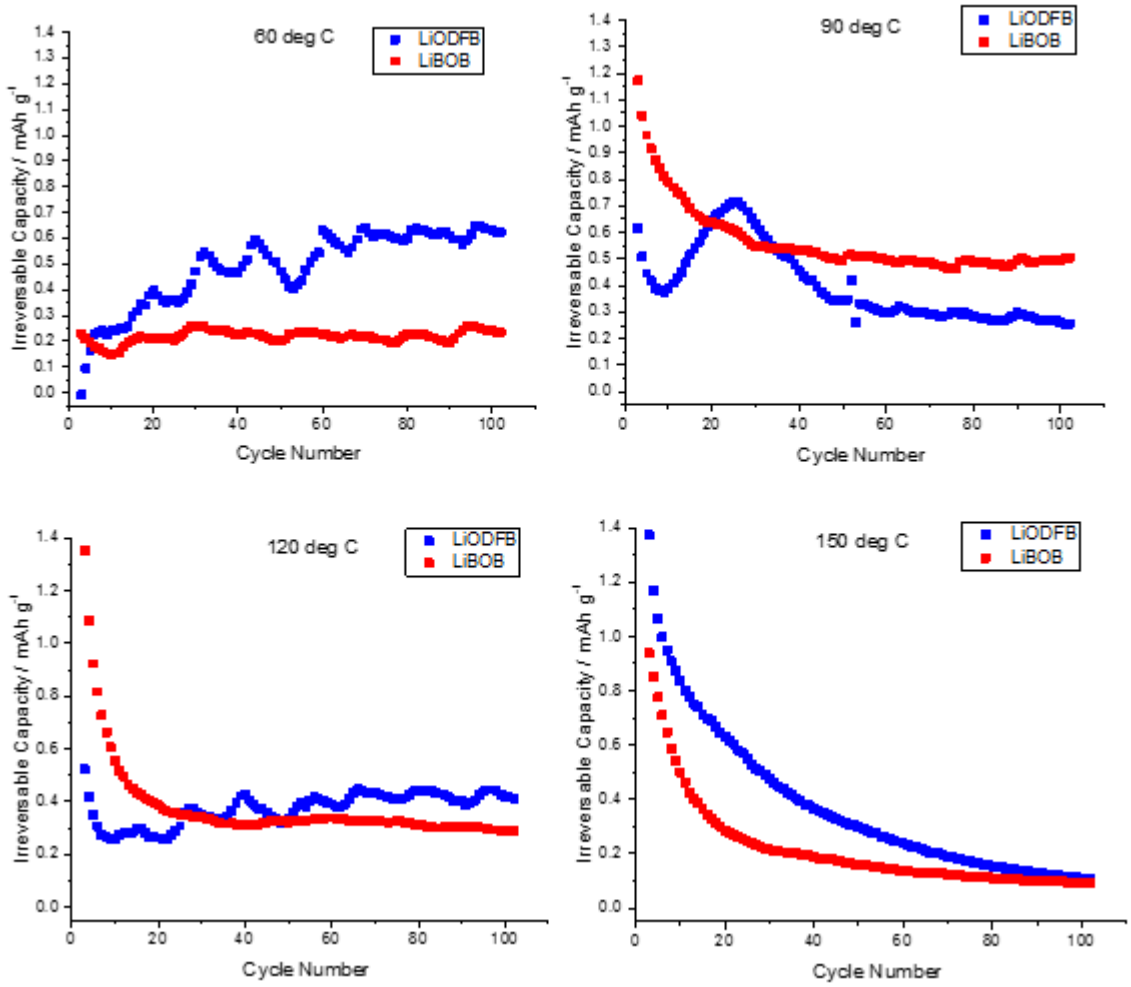

Figure 4-16 Irreversible capacity vs cycle number plots for cycles 2-102 for LiODFB and LiBOB.

4.6 Conclusions

This chapter aimed to study the effect of electrolyte salts on the performance of cells at elevated temperatures. At 120 ^{o}C the capacity after 100 cycles was 130 mAh g^{-1} equating to a 76% capacity retention. At 150 ^{o}C however, the capacity fade was much more rapid, with 50 % capacity loss after 20 cycles for LiODFB and 10 cycles for LiBOB. At 150 ^{o}C LiODFB performed much better than LiBOB with a slower degrade in capacity observed, however this performance can still be much improved since cycle life is low at this temperature. Further work should look the reproducibility of these experiments in order to determine the significant effects of electrolyte on high temperature performance, which should include the use of full lithium-ion pouch cells.

Further work should look at improving the high temperature performance and to find the causes of failure at high temperature. The causes of the large irreversible capacity losses should be investigated. In particular the large extra charged passed on the first cycle should be investigated to find the causes of this in order to find solutions to the problem.

Chapter 5 Effect of Electrode Binders at Elevated Temperatures

5.1 Introduction

In chapter 4 the effect of temperature on electrolytes was investigated and it was demonstrated that two lithium salts, LiBOB and LiODFB gave satisfactory performance during galvanostatic cycling at temperatures of 60, 90, 120 and 150 ^{o}C with lithium iron phosphate electrodes. After 100 cycles, the capacity dropped to 155 mAh g^{-1} at 60 ^{o}C and to 160 mAh g^{-1} at 90 ^{o}C. The higher capacity values at 90 ^{o}C have been attributed to increased kinetics with processes such as lithium insertion and de-insertion occurring at an increased rate. Literature[22,125] suggests that capacity increases in lithium iron phosphate electrodes with temperature due to:

1. Improved wetting of the surface of the positive electrode i.e. better contact of the electrode and electrolyte.
2. Improved electrolyte conductivity.
3. Improved ionic diffusion due to decreasing ionic resistance.

The effect of capacity loss becomes more apparent at 120 and 150 ^{o}C with a discharge capacity of 135 mAh g^{-1} observed after 100 cycles at 120 ^{o}C and 20 mAh g^{-1} at 150 ^{o}C. The capacity fade was fast at 150 ^{o}C showing a 50 % capacity loss after 20 cycles for LiODFB and 10 cycles for LiBOB. In chapter 4 it was observed that at 120 and 150 ^{o}C the charge capacity on the first cycle was higher than the theoretical capacity of lithium iron phosphate which is 170 mAh g^{-1}. The excess charge that is passed on this first cycle is not that of lithium de-insertion but of side reactions occurring at the electrode/ electrolyte interface.

The source of this capacity fade could be caused by several factors but could be:

- Electrolyte breakdown- at higher temperatures the kinetics of side reactions at the electrode/ electrolyte increase. These reactions consume electrolyte and form increasing resistive passivation layers which leads to capacity fade.
- Binder failure- at higher temperatures the binder which is a polymer can either melt or degrade which leads to contact losses of the electrode particles and the current collector.

This can then lead to the exposure of the aluminium current collector, which the electrolyte and the lithium can react with causing corrosion of the aluminium current collector.

It has been identified that binder failure could be a cause of degradation reactions at higher temperatures, this chapter will explore the role of binders on the capacity losses at higher temperatures. For this study three binders were investigated polyvinylidene fluoride (PVDF 5130), polyacrylonitrile (PAN) and polyamide imide (PAI). PAI and PAN were investigated due to the fact that these binders have been shown to be more effective than PVDF at elevated temperatures.[131,135–138] In chapter 3 it was shown that both PAN and PAI outperform PVDF at 60 ˚C when used with graphite and hard carbon electrodes using conventional carbonate electrolytes (LP30 and LP57). Literature has shown that both PAN and PAI give better stability on cycling compared to PVDF because of the higher thermal stability and greater adhesion properties.[131,135–138] To further investigate these binders it was decided to perform tests with higher temperature electrolytes as detailed in chapter 4. It was decided that the electrolyte to be used was 1M LiODFB in EC since this proved to be the most stable electrolyte out of the two electrolytes tested in chapter 4. In chapter 4 it was concluded that PVDF at elevated temperatures can soften towards 150 ^{o}C and cause contact losses between electrode particles and the contact to the current collector which can lead to reactions occurring between the current collector and the electrolyte and the lithium leading to capacity fade.

5.2 Aims and Objectives

The aims of this chapter were:

To investigate the effect of binders on high temperature performance of lithium iron phosphate electrodes at 60, 90, 120 and 150 ^{o}C.

The objectives of this chapter were:

To understand the role of binders on the discharge capacities and capacity loss of lithium iron phosphate electrodes at elevated temperatures of 60, 90, 120 and 150 ^{o}C.

5.3 Experimental Details

In order to evaluate the effect of binders for high temperature lithium ion batteries thermal studies were conducted on the binders using both TGA and DSC, since TGA shows mass loss due to breakdown and DSC can show phase transitions such as melting or glass transition temperatures. To study the effect of the binder on high temperature stability during operation galvanostatic cycling was performed on lithium iron phosphate electrodes made using PVDF, PAI and PAN binders at 60, 90, 120 and 150 ^{o}C. Both $LiFePO_4$ electrodes and $Li_{0.5}FePO_4$ electrodes were made using PVDF, PAN and PAI as the binder. $LiFePO_4$ electrodes were made using 76% $LiFePO_4$, 12% binder and 12% carbon black, $Li_{0.5}FePO_4$ electrodes were made using the same percentage of active material but using a 1:1 ratio of $LiFePO_4$ and $FePO_4$. The binders used were PAN, PAI and PVDF 5130 used in the same ratio as above and subjected to the same calendaring and drying techniques except for PAI which had an additional drying stage at 240 ˚C to cure the polymer, something which is described in chapter 3.

Swagelok cells were built with $LiFePO_4$ as the working electrode, $Li_{0.5}FePO_4$ as the reference and counter electrode, two glass fibre separators, and 120 µl of electrolyte. Cells were then put into ovens and heated for 1 hour prior to cycling, the cells were then cycled for 1 cycle at C/10 as a formation cycle and then cycled at 1C for 101 cycles between 4.5 V and 2.5 V. The electrolyte used was 1M LiODFB in EC, it was chosen since in chapter 4 it was demonstrated to perform better than LiBOB showing better discharge capacities and coulombic efficiency over 100 cycles.

5.4 Results from TGA and DSC of Polymers

5.4.1 TGA of PVDF, PAN and PAI

Figure 5-1 shows a plot of the TGA for PVDF 5130, PAN and PAI from 20 to 400 ˚C. The graph shows that PAI is the most thermally stable binder not showing weight loss due to decomposition between 20 and 400 ^{o}C. The least stable binder has shown to be PAN which is showing that decomposition is starting at 250 ˚C, whereas for the PVDF this occurs at 340 ˚C. These results only show results for thermal breakdown of the polymers themselves and do not show any phase changes in the polymers i.e. melting or glass transition temperatures. For this DSC analysis is required, DSC shows heat flow and so endothermic processes associated with melting or glass transition show a negative heat flow, the results of which can be seen in section 5.4.2.

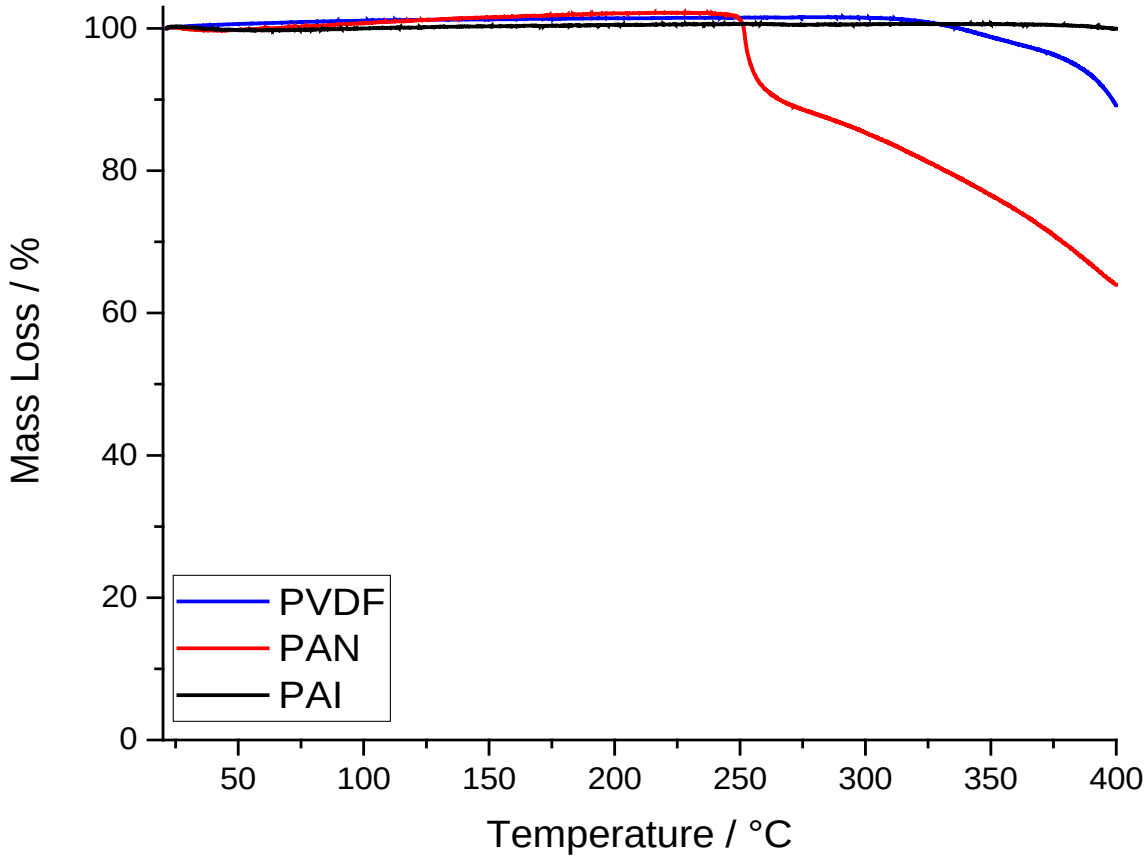

Figure 5-1 TGA plot of percentage mass loss vs temperature for PVDF 5130, PAN and PAI under argon gas. Heating rate of 1 ^{o}C per minute was used.

5.4.2 DSC of PVDF, PAN and PAI

The results for the DSC analysis for PVDF, PAN and PAI between 20 and 400 ^{o}C can be seen in Figure 5-2 to Figure 5-4. Figure 5-2 shows the results of the DSC for PVDF. It can be seen that on the first heating cycle there is an endothermic double peak starting at 125 ^{o}C going to 170 ^{o}C, on the reverse cycle there is a single peak at 100 ^{o}C. Due to the sharpness of the peak it is concluded that the endothermic peak is corresponding to a melting process. This shows that there is reversibility on this process and therefore a phase change i.e. solid to liquid and then liquid to solid, however on the second heating there is the absence of the small peak at 125 ^{o}C, instead there is a single peak at 150 ^{o}C for the melting process. This shows that on the first heating cycle there is an irreversible change in the structure of the PVDF which we know is not degradation since the TGA doesn't show loss of material in the region of 125 to 150 ^{o}C. These results confirm the observations seen in chapter 4 that electrodes made with PVDF binder have much less capacity retention at 120 and 150 ^{o}C. It is speculated that this capacity fade could be due to the PVDF softening at 120 and 150 ^{o}C, compromising the mechanical stability of the electrodes which then causes reactions of the electrolyte with the carbon particles and the surface of the aluminium current collector.

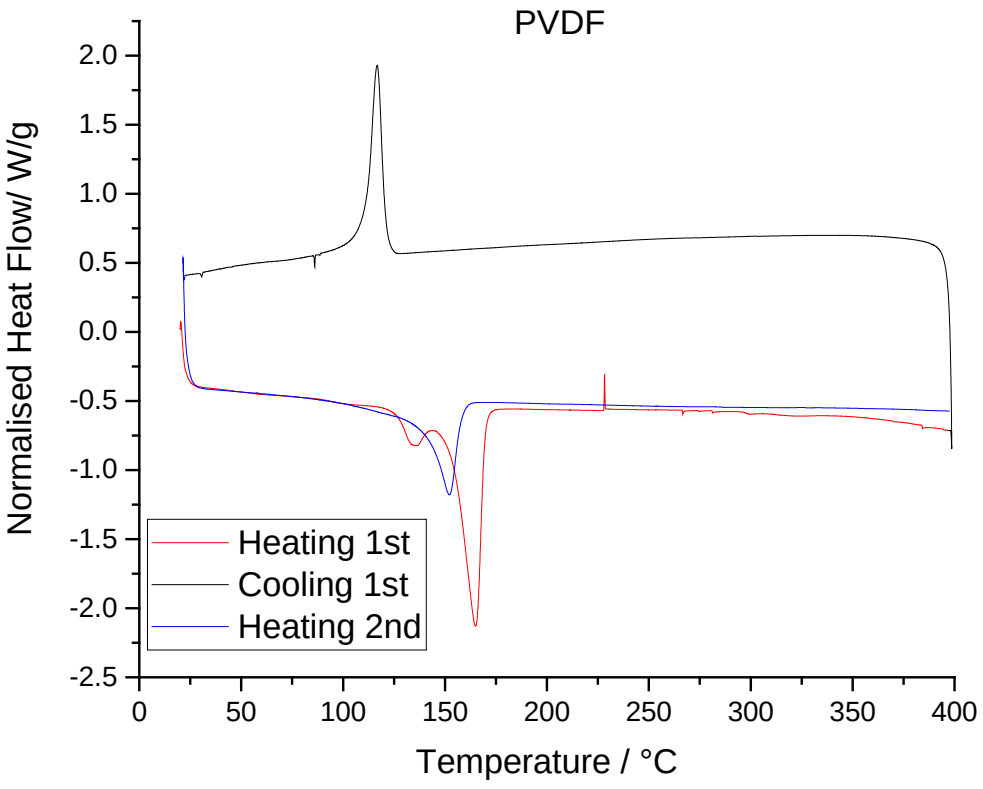

Figure 5-2 DSC plot of normalised heat flow vs temperature for PVDF 5130.

Figure 5-3 shows the results of the DSC for PAI. It can be seen from the trace that there is initially a large endothermic peak between 20 and 150 ^{o}C, this is an irreversible process since it does not appear in either the cooling cycle or the 2nd heating cycle. Literature has suggested that this is due to moisture removal out of the bulk[159]. However, there is a reversible process at 275 ^{o}C, since this peak is also seen on the cooling cycle and the second heating cycle, probably a change in the phase of the material, we know it is not a degradation reaction since the TGA shows no mass loss at this temperature and the process is reversed. Literature has shown that this is the glass transition temperature of the PAI quoted as 277 ^{o}C by *Diaham et al* [159], this is considerably higher than that of PVDF and therefore meaning that it will not soften at 150 ^{o}C.

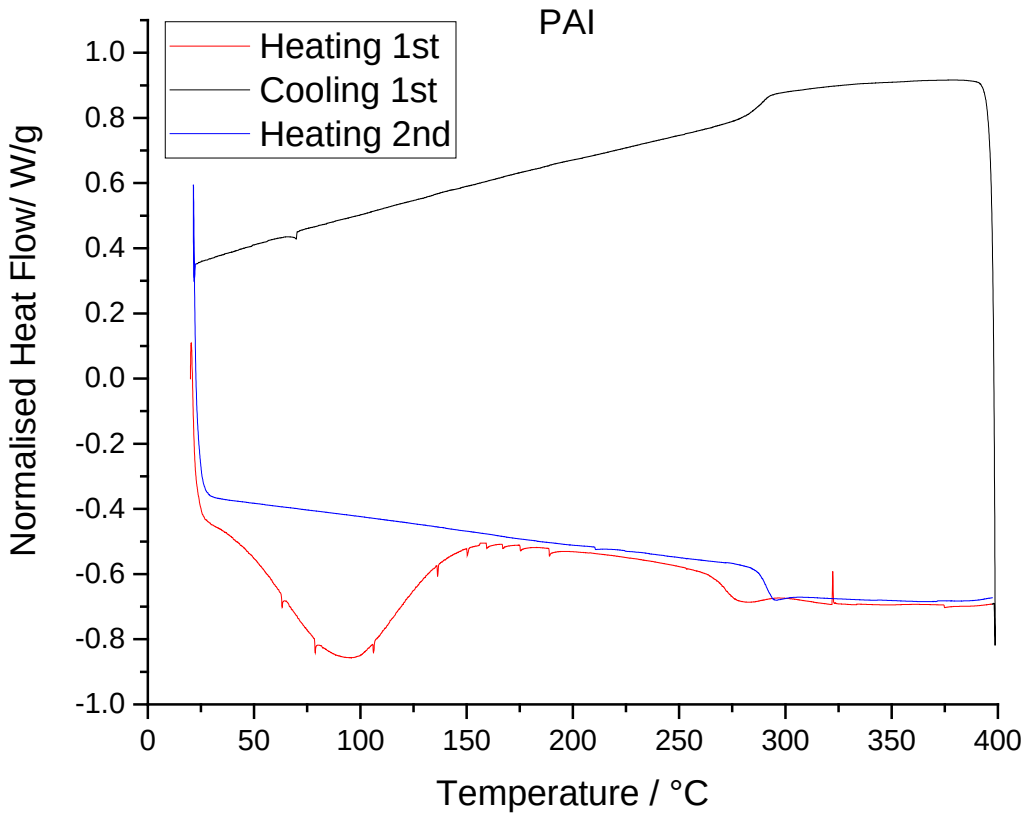

Figure 5-3 DSC plot of normalised heat flow vs temperature for PAI.

Figure 5-4 shows the results of the DSC for PAN. It can be seen that from the graph that there is the presence of two peaks in the region of 100 to 120 ^{o}C. Literature[160] has shown that there are two glass transitions for PAN one which is in the region of 80-100 ^{o}C and one near 140 ^{o}C. There is then the presence of a large exothermic peak at 300 ^{o}C, this exothermic peak corresponds to a degradation process since the TGA shows mass loss at this temperature[160,161]. The literature[160] has also shown that PAN is not stable up to the melting point and so it degrades before reaching the

melting and the reason why the melting point isn't seen on the DSC plot and only that of the degradation process.

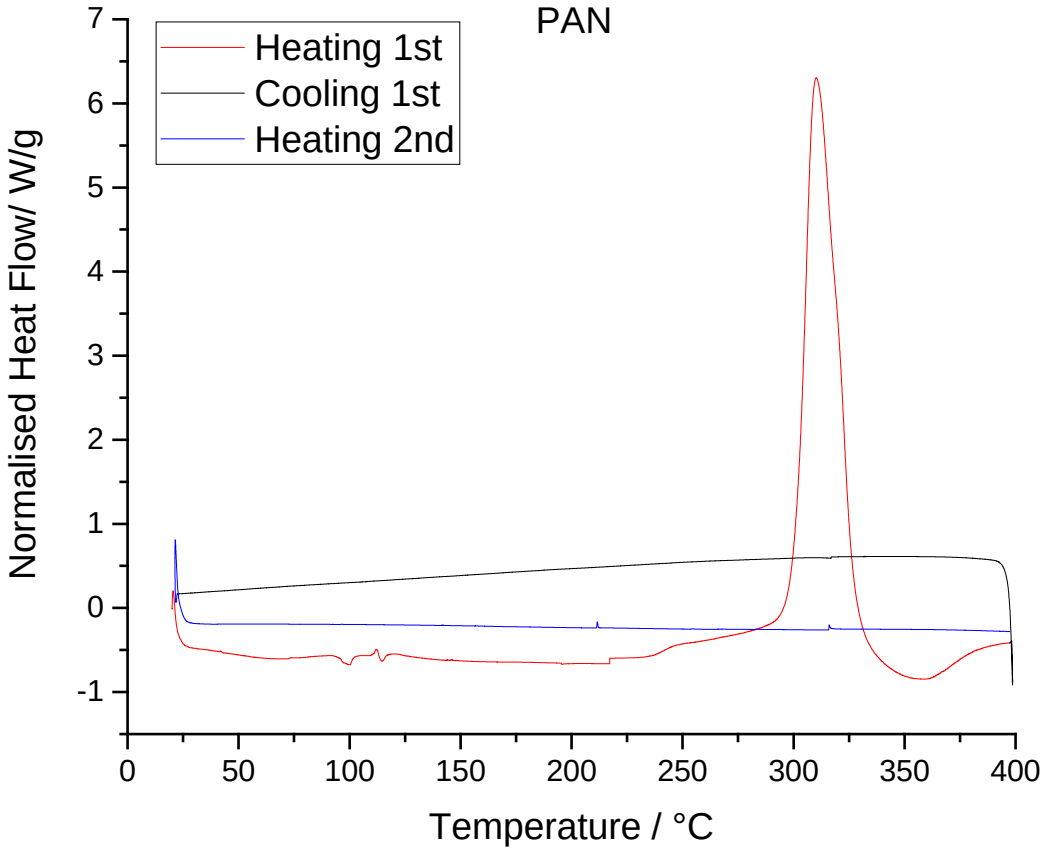

Figure 5-4 DSC plot of normalised heat flow vs temperature for PAN.

5.5 Results from Galvanostatic Cycling of PVDF, PAI and PAN

5.5.1 Cycle 1 Charge/Discharge Cycle

In the introduction to this chapter it was discussed that when lithium iron phosphate is cycled at elevated temperatures the first cycle charge capacity exceeds that of the theoretical capacity i.e. a charge capacity of >170 mAh g^{-1}. Figure 5-5 shows the comparison of the first cycle charge/ discharge cycle for the galvanostatic cycling at 60, 90, 120 and 150 ˚C for lithium iron phosphate electrodes made using PVDF, PAN and PAI as the electrode binders. It is observed that at 60 ˚C for all binders tested the excess charge passed on the first cycle charge is low which means that there is less degradation reactions occurring. This can be seen in Figure 5-6 which shows the excess charge passed on the first charge cycle, this was calculated by subtracting the theoretical capacity for lithium iron phosphate from the charge capacity. It is observed for 60 ˚C that the largest excess charge passed is for PAI with the lowest being PAN. Going to 90 ˚C and above it is observed that for both PVDF and PAN there is a large excess of charge passed on the first cycle charge process compared to that of PAI. It is observed that at 90 ˚C the capacity values are very similar for both the PDVF and PAN binders showing a charge capacity of around 300 mAh g^{-1}. This is 130 mAh g^{-1} excess charge passed which relates to side reactions, which relates to 1.6C of excess charge which is passed for these side reactions. Going to 120 ˚C it is observed that the highest excess charge is for PAN showing an excess charge passed of 325 mAh g^{-1} which results in very poor cycling stability showing 42% capacity retention after 100 cycles. However, at 150 ˚C is observed that the first cycle excess charge passed is less than at 120 ˚C, this is also an observation that was also seen in chapter 4. This has been attributed to the higher kinetics at 150 ˚C.

The exact causes of this first cycle large charge excess are unknown however looking at Figure 5-5 and Figure 5-6 it can be seen that the first cycle excess charge is influenced by the binder. This is because the binders which have poor capacity retention on cycling, PVDF and PAN both show large excesses of charge on the first cycle charge. Whereas PAI, which has a much higher capacity retention on cycling shows a much lower excess of charge passed on the first cycle. PAI also has very little change in the first cycle charge capacity with temperature, this can be seen in Figure 5-6. The better performance of the PAI binder is likely to be due to the higher thermal stability, seen in section 5.4 and the stronger adhesion properties of the PAI compared to that of the PVDF and PAN.

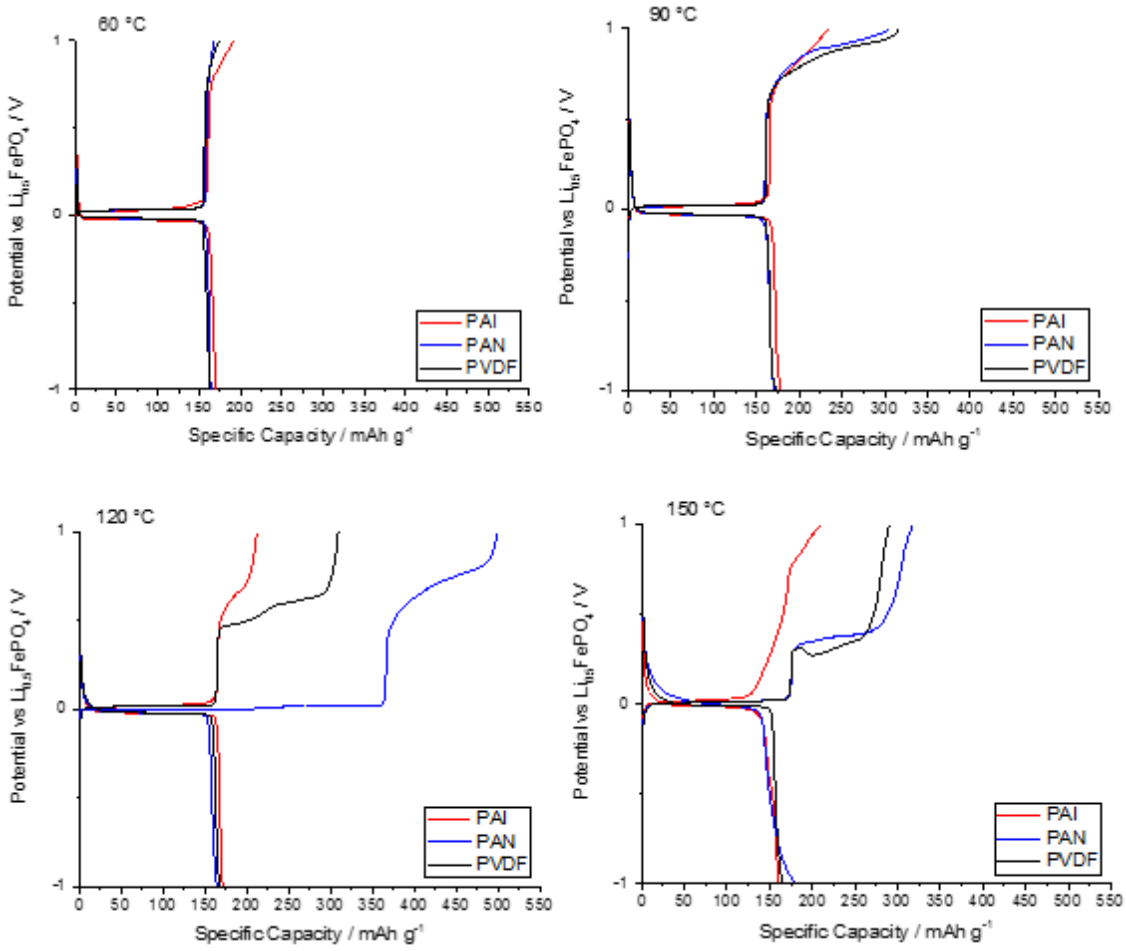

Figure 5-5 Potential vs Specific discharge capacity for cycle 1 for cells cycled with binders PAN, PAI and PVDF at 60, 90, 120 and 150 ˚C.

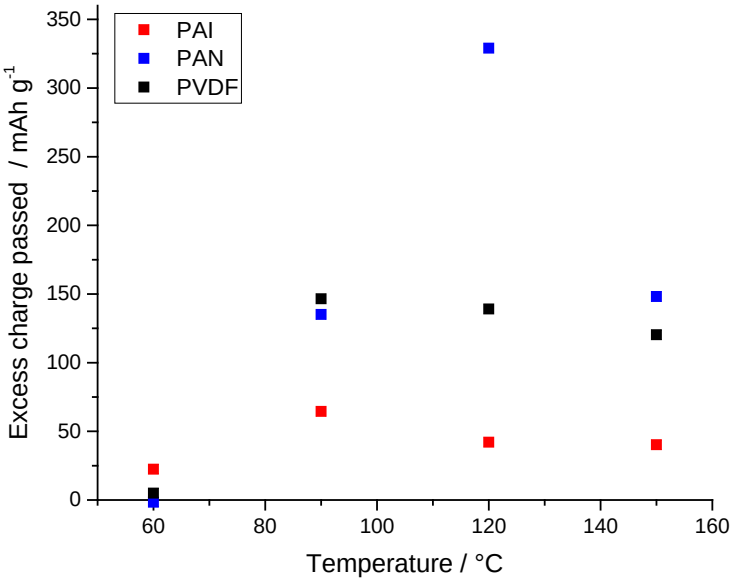

Figure 5-6 Plot showing the excess charge passed for cycle 1 of the charge cycle for cells cycled with binders PAN, PAI and PVDF at 60, 90, 120 and 150 ˚C.

5.5.2 Specific Discharge Capacity

Figure 5-7 shows the plots of the specific discharge capacity vs cycle number for the galvanostatic cycling for the three binders, it is observed that there is significant differences between the binders as the temperature increases. In chapter 3 it was observed that PAN had better capacity retention compared to PVDF when used in graphite electrodes at 60 ˚C, this was attributed to a better thermal and mechanical stability compared to PVDF binder. It can be seen from Figure 5-7 that at 60 ˚C that PAN has a higher capacity retention on cycling compared to PVDF and PAI. However, when the temperature is increased to 90 ˚C PAN shows lower discharge capacities on cycling compared to PVDF and PAI, this trend is also observed at 120 and 150 ˚C.

It is observed that at 90, 120 and 150 ˚C PAI outperforms PVDF and PAN with higher discharge capacities observed for PAI over 102 cycles at 90, 120 and 150 ˚C. The TGA and DSC traces shown in section 5.4 show that PAI is stable to a temperature of greater than 400 ˚C. Studies of PAI have also shown that PAI possess high mechanical stability due to the chemical interactions between the amide and imide units in the polymer. Hydrogen bonding occurs between the amide groups and intermolecular interactions occur between the imide groups in the polymer increase the mechanical stability.[131,134] The high mechanical stability of PAI has been used to increase the stability of silicon electrodes by *Choi et al*[135]. It shown that PAI is much more stable on cycling than PVDF with silicon, due to the fact that the PAI is able to maintain the mechanical stability of the electrode. *Morishita et al*[131] showed that NMC with PAI binder performed much better than that of NMC with PVDF binder when cycled at 60 ˚C. The mechanical properties of the PAI and PVDF were compared and it was shown that the tensile strength, elongation and elastic modulus were all higher for PAI compared for PVDF at 100 ˚C for 10 hours.

It was observed in section 5.4 that PVDF softens in the region of 120 to 150 ˚C, this would then cause contact losses between the lithium iron phosphate particles, carbon black and the electrode surface. In section 5.4 it was also observed that PAN doesn't start to decompose until around 275 ˚C and the DSC trace did not show any noticeable melting or softening occurring. This doesn't explain why such poor first cycle charge capacities and poor capacity retention on cycling at temperatures 90 ˚C and above. The poor performance of PAN at temperatures 90 ˚C and above could be down to the fact that EC is a strong polar solvent which has the ability to dissolve PAN.[162] However literature[163] has also shown that is EC is a plasticiser towards PAN, with *Flora et al* using EC as a plasticiser in a Li-ion polymer electrolyte. Other authors have also used EC as a component of polymer electrolytes[164,165] means that an electrolyte consisting primarily of EC would dissolve/

plasticise the PAN in the electrodes so when the PAN is subjected to higher temperatures there is contact losses with the electrode materials with more PAN dissolving.

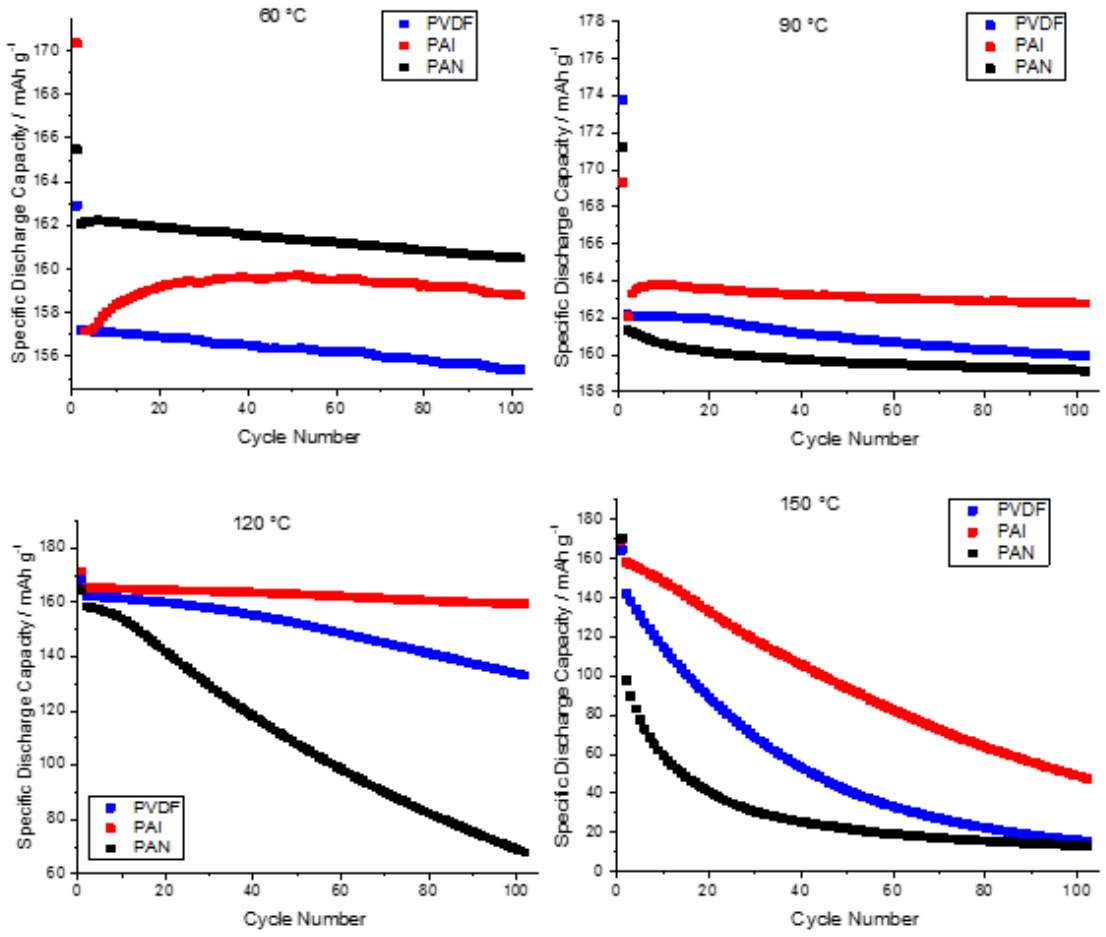

Figure 5-7 Specific discharge capacity vs cycle number plots for cells cycled with binders PAN, PAI and PVDF at 60, 90, 120 and 150 ˚C.

5.5.3 Irreversible Capacity

Figure 5-8 and Figure 5-9 show the irreversible capacity loss on cycling of the cells with PAN, PAI and PVDF at 60, 90, 120 and 150 ˚C. Figure 5-8 shows the first cycle irreversible capacity plots vs temperature as can be seen from the plot at 60 ˚C the first cycle irreversible capacity is low for all three binders in order of largest to smallest is PAI > PVDF > PAN, however the differences at this temperature are negligible. As was seen above in Figure 5-7 PAN has a larger discharge capacity on cycling at 60 ˚C, looking at Figure 5-9 it can be seen that on long term cycling PAN has a lower irreversible capacity than PVDF, however PAI has the lowest of the binders after cycle 2 at 60 ˚C. At 90 ˚C and above PAI has the lowest irreversible capacity on first cycle with PVDF and PAN having much higher irreversible capacities, as seen in Figure 5-8. On long term cycling at 90 and 120 ˚C PAI has the lowest irreversible capacity, however at 150 ˚C it has the largest irreversible capacity of all three binders despite having a much better discharge capacity as seen in Figure 5-7. At 150 ˚C, the irreversible capacities are all very similar to each other after cycle 2. What is apparent from these observations is that the first charge discharge cycle appears to influence the long-term cycling stability at elevated temperatures. Where a large irreversible first cycle capacity is observed the long-term cycling stability is much decreased than compared to one with a much lower first cycle irreversible capacity.

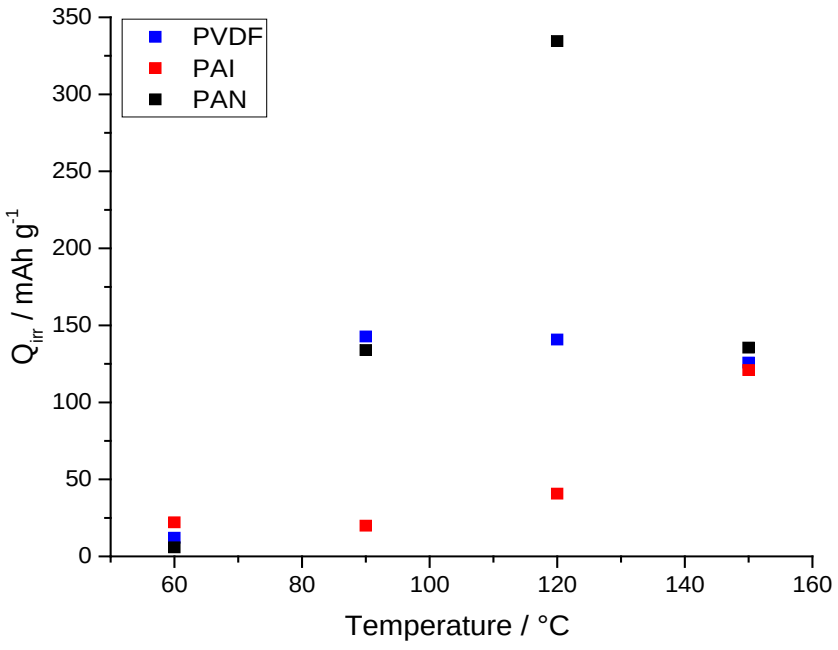

Figure 5-8 Irreversible capacity vs temperature for cycle 1 for cells cycled with binders PAN, PAI and PVDF.

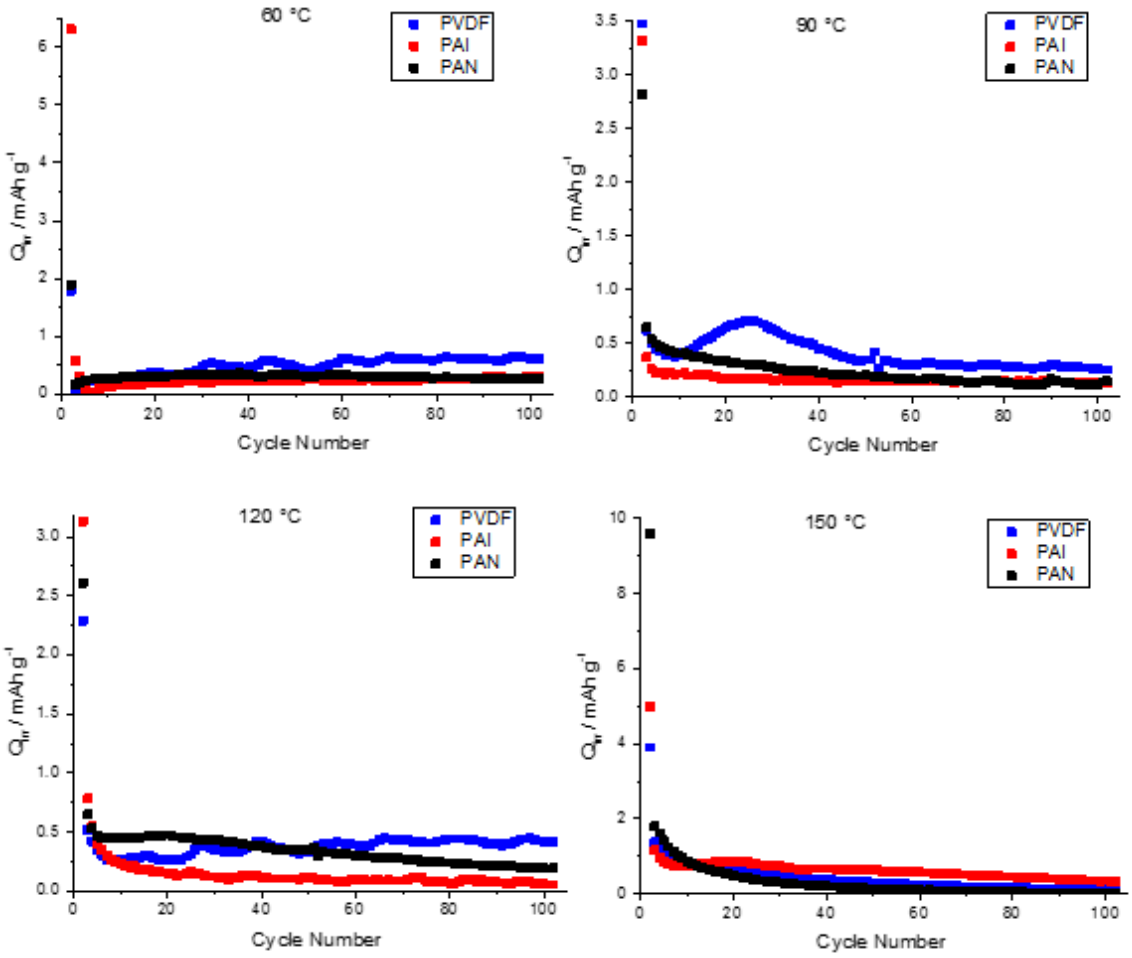

Figure 5-9 Irreversible capacity vs cycle number for cells cycled with binders PAN, PAI and PVDF at 60, 90, 120 and 150 ˚C.

5.5.4 Coulombic Efficiency

Figure 5-10 and Figure 5-11 show the coulombic efficiency on cycling of the cells with PAN, PAI and PVDF at 60, 90, 120 and 150 ˚C. Figure 5-10 shows the coulombic efficiency for the first cycles with temperature. It can be seen that for 60 ˚C the highest coulombic efficiency seen is for PAN, this ties up with the higher discharge capacities and lower irreversible capacities observed at this temperature. At 90, 120 and 150 ˚C the coulombic efficiencies are much higher than those of both PVDF and PAI, this is reflected in the higher discharge capacities seen in Figure 5-7. The lowest coulombic efficiencies observed are for PAN which are reflected by the lower discharge capacities observed in Figure 5-7. The largest differences in coulombic efficiency are observed at 90 and 120 ˚C, this is where the PAI seems to have the largest impact in terms of performance is observed. This is particularly the case at 120 ˚C where there are huge differences in the discharge capacities on long term cycling are observed, at this point the binder choice is having a significant impact.

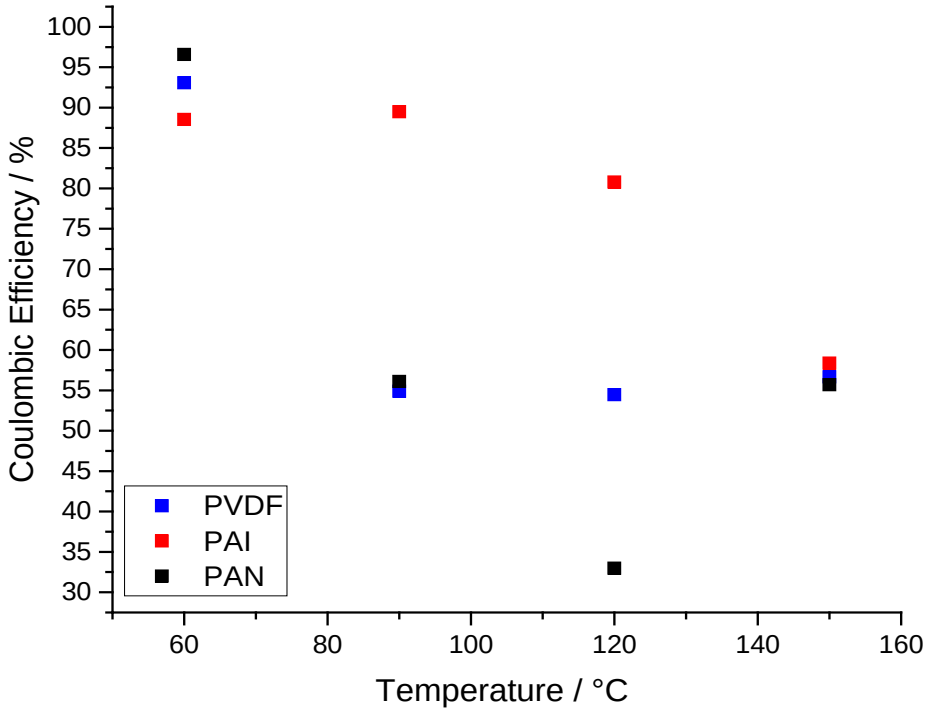

Figure 5-10 Coulombic efficiency vs temperature for cycle 1 for cells cycled with binders PAN, PAI and PVDF.

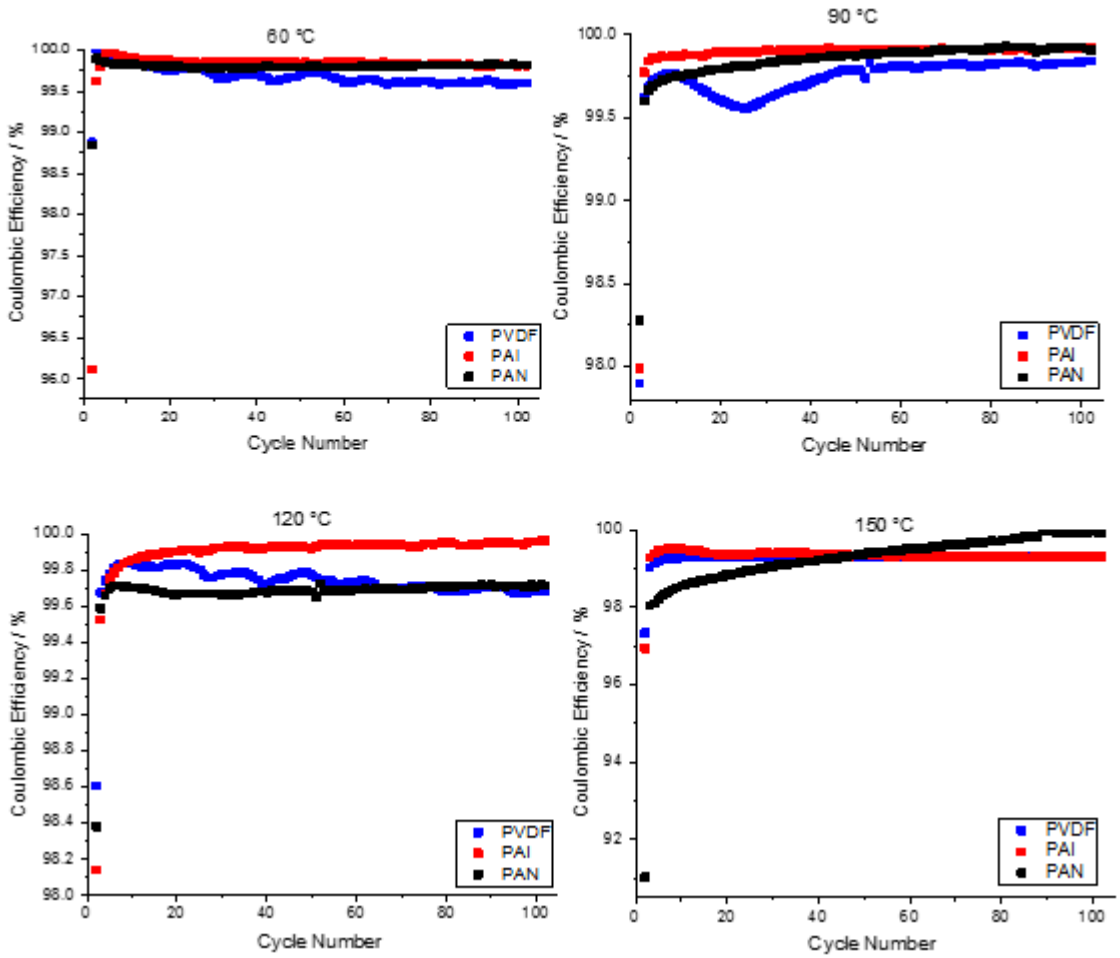

Figure 5-11 Coulombic efficiency vs cycle number for cells cycled with binders PAN, PAI and PVDF at 60, 90, 120 and 150 ˚C.

5.5.5 Overall Comparison

Table 5-1 shows the summary of the specific discharge capacities for cells cycled with three different binders PVDF, PAI and PAN at temperatures of 60, 90, 120 and 150 ˚C. The table also details the capacity retention after 100 cycles. It can be seen that at 60 ˚C the most suitable binder is PAN since the capacity retention after 100 cycles is 98% compared to 95% observed for PVDF and 94% for PAI. This was seen in the case for PAN in chapter 3 where graphite and hard carbon electrodes had much better capacity retention compared to PVDF at 60 ˚C. At 90 ˚C and above PAI outperforms PVDF and PAN. At 90 ˚C PAI has a capacity retention of 96% compared to 92% for PVDF and 93% for PAN after 100 cycles, at this temperature the binder only appears to have a small impact on the long-term stability. However, at 120 and 150 ˚C this impact is much stronger showing much more influence of the binder on high temperature performance. At 120 ˚C PAI has a 93% capacity retention compared to 42% for PAN and 80% for PVDF. At 150 ˚C PAI has a 29% capacity retention compared to 8% for PAN and 10% for PVDF.

At 120 ˚C PVDF also performs relatively well showing an 80% capacity retention after 100 cycles, however at 150 ˚C this performance decreases rapidly to 10%. This is down to the fact that it was observed in the DSC that PVDF is likely to be softening at this temperature which would compromise the electrode mechanical stability. This would cause contact losses with the electrode surface and reactions of the electrolyte with the electrode materials for example the aluminium foil and carbons leading to rapid capacity fade. At 150 ˚C even the capacity fade for PAI increases rapidly from 93% at 120 ˚C to 29% at 150 ˚C. It is likely at this temperature that there is significant reactions at the electrode/ electrolyte interface for example electrolyte breakdown leading to large capacity fade.

Further work should look the reproducibility of these experiments in order to determine the significant effects of binders on high temperature performance, which should include the use of full lithium-ion pouch cells.

Table 5-1 Summary table showing specific discharge capacity for cells cycled with binders PAN, PAI and PVDF at 60, 90, 120 and 150 ˚C.

	60 °C			90 °C			120 °C			150 °C		
Cycle	**PVDF**	**PAN**	**PAI**	**PVDF**	**PAN**	**PAI**	**PVDF**	**PAN**	**PAI**	**PVDF**	**PAN**	**PAI**
1	163	165	170	174	171	169	168	165	171	165	170	170
2	157	162	156	162	161	162	162	159	165	142	98	158
3	157	162	157	162	161	163	162	158	165	138	90	157
4	157	162	157	162	161	164	162	158	165	134	83	156
5	157	162	157	162	161	164	162	157	165	131	78	155
6	157	162	158	162	161	164	162	157	165	127	73	154
7	157	162	158	162	161	164	162	156	165	124	69	152
8	157	162	158	162	161	164	162	156	165	121	65	151
9	157	162	158	162	161	164	162	155	165	118	62	150
10	157	162	158	162	161	164	161	154	165	115	59	148
20	157	162	159	162	160	164	160	142	164	89	41	133
30	157	162	159	162	160	163	158	129	164	69	31	118
40	157	162	159	161	160	163	155	118	164	53	25	106
50	156	161	159	161	160	163	152	108	163	42	22	94
60	156	161	159	161	160	163	149	99	162	33	19	83
70	156	161	159	160	159	163	145	90	161	27	17	73
80	156	161	159	160	159	163	141	82	161	22	16	64
90	156	161	159	160	159	163	137	75	160	19	14	56
100	155	161	159	160	159	163	134	69	159	16	13	49
Capacity retention %	95	98	94	92	93	96	80	42	93	10	8	29

5.6 Conclusions

This chapter studied the effect of binders (PVDF 5130, PAI and PAN) on the cycling performance of lithium iron phosphate cells at elevated temperatures (60, 90, 120 and 150 ˚C) using the best performing electrolyte investigated in chapter 4 (1M LiODFB in EC). Results showed that at 60 ˚C PAN had the best capacity retention on cycling compared to both PVDF and PAI. These results agree with the observations in chapter 3 where it was shown that PAN had a much better capacity retention at 60 ˚C with graphite half cells compared to PVDF. However, at 90 ˚C and above PAI had the best capacity retention on cycling compared with both PVDF and PAN, with PAN showing rapid capacity fade particularly at 120 and 150 ˚C. It is observed that at 90, 120 and 150 ˚C PAI outperforms PVDF and PAN with higher discharge capacities observed for PAI over 102 cycles at 90, 120 and 150 ˚C. The TGA and DSC traces shown in section 5.4 show that PAI is stable to a temperature of greater than 400 ˚C. Studies of PAI have also shown that PAI possess high mechanical stability due to the chemical interactions between the amide and imide units in the polymer. Hydrogen bonding occurs between the amide groups and intermolecular interactions occur between the imide groups in the polymer increase the mechanical stability.[131,134] It was observed in section 5.4 that PVDF softens in the region of 120 to 150 ˚C, this would then cause contact losses between the lithium iron phosphate particles and the carbon black and also the particles on electrode surface. This would lead to conductivity problems and lead to reactions between the electrolyte and the aluminium current collector and the carbon black, causing a decline in capacity. In section 5.4 it was also observed that PAN doesn't start to decompose until around 275 ˚C and the DSC trace did not show any noticeable melting or softening occurring. The poor performance of PAN at temperatures 90 ˚C and above could be down to the fact that EC is a strong polar solvent which has the ability to dissolve PAN.[162] However literature[163] has also shown that is EC is a plasticiser towards PAN, this means that an electrolyte consisting primarily of EC would dissolve/ plasticise the PAN in the electrodes so when the PAN is subjected to higher temperatures there is contact losses with the electrode materials with more PAN dissolving.

Chapter 6 Corrosion of the Aluminium Current Collector at Elevated Temperatures

6.1 Introduction

In chapter 5 the role of binders on the high temperature galvanostatic cycling of lithium iron phosphate electrodes was investigated. Results showed that PVDF was susceptible to melting in the region of 120 to 150 ^{o}C which lead to a large irreversible capacity on the first cycle and lead to a rapid capacity fade on cycling. It was believed that the softening of PVDF was compromising the mechanical stability of the electrode surface which could cause the following effects:

1. The exposure of the electrode particles and conductive carbon, the electrolyte could then react with these causing side reactions between the electrode materials and the electrolyte.
2. The exposure of the aluminium current collector, the electrolyte could then penetrate the aluminium current collector, causing corrosion of the aluminium.

The effect can be particularly seen in the first charge cycle, which can be seen in Figure 6-1 showing a potential vs capacity plot for lithium iron phosphate with PVDF binder cycled at C/10 at 120 ^{o}C using 1M LiODFB in EC. It can be seen that at 0.45 V vs $Li_{0.5}FePO_4$ the cell is already at the theoretical capacity of 170 mAh g^{-1} due to the increased kinetics of lithium transfer at 120 ^{o}C. The excess charge that is passed on this first cycle is not that of lithium de-insertion but of side reactions occurring at the electrode/ electrolyte interface. It can be seen in Figure 6-1 that there is the presence of an extra plateaux after 0.45 V vs $Li_{0.5}FePO_4$, at this point the reactions occurring at the electrode surface have gone from passive to active, this continues to around 0.75 V vs $Li_{0.5}FePO_4$ by where after that the reactions then go passive again. These passive and active regions are typical of corrosion processes and therefore it is believed that aluminium current collector corrosion is a major cause of the irreversible capacity loss on the first cycle and also capacity fade on cycling. While knowledge on corrosion of metals in aqueous media is well studied the corrosion of metals in non-aqueous media is not as well understood. In particular that of the corrosion of battery current collectors is even less studied since most work concentrates on the study of the electrode/ electrolyte interface and not that of the current collector/ electrolyte interface.[166] Considering the

fact that the current collector is responsible for 90 % of the electronic conductivity and mechanical stability of the electrode, the study of this important battery component is poorly understood.[167]

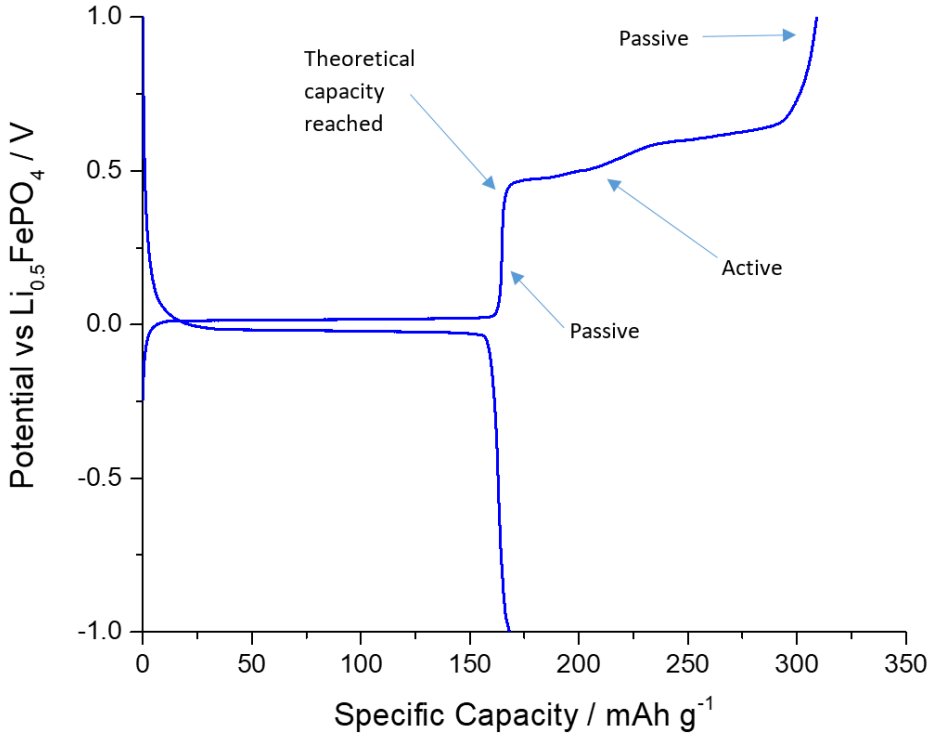

Figure 6-1 Potential vs Specific discharge capacity for cycle 1 for lithium iron phosphate electrodes made using PVDF binder at 120 ˚C showing the passive and active reactions occurring during the charge cycle.

Corrosion occurs when a metal is oxidised, releasing electrons in the process, according to equation 1-6:

$M \rightarrow M^{n+} + ne^-$ Equation 6-1

Aluminium is a metal which forms a natural passivation layer of Al_2O_3 on its surface, this layer forms instantaneously on the exposure of the fresh Al to the atmosphere, the role of this is to act as a passivation layer in order to protect the surface of aluminium from further corrosion. This layer is usually a few nm thick.[168]

The aluminium current collector used in lithium ion battery positive electrodes isn't stable with respect to the electrolyte, however the surface of the aluminium current collector is passivated by the $LiPF_6$ in the electrolyte. $LiPF_6$ is used because it improves the corrosion resistance of the aluminium current collector, literature shows that $LiPF_6$ forms both Al_2O_3 and AlF_3 layers on aluminium current collectors to passivate them.[50–55] However the passivation layer formed by the lithium salt can fail under extreme conditions such as elevated temperatures leading to the corrosion of the aluminium current collector.[169] Aluminium current collector corrosion has been investigated in the literature by *Sayed et al* [170] *Ma et al*[171], *Krämer et al* , *Mun et al*[54] and *Braithwaite et al*[169] with the work by *Sayed et al* focussing on the corrosion and passivation of current collectors at high temperatures. However, this study investigated the use of LiTFSI as the lithium salt and an ionic liquid (PIP-TFSI) as the electrolyte solvent, so this study isn't comparable with the system being investigated in this study. Another study by *Mun et al*[54] also investigates the effect of temperature on aluminium corrosion but again this study investigates the use of ionic liquids as the electrolyte solvent, however the effect of different electrolyte salts (LiTFSI, LiBETI, $LiPF_6$, $LiBF_4$) is also investigated. *Ma et al*[171] have investigated the corrosion of aluminium with 1.2M $LiPF_6$ in EC/ EMC at room temperature and proposed a mechanism for the process. Contrary to what is widely believed in the literature that $LiPF_6$ breaks down to produce HF which then converts the Al_2O_3 to AlF_3 to passivate the aluminium, it is believed that it is in fact the solvent molecules which are involved in the process. It is believed that EC can electrochemically oxidise to produce H^+ ions which then react with the Al_2O_3 leaving the aluminium surface prone to further oxidation.

This chapter will investigate the effect of temperature on the corrosion of the aluminium current collector using incremental potential staircase tests used in the literature by *Ma et al*[171] and then analysing the aluminium foils using SEM coupled with EDX analysis. The other technique used to assess the corrosion is constant current charging to assess the excess charge passed on the first charge cycle.

6.2 Aims and Objectives

The aims of this chapter were:

To investigate the role of the aluminium current collector in the capacity loss at elevated temperatures.

The objectives of this chapter were:

To understand and characterise the mechanisms that lead to the corrosion of the aluminium current collector at elevated temperatures.

6.3 Experimental Details

To assess the corrosion of the aluminium current collectors two methods were used. The first method used was an incremental potential staircase test used in the literature by *Ma et al*[171], the method is as follows:

1. Swagelok cells were fabricated using an aluminium foil, two glass fibre separators soaked with 1M LiODFB in EC and a lithium metal foil disk.
2. Cells were then put into ovens at 60, 90, 120 and 150 ^{o}C and heated for 1 hour.
3. The cells were then charged to 3.6 V vs Li/Li^{+} using a constant current of 0.024 mA (as per the method by *Ma et al* [171])
4. The cells were then held at a constant potential for 10 hours and the current was recorded.
5. This process was then repeated in 0.1V vs Li/Li^{+} increments to a potential of 4.5 V vs Li/Li^{+}.

The voltage and current profiles were then evaluated for the constant potential steps using a parabolic rate law relationship. The cells were then disassembled and the aluminium disks were then washed with ethanol to remove electrolyte and dried overnight under vacuum (Buchi drying oven < 4 x 10^{-1} mBar 80 ˚C). The aluminium disks were then imaged using SEM coupled with EDX to look for aluminium corrosion.

The second method the constant current charging experiment uses a constant current of 0.04 mA to charge the aluminium and carbon coated aluminium half cells to 3.8 V vs Li/Li^{+}. A current of 0.04 mA was chosen since this was the average current used to charge the lithium iron phosphate cells at a C-rate of C/10 during galvanostatic cycling. Carbon coated aluminium foil was made using the ink method as described in chapter 2 using 12% PVDF as the binder. To compare the effect of temperature on aluminium foil and carbon coated aluminium foil, the charge (mAh) was evaluated for the aluminium and carbon coated aluminium. This was then compared with that of the lithium iron phosphate, to allow a comparison of aluminium and carbon coated aluminium, both which don't have any lithium storage capacity, the theoretical capacity (170 mAh g^{-1}) was subtracted from the lithium iron phosphate charge. This then only gave the charge associated with contribution of the side reactions i.e. the corrosion rather than any charge associated with that of lithium storage in the lithium iron phosphate.

6.4 Results from Incremental Potential Staircase Tests

Figure 6-2 to Figure 6-9 show the voltage and current profiles for the incremental potential staircase tests between 3.6 V to 4.5 V at 60, 90, 120 and 150 ˚C. It is observed at 60 ^{o}C, seen in Figure 6-2 and Figure 6-3, that there is an initial increase in the current followed by a decay, with Figure 6-3 showing this in detail for the case of an applied potential of 3.6V. Integration of the current with time gives the total charge associated to the formation of the passivation layer on the aluminium surface. The subsequent voltage steps (3.7 to 4.5 V) show very low current which shows that the initial 3.6 V step is sufficient to give an appropriate passivation layer. The charge passed during the constant potential steps can be seen clearer in Figure 6-10 by where it can be seen that there is an initially high charge associated with the corrosion/ passivation step at 3.6 V followed by a much lower charge on subsequent potential steps.

The effect of temperature can start to be seen at 90 ˚C, seen in Figure 6-4 and Figure 6-5. It is observed that just like at 60 ˚C, there is a passivation of the aluminium surface at 3.6 V, seen in Figure 6-5. It can be seen that the current at 90 ˚C, observed by the greater area under the curve in Figure 6-5 suggesting a higher degree of aluminium oxide formed on the aluminium surface. It can also be seen that the charge passed during the potential hold steps are higher for 90 ˚C compared to of that of 60 ˚C, seen in Figure 6-10. This suggests that there is corrosion events occurring at 90 ˚C, this becomes more evident from 4.0 V to 4.5 V where the charge during the potential hold steps increases with increasing temperature. It is observed in Figure 6-4 that for 4.4 V and 4.5 V that there is current spiking during the constant potential steps suggesting that corrosion is significant during these steps.

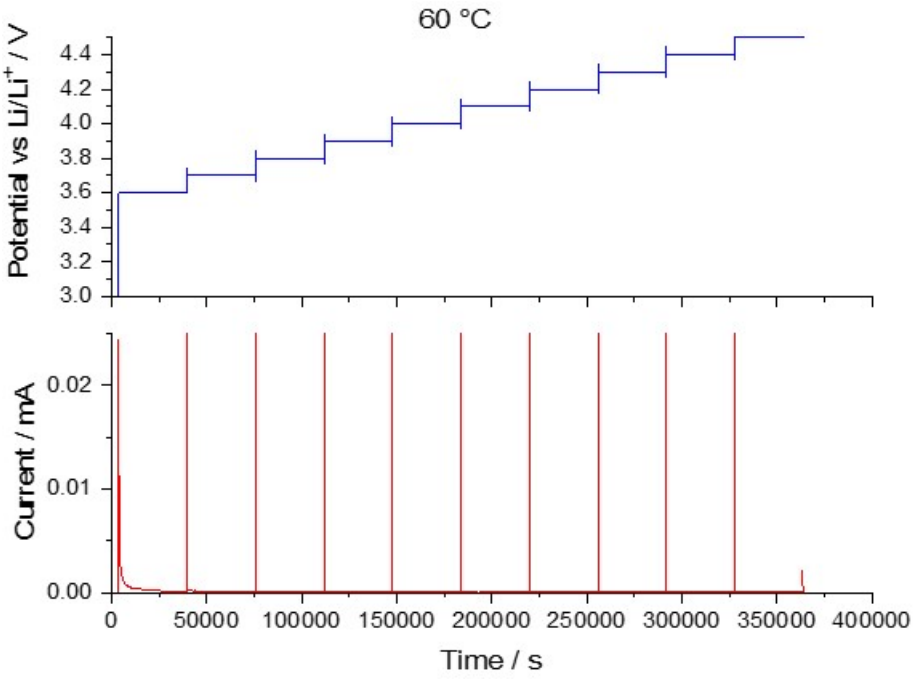

Figure 6-2 Voltage and current profile for the incremental potential staircase experiment at 60 ˚C.

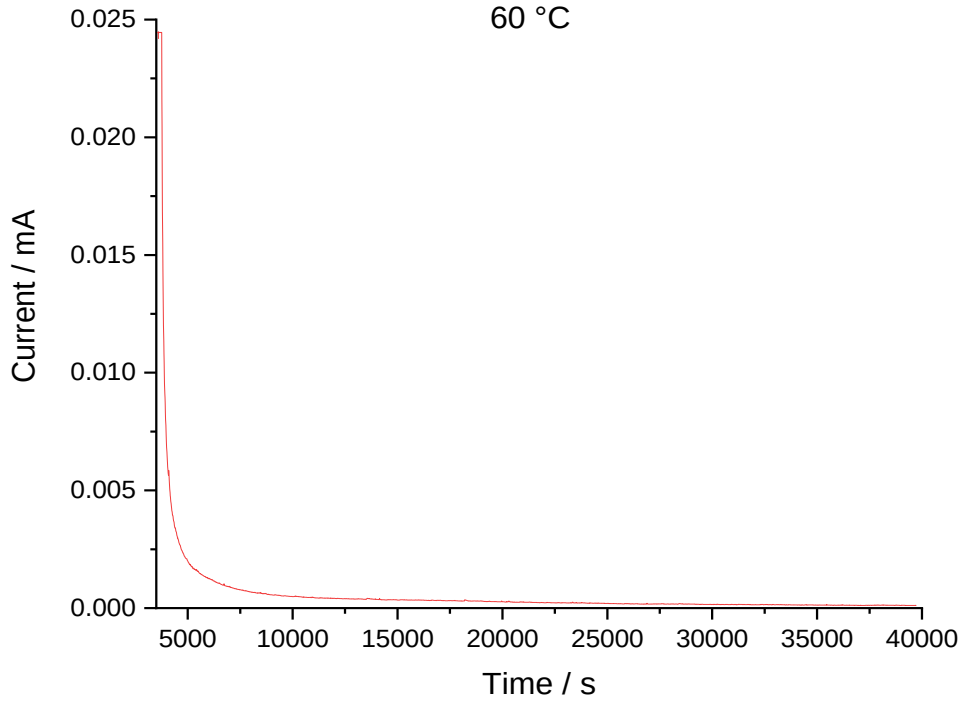

Figure 6-3 Current profile at 3.6 V for the incremental potential staircase experiment at 60 ˚C.

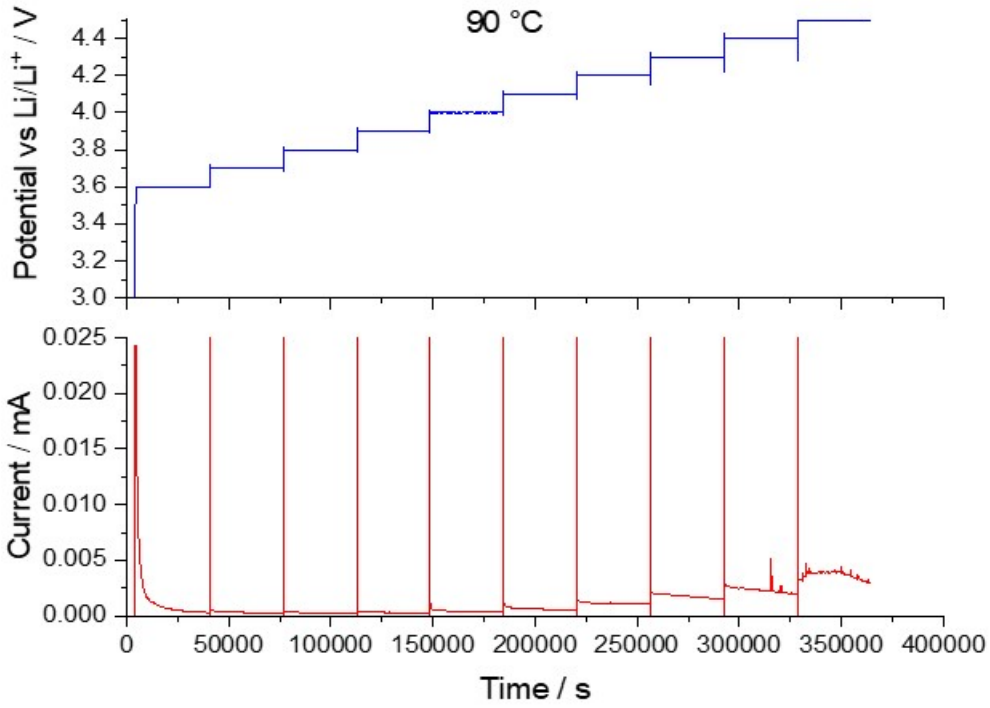

Figure 6-4 Voltage and current profile for the incremental potential staircase experiment at 90 ˚C.

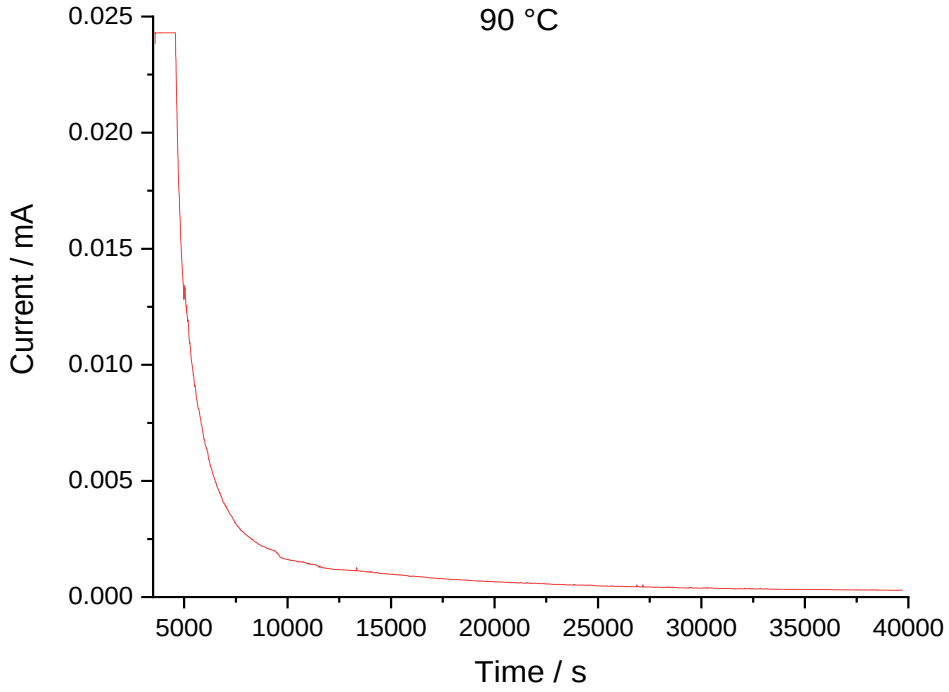

Figure 6-5 Current profile at 3.6 V for the incremental potential staircase experiment at 90 ˚C.

It can be seen at 120 ˚C that the measured current values are much larger than seen at both 90 and 60 ˚C, as can be seen in Figure 6-6 and Figure 6-7. It can be seen that at 3.6 V the current for the constant potential step is much higher and there appears to be some corrosion occurring during this step, because there is a current spike followed by a current relaxation. There also appears to be significant corrosion occurring between 3.8 V and 4.5 V since the current remains high during the potential hold steps, signifying significant corrosion occurring. Figure 6-10 shows that after 3.7 V the total charge passed increases with potential until; 4.2 V by where after this it starts to decrease again.

This effect of temperature on the corrosion is even more apparent at 150 ˚C, seen in Figure 6-8 and Figure 6-9. It is observed in Figure 6-9 that the constant current step to reach 3.6 V takes much longer at 150 ˚C than the other temperatures and it is observed that the current during the constant potential step is also much higher than the other potentials. This suggests that corrosion during this initial step is occurring since much more current is passed. The higher value of current at higher temperatures could be due to a thicker aluminium oxide coating being formed. The higher value of current could also be due to electrolyte decomposition, which might compete or occur simultaneously with the oxidation of aluminium to form the aluminium oxide passivating layer. The passivation at this high temperature is not stable, since it is observed that at higher potentials, particularly between 3.8 V and 4.0 V there is a massive increase in the current which equates to a series of corrosion events, something which is confirmed via SEM and EDX in section 6.5. It is very likely that we are seeing more than aluminium corrosion here since electrolyte breakdown is enhanced in the region of 120 and 150 ˚C, this is also confirmed in section 6.5. These results can be compared to the galvanostatic cycling behaviour. It was observed that in chapter 4 that the cells showed an additional charge contribution at ca. 0.4 V vs $Li_{0.5}FePO_4$ or 3.7 V vs Li/Li^+ for 120 ˚C and 0.25 V vs $Li_{0.5}FePO_4$ or 3.85 V vs Li/Li^+. It can be seen that looking at the graphs for 120 and 150 ˚C in Figure 6-10 that the total charge starts to rise at 3.85 V for 120 ˚C and starts to rise after 3.7 V for 150 ˚C, this agrees with the voltages in the galvanostatic cycling for 120 and 150 ˚C.

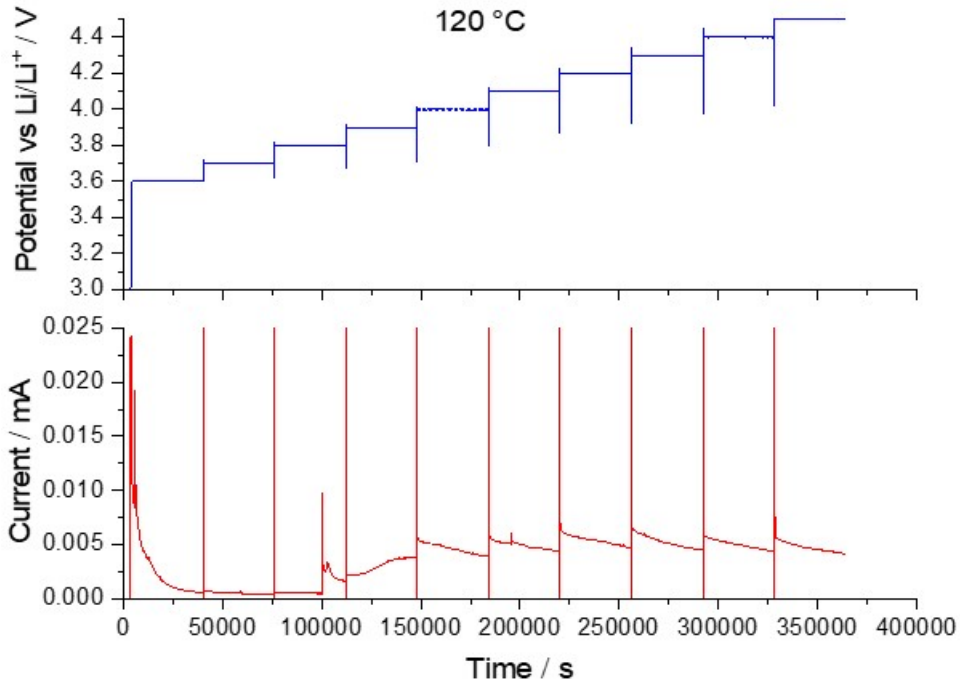

Figure 6-6 Voltage and current profile for the incremental potential staircase experiment at 120 ˚C.

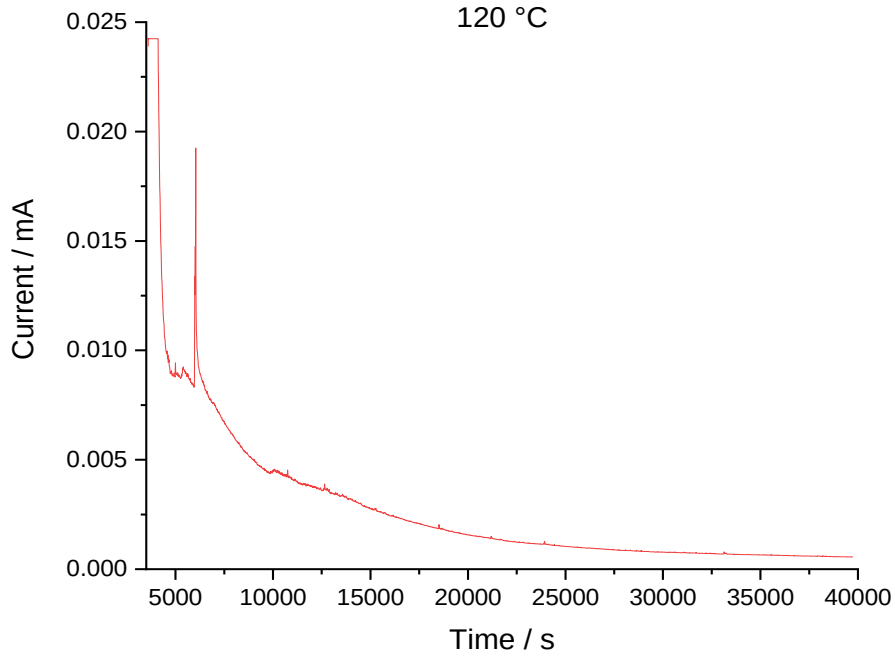

Figure 6-7 Current profile at 3.6 V for the incremental potential staircase experiment at 120 ˚C.

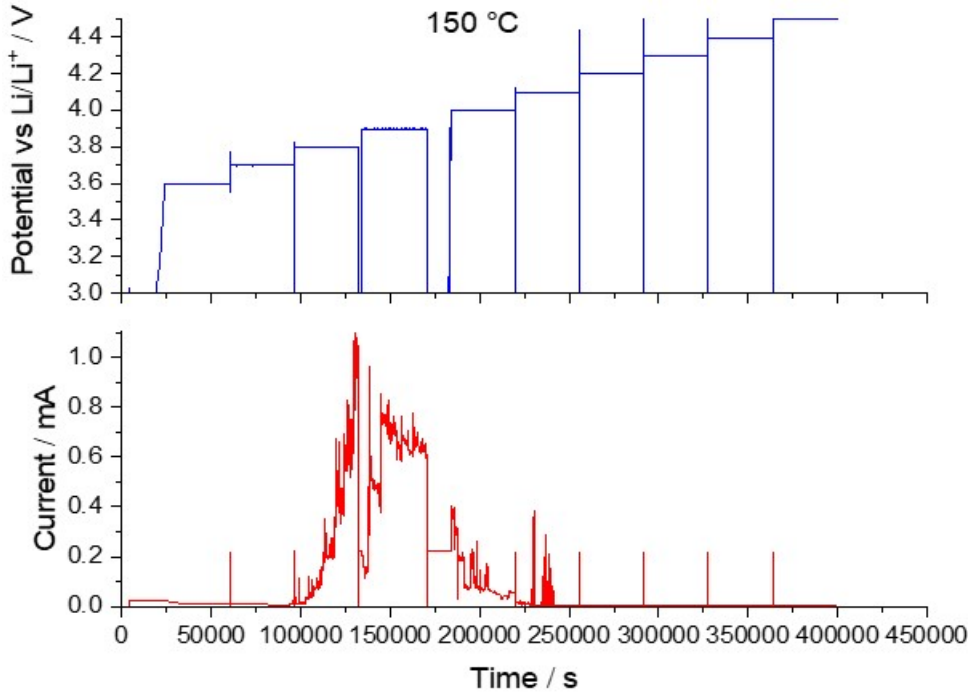

Figure 6-8 Voltage and current profile for the incremental potential staircase experiment at 150 ˚C.

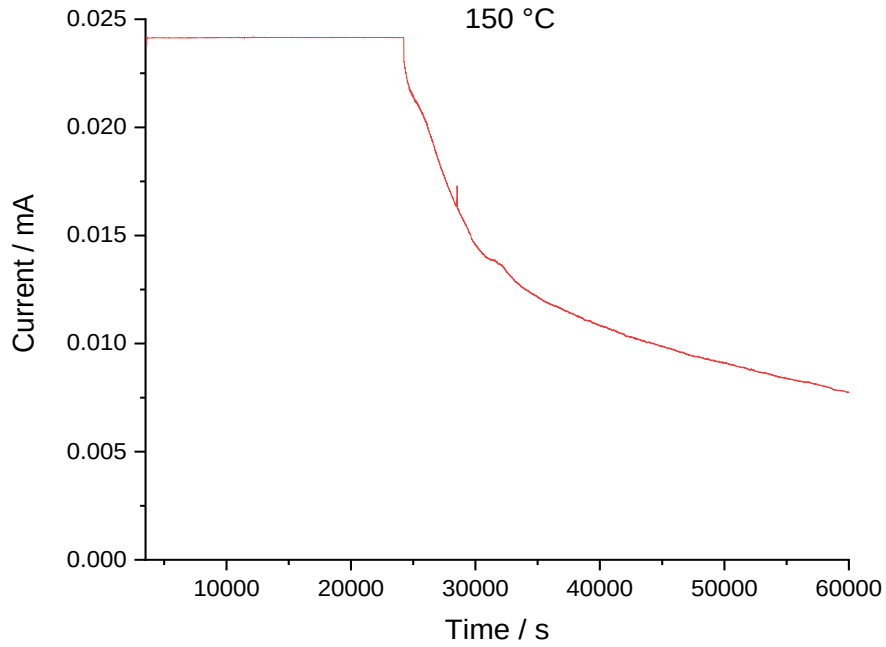

Figure 6-9 Current profile at 3.6 V for the incremental potential staircase experiment at 150 ˚C.

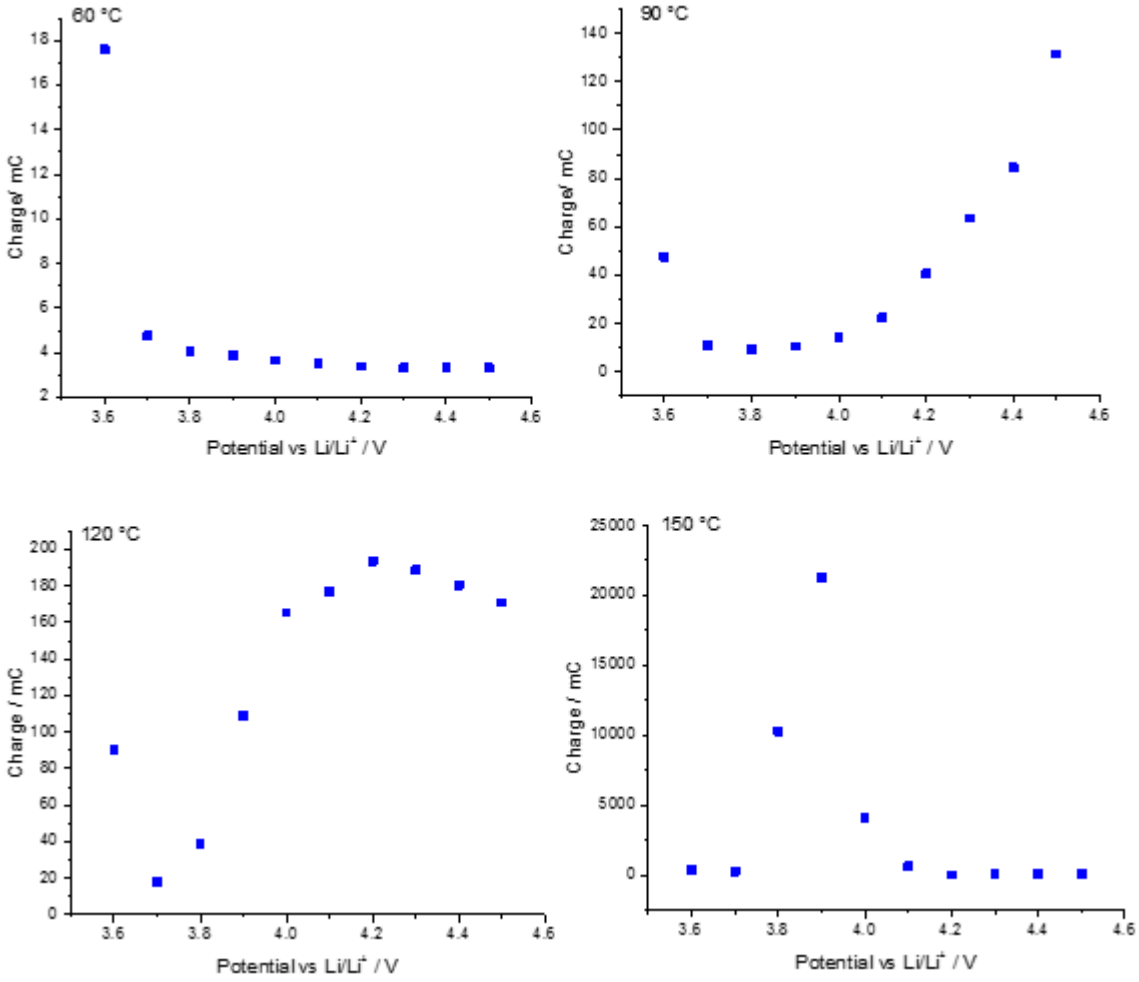

Figure 6-10 Total charge passed during the 10 hour constant potential steps for the incremental potential staircase experiment at 3.6 to 4.5 V at 60, 90, 120 and 150 ˚C.

In order to fully analyse the effect of potential and temperature on the effect of the corrosion of the aluminium current collector a model of parabolic rate law of corrosion and passivation of aluminium can be applied, seen in Equation 6-2.

$$I = [\,0.5\,k\,((t + t_0)^{-0.5})] + i_0 \qquad \text{Equation 6-2}$$

Where:

I = current

t = time

k = parabolic rate law constant

Using a solver fit on excel k, t_0 and i_0 values were used to optimise a fit to the current curve using sum of χ^2 values in order to provide a close fit to the curve as possible in order to determine an accurate k value for the kinetics of the current corrosion. Figure 6-11 shows the results of the fits for the determination of k value fits of the current curves at voltages from 3.6 V to 4.5 V for 60, 90, 120 and 150 ˚C. It is observed that at all temperatures that there is an initial high k values associated with the initial formation of the passivation of the aluminium surface, this value increases with increasing temperature as can be seen in Figure 6-11. It can also be observed that with increasing temperature that the k values for all voltages is higher with higher temperature. At 60 ˚C there is the initially higher k value with a drop to a low k value at increasing potentials, essentially showing that the electrode surface is effectively passivated, however it can be seen that a small corrosion/ passivation event occurs at 4.3 V because the k value increases returning to a low k value after 4.3 V. At 90 ˚C a similar observation is observed than seen at 60 ˚C, by where there is an initial higher k value followed by a small k value, indicating a passivated surface. Again, a spike can be seen at 4.3 V which suggests a corrosion/ passivation event and again at 4.5 V where there is much higher k value than the initial one suggesting a larger corrosion event occurring at 4.5 V. At 120 ˚C again we have an initial passivation of the surface however it can be seen that the k values are up and down, suggesting that the aluminium surface isn't entirely well passivated at this temperature suggesting a many corrosion/ passivation events occurring on the aluminium surface. The image in Figure 6-6 shows that the current plots suggest significant corrosion occurring, something which is confirmed using EDX in section 6.5. It can be seen for 150 ˚C that it appears that the surface initially passivates however at 3.9 V significant increase in k is observed peaking at 4.0 V and decreasing by 4.2 V, this can be observed in Figure 6-8 where it can be seen that there is a large increase in the current. The large spikes in current between 3.9 V and 4.1 V suggest that the surface isn't passivated and corrosion of the aluminium surface occurs.

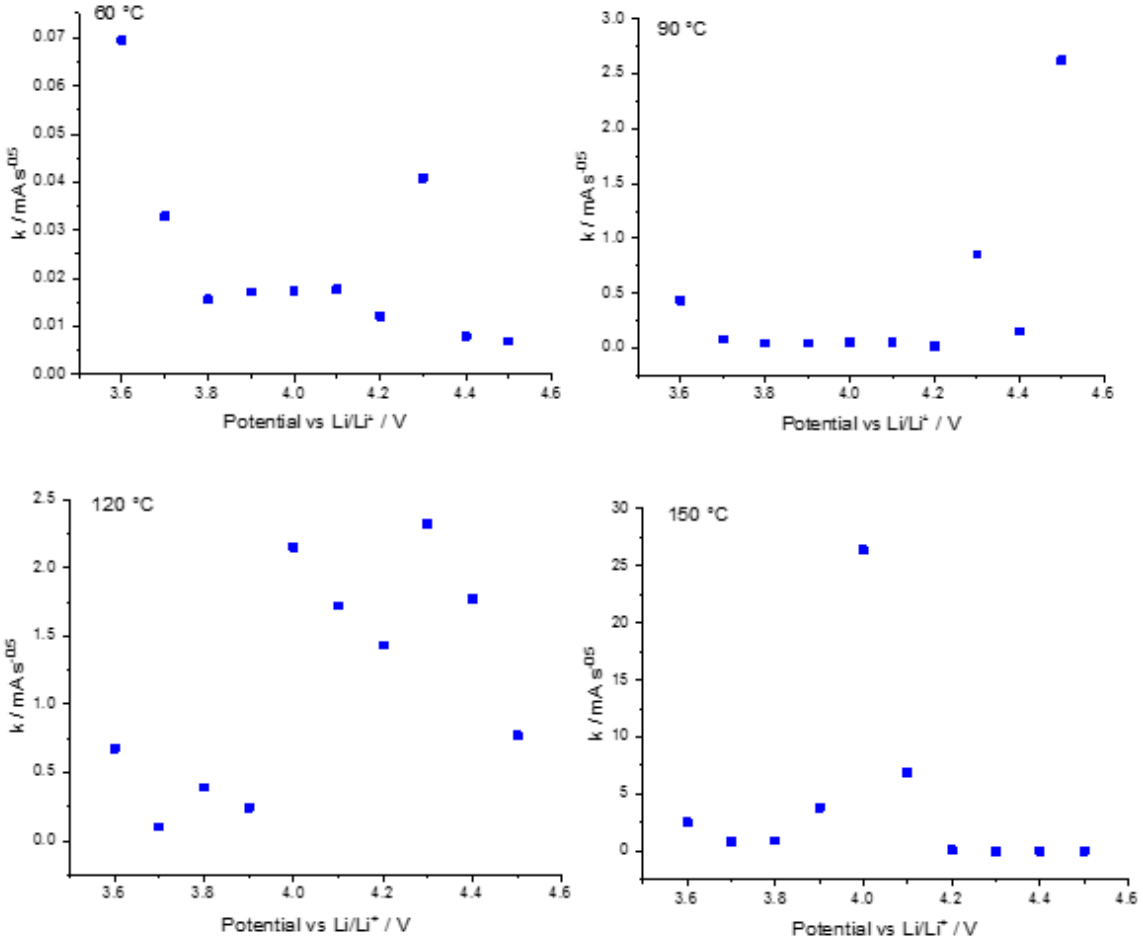

Figure 6-11 Rate constant (k) values obtained from the incremental potential staircase experiment at 3.6 to 4.5 V at 60, 90, 120 and 150 ˚C.

6.5 SEM and EDX Studies of the Aluminium Current Collectors

The following section shows the results from SEM and EDX studies of the aluminium current collectors taken from the cells used during the incremental potential staircase tests study (section 6.4). Work by *Braithwaite et al* [169] showed that aluminium corrosion occurs as localised pitting shown by SEM and used auger maps to prove that Al_2O_3 was forming in the corrosion pits. Work by *Mun et al* [54] showed that pitting corrosion occurs and showed that the formation of oxides was occurring using XPS. The cells used for the incremental potential staircase tests were disassembled and the aluminium foils were washed using ethanol to remove the electrolyte and dried at 80 ˚C prior to mounting onto SEM stubs, the samples were then mounted into the Phillips XL30 ESEM coupled with EDX.

Figure 6-12 to Figure 6-14 show the SEM/ EDX of the aluminium foil before incremental potential staircase testing, it can be seen that the aluminium surface is free of corrosion which can be confirmed by the EDX graphs in Figure 6-13 and Figure 6-14, it can be seen that the main peak in the EDX is that of Al appearing at 1.5 keV, there is also a trace of O at around 0.5 keV, this is due to natural oxidation layer which aluminium has in order to protect it from further oxidation. Two areas of the aluminium were selected a single point and a large area, both showing very similar results showing a large peak and a trace of O corresponding to the thin oxidation layer.

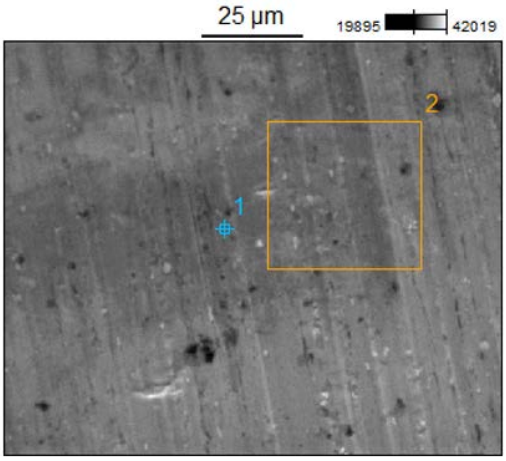

Figure 6-12 SEM image of aluminium foil before incremental potential staircase testing showing the sampling sites for the EDX. 15kv 1000X.

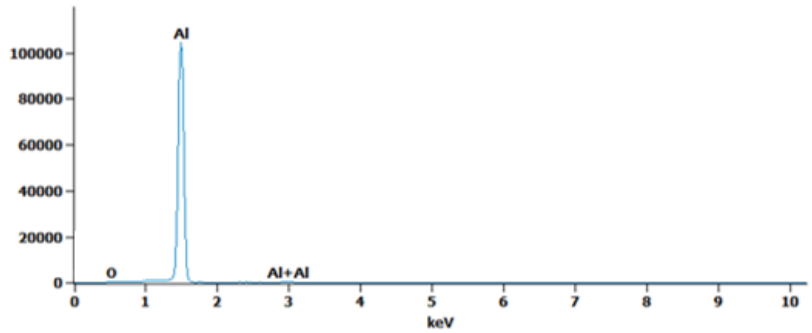

Figure 6-13 EDX site 1 of aluminium foil before incremental potential staircase testing. 15kv 1000X.

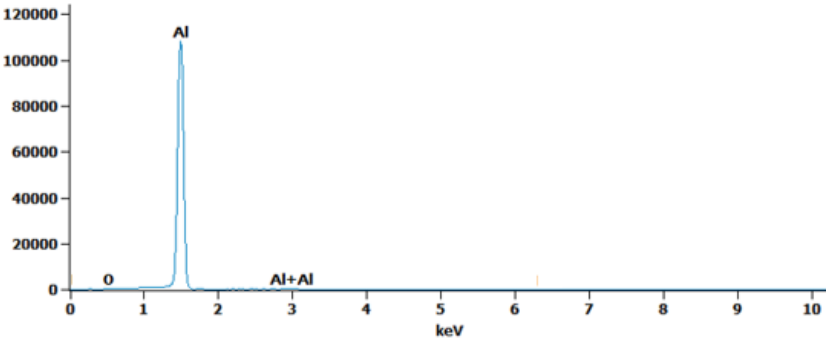

Figure 6-14 EDX site 2 of aluminium foil before incremental potential staircase testing. 15kv 1000X.

Figure 6-15 to Figure 6-18 show the SEM/ EDX of the aluminium corrosion tests at 90 ˚C. It can be seen that at 90 ˚C, that there appears to be significant corrosion of the surface indicated by the dark spots on the surface of the aluminium, there is also a large bright spot on the surface too, suggesting the growth on the surface. This growth on the surface has been analysed using EDX, the results of which are seen in Figure 6-16. It can be seen that the largest peak is O, with significant contributions from C and F, with a much smaller peak for Al than the aluminium surface itself. It is suggested that this is electrolyte breakdown on the surface, which is not surprising since it is expected that there is significant electrolyte breakdown occurring at higher temperatures. Going to spot 2 on the SEM image it can be seen that there appears to be no corrosion of the surface, this is confirmed by Figure 6-17, it can be seen that the O peak is very minimal showing that there is the normal passivation layer present. It can also be seen that there is also F present too, which could very well be the formation of AlF_3 on the surface was has been cited in previous work[50–55], since the electrolyte contains fluorine. Looking at spot 3 on Figure 6-15, it appears that there is corrosion of the aluminium surface. This is confirmed in Figure 6-18 where it is seen that there is the presence

of O and F which suggest again formation of $AlFO_3$, there is also the presence of carbon too which is a likely contribution from electrolyte breakdown. It has been shown that there is significant electrolyte breakdown and aluminium corrosion occurring at 90 ˚C, from the SEM and EDX studies.

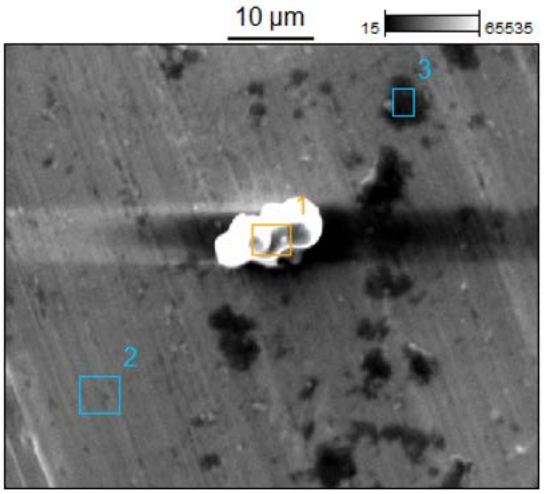

Figure 6-15 SEM image of aluminium foil subjected to incremental potential staircase testing at 90 ˚C showing the sampling sites for the EDX. 10kv 2000X.

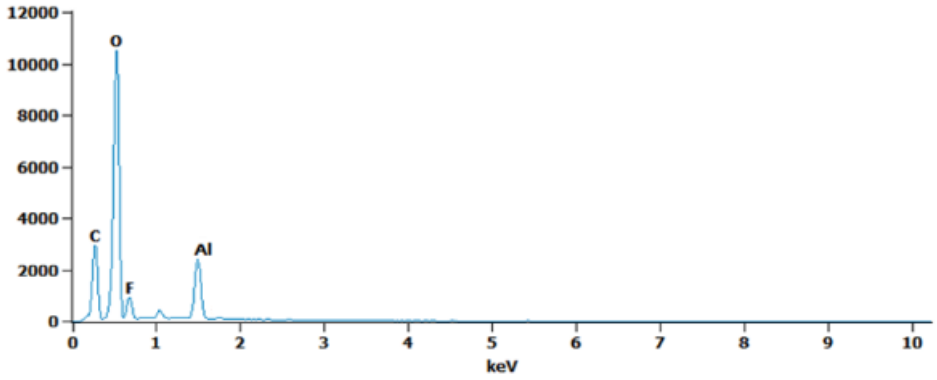

Figure 6-16 EDX site 1 of aluminium foil subjected to incremental potential staircase testing at 90 ˚C. 10kv 2000X.

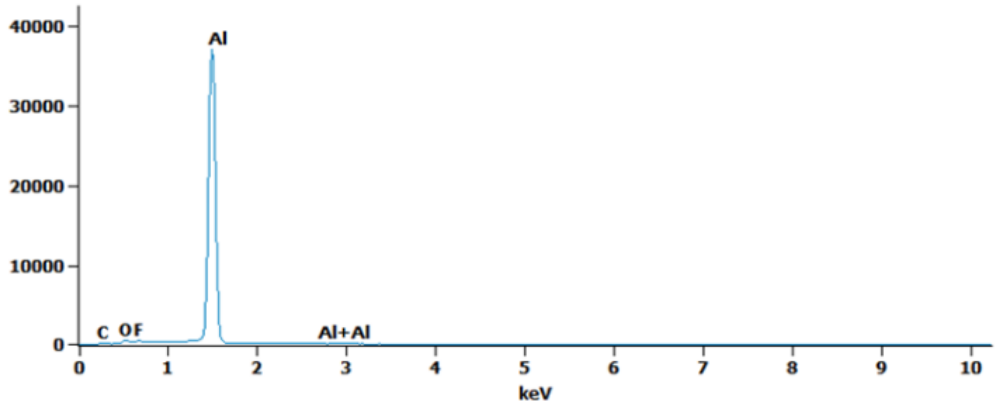

Figure 6-17 EDX site 2 of aluminium foil subjected to incremental potential staircase testing at 90 ˚C. 10kv 2000X.

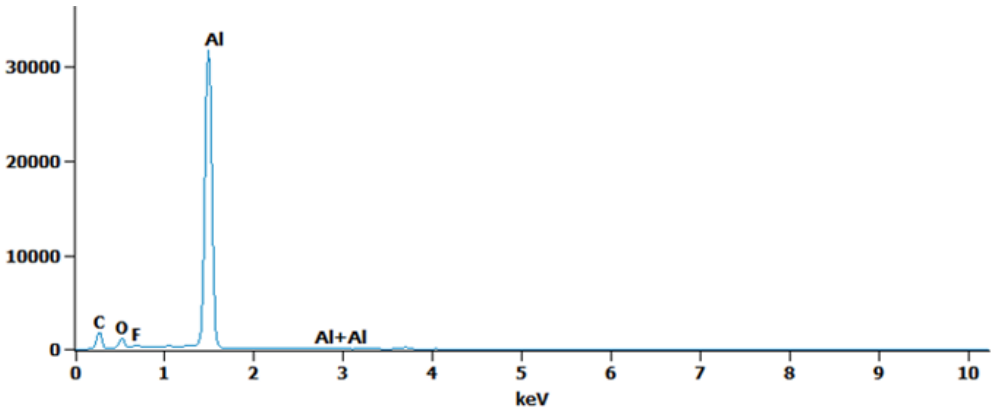

Figure 6-18 EDX site 3 of aluminium foil subjected to incremental potential staircase testing at 90 ˚C. 10kv 2000X.

Figure 6-19 to Figure 6-22 show the SEM/ EDX of the aluminium corrosion tests at 120 ˚C. What is apparent is that there seems to be much more significant corrosion occurring than at 90 ˚C. Again, it can be seen that there is a passivation layer on the aluminium surface seen from site 1, seen in Figure 6-19. Again, it appears that there is the formation of $AlFO_3$ as can be seen by the EDX Figure 6-20, this is clearly a contribution from the electrolyte itself. Looking again at Figure 6-19 it is observed that there are significant growths on the surface, these could either be corrosion or electrolyte breakdown. It can be seen that looking at Figure 6-21 and Figure 6-22 that there are significant contributions from O and F, with a small amount of C. These are likely to be formation of corrosion spots of $AlFO_3$ with electrolyte breakdown, this is the case because it has already been shown that there is electrolyte breakdown is occurring, seen at 90 ^{o}C.

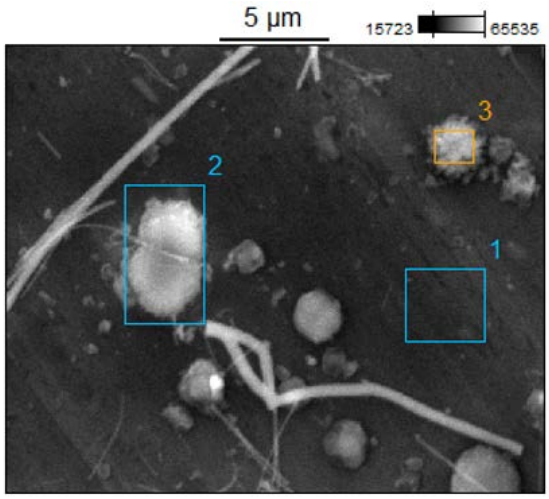

Figure 6-19 SEM image of aluminium foil subjected to incremental potential staircase testing at 120 ˚C showing the sampling sites for the EDX. 15kv 5000X.

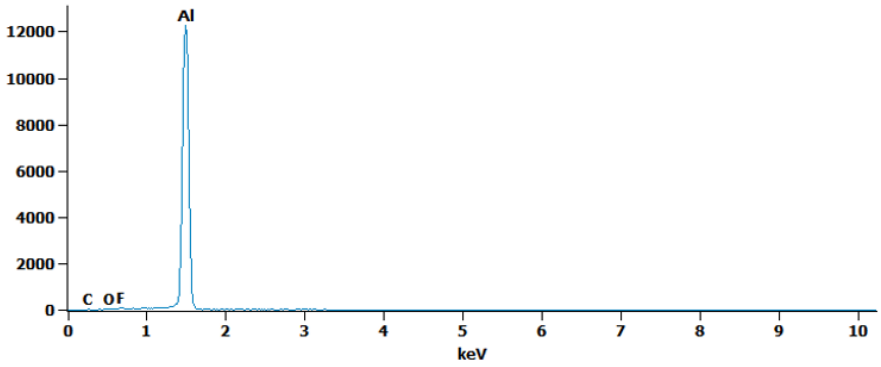

Figure 6-20 EDX site 1 of aluminium foil subjected to incremental potential staircase testing at 120 ˚C. 15kv 5000X.

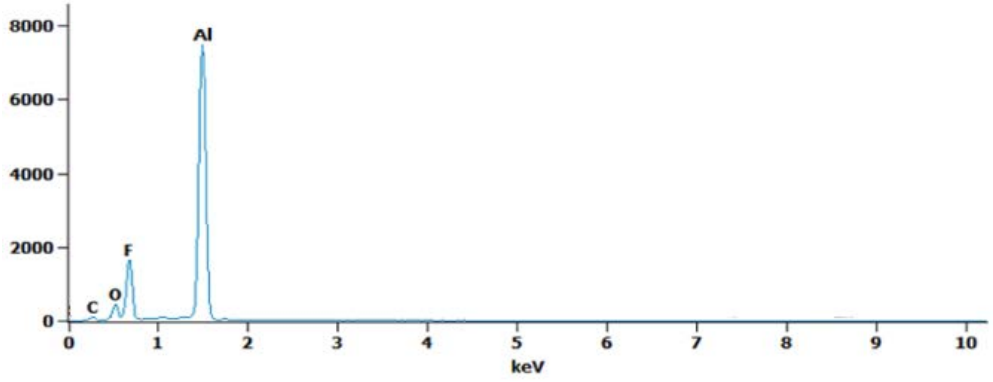

Figure 6-21 EDX site 2 of aluminium foil subjected to incremental potential staircase testing at 120 ˚C. 15kv 5000X.

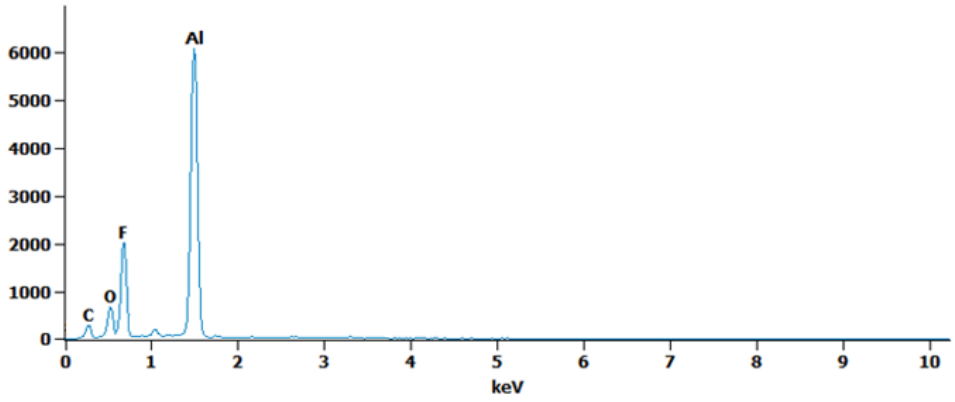

Figure 6-22 EDX site 3 of aluminium foil subjected to incremental potential staircase testing at 120 ˚C. 15kv 5000X.

Figure 6-23 to Figure 6-26 show the show the SEM/ EDX of the aluminium corrosion tests at 150 ˚C. What is immediately obvious from the SEM image in Figure 6-23 is that whole aluminium surface appears to be severely corroded, with signs of significant growth on the surface. It is shown in Figure 6-24 to Figure 6-26 that there are significant contributions of C, O and F which suggest the formation of aluminium oxides, $AlFO_3$ and electrolyte breakdown. This temperature seems to have the most significant reactions occurring from the SEM images and the EDX results and it is suggested that both aluminium corrosion and electrolyte breakdown are both contributing to the capacity fade at high temperatures. This is particularly the case where it was shown that at 150 ˚C there was huge current spikes in the corrosion tests, giving rise to high k values, with the SEM/ EDX showing significant corrosion and electrolyte breakdown, confirmed by the presence of C, O, and F.

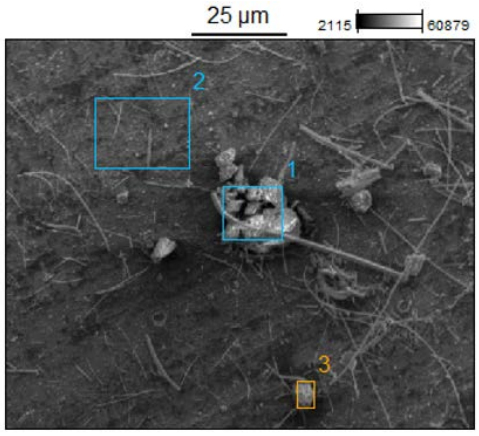

Figure 6-23 SEM image of aluminium foil subjected to incremental potential staircase testing at 150 ˚C showing the sampling sites for the EDX. 5kv 1000X.

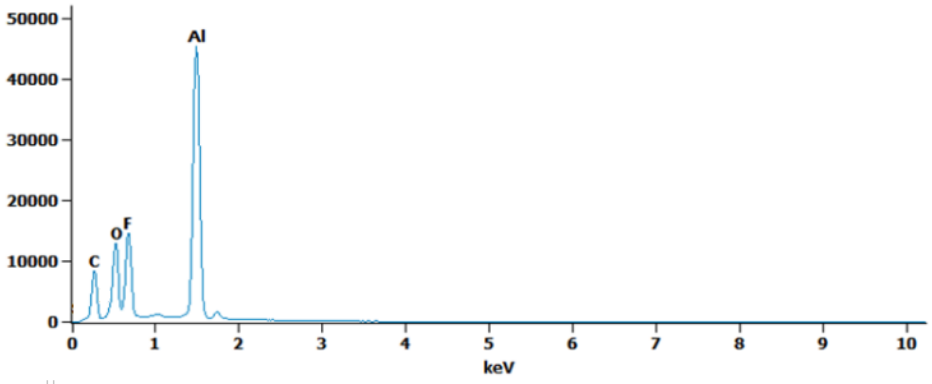

Figure 6-24 EDX site 1 of aluminium foil subjected to incremental potential staircase testing at 150 ˚C. 5kv 1000X.

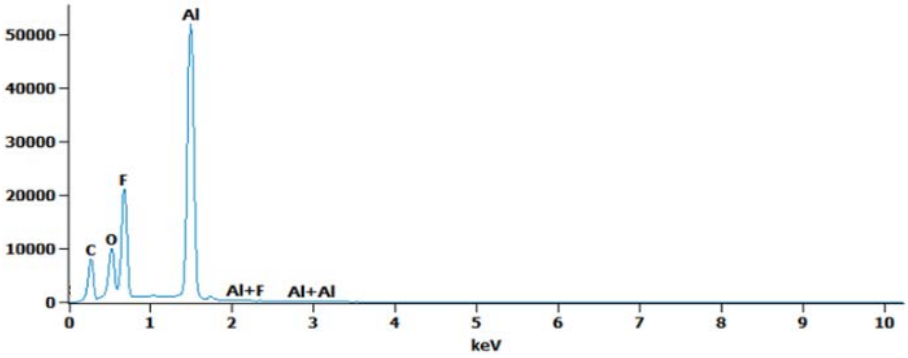

Figure 6-25 EDX site 2 of aluminium foil subjected to incremental potential staircase testing at 150 ˚C. 5kv 1000X.

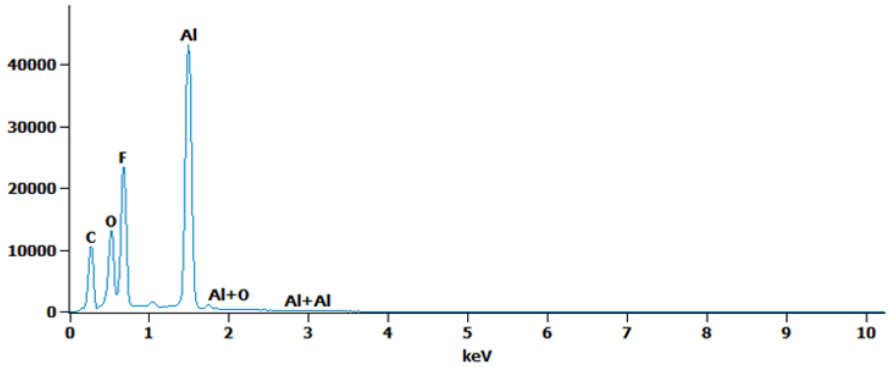

Figure 6-26 EDX site 3 of aluminium foil subjected to incremental potential staircase testing at 150 ˚C. 5kv 1000X.

6.6 Results from Constant Current Charging of Aluminium and Carbon Coated Aluminium

In chapter 4, it was found that composite $LiFePO_4$ electrodes showed a total capacity during charge higher than the theoretical capacity associated with the de-lithiation of $LiFePO_4$. This extra charge could be due to the other components present in the electrode, such as the carbon black conductive additive or the aluminium current collector, or an interplay between those extra components and the $LiFePO_4$ active material. In order to assess which component (carbon black or aluminium current collector) produced the excess charge passed during the first charge cycle cells were assembled with aluminium and carbon coated aluminium instead of $LiFePO_4$ electrodes. The cells were then charged from the open circuit potential of 2.8 V vs Li/Li^+ to 3.8 V vs Li/Li^+ with a set potential of 0.04 mA to measure how much aluminium and carbon coated aluminium contributed to the excess charge passed on the first cycle. The current of 0.04 mA was chosen because it is the typical current used in cycling cells with $LiFePO_4$ electrodes (see experimental details in the caption of Figure 6-27).

In order to understand how much excess charge is passed on the first cycle by LFP, the theoretical capacity of lithium iron phosphate was subtracted from the experimental capacities, which means that only the excess charge passed on the first charge cycle is revealed and not any associated with lithium extraction from $LiFePO_4$. The full charge profile before the subtraction of the theoretic capacity can be seen in Figure 6-27, it should also be noted that the potential has been adjusted to vs Li/Li^+ in order to compare with the rest of the results in this chapter. This is done by taking into account that the potential of the $Li_{0.5}FePO_4$ reference and counter electrode equals 3.45 V vs. Li/Li^+. It can be observed that there is excessive charge over 170 mAh g^{-1} for all temperatures. This excess charge is better understood by extracting the theoretical capacity and converting the resulting excess specific charge (mAh g^{-1}) to excess charge (mAh), this can be seen in Figure 6-28. It can be observed that the highest excess charge is for 90 ^oC giving a value of 0.4 mAh associated with side reactions, it can be observed that there is very little excess charge for 60 ^oC, compared to the other temperatures and this was also noted in chapters 5 and 6. The excess charge is also high at 120 and 150 ^oC giving values of 0.35 mAh at 120 ^oC and 0.3 mAh at 150 ^oC.

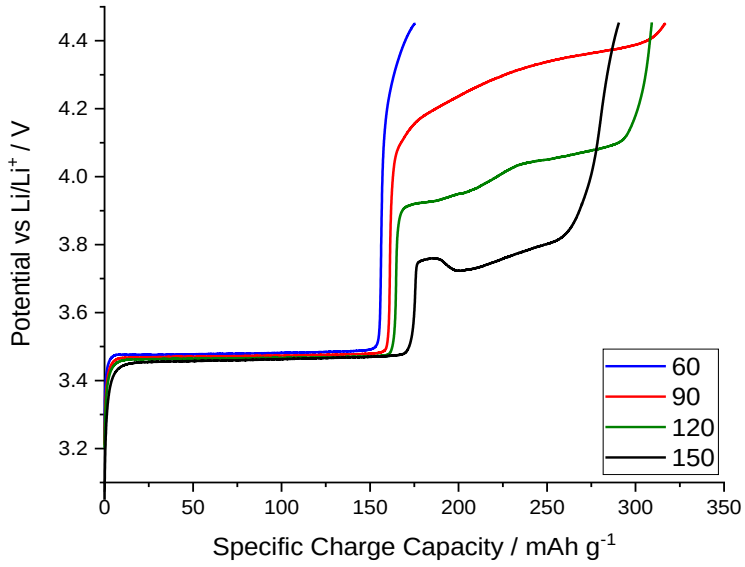

Figure 6-27 Potential vs specific charge for the first charge cycle of galvanostatic cycling of $LiFePO_4$ cells at 60, 90, 120 and 150 ˚C. The charge was done at C/10, and since the $LiFePO_4$ content was ca. 2.35 mg, the current applied was ca. 0.04 mA. The carbon content in the composite electrodes is ca 0.36mg (note that the electrodes are made with 12 %wt carbon, 12 %wt PVDF binder and 76 %wt active material).

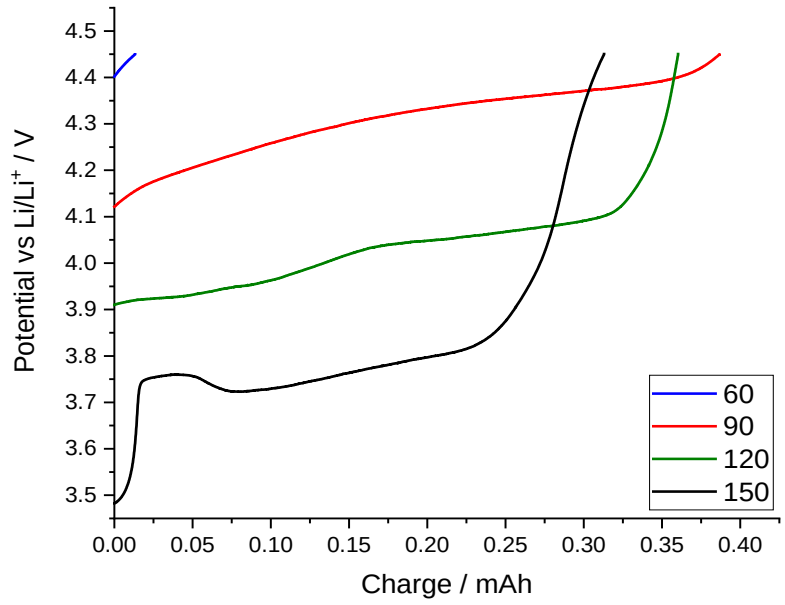

Figure 6-28 Potential vs excess charge for the first charge cycle of galvanostatic cycling of $LiFePO_4$ cells at 60, 90, 120 and 150 ˚C. The original data is plotted in Figure 6-27, and the excess charge is obtained by subtracting the theoretical capacity of 170 mAh g^{-1} to only account for the extra charge associated with side reactions.

Figure 6-29 shows the potential vs charge for the constant current charging of aluminium foil against lithium metal using the same electrolyte as in cycling $LiFePO_4$ electrodes in the results in Figure 6-27 and Figure 6-28 a 1M LiODFB in EC electrolyte at 60, 90, 120 and 150 ˚C. The current applied to the aluminium electrodes is also the same as the current applied to the $LiFePO_4$ electrodes: 0.04 mA. It can be seen that the charge of aluminium is low which is to be expected, since it is not a lithium storage material, it can be seen however that as temperature is increased the charge increases. This is likely due to the side reactions occurring namely aluminium corrosion and electrolyte breakdown occurring as was proved earlier on in this chapter. However, these charge values do not match those associated with those of the lithium iron phosphate cells, seen in Figure 6-28 and table 6-1. Looking at Figure 6-28 it can be seen that the excess charge values are 100 times larger for lithium iron phosphate compared to the aluminium meaning that it is more than the aluminium itself which is contributing to the excess charge passed. It needs to also be noted that in the constant current experiment the aluminium is charged from the open circuit potential of 2.8 V vs Li/Li^+ to 3.8 V vs Li/Li^+ and not 4.5 V vs Li/Li^+ as in the case for $LiFePO_4$. Future work should look at further set of experiments going up to 4.5 V vs Li/Li^+.

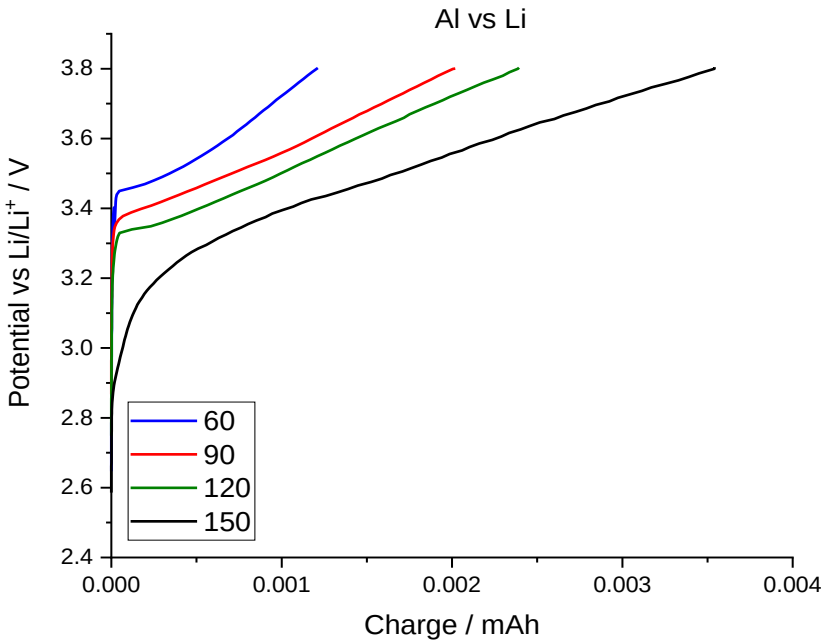

Figure 6-29 Potential vs charge for a constant current (0.04 mA) charging of Al vs Li cells at 60, 90, 120 and 150 ˚C.

Figure 6-30 and Figure 6-31 show the results of the constant current charging of carbon black coated aluminium vs Li cells at 60, 90, 120 and 150 ˚C. These electrodes were made by ink-coating an aluminium foil, producing a coating with 90 %wt of carbon black and 10 %wt of PVDF. The carbon content in these electrodes is ca. 0.67mg, which is higher than the ca 0.36mg carbon content in the $LiFePO_4$ composite electrodes. It needs to also be noted here that in the constant current experiment the carbon coated aluminium is charged from the open circuit potential of 2.8 V vs Li/Li^+ to 3.8 V vs Li/Li^+ and not 4.5 V vs Li/Li^+ as in the case for $LiFePO_4$ (Figure 6-28). Future work should look at further set of experiments going up to 4.5 V vs Li/Li^+. Figure 6-30 shows the results of constant current charge experiments for 60, 90, 120 and 150 ^oC, it should be noted that because the charge is so high at 150 ^oC, only part of the curve can be seen in Figure 6-30, therefore the full curve can be seen in Figure 6-31. Figure 6-31 shows that at 150 ^oC, polarization up to 3.8 V involves a substantial charge, of up to 2.5 mAh. In view of Figure 6-28, it is estimated that at 150 ^oC, polarization to 3.8 V vs. Li/Li^+ would involve an excess charge of around 0.3 mAh in the experiments with $LiFePO_4$ electrodes. As noted, the carbon coated aluminium electrodes contain more carbon that the $LiFePO_4$ composite electrodes. This could explain the higher charge observed in the former. In addition, the carbon coated composite electrodes could have a higher porosity, which again, could explain a higher charge. On the other hand, the carbon coated electrode shows a very small charge at lower temperatures, this can be seen in Figure 6-30. In view of Figure 6-28, it is estimated that at 60, 90 and 120 ^oC, polarization to 3.8 V vs. Li/Li^+ would involve a small or negligible excess charge for the experiments with $LiFePO_4$ electrodes. This is consistent with the fact that the carbon coated aluminium electrodes show a very small charge when charged up to these potentials (Figure 6-30).

In conclusion, comparison of the charge of $LiFePO_4$ (Figure 6-28) with carbon coated aluminium (Figure 6-30 and Figure 6-31), it can be seen that the cause of the excess of charge in the $LiFePO_4$ electrodes at 150 ^oC is very likely the presence of carbon on the electrode. Since this excess of charge is triggered by application of high temperatures, we propose that the process is due to electrolyte degradation at the surface of the carbon black. This could either be the electrolyte reacting with the carbon or the carbon acting as catalyst for electrolyte reactions, since no post-mortem analysis was performed, the exact mechanism cannot be concluded. Comparing the aluminium electrodes (Figure 6-29) with that of carbon coated aluminium electrodes (Figure 6-30 and Figure 6-31), it is seen that the aluminium electrodes produce a much smaller charge in these experiments. This can be explained by the difference in the surface area: the aluminium foil is flat, and hence has a much smaller surface area than the electrode coated with a carbon black ink.

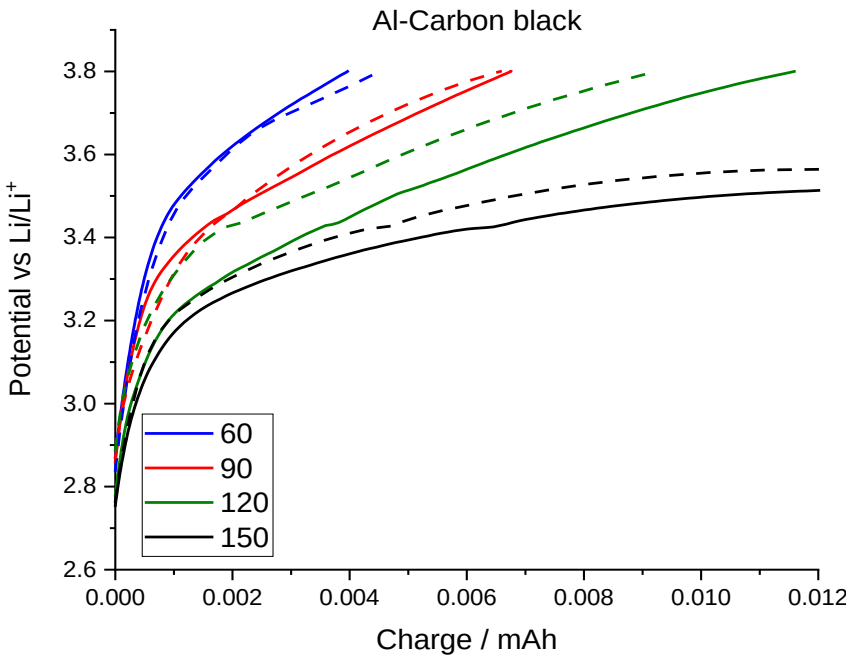

Figure 6-30 Potential vs charge for a constant current (0.04 mA) charging of carbon coated Al vs Li cells at 60, 90, 120 and 150 ˚C, dashed lines denote repeat tests. The carbon content in the composite electrodes is ca 0.67mg (note that the electrodes are made with 90 %wt carbon and 10 %wt PVDF binder).

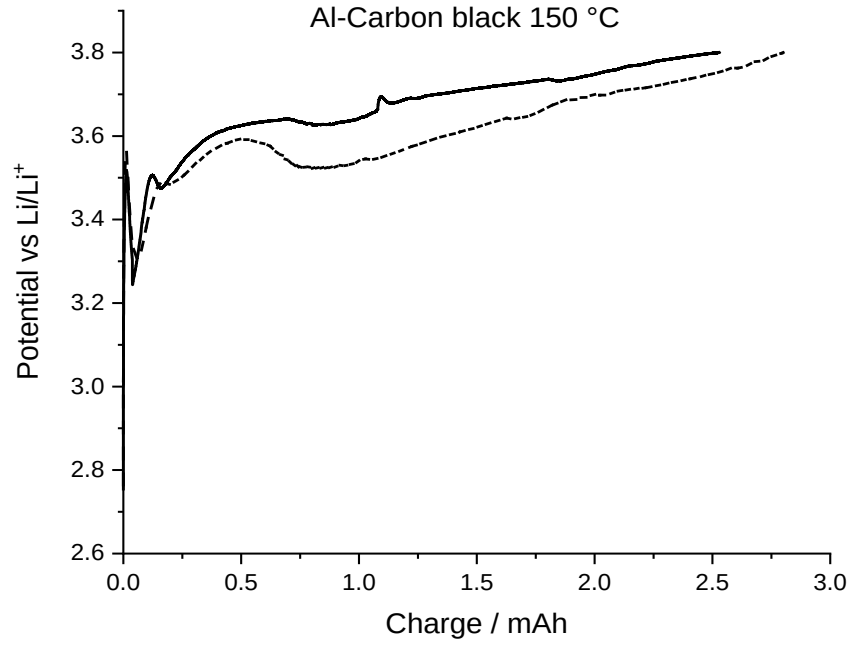

Figure 6-31 Potential vs charge for a constant current (0.04 mA) charging of carbon coated Al vs Li cells at 150 ˚C, dashed lines denote repeat tests. The carbon content in the composite electrodes is ca 0.67mg (note that the electrodes are made with 90 %wt carbon and 10 %wt PVDF binder).

Table 6-1 Summary of charge values for LFP, Al and C-Al at 60, 90, 120 and 150 ˚C.

Temperature ˚C	**Charge mAh**		
	LFP	**Al**	**C-Al**
60	0.01	0.00125	0.0040
90	0.40	0.00210	0.0070
120	0.35	0.00250	0.0118
150	0.30	0.00370	2.5000

6.7 Conclusions

This chapter aimed to identify if corrosion of the aluminium current collector occurs at elevated temperatures. The results have shown that current collector corrosion does occur at elevated temperatures, especially at temperatures above 90 ˚C, where it was shown that significant corrosion occurs to the aluminium current collector. The incremental potential staircase tests showed that at 90 ˚C that rather than the potential relaxing after a potential step, there is spikes in the current plot which signifies that current collector corrosion occurs. This effect is even more apparent at 150 ˚C, particularly between 3.8 V and 4 V there is a massive increase in the current which equates to a series of corrosion events. It is however likely that we are seeing more than aluminium corrosion here since electrolyte breakdown is also very likely in the region of 120 and 150 ˚C.

SEM with EDX was conducted on the incremental potential staircase test samples to confirm that corrosion was occurring. At 120 ˚C and 150 ˚C it was shown that significant aluminium corrosion was occurring with the SEM images showing that there are significant growths on the surface. EDX showed contributions from O and F, with a small amount of C. At 150 ˚C it was observed that there was significant aluminium corrosion and electrolyte breakdown occurring which is contributing to the capacity fade at high temperatures. This is particularly the case where it was shown that at 150 ˚C there was huge current spikes in the corrosion tests, giving rise to high k values, with the SEM/ EDX showing significant corrosion and electrolyte breakdown, confirmed by the presence of C, O, and F.

In order to assess the excess charge passed during the first charge cycle, which was discussed in section 6.1 and figure 6.1, cells were assembled with aluminium and carbon coated aluminium instead of LFP electrodes to measure how much aluminium and carbon coated aluminium contributed to the excess charge passed on the first cycle. It was shown that for aluminium as temperature is increased the charge increases due to the side reactions occurring namely aluminium corrosion and electrolyte breakdown. However, these charge values do not match those associated with those of the lithium iron phosphate cells. For the carbon coated aluminium results showed that the charge is higher than that of the aluminium foil, showing that the carbon itself does have a contribution to the excess charge passed on the first cycle. So, in addition to aluminium corrosion we also have the contribution of the side reactions of the electrolyte with the carbon. At 150 ˚C it is observed that the capacity is 2.5 mAh which is 8 times that of lithium iron phosphate at 150 ˚C, which is 0.3 mAh at 150 ˚C. This could be ascribed to the fact that the carbon content of the aluminium coated electrodes contained more carbon (ca. 0.67 mg) than the $LiFePO_4$ electrodes (0.36 mg), and also, their porosity is higher. It needs to also be noted here that in the constant

current experiments the carbon coated aluminium and the bare aluminium is charged from the open circuit potential of 2.8 V vs Li/Li^+ to 3.8 V vs Li/Li^+ and not 4.5 V vs Li/Li^+ as in the case for $LiFePO_4$. Therefore, future work should look at further set of experiments going up to 4.5 V vs Li/Li^+.

Chapter 7 Overall Conclusions and Further Work

This project aimed to investigate the high temperature operation of secondary lithium-ion batteries, giving an understanding of the temperature limitation of binders, electrolytes, positive electrode materials, negative electrode materials and current collectors.

This thesis has studied the high temperature operation of lithium ion batteries up to a temperature of 150 ^{o}C. Results have shown that the main factors which are responsible for capacity fade are the electrolyte, electrode binder and the current collector. It has been demonstrated that by replacing $LiPF_6$, for an alternative electrolyte LiODFB that lithium iron phosphate cells can be operated at higher temperatures. However, results showed that capacity fade was rapid at high temperatures, it was demonstrated that the binder was one of the causes of the first cycle irreversible capacity and had a large influence on the long-term capacity loss. It was also demonstrated that aluminium current collector corrosion was occurring during high temperature operation, this was studied in chapter 6.

In chapter 3 the effect of temperature on the galvanostatic cycling on graphite half cells was evaluated. The results showed that as temperature is increased the irreversible capacity increases, due to the formation of an increased growth of SEI with temperature. From the analysis of temperature on the irreversible capacity, using the Arrhenius equation, the effective activation energy of the irreversible reactions at the electrode/ electrolyte interface was estimated to be 11.6 kJ $^{\pm}$0.4 kJ mol^{-1}. Graphite and hard carbon were investigated as negative electrode materials and results showed that hard carbon has a large irreversible capacity loss on the first cycle. This effect was attributed to the high surface area of the hard carbon resulting in a higher amount of electrolyte breakdown. The hard carbon also didn't perform to the expected capacity which is quoted in excess of 400 mAh g^{-1}, but the observed capacity improved on heating the cells at 60 ^{o}C. A range of binders were investigated namely PVDF, PAI and PAN. Results showed that PAI was a poor performer due to high irreversible capacity losses. However, when the electrodes were subjected to an additional drying stage of 240 ^{o}C to cure the polymer results showed high coulombic efficiencies and lower irreversible capacity losses. PVDF seemed to perform well with high coulombic efficiencies and high irreversible capacity values obtained, however it didn't perform as well as PAI or PAN. PAN was only tested with graphite but results were very promising giving rise to a high coulombic efficiency and low irreversible capacity values, with a high retention of capacity on heating at 60 ^{o}C.

Chapter 4 aimed to study the effect of electrolyte salts on the performance of lithium iron phosphate cells at elevated temperatures. The capacity retention on galvanostatic cycling between

60 and 120 ^{o}C was good, at 120 ^{o}C the capacity after 100 cycles was 130 mAh g^{-1} equating to a 76% capacity retention. At 150 ^{o}C however, the capacity fade was much more rapid, with 50 % capacity loss after 20 cycles for LiODFB and 10 cycles for LiBOB. At 150 ^{o}C LiODFB performed much better than LiBOB with a slower degrade in capacity observed, however this performance can still be much improved since cycle life is low at this temperature.

Chapter 5 studied the effect of binders (PVDF 5130, PAI and PAN) on the cycling performance of lithium iron phosphate cells at elevated temperatures (60, 90, 120 and 150 ˚C) using the best performing electrolyte investigated in chapter 4 (1M LiODFB in EC). Results showed that at 60 ˚C PAN had the highest capacity retention on cycling compared to both PVDF and PAI. However, at 90 ˚C and above PAI had the highest capacity retention on cycling compared with both PVDF and PAN, with PAN showing rapid capacity fade particularly at 120 and 150 ˚C. It is observed that at 90, 120 and 150 ˚C PAI outperforms PVDF and PAN with higher discharge capacities observed for PAI over 102 cycles at 90, 120 and 150 ˚C.

Chapter 6 aimed to understand and characterise the mechanisms that lead to the corrosion of the aluminium current collector at elevated temperatures and to assess the role of the current collector in the capacity loss at elevated temperatures. The results have shown that current collector corrosion does occur at elevated temperatures, especially at temperatures above 90 ˚C, where it was shown that significant corrosion occurs to the aluminium current collector. SEM with EDX was conducted on the incremental potential staircase test samples to confirm that corrosion was occurring. At 120 ˚C and 150 ˚C it was shown that significant aluminium corrosion was occurring with the SEM images showing that there are significant growths on the surface. EDX showed contributions from O and F, with a small amount of C. At 150 ˚C it was observed that there was significant aluminium corrosion and electrolyte breakdown occurring which is contributing to the capacity fade at high temperatures. In order to assess the origin of the excess charge passed during the first charge cycle cells were assembled with aluminium and carbon coated aluminium instead of LFP electrodes to measure how much aluminium and carbon coated aluminium contributed to the excess charge passed on the first cycle. It was shown that for aluminium as temperature is increased the charge increases due to the side reactions occurring namely aluminium corrosion and electrolyte breakdown. However, these charge values do not match those associated with those of the lithium iron phosphate cells. For the carbon coated aluminium results showed that the charge is higher than that of the aluminium foil, showing that the carbon itself does have a contribution to the excess charge passed on the first cycle. So, in addition to aluminium corrosion we also have the contribution of the side reactions of the electrolyte with the carbon. At 150 ˚C it is observed that the capacity is 2.5 mAh which is 8 times that of lithium iron phosphate at 150 ˚C, which is 0.35 mAh at 150 ˚C. It needs to also be noted here that in the constant current experiments the carbon coated

aluminium and the bare aluminium is charged from the open circuit potential of 2.8 V vs Li/Li^+ to 3.8 V vs Li/Li^+ and not 4.5 V vs Li/Li^+ as in the case for $LiFePO_4$. Therefore, future work should look at further set of experiments going up to 4.5 V vs Li/Li^+.

In order to further the work that has been done during this thesis it has been identified that further work would need to be done in the following areas:

1. Electrolyte: In chapter 4 the investigation of electrolytes suitable for high temperature operation was done. However, this work could be expanded to investigate electrolyte additives in order to allow effective stabilisation of the SEI at higher temperatures. It should also include the investigation of alternative electrolyte systems such as polymers and solid-state electrolytes since it is likely that the limit of what can be achieved in carbonate systems has been reached.
2. Binder: It was effectively demonstrated in chapter 5 that binders had a huge impact on the first cycle irreversible capacity long term capacity fade. Further work should look at optimising the electrode binders, further evaluating the use of PAI as a binder for use at high temperatures, evaluating in a full Li-ion cell configuration.
3. Current Collector: It was demonstrated in chapter 6 that corrosion of the aluminium current collector was occurring at elevated temperatures. Therefore, alternative current collectors should be investigated for use at high temperatures that don't corrode when operated at 150 ^oC. The protection of the current collector could also be investigated using either coatings for the aluminium current collector or by electrolyte additives that allow effective passivation of the surface which do not fail at high temperatures.

Bibliography

1 M. V. Reddy, G. V. Subba Rao and B. V. R. Chowdari, Metal Oxides and Oxysalts as Anode Materials for Li Ion Batteries, *Chem. Rev.*, 2013, **113**, 5364–5457.

2 5,028,500, 1991, 11.

3 G. E. Blomgren, The Development and Future of Lithium Ion Batteries, *J. Electrochem. Soc.*, 2017, **164**, A5019–A5025.

4 A. K. Padhi, K. S. Nanjundaswamy and J. B. Goodenough, Phospho-olivines as Positive-Electrode Materials for Rechargeable Lithium Batteries, *J. Electrochem. Soc.*, 1997, **144**, 1188.

5 H. O. F. Batteries, D. E. Library and T. M. Companies, *Handbook of batteries*, McGraw-Hill, 2004.

6 E. B. Group, High Temperature Battery Packs for Oilfield Applications, http://excellbattery.com/industries/oil-industry/, (accessed 17 July 2015).

7 L. Bodenes, R. Naturel, H. Martinez, R. Dedryvère, M. Menetrier, L. Croguennec, J. P. Pérès, C. Tessier and F. Fischer, Lithium secondary batteries working at very high temperature: Capacity fade and understanding of aging mechanisms, *J. Power Sources*, 2013, **236**, 265–275.

8 P. Novák and P. Podhájecký, A high-temperature lithium copper oxide cell with a solid polymer electrolyte, *J. Power Sources*, 1991, **35**, 235–247.

9 M. Winter, J. O. J. Besenhard, M. E. Spahr and P. Novák, Insertion Electrode Materials for Rechargeable Lithium Batteries, *Adv. Mater.*, 1998, **10**, 725–763.

10 V. Aravindan, J. Gnanaraj, S. Madhavi and H. K. Liu, *Chem. - A Eur. J.*, 2011, 17, 14326–14346.

11 S. J. An, J. Li, C. Daniel, D. Mohanty, S. Nagpure and D. L. Wood, *Carbon N. Y.*, 2016, 105, 52–76.

12 M. Broussely, P. Biensan, F. Bonhomme, P. Blanchard, S. Herreyre, K. Nechev and R. J. Staniewicz, in *Journal of Power Sources*, 2005, vol. 146, pp. 90–96.

13 K. Edström, M. Herstedt and D. P. Abraham, in *Journal of Power Sources*, 2006, vol. 153,

pp. 380–384.

14 E. Peled, Advanced Model for Solid Electrolyte Interphase Electrodes in Liquid and Polymer Electrolytes, *J. Electrochem. Soc.*, 1997, **144**, L208.

15 J. B. Goodenough and Y. Kim, *Chem. Mater.*, 2010, 22, 587–603.

16 U. of L. D. of Chemistry, Hardwick Group, https://www.liverpool.ac.uk/chemistry/research/hardwick-group/research/, (accessed 17 August 2017).

17 J. Vetter, P. Novák, M. R. Wagner, C. Veit, K. C. Möller, J. O. Besenhard, M. Winter, M. Wohlfahrt-Mehrens, C. Vogler and A. Hammouche, Ageing mechanisms in lithium-ion batteries, *J. Power Sources*, 2005, **147**, 269–281.

18 T. Waldmann, M. Wilka, M. Kasper, M. Fleischhammer and M. Wohlfahrt-Mehrens, Temperature dependent ageing mechanisms in Lithium-ion batteries - A Post-Mortem study, *J. Power Sources*, 2014, **262**, 129–135.

19 H. Shin, J. Park, A. M. Sastry and W. Lu, Degradation of the solid electrolyte interphase induced by the deposition of manganese ions, *J. Power Sources*, 2015, **284**, 416–427.

20 H. Song, Z. Cao, Z. Zhang, Y. Lai, J. Li and Y. Liu, Effect of vinylene carbonate as electrolyte additive on cycling performance of LiFePO4 / graphite cell at elevated temperature, *Trans. Nonferrous Met. Soc. China*, 2014, **24**, 723–728.

21 A. Lewandowski, B. Kurc, A. Swiderska-Mocek and N. Kusa, Graphite|LiFePO4 lithium-ion battery working at the heat engine coolant temperature, *J. Power Sources*, 2014, **266**, 132–137.

22 C. Te Hsieh, C. T. Pai, Y. F. Chen, P. Y. Yu and R. S. Juang, Electrochemical performance of lithium iron phosphate cathodes at various temperatures, *Electrochim. Acta*, 2014, **115**, 96–102.

23 S. B. Lee and S. Il Pyun, The effect of electrolyte temperature on the passivity of solid electrolyte interphase formed on a graphite electrode, *Carbon N. Y.*, 2002, **40**, 2333–2339.

24 K. Jalkanen, J. Karppinen, L. Skogström, T. Laurila, M. Nisula and K. Vuorilehto, Cycle aging of commercial NMC / graphite pouch cells at different temperatures, *Appl. Energy*, 2015, **154**, 160–172.

25 M.-T. F. Rodrigues, G. Babu, H. Gullapalli, K. Kalaga, F. N. Sayed, K. Kato, J. Joyner and P. M.

Ajayan, A materials perspective on Li-ion batteries at extreme temperatures, *Nat. Energy*, 2017, **2**, 17108.

26 B. M. Newman, G.H., Francis, R. W., Gaines, L. H., Rao, Hazard Investigations of LiClO4 / Dioxolane Electrolyte, *J. Electrochem. Soc.*, 1980, **127**, 2025.

27 T. Batteries, Tadiran Batteries, http://www.tadiranbatteries.de/pdf/product-data-catalogue-tadiran-lithium-batteries.pdf., (accessed 5 May 2015).

28 B. Dunn, H. Kamath and J. M. Tarascon, Electrical energy storage for the grid: A battery of choices, *Science (80-.).*, 2011, **334**, 928–935.

29 X. Lu, G. Li, J. Y. Kim, D. Mei, J. P. Lemmon, V. L. Sprenkle and J. Liu, Liquid-metal electrode to enable ultra-low temperature sodium-beta alumina batteries for renewable energy storage, *Nat. Commun.*, , DOI:10.1038/ncomms5578.

30 F. Zheng, M. Kotobuki, S. Song, M. O. Lai and L. Lu, Review on solid electrolytes for all-solid-state lithium-ion batteries, *J. Power Sources*, 2018, **389**, 198–213.

31 Ilika, ILIKA_STEREAX_P180_FAQ, http://www.ilika.com/images/uploads/general/ILIKA_STEREAX_P180_FAQ_V3.0.pdf., (accessed 12 May 2017).

32 Ilika, StereaxTM P180 - Extended Temperature Range Solid State Battery: -40°C to +150°C, http://www.ilika.com/images/uploads/general/STEREAX_P180_SPECIFICATION_SHEET_V2.1.pdf., (accessed 21 August 2017).

33 K. Hayashi, Y. Nemoto, S.-I. Tobishima and J.-I. Yamaki, Mixed solvent electrolyte for high voltage lithium metal secondary cells, *Electrochim. Acta*, 1999, **44**, 2337–2344.

34 K. Xu, Nonaqueous Liquid Electrolytes for Lithium-Based Rechargeable Batteries, *Chem. Rev.*, 2004, **104**, 4303–4417.

35 S. Few, O. Schmidt, G. J. Offer, N. Brandon, J. Nelson and A. Gambhir, Prospective improvements in cost and cycle life of off-grid lithium-ion battery packs: An analysis informed by expert elicitations, *Energy Policy*, 2018, **114**, 578–590.

36 R. Fong, U. Sacken and J. R. Dahn, Studies of Lithium Intercalation into Carbons Using Nonaqueous Electrochemical Cells, *J. Electrochem. Soc.*, 1990, **137**, 2009–2013.

37 R. Yazami, Surface chemistry and lithium storage capability of the graphite-lithium electrode, *Electrochim. Acta*, 1999, **45**, 87–97.

38 C. E. L. Foss, A. M. Svensson, Ø. Gullbrekken, S. Sunde and F. Vullum-Bruer, Temperature effects on performance of graphite anodes in carbonate based electrolytes for lithium ion batteries, *J. Energy Storage*, 2018, **17**, 395–402.

39 BASF, BASF Selectilyte Electrolytes, http://www.catalysts.basf.com/p02/USWeb-Internet/catalysts/en/content/microsites/catalysts/prods-inds/batt-mats/selectilyte-electrolytes., (accessed 29 June 2015).

40 T. Kurita, J. Lu, M. Yaegashi, Y. Yamada, S. I. Nishimura, T. Tanaka, T. Uzumaki and A. Yamada, Challenges toward higher temperature operation of LiFePO4, *J. Power Sources*, 2012, **214**, 166–170.

41 L. Hu, Z. Zhang and K. Amine, Fluorinated electrolytes for Li-ion battery: An FEC-based electrolyte for high voltage LiNi0.5Mn1.5O4/graphite couple, *Electrochem. commun.*, 2013, **35**, 76–79.

42 J. Xia, R. Petibon, A. Xiao, W. M. Lamanna and J. R. Dahn, The effectiveness of electrolyte additives in fluorinated electrolytes for high voltage Li[Ni0.4Mn0.4Co0.2]O2/graphite pouch Li-ion cells, *J. Power Sources*, 2016, **330**, 175–185.

43 M. Salomon, H. Lin, E. J. Plichta and M. Hendrickson, in *Advances in Lithium-Ion Batteries*, Kluwer Academic/ Plenum Publishers, 2002, pp. 309–344.

44 A. Lewandowski and A. Świderska-Mocek, Ionic liquids as electrolytes for Li-ion batteries-An overview of electrochemical studies, *J. Power Sources*, 2009, **194**, 601–609.

45 D. Muñoz-Rojas, J. B. Leriche, C. Delacourt, P. Poizot, M. R. Palacín and J. M. Tarascon, Development and implementation of a high temperature electrochemical cell for lithium batteries, *Electrochem. commun.*, 2007, **9**, 708–712.

46 Y. Wang, K. Zaghib, A. Guerfi, F. F. C. Bazito, R. M. Torresi and J. R. Dahn, Accelerating rate calorimetry studies of the reactions between ionic liquids and charged lithium ion battery electrode materials, *Electrochim. Acta*, 2007, **52**, 6346–6352.

47 X. Lin, R. Kavian, Y. Lu, Q. Hu, Y. Shao-Horn and M. W. Grinstaff, Thermally-responsive, nonflammable phosphonium ionic liquid electrolytes for lithium metal batteries: operating at 100 degrees celsius, *Chem. Sci.*, 2015, **6**, 6601–6606.

48 M. J. Marczewski, B. Stanje, I. Hanzu, M. Wilkening and P. Johansson, “Ionic liquids-in-salt” – a promising electrolyte concept for high-temperature lithium batteries?, *Phys. Chem. Chem. Phys.*, 2014, **16**, 12341–12349.

49 K. Ababtain, G. Babu, X. Lin, M. T. F. Rodrigues, H. Gullapalli, P. M. Ajayan, M. W. Grinstaff and L. M. R. Arava, Ionic Liquid-Organic Carbonate Electrolyte Blends to Stabilize Silicon Electrodes for Extending Lithium Ion Battery Operability to 100 °C, *ACS Appl. Mater. Interfaces*, 2016, **8**, 15242–15249.

50 S.-T. Myung, Y. Sasaki, S. Sakurada, Y.-K. Sun and H. Yashiro, Electrochemical behavior of current collectors for lithium batteries in non-aqueous alkyl carbonate solution and surface analysis by ToF-SIMS, *Electrochim. Acta*, 2009, **55**, 288–297.

51 X. Zhang and T. M. Devine, Identity of Passive Film Formed on Aluminum in Li-Ion Battery Electrolytes with LiPF6, *J. Electrochem. Soc.*, 2006, **153**, B344–B351.

52 K. Kanamura, T. Okagawa and Z.-I. Takehara, Electrochemical oxidation of propylene carbonate (containing various salts) on aluminium electrodes, *J. Power Sources*, 1995, **57**, 119–123.

53 M. Dahbi, F. Ghamouss, F. Ois Tran-Van, D. Lemordant and M. Anouti, Comparative study of EC/DMC LiTFSI and LiPF6 electrolytes for electrochemical storage, *J. Power Sources*, 2011, **196**, 9743–9750.

54 J. Mun, T. Yim, C. Y. Choi, J. H. Ryu, Y. G. Kim and S. M. Oh, Linear-Sweep Thermammetry Study on Corrosion Behavior of Al Current Collector in Ionic Liquid Solvent, *Electrochem. Solid-State Lett.*, 2010, **13**, A109.

55 B. Markovsky, F. Amalraj, H. E. Gottlieb, Y. Gofer, S. K. Martha and D. Aurbach, On the Electrochemical Behavior of Aluminum Electrodes in Nonaqueous Electrolyte Solutions of Lithium Salts, *J. Electrochem. Soc.*, 2010, **157**, 423–429.

56 M. Zhou, L. Zhao, S. Okada and J. Yamaki, Quantitative Studies on the Influence of LiPF6 on the Thermal Stability of Graphite with Electrolyte, *J. Electrochem. Soc.*, 2012, **159**, A44–A48.

57 B. Electrolytes, O. N. The, P. Of and S. Batteries, EFFECT OF HF IN LiPF6 BASED ELECTROLYTES ON THE PROPERTIES OF SURFACE PASSIVATION FILMS FORMED ON GRAPHITE ELECTRODES IN Li SECONDARY BATTERIES, *Mat. Res. Soc. Symp. Proc.*, 1998, **496**, 457–462.

58 B. Ravdel, K. M. Abraham, R. Gitzendanner, J. Dicarlo, B. Lucht and C. Campion, Thermal stability of lithium-ion battery electrolytes, , DOI:10.1016/S0378-7753(03)00257-X.

59 A. Guéguen, D. Streich, M. He, M. Mendez, F. F. Chesneau, P. Novák and E. J. Berg,

Decomposition of LiPF6 in High Energy Lithium-Ion Batteries Studied with Online Electrochemical Mass Spectrometry, *J. Electrochem. Soc.*, 2016, **163**, 1095–1100.

60 B. Ravdel, K. M. Abraham, R. Gitzendanner, J. Dicarlo, B. Lucht and C. Campion, Thermal stability of lithium-ion battery electrolytes, *J. Power Sources*, 2003, **119**–**121**, 805–810.

61 C. L. Campion, W. Li, W. B. Euler, B. L. Lucht, B. Ravdel, J. F. DiCarlo, R. Gitzendanner and K. M. Abraham, Suppression of Toxic Compounds Produced in the Decomposition of Lithium-Ion Battery Electrolytes, *Electrochem. Solid-State Lett.*, 2004, **7**, A194.

62 M. Moshkovich, M. Cojocaru, H. E. Gottlieb and D. Aurbach, The study of the anodic stability of alkyl carbonate solutions by in situ FTIR spectroscopy, EQCM, NMR and MS, *J. Electroanal. Chem.*, 2001, **497**, 84–96.

63 C. L. Campion, W. Li and B. L. Lucht, Thermal Decomposition of LiPF6-Based Electrolytes for Lithium-Ion Batteries, *J. Electrochem. Soc.*, 2005, **152**, A2327–A2334.

64 B. Vortmann, S. Nowak and C. Engelhard, Rapid Characterization of Lithium Ion Battery Electrolytes and Thermal Aging Products by Low-Temperature Plasma Ambient Ionization High-Resolution Mass Spectrometry, *Am. Chem. Soc.*, 2013, **85**, 3433–3438.

65 V. Kraft, M. Grützke, W. Weber, M. Winter and S. Nowak, Ion chromatography electrospray ionization mass spectrometry method development and investigation of lithium hexafluorophosphate-based organic electrolytes and their thermal decomposition products, *J. Chromatogr. A*, 2014, **1354**, 92–100.

66 V. Kraft, W. Weber, M. Grützke, G. Grützke, M. Winter and S. Nowak, Study of decomposition products by gas chromatography-mass spectrometry and ion chromatography-electrospray ionization-mass spectrometry in thermally decomposed lithium hexafluorophosphate-based lithium ion battery electrolytes, *RSC Adv.*, 2015, **5**, 80150–80157.

67 W. Weber, R. Wagner, B. Streipert, V. Kraft, M. Winter and S. Nowak, Ion and gas chromatography mass spectrometry investigations of organophosphates in lithium ion battery electrolytes by electrochemical aging at elevated cathode potentials, *J. Power Sources*, 2016, **306**, 193–199.

68 S. Wilken, M. Treskow, J. Scheers, P. Johansson and P. Jacobsson, Initial stages of thermal decomposition of LiPF6-based lithium ion battery electrolytes by detailed Raman and NMR spectroscopy, *RSC Adv.*, 2013, **3**, 16359–16364.

69 S. Nowak and M. Winter, Review-Chemical Analysis for a Better Understanding of Aging and Degradation Mechanisms of Non-Aqueous Electrolytes for Lithium Ion Batteries: Method Development, Application and Lessons Learned Importance of Chemical Analysis for LIBs, *J. Electrochem. Soc.*, 2015, **162**, 2500–2508.

70 D. Aurbach, B. Markovsky, G. Salitra, E. Markevich, Y. Talyossef, M. Koltypin, L. Nazar, B. Ellis and D. Kovacheva, Review on electrode-electrolyte solution interactions, related to cathode materials for Li-ion batteries, *J. Power Sources*, 2007, **165**, 491–499.

71 K. Xu, S. S. Zhang, U. Lee, J. L. Allen and T. R. Jow, in *Journal of Power Sources*, 2005, vol. 146, pp. 79–85.

72 K. Xu, S. Zhang, T. R. Jow, W. Xu and C. A. Angell, LiBOB as Salt for Lithium-Ion Batteries:A Possible Solution for High Temperature Operation, *Electrochem. Solid-State Lett.*, 2002, **5**, A26.

73 K. Xu, S. Zhang and R. Jow, Electrochemical impedance study of graphite/electrolyte interface formed in LiBOB/PC electrolyte, *J. Power Sources*, 2005, **143**, 197–202.

74 S. S. Zhang, K. Xu and T. R. Jow, LiBOB-based gel electrolyte Li-ion battery for high temperature operation, *J. Power Sources*, 2006, **154**, 276–280.

75 K. Xu, B. Deveney, K. Nechev, Y. Lam and T. R. Jow, Evaluating LiBOB/Lactone Electrolytes in Large-Format Lithium-Ion Cells Based on Nickelate and Iron Phosphate, *J. Electrochem. Soc.*, 2008, **155**, 12–959.

76 S. Shui Zhang, An unique lithium salt for the improved electrolyte of Li-ion battery, *Electrochem. commun.*, 2006, **8**, 1423–1428.

77 J. Li, K. Xie, Y. Lai, Z. Zhang, F. Li, X. Hao, X. Chen and Y. Liu, Lithium oxalyldifluroborate/carbonate electrolytes for LiFePO4/artifical graphite lithium-ion cells, *J. Power Sources*, 2010, **195**, 5344–5350.

78 H. Zhou, F. Liu and J. Li, Preparation, Thermal Stability and Electrochemical Properties of LiODFB, *J. Mater. Sci. Technol.*, 2012, **28**, 723–727.

79 L. J. Krause, W. Lamanna, J. Summerfield, M. Engle, G. Korba, R. Loch and R. Atanasoski, *Corrosion of aluminum at high voltages in non-aqueous electrolytes containing perfluoroalkylsulfonyl imides; new lithium salts for lithium-ion cells*, 1997, vol. 68.

80 H.-B. Han, S.-S. Zhou, D.-J. Zhang, S.-W. Feng, L.-F. Li, K. Liu, W.-F. Feng, J. Nie, H. Li, X.-J.

Huang, M. Armand and Z.-B. Zhou, Lithium bis(fluorosulfonyl)imide (LiFSI) as conducting salt for nonaqueous liquid electrolytes for lithium-ion batteries: Physicochemical and electrochemical properties, *J. Power Sources*, 2011, **196**, 3623–3632.

81 A. Abouimrane, J. Ding and I. J. Davidson, Liquid electrolyte based on lithium bis-fluorosulfonyl imide salt: Aluminum corrosion studies and lithium ion battery investigations, *J. Power Sources*, 2009, **189**, 693–696.

82 B. Garcia and M. Armand, Aluminium corrosion in room temperature molten salt, *J. Power Sources*, 2004, **132**, 206–208.

83 X. Chen, W. Xu, M. H. Engelhard, J. Zheng, Y. Zhang, F. Ding, J. Qian and J.-G. Zhang, Mixed salts of LiTFSI and LiBOB for stable LiFePO4-based batteries at elevated temperatures, *J. Mater. Chem. A*, 2014, **2**, 2346.

84 F. Li, Y. Gong, G. Jia, Q. Wang, Z. Peng, W. Fan and B. Bai, A novel dual-salts of LiTFSI and LiODFB in LiFePO4-based batteries for suppressing aluminum corrosion and improving cycling stability, *J. Power Sources*, 2015, **295**, 47–54.

85 J. Zheng, M. H. Engelhard, D. Mei, S. Jiao, B. J. Polzin, J. G. Zhang and W. Xu, Electrolyte additive enabled fast charging and stable cycling lithium metal batteries, *Nat. Energy*, , DOI:10.1038/nenergy.2017.12.

86 M. Herstedt, H. Rensmo, H. Siegbahn and K. Edström, Electrolyte additives for enhanced thermal stability of the graphite anode interface in a Li-ion battery, *Electrochim. Acta*, 2004, **49**, 2351–2359.

87 Y. Fu, C. Chen, C. Qiu and X. Ma, Vinyl ethylene carbonate as an additive to ionic liquid electrolyte for lithium ion batteries, *J. Appl. Electrochem.*, 2009, **39**, 2597–2603.

88 D. Aurbach, K. Gamolsky, B. Markovsky, Y. Gofer, M. Schmidt and U. Heider, On the use of vinylene carbonate (VC) as an additive to electrolyte solutions for Li-ion batteries, *Electrochim. Acta*, 2002, **47**, 1423–1439.

89 R. D. Deshpande, P. Ridgway, Y. Fu, W. Zhang, J. Cai and V. Battaglia, The Limited Effect of VC in Graphite/NMC Cells, *J. Electrochem. Soc.*, 2014, **162**, A330–A338.

90 M. Herstedt, M. Stjerndahl and T. Gustafsson, Anion receptor for enhanced thermal stability of the graphite anode interface in a Li-ion battery, *Electrochem. commun.*, 2003, **5**, 467–472.

91 M. Ryou, J. Lee, D. Jin, W. Kim, J. Wook, J. Park and Y. Min, 2-(triphenylphosphoranylidene) succinic anhydride as a new electrolyte additive to improve high temperature cycle performance of LiMn2O4 / graphite Li-ion batteries, *Electrochim. Acta*, 2013, **102**, 97–103.

92 M. Ryou, G. Han, Y. Min, J. Lee, D. Jin, Y. Ok and J. Park, Effect of fluoroethylene carbonate on high temperature capacity retention of LiMn2O4 / graphite Li-ion cells, *Electrochim. Acta*, 2010, **55**, 2073–2077.

93 K. Yamagiwa, D. Morita, N. Yabuuchi, T. H. P. and S. C. of G. L.-I. C. by F.-B. E. A. Tanaka, M. Fukunishi, T. Taki, H. Watanabe, T. Otsuka, T. Yano, J. Y. Son, Y. T. Cui, H. Oji and S. Komaba, Improved High-Temperature Performance and Surface Chemistry of Graphite/LiMn2O4 Li-Ion Cells by Fluorosilane-Based Electrolyte Additive, *Electrochim. Acta*, 2015, **160**, 347–356.

94 H. Rong, M. Xu, B. Xie, H. Lin, Y. Zhu, X. Zheng, W. Huang, Y. Liao, L. Xing and W. Li, A novel imidazole-based electrolyte additive for improved electrochemical performance at elevated temperature of high-voltage LiNi0.5Mn1.5O4 cathodes, *J. Power Sources*, 2016, **329**, 586–593.

95 Y. Liu, L. Tan and L. Li, Tris(trimethylsilyl) borate as an electrolyte additive to improve the cyclability of LiMn2O4 cathode for lithium-ion battery, *J. Power Sources*, 2013, **221**, 90–96.

96 G.-A. Nazri and G. Pistola, *Lithium Batteries: Science and Technology*, Springer, New York, 2004.

97 D. Y. W. Yu, M. Zhao and H. E. Hoster, Real-Time Measurement of Expansion and Contraction of Silicon Electrodes in Lithium-Ion Batteries, *Meet. Abstr.*, 2014, **MA2014-04**, 631–631.

98 H. Wang and M. Yoshio, *Electrochemical performance of raw natural graphite flakes as an anode material for lithium-ion batteries at the elevated temperature*, 2003, vol. 79.

99 S. S. Zhang, T. R. Jow, K. Amine and G. L. Henriksen, LiPF6-EC-EMC electrolyte for Li-ion battery, *J. Power Sources*, 2002, **107**, 18–23.

100 S. Flandrois and B. Simon, *Carbon N. Y.*, 1999, 37, 165–180.

101 J. O. Besenhard and H. P. Fritz, *Angew. Chemie Int. Ed. English*, 1983, 22, 950–975.

102 A. M. Andersson, K. Edstrom, N. Rao and A. Wendsjö, *Temperature dependence of the*

passivation layer on graphite, 1999, vol. 81–82.

103 E. Markevich, E. Pollak, G. Salitra and D. Aurbach, On the performance of graphitized meso carbon microbeads (MCMB)-meso carbon fibers (MCF) and synthetic graphite electrodes at elevated temperatures, *J. Power Sources*, 2007, **174**, 1263–1269.

104 A. M. Andersson and K. Edström, Chemical Composition and Morphology of the Elevated Temperature SEI on Graphite, *J. Electrochem. Soc.*, 2001, **148**, 1100–1109.

105 P. Liu, J. Wang, J. Hicks-garner, E. Sherman, S. Soukiazian, M. Verbrugge, H. Tataria, J. Musser, P. Finamore, J. Deere, S. Engineering and N. Carolina, Aging Mechanisms of LiFePO 4 Batteries Deduced by Electrochemical and Structural Analyses, *J. Electrochem. Soc.*, 2010, **157**, 499–507.

106 H. Fujimoto, K. Tokumitsu, A. Mabuchi, N. Chinnasamy and T. Kasuh, The anode performance of the hard carbon for the lithium ion battery derived from the oxygen-containing aromatic precursors, *J. Power Sources*, 2010, **195**, 7452–7456.

107 M. Alamgir, Q. Zuo and K. M. Abraham, The Behavior of Carbon Electrodes Derived from Poly(p-phenylene) in Polyacrylonitrile-Based Polymer Electrolyte Cells, *Electrochem. Soc. Lett.*, 1994, **11**, L143–L144.

108 T. Yamabe, K. Tanaka, H. Ago, K. Yoshizawa and S. Yata, Structure and properties of deeply Li-doped polyacenic semiconductor materials beyond C6Li stage, *Synth. Met.*, 1997, **62**, 153–158.

109 T. Zheng, J. S. Xue and J. R. Dahn, Lithium insertion in hydrogen-containing carbonaceous materials, *Chem. Mater.*, 1996, **8**, 389–393.

110 T. Zheng, Y. Liu, E. W. Fuller, S. Tseng, U. Sacken and J. R. Dahn, Lithium Insertion in High Capacity Carbonaceous Materials, *J. Electrochem. Soc*, 1995, **142**, 2581–2590.

111 Y. Mori, T. Iriyama, T. Hashimoto, S. Yamazaki, F. Kawakami, H. Shiroki and T. Yamabe, Lithium dopinghndoping in disordered coke carbons, *J. Power Sources*, 1995, **56**, 205–208.

112 H. Fujimoto, A. Mabuchi, K. Tokumitsu and T. Kasuh, Irreversible capacity of lithium secondary battery using meso-carbon micro beads as anode material, *J. Power Sources*, 1995, **54**, 440–443.

113 J. S. Xue and J. R. Dahn, *Dramatic Effect of Oxidation on Lithium Insertion in Carbons Made from Epoxy Resins*, Electrochemical Society, 1995, vol. 142.

114 S. Yata, Y. Hato, H. Kinoshita, N. Ando, A. Anekawa, T. Hashimoto, M. Yamaguchi, K. Tanaka and T. Yamabe, Characteristics of deeply Li-doped polyacenic semiconductor material and fabrication of a Li secondary battery, *Synth. Met.*, 1995, **73**, 273–277.

115 F. Béguin, F. Chevallier, C. Vix-Guterl, S. Saadallah, V. Bertagna, J. N. Rouzaud and E. Frackowiak, Correlation of the irreversible lithium capacity with the active surface area of modified carbons, *Carbon N. Y.*, 2005, **2005**, 2160–2167.

116 D. D. Macneil, D. Larcher and J. R. Dahn, *Comparison of the Reactivity of Various Carbon Electrode Materials with Electrolyte at Elevated Temperature*, 1999, vol. 146.

117 H. Zheng, Q. Qu, L. Zhang, G. Liu and V. S. Battaglia, Hard carbon: a promising lithium-ion battery anode for high temperature applications with ionic electrolyte, *RSC Adv.*, 2012, **2**, 4904–4912.

118 K. Mizushima, P. C. Jones, P. J. Wiseman and J. B. Goodenough, LixCoO2(0<x<-1): A new cathode material for batteries of high energy density, *Mater. Res. Bull.*, 1980, **15**, 783–789.

119 J. B. Goodenough, K. Mizushima and T. Takeda, Solid-solution oxides for storage-battery electrodes, *Jpn. J. Appl. Phys.*, 1980, **19**, 305–313.

120 T. Ohzuku and R. J. Brodd, An overview of positive-electrode materials for advanced lithium-ion batteries, *J. Power Sources*, 2007, **174**, 449–456.

121 R. Jung, M. Metzger, F. Maglia, C. Stinner and H. A. Gasteiger, Chemical versus Electrochemical Electrolyte Oxidation on NMC111, NMC622, NMC811, LNMO, and Conductive Carbon, , DOI:10.1021/acs.jpclett.7b01927.

122 R. Jung, M. Metzger, F. Maglia, C. Stinner and H. A. Gasteiger, Oxygen Release and Its Effect on the Cycling Stability of LiNixMnyCozO2 (NMC) Cathode Materials for Li-Ion Batteries, *J. Electrochem. Soc.*, 2017, **164**, 1361–1377.

123 M. M. Thackeray, L. A. de Picciotto, A. de Kock, P. J. Johnson, V. A. Nicholas and K. T. Adendorff, Spinel electrodes for lithium batteries - A review, *J. Power Sources*, 1987, **21**, 1–8.

124 C. Delacourt, P. Poizot, J.-M. Tarascon and C. Masquelier, The existence of a temperature-driven solid solution in LixFePO4 for 0 ≤ x ≤ 1, *Nat. Mater.*, 2005, **4**, 254–260.

125 K. Amine, J. Liu and I. Belharouak, High-temperature storage and cycling of C-LiFePO/graphite Li-ion cells, *Electrochem. commun.*, 2005, **7**, 669–673.

126 C.-T. Hsieh, C.-T. Pai, Y.-F. Chen, P.-Y. Yu and R.-S. Juang, Electrochemical performance of lithium iron phosphate cathodes at various temperatures, *Electrochim. Acta*, 2014, **115**, 96–102.

127 Y. Huang, Y.-C. Lin, D. M. Jenkins, N. A. Chernova, Y. Chung, B. Radhakrishnan, I.-H. Chu, J. Fang, Q. Wang, F. Omenya, S. P. Ong and M. S. Whittingham, Thermal Stability and Reactivity of Cathode Materials for Li-Ion Batteries, *ACS Appl. Mater. Interfaces*, 2016, **8**, 7013–7021.

128 G. Liu, H. Zheng, X. Song and V. S. Battaglia, Particles and Polymer Binder Interaction: A Controlling Factor in Lithium-Ion Electrode Performance, *J. Electrochem. Soc.*, 2012, **159**, A214–A221.

129 N.-S. Choi, S.-Y. Ha, Y. Lee, J. Y. Jang, M.-H. Jeong, W. C. Shin and M. Ue, Recent Progress on Polymeric Binders for Silicon Anodes in Lithium-Ion Batteries, *J. Electrochem. Sci. Technol.*, 2015, **6**, 35–49.

130 Y. Nishi, Lithium ion secondary batteries; past 10 years and the future, *J. Power Sources*, 2001, **100**, 101–106.

131 M. Morishita, A. Yamano, T. Kitaoka, H. Sakai, T. Ojima and T. Sakai, Polyamide-Imide Binder with Higher Adhesive Property and Thermal Stability as Positive Electrode of 4V-Class Lithium-Ion Batteries, *J. Electrochem. Soc.*, 2014, **161**, A955–A960.

132 S. L. Chou, Y. Pan, J. Z. Wang, H. K. Liu and S. X. Dou, Small things make a big difference: Binder effects on the performance of Li and Na batteries, *Phys. Chem. Chem. Phys.*, 2014, **16**, 20347–20359.

133 L. Bodenes, R. Dedryvère, H. Martinez, F. Fischer, C. Tessier and J.-P. Pérès, Lithium-Ion Batteries Working at 85 deg C: Aging Phenomena and Electrode/Electrolyte Interfaces Studied by XPS, *J. Electrochem. Soc.*, 2012, **159**, 1739–1746.

134 W. Wrasidlo and J. Augl, Aromatic Polyimide-co-Amides . I, *J. Polym. Sci. Part A-1*, 1969, **7**, 321–332.

135 N.-S. Choi, K. Han Yew, W.-U. Choi and S.-S. Kim, Enhanced electrochemical properties of a Si-based anode using an electrochemically active polyamide imide binder, *J. Power Sources*, 2008, **177**, 590–594.

136 L. Gong, M. H. T. Nguyen and E.-S. Oh, High polar polyacrylonitrile as a potential binder for negative electrodes in lithium ion batteries, *Electrochem. commun.*, 2013, **29**, 45–47.

137 L. Shen, L. Shen, Z. Wang and L. Chen, In situ thermally cross-linked polyacrylonitrile as binder for high-performance silicon as lithium ion battery anode, *ChemSusChem*, 2014, **7**, 1951–1956.

138 W. E. Org, W. Lin, J. Wang, R. Zhou, B. Wu and J. Zhao, ELECTROCHEMICAL SCIENCE Improving the Electrochemical Performance of LiNi 0.5 Mn 1.5 O 4 Cathode Materials by Surface Coating with Cyclized Polyacrylonitrile for Lithium-Ion Batteries, *Int. J. Electrochem. Sci*, 2017, **12**, 12047–12059.

139 Z. Zhang, L. Hu, H. Wu, W. Weng, M. Koh, P. C. Redfern, L. A. Curtiss and K. Amine, Fluorinated electrolytes for 5 V lithium-ion battery chemistry, *This J. is [a] R. Soc. Chem.*, 2013, **6**, 1806–1810.

140 Z. Chen, Y. Ren, A. N. Jansen, C. K. Lin, W. Weng and K. Amine, New class of nonaqueous electrolytes for long-life and safe lithium-ion batteries, *Nat. Commun.*, , DOI:10.1038/ncomms2518.

141 H. Q. Pham, E.-H. Hwang, Y.-G. Kwon and S.-W. Song, Understanding the interfacial phenomena of a 4.7 V and 55 °C Li-ion battery with Li-rich layered oxide cathode and graphite anode and its correlation to high-energy cycling performance, *J. Power Sources*, 2016, **323**, 220–230.

142 Y. Qin, Z. Chen, J. Liu and K. Amine, Lithium Tetrafluoro Oxalato Phosphate as Electrolyte Additive for Lithium-Ion Cells, *Electrochem. Solid-State Lett.*, 2010, **12**, A11–A14.

143 K. S. Kang, S. Choi, J. Song, S.-G. Woo, Y. N. Jo, J. Choi, T. Yim, J.-S. Yu and Y.-J. Kim, Effect of additives on electrochemical performance of lithium nickel cobalt manganese oxide at high temperature, *J. Power Sources*, 2014, **253**, 48–54.

144 D. P. Kong, P. Ping, Q. S. Wang and J. H. Sun, Study on High Temperature Stability of LiNi0.33Co0.33Mn0.33O2 / Li4TiO12 Cells from the Safety Perspective, *J. Electrochem. Soc.*, 2016, **163**, 1697–1704.

145 J. Li, Y. Zhu, L. Wang and C. Cao, Lithium titanate epitaxial coating on spinel lithium manganese oxide surface for improving the performance of lithium storage capability, *ACS Appl. Mater. Interfaces*, 2014, **6**, 18742–18750.

146 H. Han, J. Guo, D. Zhang, S. Feng, W. Feng, J. Nie and Z. Zhou, Lithium (fluorosulfonyl)(nonafluorobutanesulfonyl)imide (LiFNFSI) as conducting salt to improve the high-temperature resilience of lithium-ion cells, *Electrochem. commun.*, 2011, **13**, 265–

268.

147 Y. Cho, J. Eom and J. Cho, High Performance LiCoO[sub 2] Cathode Materials at 60°C for Lithium Secondary Batteries Prepared by the Facile Nanoscale Dry-Coating Method, *J. Electrochem. Soc.*, 2010, **157**, A617–A624.

148 D. Li, Z. Ma, J. Xu, Y. Li and K. Xie, High temperature property of all-solid-state thin film lithium battery using LiPON electrolyte, *Mater. Lett.*, **134**, 237–239.

149 X. Wang, Z. Liu, C. Zhang, Q. Kong, J. Yao, P. Han, W. Jiang, H. Xu and G. Cui, Exploring polymeric lithium tartaric acid borate for thermally resistant polymer electrolyte of lithium batteries, *Electrochim. Acta*, 2013, **92**, 132–138.

150 Q. Hu, S. Osswald, R. Daniel, Y. Zhu, S. Wesel, L. Ortiz and D. R. Sadoway, Graft copolymer-based lithium-ion battery for high-temperature operation, *J. Power Sources*, 2011, **196**, 5604–5610.

151 J. Zhang, L. Yue, Q. Kong, Z. Liu, X. Zhou, C. Zhang, Q. Xu, B. Zhang, G. Ding, B. Qin, Y. Duan, Q. Wang, J. Yao, G. Cui and L. Chen, Sustainable, heat-resistant and flame-retardant cellulose-based composite separator for high-performance lithium ion battery, *Sci. Rep.*, , DOI:10.1038/srep03935.

152 H. S. Yang, S.-H. Kim, A. G. Kannan, S. K. Kim, C. Park and D.-W. Kim, Performance Enhancement of Silicon Alloy-Based Anodes Using Thermally Treated Poly(amide imide) as a Polymer Binder for High Performance Lithium-Ion Batteries, *Langmuir*, 2016, **32**, 3300–3307.

153 T. Zheng, A. S. Gozdz and G. G. Amatucci, Reactivity of the Solid Electrolyte Interface on Carbon Electrodes at Elevated Temperatures, *J. Electrochem. Soc.*, 1999, **146**, 4014–4018.

154 Kuraray, Anode Material for Lithium-ion Secondary Battery Biocarbotron, www.kuraray.co.jp/en/, (accessed 5 January 2016).

155 China Steel Chemical Corporation, Certificate of Analysis MGPA, www.cscc.com.tw.

156 C. V. Ramana, A. Mauger, F. Gendron, C. M. Julien and K. Zaghib, Study of the Li-insertion/extraction process in LiFePO4/FePO4, *J. Power Sources*, 2009, **187**, 555–564.

157 N. Intaranont, N. Garcia-Araez, A. L. Hector, J. A. Milton and J. R. Owen, Selective lithium extraction from brines by chemical reaction with battery materials, *J. Mater. Chem. A*, 2014, **2**, 6374–6377.

158 H. Yang, G. V. Zhuang and P. N. Ross, Thermal stability of LiPF6 salt and Li-ion battery electrolytes containing LiPF6, *J. Power Sources*, 2006, **161**, 573–579.

159 S. Diaham and M. -l. Locatelli, Novel high glass transition polyamide-imide: Tg influence on electrical conductivity at high temperature, *IEEE Trans. Dielectr. Electr. Insul.*, 2015, **22**, 3053–3058.

160 O. Olabisi, in *Handook of thermoplastics*, 1997, p. 185.

161 Z. Bashir, *Polyacrylonitrile, an unusual linear homopolymer with two glass transitions*, 1999, vol. 24.

162 IGTPAN, The first innovation and technology center dedicated for researching Polyacrylonitrile, http://www.igtpan.com/Ingles/propriedade-poli.asp, (accessed 15 August 2018).

163 X. H. Flora, M. Ulaganathan and S. Rajendran, Role of different plasticizers in li-ion conducting poly(acrylonitrile)- poly(methyl methacrylate) hybrid polymer electrolyte, *Int. J. Polym. Mater. Polym. Biomater.*, 2013, **62**, 737–742.

164 F. Croce, S. D. Brown, S. G. Greenbaum, S. M. Slane, M. Salomon and U. Army EPSD, *Lithium-7 NMR and Ionic Conductivity Studies of Gel Electrolytes Based on Poly(acrylonitrile)*, 1993, vol. 5.

165 Z. Bashir, S. P. Church and D. M. Price, The formation of polymer-solvent complexes of polyacrylonitrile from organic solvents containing carbonyl groups, *Acta Polym.*, 1993, **44**, 211–218.

166 M.-T. F. Rodrigues, G. Babu, H. Gullapalli, K. Kalaga, F. N. Sayed, K. Kato, J. Joyner and P. M. Ajayan, A materials perspective on Li-ion batteries at extreme temperatures, *Nat. Energy*, 2017, **2**, 17108.

167 M. Wang, A. V. Le, Y. Shi, D. J. Noelle and Y. Qiao, Heterogeneous current collector in lithium-ion battery for thermal-runaway mitigation, *Appl. Phys. Lett.*, , DOI:10.1063/1.4975799.

168 C. Vargel, *Corrosion of Aluminium*, Elsevier, 2004.

169 J. W. Braithwaite, A. Gonzales, G. Nagasubramanian, S. J. Lucero, D. E. Peebles, J. A. Ohlhausen and W. R. Cieslak, *Corrosion of Lithium-Ion Battery Current Collectors*, 1999, vol. 146.

170 F. N. Sayed, M.-T. F. Rodrigues, K. Kalaga, H. Gullapalli and P. M. Ajayan, Curious Case of Positive Current Collectors: Corrosion and Passivation at High Temperature, *ACS Appl. Mater. Interfaces*, 2017, **9**, 43623–43631.

171 T. Ma, G.-L. Xu, Y. Li, L. Wang, X. He, J. Zheng, J. Liu, M. H. Engelhard, P. Zapol, L. A. Curtiss, J. Jorne, Khalil Amine and Z. Chen, Revisiting the Corrosion of the Aluminum Current Collector in Lithium-Ion Batteries, *J. Phys. Chem. Lett.*, 2017, **8**, 1072–1077.

RE: Use of SEI image on Hardwick Group website

Hardwick, Laurence <Laurence.Hardwick@liverpool.ac.uk>

Tue 05/02/2019 11:05

To:Wright D.R. <D.R.Wright@soton.ac.uk>;

Dear Dan

That will be fine

Best

Laurence

Prof. Laurence Hardwick
Director of the Stephenson Institute for Renewable Energy
Department of Chemistry
The University of Liverpool
Chadwick Building, Peach Street, Liverpool, L69 7ZF, UK
Phone: +44 (0)151 794 3493
Email: hardwick@liverpool.ac.uk
http://www.liverpool.ac.uk/chemistry/research/hardwick-group/

From: Wright D.R. <D.R.Wright@soton.ac.uk>
Sent: 05 February 2019 10:19
To: Hardwick, Laurence <hardwick@liverpool.ac.uk>
Subject: Use of SEI image on Hardwick Group website

Dear Professor Hardwick,

I am currently finishing off my PhD and am obtaining permissions to use images I have taken from sources. I have used the image of the peled model of the SEI in my thesis from your research group page.

Could I please obtain permission from you to use this image in my thesis if possible please?

Many thanks,

Dan.

Daniel Wright BSc (hons.), MSc, MCSM
Senior Research Assistant
Faculty of Engineering and the Environment- Energy Technology Group
University of Southampton, Highfield Campus, B25/R2033

SPRINGER NATURE LICENSE TERMS AND CONDITIONS

Feb 05, 2019

This Agreement between Daniel R Wright ("You") and Springer Nature ("Springer Nature") consists of your license details and the terms and conditions provided by Springer Nature and Copyright Clearance Center.

License Number	4522491306267
License date	Feb 05, 2019
Licensed Content Publisher	Springer Nature
Licensed Content Publication	Nature Energy
Licensed Content Title	A materials perspective on Li-ion batteries at extreme temperatures
Licensed Content Author	Marco-Tulio F. Rodrigues, Ganguli Babu, Hemtej Gullapalli, Kaushik Kalaga, Farheen N. Sayed et al.
Licensed Content Date	Jul 24, 2017
Licensed Content Volume	2
Licensed Content Issue	8
Type of Use	Thesis/Dissertation
Requestor type	academic/university or research institute
Format	print and electronic
Portion	figures/tables/illustrations
Number of figures/tables/illustrations	1
High-res required	no
Will you be translating?	no
Circulation/distribution	<501
Author of this Springer Nature content	no
Title	Mr
Institution name	University of Southampton
Expected presentation date	Mar 2019
Portions	Figure 2
Requestor Location	Daniel R Wright Flat 17 Westfield Corner Wide Lane Southampton, Hampshire SO18 2LE United Kingdom Attn:
Billing Type	Invoice
Billing Address	Daniel R Wright Flat 17 Westfield Corner Wide Lane Southampton, United Kingdom SO18 2LE Attn:

Total 0.00 GBP

Terms and Conditions

Springer Nature Terms and Conditions for RightsLink Permissions

Springer Nature Customer Service Centre GmbH (the Licensor) hereby grants you a non-exclusive, world-wide licence to reproduce the material and for the purpose and requirements specified in the attached copy of your order form, and for no other use, subject to the conditions below:

1. The Licensor warrants that it has, to the best of its knowledge, the rights to license reuse of this material. However, you should ensure that the material you are requesting is original to the Licensor and does not carry the copyright of another entity (as credited in the published version).

   If the credit line on any part of the material you have requested indicates that it was reprinted or adapted with permission from another source, then you should also seek permission from that source to reuse the material.

2. Where **print only** permission has been granted for a fee, separate permission must be obtained for any additional electronic re-use.

3. Permission granted **free of charge** for material in print is also usually granted for any electronic version of that work, provided that the material is incidental to your work as a whole and that the electronic version is essentially equivalent to, or substitutes for, the print version.

4. A licence for 'post on a website' is valid for 12 months from the licence date. This licence does not cover use of full text articles on websites.

5. Where **'reuse in a dissertation/thesis'** has been selected the following terms apply: Print rights of the final author's accepted manuscript (for clarity, NOT the published version) for up to 100 copies, electronic rights for use only on a personal website or institutional repository as defined by the Sherpa guideline (www.sherpa.ac.uk/romeo/).

6. Permission granted for books and journals is granted for the lifetime of the first edition and does not apply to second and subsequent editions (except where the first edition permission was granted free of charge or for signatories to the STM Permissions Guidelines http://www.stm-assoc.org/copyright-legal-affairs/permissions/permissions-guidelines/), and does not apply for editions in other languages unless additional translation rights have been granted separately in the licence.

7. Rights for additional components such as custom editions and derivatives require additional permission and may be subject to an additional fee. Please apply to Journalpermissions@springernature.com/bookpermissions@springernature.com for these rights.

8. The Licensor's permission must be acknowledged next to the licensed material in print. In electronic form, this acknowledgement must be visible at the same time as the figures/tables/illustrations or abstract, and must be hyperlinked to the journal/book's homepage. Our required acknowledgement format is in the Appendix below.

9. Use of the material for incidental promotional use, minor editing privileges (this does not include cropping, adapting, omitting material or any other changes that affect the meaning, intention or moral rights of the author) and copies for the disabled are permitted under this licence.

10. Minor adaptations of single figures (changes of format, colour and style) do not require the Licensor's approval. However, the adaptation should be credited as shown in Appendix below.

Appendix — Acknowledgements:

For Journal Content:
Reprinted by permission from [**the Licensor**]: [**Journal Publisher** (e.g. Nature/Springer/Palgrave)] [**JOURNAL NAME**] [**REFERENCE CITATION** (Article name, Author(s) Name), [**COPYRIGHT**] (year of publication)

For **Advance Online Publication papers:**
Reprinted by permission from [**the Licensor**]: [**Journal Publisher** (e.g. Nature/Springer/Palgrave)] [**JOURNAL NAME**] [**REFERENCE CITATION** (Article name, Author(s) Name), [**COPYRIGHT**] (year of publication), advance online publication, day month year (doi: 10.1038/sj.[JOURNAL ACRONYM].)

For Adaptations/Translations:
Adapted/Translated by permission from [**the Licensor**]: [**Journal Publisher** (e.g. Nature/Springer/Palgrave)] [**JOURNAL NAME**] [**REFERENCE CITATION** (Article name, Author(s) Name), [**COPYRIGHT**] (year of publication)

Note: For any republication from the British Journal of Cancer, the following credit line style applies:

Reprinted/adapted/translated by permission from [**the Licensor**]: on behalf of Cancer Research UK: : [**Journal Publisher** (e.g. Nature/Springer/Palgrave)] [**JOURNAL NAME**] [**REFERENCE CITATION** (Article name, Author(s) Name), [**COPYRIGHT**] (year of publication)

For **Advance Online Publication** papers:
Reprinted by permission from The [**the Licensor**]: on behalf of Cancer Research UK: [**Journal Publisher** (e.g. Nature/Springer/Palgrave)] [**JOURNAL NAME**] [**REFERENCE CITATION** (Article name, Author(s) Name), [**COPYRIGHT**] (year of publication), advance online publication, day month year (doi: 10.1038/sj.[JOURNAL ACRONYM])

For Book content:
Reprinted/adapted by permission from [**the Licensor**]: [**Book Publisher** (e.g. Palgrave Macmillan, Springer etc) [**Book Title**] by [**Book author**(s)] [**COPYRIGHT**] (year of publication)

Other Conditions:

Version 1.1

Questions? customercare@copyright.com or +1-855-239-3415 (toll free in the US) or +1-978-646-2777.

This page is available in the following languages:

Creative Commons License Deed

Attribution 4.0 International (CC BY 4.0)

This is a human-readable summary of (and not a substitute for) the license.

You are free to:

Share — copy and redistribute the material in any medium or format

Adapt — remix, transform, and build upon the material

for any purpose, even commercially.

The licensor cannot revoke these freedoms as long as you follow the license terms.

Under the following terms:

Attribution — You must give appropriate credit, provide a link to the license, and indicate if changes were made. You may do so in any reasonable manner, but not in any way that suggests the licensor endorses you or your use.

No additional restrictions — You may not apply legal terms or technological measures that legally restrict others from doing anything the license permits.

Notices:

You do not have to comply with the license for elements of the material in the public domain or where your use is permitted by an applicable exception or limitation.

No warranties are given. The license may not give you all of the permissions necessary for your intended use. For example, other rights such as publicity, privacy, or moral rights may limit how you use the material.

ELSEVIER LICENSE
TERMS AND CONDITIONS

Feb 05, 2019

This Agreement between Daniel R Wright ("You") and Elsevier ("Elsevier") consists of your license details and the terms and conditions provided by Elsevier and Copyright Clearance Center.

License Number	4522501081092
License date	Feb 05, 2019
Licensed Content Publisher	Elsevier
Licensed Content Publication	Journal of Power Sources
Licensed Content Title	Challenges toward higher temperature operation of LiFePO4
Licensed Content Author	Tomochika Kurita,Jiechen Lu,Makoto Yaegashi,Yuki Yamada,Shin-ichi Nishimura,Tsutomu Tanaka,Takuya Uzumaki,Atsuo Yamada
Licensed Content Date	Sep 15, 2012
Licensed Content Volume	214
Licensed Content Issue	n/a
Licensed Content Pages	5
Start Page	166
End Page	170
Type of Use	reuse in a thesis/dissertation
Portion	figures/tables/illustrations
Number of figures/tables/illustrations	1
Format	both print and electronic
Are you the author of this Elsevier article?	No
Will you be translating?	No
Original figure numbers	Figure 3
Title of your thesis/dissertation	Mr
Publisher of new work	University of Southampton
Expected completion date	Mar 2019
Estimated size (number of pages)	1
Requestor Location	Daniel R Wright Flat 17 Westfield Corner Wide Lane Southampton, Hampshire SO18 2LE United Kingdom Attn:
Publisher Tax ID	GB 494 6272 12
Total	0.00 GBP
Terms and Conditions	

INTRODUCTION

1. The publisher for this copyrighted material is Elsevier. By clicking "accept" in connection with completing this licensing transaction, you agree that the following terms and conditions apply to this transaction (along with the Billing and Payment terms and conditions established by Copyright Clearance Center, Inc. ("CCC"), at the time that you opened your Rightslink account and that are available at any time at http://myaccount.copyright.com).

GENERAL TERMS

2. Elsevier hereby grants you permission to reproduce the aforementioned material subject to the terms and conditions indicated.

3. Acknowledgement: If any part of the material to be used (for example, figures) has appeared in our publication with credit or acknowledgement to another source, permission must also be sought from that source. If such permission is not obtained then that material may not be included in your publication/copies. Suitable acknowledgement to the source must be made, either as a footnote or in a reference list at the end of your publication, as follows:

"Reprinted from Publication title, Vol /edition number, Author(s), Title of article / title of chapter, Pages No., Copyright (Year), with permission from Elsevier [OR APPLICABLE SOCIETY COPYRIGHT OWNER]." Also Lancet special credit - "Reprinted from The Lancet, Vol. number, Author(s), Title of article, Pages No., Copyright (Year), with permission from Elsevier."

4. Reproduction of this material is confined to the purpose and/or media for which permission is hereby given.

5. Altering/Modifying Material: Not Permitted. However figures and illustrations may be altered/adapted minimally to serve your work. Any other abbreviations, additions, deletions and/or any other alterations shall be made only with prior written authorization of Elsevier Ltd. (Please contact Elsevier at permissions@elsevier.com). No modifications can be made to any Lancet figures/tables and they must be reproduced in full.

6. If the permission fee for the requested use of our material is waived in this instance, please be advised that your future requests for Elsevier materials may attract a fee.

7. Reservation of Rights: Publisher reserves all rights not specifically granted in the combination of (i) the license details provided by you and accepted in the course of this licensing transaction, (ii) these terms and conditions and (iii) CCC's Billing and Payment terms and conditions.

8. License Contingent Upon Payment: While you may exercise the rights licensed immediately upon issuance of the license at the end of the licensing process for the transaction, provided that you have disclosed complete and accurate details of your proposed use, no license is finally effective unless and until full payment is received from you (either by publisher or by CCC) as provided in CCC's Billing and Payment terms and conditions. If full payment is not received on a timely basis, then any license preliminarily granted shall be deemed automatically revoked and shall be void as if never granted. Further, in the event that you breach any of these terms and conditions or any of CCC's Billing and Payment terms and conditions, the license is automatically revoked and shall be void as if never granted. Use of materials as described in a revoked license, as well as any use of the materials beyond the scope of an unrevoked license, may constitute copyright infringement and publisher reserves the right to take any and all action to protect its copyright in the materials.

9. Warranties: Publisher makes no representations or warranties with respect to the licensed material.

10. Indemnity: You hereby indemnify and agree to hold harmless publisher and CCC, and their respective officers, directors, employees and agents, from and against any and all claims arising out of your use of the licensed material other than as specifically authorized pursuant to this license.

11. No Transfer of License: This license is personal to you and may not be sublicensed, assigned, or transferred by you to any other person without publisher's written permission.

12. No Amendment Except in Writing: This license may not be amended except in a writing signed by both parties (or, in the case of publisher, by CCC on publisher's behalf).

13. Objection to Contrary Terms: Publisher hereby objects to any terms contained in any purchase order, acknowledgment, check endorsement or other writing prepared by you, which terms are inconsistent with these terms and conditions or CCC's Billing and Payment

terms and conditions. These terms and conditions, together with CCC's Billing and Payment terms and conditions (which are incorporated herein), comprise the entire agreement between you and publisher (and CCC) concerning this licensing transaction. In the event of any conflict between your obligations established by these terms and conditions and those established by CCC's Billing and Payment terms and conditions, these terms and conditions shall control.

14. Revocation: Elsevier or Copyright Clearance Center may deny the permissions described in this License at their sole discretion, for any reason or no reason, with a full refund payable to you. Notice of such denial will be made using the contact information provided by you. Failure to receive such notice will not alter or invalidate the denial. In no event will Elsevier or Copyright Clearance Center be responsible or liable for any costs, expenses or damage incurred by you as a result of a denial of your permission request, other than a refund of the amount(s) paid by you to Elsevier and/or Copyright Clearance Center for denied permissions.

LIMITED LICENSE

The following terms and conditions apply only to specific license types:

15. **Translation**: This permission is granted for non-exclusive world **English** rights only unless your license was granted for translation rights. If you licensed translation rights you may only translate this content into the languages you requested. A professional translator must perform all translations and reproduce the content word for word preserving the integrity of the article.

16. **Posting licensed content on any Website**: The following terms and conditions apply as follows: Licensing material from an Elsevier journal: All content posted to the web site must maintain the copyright information line on the bottom of each image; A hyper-text must be included to the Homepage of the journal from which you are licensing at http://www.sciencedirect.com/science/journal/xxxxx or the Elsevier homepage for books at http://www.elsevier.com; Central Storage: This license does not include permission for a scanned version of the material to be stored in a central repository such as that provided by Heron/XanEdu.

Licensing material from an Elsevier book: A hyper-text link must be included to the Elsevier homepage at http://www.elsevier.com . All content posted to the web site must maintain the copyright information line on the bottom of each image.

Posting licensed content on Electronic reserve: In addition to the above the following clauses are applicable: The web site must be password-protected and made available only to bona fide students registered on a relevant course. This permission is granted for 1 year only. You may obtain a new license for future website posting.

17. **For journal authors:** the following clauses are applicable in addition to the above:

Preprints:

A preprint is an author's own write-up of research results and analysis, it has not been peer-reviewed, nor has it had any other value added to it by a publisher (such as formatting, copyright, technical enhancement etc.).

Authors can share their preprints anywhere at any time. Preprints should not be added to or enhanced in any way in order to appear more like, or to substitute for, the final versions of articles however authors can update their preprints on arXiv or RePEc with their Accepted Author Manuscript (see below).

If accepted for publication, we encourage authors to link from the preprint to their formal publication via its DOI. Millions of researchers have access to the formal publications on ScienceDirect, and so links will help users to find, access, cite and use the best available version. Please note that Cell Press, The Lancet and some society-owned have different preprint policies. Information on these policies is available on the journal homepage.

Accepted Author Manuscripts: An accepted author manuscript is the manuscript of an article that has been accepted for publication and which typically includes author-incorporated changes suggested during submission, peer review and editor-author communications.

Authors can share their accepted author manuscript:

- immediately

- via their non-commercial person homepage or blog
- by updating a preprint in arXiv or RePEc with the accepted manuscript
- via their research institute or institutional repository for internal institutional uses or as part of an invitation-only research collaboration work-group
- directly by providing copies to their students or to research collaborators for their personal use
- for private scholarly sharing as part of an invitation-only work group on commercial sites with which Elsevier has an agreement

- After the embargo period
  - via non-commercial hosting platforms such as their institutional repository
  - via commercial sites with which Elsevier has an agreement

In all cases accepted manuscripts should:

- link to the formal publication via its DOI
- bear a CC-BY-NC-ND license - this is easy to do
- if aggregated with other manuscripts, for example in a repository or other site, be shared in alignment with our hosting policy not be added to or enhanced in any way to appear more like, or to substitute for, the published journal article.

Published journal article (JPA): A published journal article (PJA) is the definitive final record of published research that appears or will appear in the journal and embodies all value-adding publishing activities including peer review co-ordination, copy-editing, formatting, (if relevant) pagination and online enrichment.
Policies for sharing publishing journal articles differ for subscription and gold open access articles:
Subscription Articles: If you are an author, please share a link to your article rather than the full-text. Millions of researchers have access to the formal publications on ScienceDirect, and so links will help your users to find, access, cite, and use the best available version.
Theses and dissertations which contain embedded PJAs as part of the formal submission can be posted publicly by the awarding institution with DOI links back to the formal publications on ScienceDirect.
If you are affiliated with a library that subscribes to ScienceDirect you have additional private sharing rights for others' research accessed under that agreement. This includes use for classroom teaching and internal training at the institution (including use in course packs and courseware programs), and inclusion of the article for grant funding purposes.
Gold Open Access Articles: May be shared according to the author-selected end-user license and should contain a CrossMark logo, the end user license, and a DOI link to the formal publication on ScienceDirect.
Please refer to Elsevier's posting policy for further information.
18. **For book authors** the following clauses are applicable in addition to the above:
Authors are permitted to place a brief summary of their work online only. You are not allowed to download and post the published electronic version of your chapter, nor may you scan the printed edition to create an electronic version. **Posting to a repository:** Authors are permitted to post a summary of their chapter only in their institution's repository.
19. **Thesis/Dissertation**: If your license is for use in a thesis/dissertation your thesis may be submitted to your institution in either print or electronic form. Should your thesis be published commercially, please reapply for permission. These requirements include permission for the Library and Archives of Canada to supply single copies, on demand, of the complete thesis and include permission for Proquest/UMI to supply single copies, on demand, of the complete thesis. Should your thesis be published commercially, please reapply for permission. Theses and dissertations which contain embedded PJAs as part of the formal submission can be posted publicly by the awarding institution with DOI links back to the formal publications on ScienceDirect.

Elsevier Open Access Terms and Conditions
You can publish open access with Elsevier in hundreds of open access journals or in nearly 2000 established subscription journals that support open access publishing. Permitted third

party re-use of these open access articles is defined by the author's choice of Creative Commons user license. See our open access license policy for more information.

Terms & Conditions applicable to all Open Access articles published with Elsevier:

Any reuse of the article must not represent the author as endorsing the adaptation of the article nor should the article be modified in such a way as to damage the author's honour or reputation. If any changes have been made, such changes must be clearly indicated.

The author(s) must be appropriately credited and we ask that you include the end user license and a DOI link to the formal publication on ScienceDirect.

If any part of the material to be used (for example, figures) has appeared in our publication with credit or acknowledgement to another source it is the responsibility of the user to ensure their reuse complies with the terms and conditions determined by the rights holder.

Additional Terms & Conditions applicable to each Creative Commons user license:

CC BY: The CC-BY license allows users to copy, to create extracts, abstracts and new works from the Article, to alter and revise the Article and to make commercial use of the Article (including reuse and/or resale of the Article by commercial entities), provided the user gives appropriate credit (with a link to the formal publication through the relevant DOI), provides a link to the license, indicates if changes were made and the licensor is not represented as endorsing the use made of the work. The full details of the license are available at http://creativecommons.org/licenses/by/4.0.

CC BY NC SA: The CC BY-NC-SA license allows users to copy, to create extracts, abstracts and new works from the Article, to alter and revise the Article, provided this is not done for commercial purposes, and that the user gives appropriate credit (with a link to the formal publication through the relevant DOI), provides a link to the license, indicates if changes were made and the licensor is not represented as endorsing the use made of the work. Further, any new works must be made available on the same conditions. The full details of the license are available at http://creativecommons.org/licenses/by-nc-sa/4.0.

CC BY NC ND: The CC BY-NC-ND license allows users to copy and distribute the Article, provided this is not done for commercial purposes and further does not permit distribution of the Article if it is changed or edited in any way, and provided the user gives appropriate credit (with a link to the formal publication through the relevant DOI), provides a link to the license, and that the licensor is not represented as endorsing the use made of the work. The full details of the license are available at http://creativecommons.org/licenses/by-nc-nd/4.0.

Any commercial reuse of Open Access articles published with a CC BY NC SA or CC BY NC ND license requires permission from Elsevier and will be subject to a fee.

Commercial reuse includes:

- Associating advertising with the full text of the Article
- Charging fees for document delivery or access
- Article aggregation
- Systematic distribution via e-mail lists or share buttons

Posting or linking by commercial companies for use by customers of those companies.

20. **Other Conditions**:

v1.9

Questions? customercare@copyright.com or +1-855-239-3415 (toll free in the US) or +1-978-646-2777.

ELSEVIER LICENSE
TERMS AND CONDITIONS

Feb 05, 2019

This Agreement between Daniel R Wright ("You") and Elsevier ("Elsevier") consists of your license details and the terms and conditions provided by Elsevier and Copyright Clearance Center.

License Number	4522510282959
License date	Feb 05, 2019
Licensed Content Publisher	Elsevier
Licensed Content Publication	Electrochemistry Communications
Licensed Content Title	An unique lithium salt for the improved electrolyte of Li-ion battery
Licensed Content Author	Sheng Shui Zhang
Licensed Content Date	Sep 1, 2006
Licensed Content Volume	8
Licensed Content Issue	9
Licensed Content Pages	6
Start Page	1423
End Page	1428
Type of Use	reuse in a thesis/dissertation
Portion	figures/tables/illustrations
Number of figures/tables/illustrations	1
Format	both print and electronic
Are you the author of this Elsevier article?	No
Will you be translating?	No
Original figure numbers	Reaction of LiODFB on page 1425
Title of your thesis/dissertation	Mr
Publisher of new work	University of Southampton
Expected completion date	Mar 2019
Estimated size (number of pages)	1
Requestor Location	Daniel R Wright Flat 17 Westfield Corner Wide Lane Southampton, Hampshire SO18 2LE United Kingdom Attn:
Publisher Tax ID	GB 494 6272 12
Total	0.00 GBP
Terms and Conditions	

INTRODUCTION

1. The publisher for this copyrighted material is Elsevier. By clicking "accept" in connection with completing this licensing transaction, you agree that the following terms and conditions

apply to this transaction (along with the Billing and Payment terms and conditions established by Copyright Clearance Center, Inc. ("CCC"), at the time that you opened your Rightslink account and that are available at any time at http://myaccount.copyright.com).

GENERAL TERMS

2. Elsevier hereby grants you permission to reproduce the aforementioned material subject to the terms and conditions indicated.
3. Acknowledgement: If any part of the material to be used (for example, figures) has appeared in our publication with credit or acknowledgement to another source, permission must also be sought from that source. If such permission is not obtained then that material may not be included in your publication/copies. Suitable acknowledgement to the source must be made, either as a footnote or in a reference list at the end of your publication, as follows:
"Reprinted from Publication title, Vol /edition number, Author(s), Title of article / title of chapter, Pages No., Copyright (Year), with permission from Elsevier [OR APPLICABLE SOCIETY COPYRIGHT OWNER]." Also Lancet special credit - "Reprinted from The Lancet, Vol. number, Author(s), Title of article, Pages No., Copyright (Year), with permission from Elsevier."
4. Reproduction of this material is confined to the purpose and/or media for which permission is hereby given.
5. Altering/Modifying Material: Not Permitted. However figures and illustrations may be altered/adapted minimally to serve your work. Any other abbreviations, additions, deletions and/or any other alterations shall be made only with prior written authorization of Elsevier Ltd. (Please contact Elsevier at permissions@elsevier.com). No modifications can be made to any Lancet figures/tables and they must be reproduced in full.
6. If the permission fee for the requested use of our material is waived in this instance, please be advised that your future requests for Elsevier materials may attract a fee.
7. Reservation of Rights: Publisher reserves all rights not specifically granted in the combination of (i) the license details provided by you and accepted in the course of this licensing transaction, (ii) these terms and conditions and (iii) CCC's Billing and Payment terms and conditions.
8. License Contingent Upon Payment: While you may exercise the rights licensed immediately upon issuance of the license at the end of the licensing process for the transaction, provided that you have disclosed complete and accurate details of your proposed use, no license is finally effective unless and until full payment is received from you (either by publisher or by CCC) as provided in CCC's Billing and Payment terms and conditions. If full payment is not received on a timely basis, then any license preliminarily granted shall be deemed automatically revoked and shall be void as if never granted. Further, in the event that you breach any of these terms and conditions or any of CCC's Billing and Payment terms and conditions, the license is automatically revoked and shall be void as if never granted. Use of materials as described in a revoked license, as well as any use of the materials beyond the scope of an unrevoked license, may constitute copyright infringement and publisher reserves the right to take any and all action to protect its copyright in the materials.
9. Warranties: Publisher makes no representations or warranties with respect to the licensed material.
10. Indemnity: You hereby indemnify and agree to hold harmless publisher and CCC, and their respective officers, directors, employees and agents, from and against any and all claims arising out of your use of the licensed material other than as specifically authorized pursuant to this license.
11. No Transfer of License: This license is personal to you and may not be sublicensed, assigned, or transferred by you to any other person without publisher's written permission.
12. No Amendment Except in Writing: This license may not be amended except in a writing signed by both parties (or, in the case of publisher, by CCC on publisher's behalf).
13. Objection to Contrary Terms: Publisher hereby objects to any terms contained in any purchase order, acknowledgment, check endorsement or other writing prepared by you, which terms are inconsistent with these terms and conditions or CCC's Billing and Payment terms and conditions. These terms and conditions, together with CCC's Billing and Payment terms and conditions (which are incorporated herein), comprise the entire agreement

between you and publisher (and CCC) concerning this licensing transaction. In the event of any conflict between your obligations established by these terms and conditions and those established by CCC's Billing and Payment terms and conditions, these terms and conditions shall control.

14. Revocation: Elsevier or Copyright Clearance Center may deny the permissions described in this License at their sole discretion, for any reason or no reason, with a full refund payable to you. Notice of such denial will be made using the contact information provided by you. Failure to receive such notice will not alter or invalidate the denial. In no event will Elsevier or Copyright Clearance Center be responsible or liable for any costs, expenses or damage incurred by you as a result of a denial of your permission request, other than a refund of the amount(s) paid by you to Elsevier and/or Copyright Clearance Center for denied permissions.

LIMITED LICENSE

The following terms and conditions apply only to specific license types:

15. **Translation**: This permission is granted for non-exclusive world **English** rights only unless your license was granted for translation rights. If you licensed translation rights you may only translate this content into the languages you requested. A professional translator must perform all translations and reproduce the content word for word preserving the integrity of the article.

16. **Posting licensed content on any Website**: The following terms and conditions apply as follows: Licensing material from an Elsevier journal: All content posted to the web site must maintain the copyright information line on the bottom of each image; A hyper-text must be included to the Homepage of the journal from which you are licensing at http://www.sciencedirect.com/science/journal/xxxxx or the Elsevier homepage for books at http://www.elsevier.com; Central Storage: This license does not include permission for a scanned version of the material to be stored in a central repository such as that provided by Heron/XanEdu.

Licensing material from an Elsevier book: A hyper-text link must be included to the Elsevier homepage at http://www.elsevier.com . All content posted to the web site must maintain the copyright information line on the bottom of each image.

Posting licensed content on Electronic reserve: In addition to the above the following clauses are applicable: The web site must be password-protected and made available only to bona fide students registered on a relevant course. This permission is granted for 1 year only. You may obtain a new license for future website posting.

17. **For journal authors:** the following clauses are applicable in addition to the above:

Preprints:

A preprint is an author's own write-up of research results and analysis, it has not been peer-reviewed, nor has it had any other value added to it by a publisher (such as formatting, copyright, technical enhancement etc.).

Authors can share their preprints anywhere at any time. Preprints should not be added to or enhanced in any way in order to appear more like, or to substitute for, the final versions of articles however authors can update their preprints on arXiv or RePEc with their Accepted Author Manuscript (see below).

If accepted for publication, we encourage authors to link from the preprint to their formal publication via its DOI. Millions of researchers have access to the formal publications on ScienceDirect, and so links will help users to find, access, cite and use the best available version. Please note that Cell Press, The Lancet and some society-owned have different preprint policies. Information on these policies is available on the journal homepage.

Accepted Author Manuscripts: An accepted author manuscript is the manuscript of an article that has been accepted for publication and which typically includes author-incorporated changes suggested during submission, peer review and editor-author communications.

Authors can share their accepted author manuscript:

- immediately
  - via their non-commercial person homepage or blog
  - by updating a preprint in arXiv or RePEc with the accepted manuscript

- via their research institute or institutional repository for internal institutional uses or as part of an invitation-only research collaboration work-group
- directly by providing copies to their students or to research collaborators for their personal use
- for private scholarly sharing as part of an invitation-only work group on commercial sites with which Elsevier has an agreement

- After the embargo period
  - via non-commercial hosting platforms such as their institutional repository
  - via commercial sites with which Elsevier has an agreement

In all cases accepted manuscripts should:

- link to the formal publication via its DOI
- bear a CC-BY-NC-ND license - this is easy to do
- if aggregated with other manuscripts, for example in a repository or other site, be shared in alignment with our hosting policy not be added to or enhanced in any way to appear more like, or to substitute for, the published journal article.

Published journal article (JPA): A published journal article (PJA) is the definitive final record of published research that appears or will appear in the journal and embodies all value-adding publishing activities including peer review co-ordination, copy-editing, formatting, (if relevant) pagination and online enrichment.
Policies for sharing publishing journal articles differ for subscription and gold open access articles:
Subscription Articles: If you are an author, please share a link to your article rather than the full-text. Millions of researchers have access to the formal publications on ScienceDirect, and so links will help your users to find, access, cite, and use the best available version. Theses and dissertations which contain embedded PJAs as part of the formal submission can be posted publicly by the awarding institution with DOI links back to the formal publications on ScienceDirect.
If you are affiliated with a library that subscribes to ScienceDirect you have additional private sharing rights for others' research accessed under that agreement. This includes use for classroom teaching and internal training at the institution (including use in course packs and courseware programs), and inclusion of the article for grant funding purposes.
Gold Open Access Articles: May be shared according to the author-selected end-user license and should contain a CrossMark logo, the end user license, and a DOI link to the formal publication on ScienceDirect.
Please refer to Elsevier's posting policy for further information.
18. **For book authors** the following clauses are applicable in addition to the above: Authors are permitted to place a brief summary of their work online only. You are not allowed to download and post the published electronic version of your chapter, nor may you scan the printed edition to create an electronic version. **Posting to a repository:** Authors are permitted to post a summary of their chapter only in their institution's repository.
19. **Thesis/Dissertation**: If your license is for use in a thesis/dissertation your thesis may be submitted to your institution in either print or electronic form. Should your thesis be published commercially, please reapply for permission. These requirements include permission for the Library and Archives of Canada to supply single copies, on demand, of the complete thesis and include permission for Proquest/UMI to supply single copies, on demand, of the complete thesis. Should your thesis be published commercially, please reapply for permission. Theses and dissertations which contain embedded PJAs as part of the formal submission can be posted publicly by the awarding institution with DOI links back to the formal publications on ScienceDirect.

Elsevier Open Access Terms and Conditions
You can publish open access with Elsevier in hundreds of open access journals or in nearly 2000 established subscription journals that support open access publishing. Permitted third party re-use of these open access articles is defined by the author's choice of Creative Commons user license. See our open access license policy for more information.

ELSEVIER LICENSE
TERMS AND CONDITIONS

Feb 05, 2019

This Agreement between Daniel R Wright ("You") and Elsevier ("Elsevier") consists of your license details and the terms and conditions provided by Elsevier and Copyright Clearance Center.

License Number	4522510907455
License date	Feb 05, 2019
Licensed Content Publisher	Elsevier
Licensed Content Publication	Journal of Power Sources
Licensed Content Title	Lithium oxalyldifluoroborate/carbonate electrolytes for LiFePO4/artificial graphite lithium-ion cells
Licensed Content Author	Jie Li,Keyu Xie,Yanqing Lai,Zhi'an Zhang,Fanqun Li,Xin Hao,Xujie Chen,Yexiang Liu
Licensed Content Date	Aug 15, 2010
Licensed Content Volume	195
Licensed Content Issue	16
Licensed Content Pages	7
Start Page	5344
End Page	5350
Type of Use	reuse in a thesis/dissertation
Portion	figures/tables/illustrations
Number of figures/tables/illustrations	1
Format	both print and electronic
Are you the author of this Elsevier article?	No
Will you be translating?	No
Original figure numbers	figure 10
Title of your thesis/dissertation	Mr
Publisher of new work	University of Southampton
Expected completion date	Mar 2019
Estimated size (number of pages)	1
Requestor Location	Daniel R Wright Flat 17 Westfield Corner Wide Lane Southampton, Hampshire SO18 2LE United Kingdom Attn:
Publisher Tax ID	GB 494 6272 12
Total	0.00 GBP
Terms and Conditions	

INTRODUCTION

1. The publisher for this copyrighted material is Elsevier. By clicking "accept" in connection with completing this licensing transaction, you agree that the following terms and conditions apply to this transaction (along with the Billing and Payment terms and conditions established by Copyright Clearance Center, Inc. ("CCC"), at the time that you opened your Rightslink account and that are available at any time at http://myaccount.copyright.com).

GENERAL TERMS

2. Elsevier hereby grants you permission to reproduce the aforementioned material subject to the terms and conditions indicated.

3. Acknowledgement: If any part of the material to be used (for example, figures) has appeared in our publication with credit or acknowledgement to another source, permission must also be sought from that source. If such permission is not obtained then that material may not be included in your publication/copies. Suitable acknowledgement to the source must be made, either as a footnote or in a reference list at the end of your publication, as follows:

"Reprinted from Publication title, Vol /edition number, Author(s), Title of article / title of chapter, Pages No., Copyright (Year), with permission from Elsevier [OR APPLICABLE SOCIETY COPYRIGHT OWNER]." Also Lancet special credit - "Reprinted from The Lancet, Vol. number, Author(s), Title of article, Pages No., Copyright (Year), with permission from Elsevier."

4. Reproduction of this material is confined to the purpose and/or media for which permission is hereby given.

5. Altering/Modifying Material: Not Permitted. However figures and illustrations may be altered/adapted minimally to serve your work. Any other abbreviations, additions, deletions and/or any other alterations shall be made only with prior written authorization of Elsevier Ltd. (Please contact Elsevier at permissions@elsevier.com). No modifications can be made to any Lancet figures/tables and they must be reproduced in full.

6. If the permission fee for the requested use of our material is waived in this instance, please be advised that your future requests for Elsevier materials may attract a fee.

7. Reservation of Rights: Publisher reserves all rights not specifically granted in the combination of (i) the license details provided by you and accepted in the course of this licensing transaction, (ii) these terms and conditions and (iii) CCC's Billing and Payment terms and conditions.

8. License Contingent Upon Payment: While you may exercise the rights licensed immediately upon issuance of the license at the end of the licensing process for the transaction, provided that you have disclosed complete and accurate details of your proposed use, no license is finally effective unless and until full payment is received from you (either by publisher or by CCC) as provided in CCC's Billing and Payment terms and conditions. If full payment is not received on a timely basis, then any license preliminarily granted shall be deemed automatically revoked and shall be void as if never granted. Further, in the event that you breach any of these terms and conditions or any of CCC's Billing and Payment terms and conditions, the license is automatically revoked and shall be void as if never granted. Use of materials as described in a revoked license, as well as any use of the materials beyond the scope of an unrevoked license, may constitute copyright infringement and publisher reserves the right to take any and all action to protect its copyright in the materials.

9. Warranties: Publisher makes no representations or warranties with respect to the licensed material.

10. Indemnity: You hereby indemnify and agree to hold harmless publisher and CCC, and their respective officers, directors, employees and agents, from and against any and all claims arising out of your use of the licensed material other than as specifically authorized pursuant to this license.

11. No Transfer of License: This license is personal to you and may not be sublicensed, assigned, or transferred by you to any other person without publisher's written permission.
12. No Amendment Except in Writing: This license may not be amended except in a writing signed by both parties (or, in the case of publisher, by CCC on publisher's behalf).
13. Objection to Contrary Terms: Publisher hereby objects to any terms contained in any purchase order, acknowledgment, check endorsement or other writing prepared by you, which terms are inconsistent with these terms and conditions or CCC's Billing and Payment terms and conditions. These terms and conditions, together with CCC's Billing and Payment terms and conditions (which are incorporated herein), comprise the entire agreement between you and publisher (and CCC) concerning this licensing transaction. In the event of any conflict between your obligations established by these terms and conditions and those established by CCC's Billing and Payment terms and conditions, these terms and conditions shall control.
14. Revocation: Elsevier or Copyright Clearance Center may deny the permissions described in this License at their sole discretion, for any reason or no reason, with a full refund payable to you. Notice of such denial will be made using the contact information provided by you. Failure to receive such notice will not alter or invalidate the denial. In no event will Elsevier or Copyright Clearance Center be responsible or liable for any costs, expenses or damage incurred by you as a result of a denial of your permission request, other than a refund of the amount(s) paid by you to Elsevier and/or Copyright Clearance Center for denied permissions.

LIMITED LICENSE

The following terms and conditions apply only to specific license types:
15. **Translation**: This permission is granted for non-exclusive world **English** rights only unless your license was granted for translation rights. If you licensed translation rights you may only translate this content into the languages you requested. A professional translator must perform all translations and reproduce the content word for word preserving the integrity of the article.
16. **Posting licensed content on any Website**: The following terms and conditions apply as follows: Licensing material from an Elsevier journal: All content posted to the web site must maintain the copyright information line on the bottom of each image; A hyper-text must be included to the Homepage of the journal from which you are licensing at http://www.sciencedirect.com/science/journal/xxxxx or the Elsevier homepage for books at http://www.elsevier.com; Central Storage: This license does not include permission for a scanned version of the material to be stored in a central repository such as that provided by Heron/XanEdu.
Licensing material from an Elsevier book: A hyper-text link must be included to the Elsevier homepage at http://www.elsevier.com . All content posted to the web site must maintain the copyright information line on the bottom of each image.

Posting licensed content on Electronic reserve: In addition to the above the following clauses are applicable: The web site must be password-protected and made available only to bona fide students registered on a relevant course. This permission is granted for 1 year only. You may obtain a new license for future website posting.
17. **For journal authors:** the following clauses are applicable in addition to the above:
Preprints:
A preprint is an author's own write-up of research results and analysis, it has not been peer-reviewed, nor has it had any other value added to it by a publisher (such as formatting, copyright, technical enhancement etc.).
Authors can share their preprints anywhere at any time. Preprints should not be added to or enhanced in any way in order to appear more like, or to substitute for, the final versions of articles however authors can update their preprints on arXiv or RePEc with their Accepted Author Manuscript (see below).

If accepted for publication, we encourage authors to link from the preprint to their formal publication via its DOI. Millions of researchers have access to the formal publications on ScienceDirect, and so links will help users to find, access, cite and use the best available version. Please note that Cell Press, The Lancet and some society-owned have different preprint policies. Information on these policies is available on the journal homepage.
Accepted Author Manuscripts: An accepted author manuscript is the manuscript of an article that has been accepted for publication and which typically includes author-incorporated changes suggested during submission, peer review and editor-author communications.
Authors can share their accepted author manuscript:

- immediately
  - via their non-commercial person homepage or blog
  - by updating a preprint in arXiv or RePEc with the accepted manuscript
  - via their research institute or institutional repository for internal institutional uses or as part of an invitation-only research collaboration work-group
  - directly by providing copies to their students or to research collaborators for their personal use
  - for private scholarly sharing as part of an invitation-only work group on commercial sites with which Elsevier has an agreement
- After the embargo period
  - via non-commercial hosting platforms such as their institutional repository
  - via commercial sites with which Elsevier has an agreement

In all cases accepted manuscripts should:

- link to the formal publication via its DOI
- bear a CC-BY-NC-ND license - this is easy to do
- if aggregated with other manuscripts, for example in a repository or other site, be shared in alignment with our hosting policy not be added to or enhanced in any way to appear more like, or to substitute for, the published journal article.

Published journal article (JPA): A published journal article (PJA) is the definitive final record of published research that appears or will appear in the journal and embodies all value-adding publishing activities including peer review co-ordination, copy-editing, formatting, (if relevant) pagination and online enrichment.
Policies for sharing publishing journal articles differ for subscription and gold open access articles:
Subscription Articles: If you are an author, please share a link to your article rather than the full-text. Millions of researchers have access to the formal publications on ScienceDirect, and so links will help your users to find, access, cite, and use the best available version.
Theses and dissertations which contain embedded PJAs as part of the formal submission can be posted publicly by the awarding institution with DOI links back to the formal publications on ScienceDirect.
If you are affiliated with a library that subscribes to ScienceDirect you have additional private sharing rights for others' research accessed under that agreement. This includes use for classroom teaching and internal training at the institution (including use in course packs and courseware programs), and inclusion of the article for grant funding purposes.
Gold Open Access Articles: May be shared according to the author-selected end-user license and should contain a CrossMark logo, the end user license, and a DOI link to the formal publication on ScienceDirect.
Please refer to Elsevier's posting policy for further information.

18. **For book authors** the following clauses are applicable in addition to the above:
Authors are permitted to place a brief summary of their work online only. You are not allowed to download and post the published electronic version of your chapter, nor may you scan the printed edition to create an electronic version. **Posting to a repository:** Authors are permitted to post a summary of their chapter only in their institution's repository.
19. **Thesis/Dissertation**: If your license is for use in a thesis/dissertation your thesis may be submitted to your institution in either print or electronic form. Should your thesis be published commercially, please reapply for permission. These requirements include permission for the Library and Archives of Canada to supply single copies, on demand, of the complete thesis and include permission for Proquest/UMI to supply single copies, on demand, of the complete thesis. Should your thesis be published commercially, please reapply for permission. Theses and dissertations which contain embedded PJAs as part of the formal submission can be posted publicly by the awarding institution with DOI links back to the formal publications on ScienceDirect.

Elsevier Open Access Terms and Conditions
You can publish open access with Elsevier in hundreds of open access journals or in nearly 2000 established subscription journals that support open access publishing. Permitted third party re-use of these open access articles is defined by the author's choice of Creative Commons user license. See our open access license policy for more information.
Terms & Conditions applicable to all Open Access articles published with Elsevier:
Any reuse of the article must not represent the author as endorsing the adaptation of the article nor should the article be modified in such a way as to damage the author's honour or reputation. If any changes have been made, such changes must be clearly indicated.
The author(s) must be appropriately credited and we ask that you include the end user license and a DOI link to the formal publication on ScienceDirect.
If any part of the material to be used (for example, figures) has appeared in our publication with credit or acknowledgement to another source it is the responsibility of the user to ensure their reuse complies with the terms and conditions determined by the rights holder.
Additional Terms & Conditions applicable to each Creative Commons user license:
CC BY: The CC-BY license allows users to copy, to create extracts, abstracts and new works from the Article, to alter and revise the Article and to make commercial use of the Article (including reuse and/or resale of the Article by commercial entities), provided the user gives appropriate credit (with a link to the formal publication through the relevant DOI), provides a link to the license, indicates if changes were made and the licensor is not represented as endorsing the use made of the work. The full details of the license are available at http://creativecommons.org/licenses/by/4.0.
CC BY NC SA: The CC BY-NC-SA license allows users to copy, to create extracts, abstracts and new works from the Article, to alter and revise the Article, provided this is not done for commercial purposes, and that the user gives appropriate credit (with a link to the formal publication through the relevant DOI), provides a link to the license, indicates if changes were made and the licensor is not represented as endorsing the use made of the work. Further, any new works must be made available on the same conditions. The full details of the license are available at http://creativecommons.org/licenses/by-nc-sa/4.0.
CC BY NC ND: The CC BY-NC-ND license allows users to copy and distribute the Article, provided this is not done for commercial purposes and further does not permit distribution of the Article if it is changed or edited in any way, and provided the user gives appropriate credit (with a link to the formal publication through the relevant DOI), provides a link to the license, and that the licensor is not represented as endorsing the use made of the work. The full details of the license are available at http://creativecommons.org/licenses/by-nc-nd/4.0.
Any commercial reuse of Open Access articles published with a CC BY NC SA or CC BY NC ND license requires permission from Elsevier and will be subject to a fee.
Commercial reuse includes:

- Associating advertising with the full text of the Article
- Charging fees for document delivery or access
- Article aggregation
- Systematic distribution via e-mail lists or share buttons

Posting or linking by commercial companies for use by customers of those companies.

20. **Other Conditions**:

v1.9

Questions? customercare@copyright.com or +1-855-239-3415 (toll free in the US) or +1-978-646-2777.

SPRINGER NATURE LICENSE TERMS AND CONDITIONS

Feb 05, 2019

This Agreement between Daniel R Wright ("You") and Springer Nature ("Springer Nature") consists of your license details and the terms and conditions provided by Springer Nature and Copyright Clearance Center.

License Number	4522520468685
License date	Feb 05, 2019
Licensed Content Publisher	Springer Nature
Licensed Content Publication	Nature Energy
Licensed Content Title	Electrolyte additive enabled fast charging and stable cycling lithium metal batteries
Licensed Content Author	Jianming Zheng, Mark H. Engelhard, Donghai Mei, Shuhong Jiao, Bryant J. Polzin et al.
Licensed Content Date	Mar 1, 2017
Licensed Content Volume	2
Licensed Content Issue	3
Type of Use	Thesis/Dissertation
Requestor type	academic/university or research institute
Format	print and electronic
Portion	figures/tables/illustrations
Number of figures/tables/illustrations	1
High-res required	no
Will you be translating?	no
Circulation/distribution	<501
Author of this Springer Nature content	no
Title	Mr
Institution name	University of Southampton
Expected presentation date	Mar 2019
Portions	Figure 1
Requestor Location	Daniel R Wright Flat 17 Westfield Corner Wide Lane Southampton, Hampshire SO18 2LE United Kingdom Attn:
Billing Type	Invoice
Billing Address	Daniel R Wright Flat 17 Westfield Corner Wide Lane Southampton, United Kingdom SO18 2LE Attn: Daniel R Wright
Total	0.00 GBP
Terms and Conditions	

Springer Nature Terms and Conditions for RightsLink Permissions

Springer Nature Customer Service Centre GmbH (the Licensor) hereby grants you a non-exclusive, world-wide licence to reproduce the material and for the purpose and requirements specified in the attached copy of your order form, and for no other use, subject to the conditions below:

1. The Licensor warrants that it has, to the best of its knowledge, the rights to license reuse of this material. However, you should ensure that the material you are requesting is original to the Licensor and does not carry the copyright of another entity (as credited in the published version).

   If the credit line on any part of the material you have requested indicates that it was reprinted or adapted with permission from another source, then you should also seek permission from that source to reuse the material.

2. Where **print only** permission has been granted for a fee, separate permission must be obtained for any additional electronic re-use.

3. Permission granted **free of charge** for material in print is also usually granted for any electronic version of that work, provided that the material is incidental to your work as a whole and that the electronic version is essentially equivalent to, or substitutes for, the print version.

4. A licence for 'post on a website' is valid for 12 months from the licence date. This licence does not cover use of full text articles on websites.

5. Where **'reuse in a dissertation/thesis'** has been selected the following terms apply: Print rights of the final author's accepted manuscript (for clarity, NOT the published version) for up to 100 copies, electronic rights for use only on a personal website or institutional repository as defined by the Sherpa guideline (www.sherpa.ac.uk/romeo/).

6. Permission granted for books and journals is granted for the lifetime of the first edition and does not apply to second and subsequent editions (except where the first edition permission was granted free of charge or for signatories to the STM Permissions Guidelines http://www.stm-assoc.org/copyright-legal-affairs/permissions/permissions-guidelines/), and does not apply for editions in other languages unless additional translation rights have been granted separately in the licence.

7. Rights for additional components such as custom editions and derivatives require additional permission and may be subject to an additional fee. Please apply to Journalpermissions@springernature.com/bookpermissions@springernature.com for these rights.

8. The Licensor's permission must be acknowledged next to the licensed material in print. In electronic form, this acknowledgement must be visible at the same time as the figures/tables/illustrations or abstract, and must be hyperlinked to the journal/book's homepage. Our required acknowledgement format is in the Appendix below.

9. Use of the material for incidental promotional use, minor editing privileges (this does not include cropping, adapting, omitting material or any other changes that affect the meaning, intention or moral rights of the author) and copies for the disabled are permitted under this licence.

10. Minor adaptations of single figures (changes of format, colour and style) do not require the Licensor's approval. However, the adaptation should be credited as shown in Appendix below.

Appendix — Acknowledgements:

For Journal Content:

Reprinted by permission from [**the Licensor**]: [**Journal Publisher** (e.g. Nature/Springer/Palgrave)] [**JOURNAL NAME**] [**REFERENCE CITATION** (Article name, Author(s) Name), [**COPYRIGHT**] (year of publication)

For **Advance Online Publication papers:**
Reprinted by permission from [**the Licensor**]: [**Journal Publisher** (e.g. Nature/Springer/Palgrave)] [**JOURNAL NAME**] [**REFERENCE CITATION** (Article name, Author(s) Name), [**COPYRIGHT**] (year of publication), advance online publication, day month year (doi: 10.1038/sj.[JOURNAL ACRONYM].)

For Adaptations/Translations:
Adapted/Translated by permission from [**the Licensor**]: [**Journal Publisher** (e.g. Nature/Springer/Palgrave)] [**JOURNAL NAME**] [**REFERENCE CITATION** (Article name, Author(s) Name), [**COPYRIGHT**] (year of publication)

Note: For any republication from the British Journal of Cancer, the following credit line style applies:

Reprinted/adapted/translated by permission from [**the Licensor**]: on behalf of Cancer Research UK: : [**Journal Publisher** (e.g. Nature/Springer/Palgrave)] [**JOURNAL NAME**] [**REFERENCE CITATION** (Article name, Author(s) Name), [**COPYRIGHT**] (year of publication)

For **Advance Online Publication** papers:
Reprinted by permission from The [**the Licensor**]: on behalf of Cancer Research UK: [**Journal Publisher** (e.g. Nature/Springer/Palgrave)] [**JOURNAL NAME**] [**REFERENCE CITATION** (Article name, Author(s) Name), [**COPYRIGHT**] (year of publication), advance online publication, day month year (doi: 10.1038/sj.[JOURNAL ACRONYM])

For Book content:
Reprinted/adapted by permission from [**the Licensor**]: [**Book Publisher** (e.g. Palgrave Macmillan, Springer etc) [**Book Title**] by [**Book author**(s)] [**COPYRIGHT**] (year of publication)

Other Conditions:

Version 1.1

Questions? customercare@copyright.com or +1-855-239-3415 (toll free in the US) or +1-978-646-2777.

ELSEVIER LICENSE
TERMS AND CONDITIONS

Feb 05, 2019

This Agreement between Daniel R Wright ("You") and Elsevier ("Elsevier") consists of your license details and the terms and conditions provided by Elsevier and Copyright Clearance Center.

License Number	4522520768983
License date	Feb 05, 2019
Licensed Content Publisher	Elsevier
Licensed Content Publication	Electrochimica Acta
Licensed Content Title	Improved High-Temperature Performance and Surface Chemistry of Graphite/LiMn2O4 Li-Ion Cells by Fluorosilane-Based Electrolyte Additive
Licensed Content Author	Kiyofumi Yamagiwa,Daichi Morita,Naoaki Yabuuchi,Tatsuya Tanaka,Mika Fukunishi,Takayuki Taki,Hiroaki Watanabe,Takahiro Otsuka,Toru Yano,Jin-Young Son,Yi-Tao Cui,Hiroshi Oji,Shinichi Komaba
Licensed Content Date	Apr 1, 2015
Licensed Content Volume	160
Licensed Content Issue	n/a
Licensed Content Pages	10
Start Page	347
End Page	356
Type of Use	reuse in a thesis/dissertation
Intended publisher of new work	other
Portion	figures/tables/illustrations
Number of figures/tables/illustrations	1
Format	both print and electronic
Are you the author of this Elsevier article?	No
Will you be translating?	No
Original figure numbers	Figure 5
Title of your thesis/dissertation	Mr
Publisher of new work	University of Southampton
Expected completion date	Mar 2019
Estimated size (number of pages)	1
Requestor Location	Daniel R Wright Flat 17 Westfield Corner Wide Lane Southampton, Hampshire SO18 2LE United Kingdom Attn:
Publisher Tax ID	GB 494 6272 12

Total 0.00 GBP

Terms and Conditions

INTRODUCTION

1. The publisher for this copyrighted material is Elsevier. By clicking "accept" in connection with completing this licensing transaction, you agree that the following terms and conditions apply to this transaction (along with the Billing and Payment terms and conditions established by Copyright Clearance Center, Inc. ("CCC"), at the time that you opened your Rightslink account and that are available at any time at http://myaccount.copyright.com).

GENERAL TERMS

2. Elsevier hereby grants you permission to reproduce the aforementioned material subject to the terms and conditions indicated.
3. Acknowledgement: If any part of the material to be used (for example, figures) has appeared in our publication with credit or acknowledgement to another source, permission must also be sought from that source. If such permission is not obtained then that material may not be included in your publication/copies. Suitable acknowledgement to the source must be made, either as a footnote or in a reference list at the end of your publication, as follows:
"Reprinted from Publication title, Vol /edition number, Author(s), Title of article / title of chapter, Pages No., Copyright (Year), with permission from Elsevier [OR APPLICABLE SOCIETY COPYRIGHT OWNER]." Also Lancet special credit - "Reprinted from The Lancet, Vol. number, Author(s), Title of article, Pages No., Copyright (Year), with permission from Elsevier."
4. Reproduction of this material is confined to the purpose and/or media for which permission is hereby given.
5. Altering/Modifying Material: Not Permitted. However figures and illustrations may be altered/adapted minimally to serve your work. Any other abbreviations, additions, deletions and/or any other alterations shall be made only with prior written authorization of Elsevier Ltd. (Please contact Elsevier at permissions@elsevier.com). No modifications can be made to any Lancet figures/tables and they must be reproduced in full.
6. If the permission fee for the requested use of our material is waived in this instance, please be advised that your future requests for Elsevier materials may attract a fee.
7. Reservation of Rights: Publisher reserves all rights not specifically granted in the combination of (i) the license details provided by you and accepted in the course of this licensing transaction, (ii) these terms and conditions and (iii) CCC's Billing and Payment terms and conditions.
8. License Contingent Upon Payment: While you may exercise the rights licensed immediately upon issuance of the license at the end of the licensing process for the transaction, provided that you have disclosed complete and accurate details of your proposed use, no license is finally effective unless and until full payment is received from you (either by publisher or by CCC) as provided in CCC's Billing and Payment terms and conditions. If full payment is not received on a timely basis, then any license preliminarily granted shall be deemed automatically revoked and shall be void as if never granted. Further, in the event that you breach any of these terms and conditions or any of CCC's Billing and Payment terms and conditions, the license is automatically revoked and shall be void as if never granted. Use of materials as described in a revoked license, as well as any use of the materials beyond the scope of an unrevoked license, may constitute copyright infringement and publisher reserves the right to take any and all action to protect its copyright in the materials.
9. Warranties: Publisher makes no representations or warranties with respect to the licensed material.
10. Indemnity: You hereby indemnify and agree to hold harmless publisher and CCC, and their respective officers, directors, employees and agents, from and against any and all claims arising out of your use of the licensed material other than as specifically authorized pursuant to this license.
11. No Transfer of License: This license is personal to you and may not be sublicensed, assigned, or transferred by you to any other person without publisher's written permission.

12. No Amendment Except in Writing: This license may not be amended except in a writing signed by both parties (or, in the case of publisher, by CCC on publisher's behalf).
13. Objection to Contrary Terms: Publisher hereby objects to any terms contained in any purchase order, acknowledgment, check endorsement or other writing prepared by you, which terms are inconsistent with these terms and conditions or CCC's Billing and Payment terms and conditions. These terms and conditions, together with CCC's Billing and Payment terms and conditions (which are incorporated herein), comprise the entire agreement between you and publisher (and CCC) concerning this licensing transaction. In the event of any conflict between your obligations established by these terms and conditions and those established by CCC's Billing and Payment terms and conditions, these terms and conditions shall control.
14. Revocation: Elsevier or Copyright Clearance Center may deny the permissions described in this License at their sole discretion, for any reason or no reason, with a full refund payable to you. Notice of such denial will be made using the contact information provided by you. Failure to receive such notice will not alter or invalidate the denial. In no event will Elsevier or Copyright Clearance Center be responsible or liable for any costs, expenses or damage incurred by you as a result of a denial of your permission request, other than a refund of the amount(s) paid by you to Elsevier and/or Copyright Clearance Center for denied permissions.

LIMITED LICENSE

The following terms and conditions apply only to specific license types:
15. **Translation**: This permission is granted for non-exclusive world **English** rights only unless your license was granted for translation rights. If you licensed translation rights you may only translate this content into the languages you requested. A professional translator must perform all translations and reproduce the content word for word preserving the integrity of the article.
16. **Posting licensed content on any Website**: The following terms and conditions apply as follows: Licensing material from an Elsevier journal: All content posted to the web site must maintain the copyright information line on the bottom of each image; A hyper-text must be included to the Homepage of the journal from which you are licensing at http://www.sciencedirect.com/science/journal/xxxxx or the Elsevier homepage for books at http://www.elsevier.com; Central Storage: This license does not include permission for a scanned version of the material to be stored in a central repository such as that provided by Heron/XanEdu.
Licensing material from an Elsevier book: A hyper-text link must be included to the Elsevier homepage at http://www.elsevier.com . All content posted to the web site must maintain the copyright information line on the bottom of each image.

Posting licensed content on Electronic reserve: In addition to the above the following clauses are applicable: The web site must be password-protected and made available only to bona fide students registered on a relevant course. This permission is granted for 1 year only. You may obtain a new license for future website posting.
17. **For journal authors:** the following clauses are applicable in addition to the above:
Preprints:
A preprint is an author's own write-up of research results and analysis, it has not been peer-reviewed, nor has it had any other value added to it by a publisher (such as formatting, copyright, technical enhancement etc.).
Authors can share their preprints anywhere at any time. Preprints should not be added to or enhanced in any way in order to appear more like, or to substitute for, the final versions of articles however authors can update their preprints on arXiv or RePEc with their Accepted Author Manuscript (see below).
If accepted for publication, we encourage authors to link from the preprint to their formal publication via its DOI. Millions of researchers have access to the formal publications on ScienceDirect, and so links will help users to find, access, cite and use the best available version. Please note that Cell Press, The Lancet and some society-owned have different preprint policies. Information on these policies is available on the journal homepage.
Accepted Author Manuscripts: An accepted author manuscript is the manuscript of an article that has been accepted for publication and which typically includes author-

incorporated changes suggested during submission, peer review and editor-author communications.
Authors can share their accepted author manuscript:

- immediately
  - via their non-commercial person homepage or blog
  - by updating a preprint in arXiv or RePEc with the accepted manuscript
  - via their research institute or institutional repository for internal institutional uses or as part of an invitation-only research collaboration work-group
  - directly by providing copies to their students or to research collaborators for their personal use
  - for private scholarly sharing as part of an invitation-only work group on commercial sites with which Elsevier has an agreement
- After the embargo period
  - via non-commercial hosting platforms such as their institutional repository
  - via commercial sites with which Elsevier has an agreement

In all cases accepted manuscripts should:

- link to the formal publication via its DOI
- bear a CC-BY-NC-ND license - this is easy to do
- if aggregated with other manuscripts, for example in a repository or other site, be shared in alignment with our hosting policy not be added to or enhanced in any way to appear more like, or to substitute for, the published journal article.

Published journal article (JPA): A published journal article (PJA) is the definitive final record of published research that appears or will appear in the journal and embodies all value-adding publishing activities including peer review co-ordination, copy-editing, formatting, (if relevant) pagination and online enrichment.
Policies for sharing publishing journal articles differ for subscription and gold open access articles:
Subscription Articles: If you are an author, please share a link to your article rather than the full-text. Millions of researchers have access to the formal publications on ScienceDirect, and so links will help your users to find, access, cite, and use the best available version.
Theses and dissertations which contain embedded PJAs as part of the formal submission can be posted publicly by the awarding institution with DOI links back to the formal publications on ScienceDirect.
If you are affiliated with a library that subscribes to ScienceDirect you have additional private sharing rights for others' research accessed under that agreement. This includes use for classroom teaching and internal training at the institution (including use in course packs and courseware programs), and inclusion of the article for grant funding purposes.
Gold Open Access Articles: May be shared according to the author-selected end-user license and should contain a CrossMark logo, the end user license, and a DOI link to the formal publication on ScienceDirect.
Please refer to Elsevier's posting policy for further information.
18. **For book authors** the following clauses are applicable in addition to the above: Authors are permitted to place a brief summary of their work online only. You are not allowed to download and post the published electronic version of your chapter, nor may you scan the printed edition to create an electronic version. **Posting to a repository:** Authors are permitted to post a summary of their chapter only in their institution's repository.
19. **Thesis/Dissertation**: If your license is for use in a thesis/dissertation your thesis may be submitted to your institution in either print or electronic form. Should your thesis be published commercially, please reapply for permission. These requirements include permission for the Library and Archives of Canada to supply single copies, on demand, of the complete thesis and include permission for Proquest/UMI to supply single copies, on demand, of the complete thesis. Should your thesis be published commercially, please reapply for permission. Theses and dissertations which contain embedded PJAs as part of

the formal submission can be posted publicly by the awarding institution with DOI links back to the formal publications on ScienceDirect.

Elsevier Open Access Terms and Conditions

You can publish open access with Elsevier in hundreds of open access journals or in nearly 2000 established subscription journals that support open access publishing. Permitted third party re-use of these open access articles is defined by the author's choice of Creative Commons user license. See our open access license policy for more information.

Terms & Conditions applicable to all Open Access articles published with Elsevier:

Any reuse of the article must not represent the author as endorsing the adaptation of the article nor should the article be modified in such a way as to damage the author's honour or reputation. If any changes have been made, such changes must be clearly indicated.

The author(s) must be appropriately credited and we ask that you include the end user license and a DOI link to the formal publication on ScienceDirect.

If any part of the material to be used (for example, figures) has appeared in our publication with credit or acknowledgement to another source it is the responsibility of the user to ensure their reuse complies with the terms and conditions determined by the rights holder.

Additional Terms & Conditions applicable to each Creative Commons user license:

CC BY: The CC-BY license allows users to copy, to create extracts, abstracts and new works from the Article, to alter and revise the Article and to make commercial use of the Article (including reuse and/or resale of the Article by commercial entities), provided the user gives appropriate credit (with a link to the formal publication through the relevant DOI), provides a link to the license, indicates if changes were made and the licensor is not represented as endorsing the use made of the work. The full details of the license are available at http://creativecommons.org/licenses/by/4.0.

CC BY NC SA: The CC BY-NC-SA license allows users to copy, to create extracts, abstracts and new works from the Article, to alter and revise the Article, provided this is not done for commercial purposes, and that the user gives appropriate credit (with a link to the formal publication through the relevant DOI), provides a link to the license, indicates if changes were made and the licensor is not represented as endorsing the use made of the work. Further, any new works must be made available on the same conditions. The full details of the license are available at http://creativecommons.org/licenses/by-nc-sa/4.0.

CC BY NC ND: The CC BY-NC-ND license allows users to copy and distribute the Article, provided this is not done for commercial purposes and further does not permit distribution of the Article if it is changed or edited in any way, and provided the user gives appropriate credit (with a link to the formal publication through the relevant DOI), provides a link to the license, and that the licensor is not represented as endorsing the use made of the work. The full details of the license are available at http://creativecommons.org/licenses/by-nc-nd/4.0.

Any commercial reuse of Open Access articles published with a CC BY NC SA or CC BY NC ND license requires permission from Elsevier and will be subject to a fee.

Commercial reuse includes:

- Associating advertising with the full text of the Article
- Charging fees for document delivery or access
- Article aggregation
- Systematic distribution via e-mail lists or share buttons

Posting or linking by commercial companies for use by customers of those companies.

20. **Other Conditions**:

v1.9

Questions? customercare@copyright.com or +1-855-239-3415 (toll free in the US) or +1-978-646-2777.

JOHN WILEY AND SONS LICENSE TERMS AND CONDITIONS

Feb 05, 2019

This Agreement between Daniel R Wright ("You") and John Wiley and Sons ("John Wiley and Sons") consists of your license details and the terms and conditions provided by John Wiley and Sons and Copyright Clearance Center.

License Number	4522530159856
License date	Feb 05, 2019
Licensed Content Publisher	John Wiley and Sons
Licensed Content Publication	Advanced Materials
Licensed Content Title	Insertion Electrode Materials for Rechargeable Lithium Batteries
Licensed Content Author	Martin Winter, Jürgen O. Besenhard, Michael E. Spahr, et al
Licensed Content Date	Jan 26, 1999
Licensed Content Volume	10
Licensed Content Issue	10
Licensed Content Pages	39
Type of use	Dissertation/Thesis
Requestor type	University/Academic
Format	Print and electronic
Portion	Figure/table
Number of figures/tables	4
Original Wiley figure/table number(s)	Figure 5, figure 6 a, figure 7, figure 8
Will you be translating?	No
Title of your thesis / dissertation	Mr
Expected completion date	Mar 2019
Expected size (number of pages)	1
Requestor Location	Daniel R Wright Flat 17 Westfield Corner Wide Lane Southampton, Hampshire SO18 2LE United Kingdom Attn:
Publisher Tax ID	EU826007151
Total	0.00 GBP
Terms and Conditions	

TERMS AND CONDITIONS

This copyrighted material is owned by or exclusively licensed to John Wiley & Sons, Inc. or one of its group companies (each a"Wiley Company") or handled on behalf of a society with which a Wiley Company has exclusive publishing rights in relation to a particular work (collectively "WILEY"). By clicking "accept" in connection with completing this licensing transaction, you agree that the following terms and conditions apply to this transaction (along with the billing and payment terms and conditions established by the Copyright Clearance Center Inc., ("CCC's Billing and Payment terms and conditions"), at the time that

you opened your RightsLink account (these are available at any time at http://myaccount.copyright.com).

Terms and Conditions

- The materials you have requested permission to reproduce or reuse (the "Wiley Materials") are protected by copyright.

- You are hereby granted a personal, non-exclusive, non-sub licensable (on a stand-alone basis), non-transferable, worldwide, limited license to reproduce the Wiley Materials for the purpose specified in the licensing process. This license, **and any CONTENT (PDF or image file) purchased as part of your order,** is for a one-time use only and limited to any maximum distribution number specified in the license. The first instance of republication or reuse granted by this license must be completed within two years of the date of the grant of this license (although copies prepared before the end date may be distributed thereafter). The Wiley Materials shall not be used in any other manner or for any other purpose, beyond what is granted in the license. Permission is granted subject to an appropriate acknowledgement given to the author, title of the material/book/journal and the publisher. You shall also duplicate the copyright notice that appears in the Wiley publication in your use of the Wiley Material. Permission is also granted on the understanding that nowhere in the text is a previously published source acknowledged for all or part of this Wiley Material. Any third party content is expressly excluded from this permission.

- With respect to the Wiley Materials, all rights are reserved. Except as expressly granted by the terms of the license, no part of the Wiley Materials may be copied, modified, adapted (except for minor reformatting required by the new Publication), translated, reproduced, transferred or distributed, in any form or by any means, and no derivative works may be made based on the Wiley Materials without the prior permission of the respective copyright owner.**For STM Signatory Publishers clearing permission under the terms of the STM Permissions Guidelines only, the terms of the license are extended to include subsequent editions and for editions in other languages, provided such editions are for the work as a whole in situ and does not involve the separate exploitation of the permitted figures or extracts,** You may not alter, remove or suppress in any manner any copyright, trademark or other notices displayed by the Wiley Materials. You may not license, rent, sell, loan, lease, pledge, offer as security, transfer or assign the Wiley Materials on a stand-alone basis, or any of the rights granted to you hereunder to any other person.

- The Wiley Materials and all of the intellectual property rights therein shall at all times remain the exclusive property of John Wiley & Sons Inc, the Wiley Companies, or their respective licensors, and your interest therein is only that of having possession of and the right to reproduce the Wiley Materials pursuant to Section 2 herein during the continuance of this Agreement. You agree that you own no right, title or interest in or to the Wiley Materials or any of the intellectual property rights therein. You shall have no rights hereunder other than the license as provided for above in Section 2. No right, license or interest to any trademark, trade name, service mark or other branding ("Marks") of WILEY or its licensors is granted hereunder, and you agree that you shall not assert any such right, license or interest with respect thereto

- NEITHER WILEY NOR ITS LICENSORS MAKES ANY WARRANTY OR REPRESENTATION OF ANY KIND TO YOU OR ANY THIRD PARTY, EXPRESS, IMPLIED OR STATUTORY, WITH RESPECT TO THE MATERIALS OR THE ACCURACY OF ANY INFORMATION CONTAINED IN THE MATERIALS, INCLUDING, WITHOUT LIMITATION, ANY IMPLIED WARRANTY OF MERCHANTABILITY, ACCURACY, SATISFACTORY QUALITY, FITNESS FOR A PARTICULAR PURPOSE, USABILITY, INTEGRATION OR NON-INFRINGEMENT AND ALL SUCH WARRANTIES

ARE HEREBY EXCLUDED BY WILEY AND ITS LICENSORS AND WAIVED BY YOU.

- WILEY shall have the right to terminate this Agreement immediately upon breach of this Agreement by you.
- You shall indemnify, defend and hold harmless WILEY, its Licensors and their respective directors, officers, agents and employees, from and against any actual or threatened claims, demands, causes of action or proceedings arising from any breach of this Agreement by you.
- IN NO EVENT SHALL WILEY OR ITS LICENSORS BE LIABLE TO YOU OR ANY OTHER PARTY OR ANY OTHER PERSON OR ENTITY FOR ANY SPECIAL, CONSEQUENTIAL, INCIDENTAL, INDIRECT, EXEMPLARY OR PUNITIVE DAMAGES, HOWEVER CAUSED, ARISING OUT OF OR IN CONNECTION WITH THE DOWNLOADING, PROVISIONING, VIEWING OR USE OF THE MATERIALS REGARDLESS OF THE FORM OF ACTION, WHETHER FOR BREACH OF CONTRACT, BREACH OF WARRANTY, TORT, NEGLIGENCE, INFRINGEMENT OR OTHERWISE (INCLUDING, WITHOUT LIMITATION, DAMAGES BASED ON LOSS OF PROFITS, DATA, FILES, USE, BUSINESS OPPORTUNITY OR CLAIMS OF THIRD PARTIES), AND WHETHER OR NOT THE PARTY HAS BEEN ADVISED OF THE POSSIBILITY OF SUCH DAMAGES. THIS LIMITATION SHALL APPLY NOTWITHSTANDING ANY FAILURE OF ESSENTIAL PURPOSE OF ANY LIMITED REMEDY PROVIDED HEREIN.
- Should any provision of this Agreement be held by a court of competent jurisdiction to be illegal, invalid, or unenforceable, that provision shall be deemed amended to achieve as nearly as possible the same economic effect as the original provision, and the legality, validity and enforceability of the remaining provisions of this Agreement shall not be affected or impaired thereby.
- The failure of either party to enforce any term or condition of this Agreement shall not constitute a waiver of either party's right to enforce each and every term and condition of this Agreement. No breach under this agreement shall be deemed waived or excused by either party unless such waiver or consent is in writing signed by the party granting such waiver or consent. The waiver by or consent of a party to a breach of any provision of this Agreement shall not operate or be construed as a waiver of or consent to any other or subsequent breach by such other party.
- This Agreement may not be assigned (including by operation of law or otherwise) by you without WILEY's prior written consent.
- Any fee required for this permission shall be non-refundable after thirty (30) days from receipt by the CCC.
- These terms and conditions together with CCC's Billing and Payment terms and conditions (which are incorporated herein) form the entire agreement between you and WILEY concerning this licensing transaction and (in the absence of fraud) supersedes all prior agreements and representations of the parties, oral or written. This Agreement may not be amended except in writing signed by both parties. This Agreement shall be binding upon and inure to the benefit of the parties' successors, legal representatives, and authorized assigns.
- In the event of any conflict between your obligations established by these terms and conditions and those established by CCC's Billing and Payment terms and conditions, these terms and conditions shall prevail.

- WILEY expressly reserves all rights not specifically granted in the combination of (i) the license details provided by you and accepted in the course of this licensing transaction, (ii) these terms and conditions and (iii) CCC's Billing and Payment terms and conditions.

- This Agreement will be void if the Type of Use, Format, Circulation, or Requestor Type was misrepresented during the licensing process.

- This Agreement shall be governed by and construed in accordance with the laws of the State of New York, USA, without regards to such state's conflict of law rules. Any legal action, suit or proceeding arising out of or relating to these Terms and Conditions or the breach thereof shall be instituted in a court of competent jurisdiction in New York County in the State of New York in the United States of America and each party hereby consents and submits to the personal jurisdiction of such court, waives any objection to venue in such court and consents to service of process by registered or certified mail, return receipt requested, at the last known address of such party.

WILEY OPEN ACCESS TERMS AND CONDITIONS

Wiley Publishes Open Access Articles in fully Open Access Journals and in Subscription journals offering Online Open. Although most of the fully Open Access journals publish open access articles under the terms of the Creative Commons Attribution (CC BY) License only, the subscription journals and a few of the Open Access Journals offer a choice of Creative Commons Licenses. The license type is clearly identified on the article.

The Creative Commons Attribution License

The Creative Commons Attribution License (CC-BY) allows users to copy, distribute and transmit an article, adapt the article and make commercial use of the article. The CC-BY license permits commercial and non-

Creative Commons Attribution Non-Commercial License

The Creative Commons Attribution Non-Commercial (CC-BY-NC)License permits use, distribution and reproduction in any medium, provided the original work is properly cited and is not used for commercial purposes.(see below)

Creative Commons Attribution-Non-Commercial-NoDerivs License

The Creative Commons Attribution Non-Commercial-NoDerivs License (CC-BY-NC-ND) permits use, distribution and reproduction in any medium, provided the original work is properly cited, is not used for commercial purposes and no modifications or adaptations are made. (see below)

Use by commercial "for-profit" organizations

Use of Wiley Open Access articles for commercial, promotional, or marketing purposes requires further explicit permission from Wiley and will be subject to a fee.

Further details can be found on Wiley Online Library

http://olabout.wiley.com/WileyCDA/Section/id-410895.html

Other Terms and Conditions:

v1.10 Last updated September 2015

Questions? customercare@copyright.com or +1-855-239-3415 (toll free in the US) or +1-978-646-2777.

ELSEVIER LICENSE
TERMS AND CONDITIONS

Feb 05, 2019

This Agreement between Daniel R Wright ("You") and Elsevier ("Elsevier") consists of your license details and the terms and conditions provided by Elsevier and Copyright Clearance Center.

License Number	4522530542220
License date	Feb 05, 2019
Licensed Content Publisher	Elsevier
Licensed Content Publication	Journal of Power Sources
Licensed Content Title	An overview of positive-electrode materials for advanced lithium-ion batteries
Licensed Content Author	Tsutomu Ohzuku,Ralph J. Brodd
Licensed Content Date	Dec 6, 2007
Licensed Content Volume	174
Licensed Content Issue	2
Licensed Content Pages	8
Start Page	449
End Page	456
Type of Use	reuse in a thesis/dissertation
Intended publisher of new work	other
Portion	figures/tables/illustrations
Number of figures/tables/illustrations	1
Format	both print and electronic
Are you the author of this Elsevier article?	No
Will you be translating?	No
Original figure numbers	Figure 5
Title of your thesis/dissertation	Mr
Publisher of new work	University of Southampton
Expected completion date	Mar 2019
Estimated size (number of pages)	1
Requestor Location	Daniel R Wright Flat 17 Westfield Corner Wide Lane Southampton, Hampshire SO18 2LE United Kingdom Attn:
Publisher Tax ID	GB 494 6272 12
Total	0.00 GBP
Terms and Conditions	

INTRODUCTION

1. The publisher for this copyrighted material is Elsevier. By clicking "accept" in connection with completing this licensing transaction, you agree that the following terms and conditions apply to this transaction (along with the Billing and Payment terms and conditions established by Copyright Clearance Center, Inc. ("CCC"), at the time that you opened your Rightslink account and that are available at any time at http://myaccount.copyright.com).

GENERAL TERMS

2. Elsevier hereby grants you permission to reproduce the aforementioned material subject to the terms and conditions indicated.
3. Acknowledgement: If any part of the material to be used (for example, figures) has appeared in our publication with credit or acknowledgement to another source, permission must also be sought from that source. If such permission is not obtained then that material may not be included in your publication/copies. Suitable acknowledgement to the source must be made, either as a footnote or in a reference list at the end of your publication, as follows:
"Reprinted from Publication title, Vol /edition number, Author(s), Title of article / title of chapter, Pages No., Copyright (Year), with permission from Elsevier [OR APPLICABLE SOCIETY COPYRIGHT OWNER]." Also Lancet special credit - "Reprinted from The Lancet, Vol. number, Author(s), Title of article, Pages No., Copyright (Year), with permission from Elsevier."
4. Reproduction of this material is confined to the purpose and/or media for which permission is hereby given.
5. Altering/Modifying Material: Not Permitted. However figures and illustrations may be altered/adapted minimally to serve your work. Any other abbreviations, additions, deletions and/or any other alterations shall be made only with prior written authorization of Elsevier Ltd. (Please contact Elsevier at permissions@elsevier.com). No modifications can be made to any Lancet figures/tables and they must be reproduced in full.
6. If the permission fee for the requested use of our material is waived in this instance, please be advised that your future requests for Elsevier materials may attract a fee.
7. Reservation of Rights: Publisher reserves all rights not specifically granted in the combination of (i) the license details provided by you and accepted in the course of this licensing transaction, (ii) these terms and conditions and (iii) CCC's Billing and Payment terms and conditions.
8. License Contingent Upon Payment: While you may exercise the rights licensed immediately upon issuance of the license at the end of the licensing process for the transaction, provided that you have disclosed complete and accurate details of your proposed use, no license is finally effective unless and until full payment is received from you (either by publisher or by CCC) as provided in CCC's Billing and Payment terms and conditions. If full payment is not received on a timely basis, then any license preliminarily granted shall be deemed automatically revoked and shall be void as if never granted. Further, in the event that you breach any of these terms and conditions or any of CCC's Billing and Payment terms and conditions, the license is automatically revoked and shall be void as if never granted. Use of materials as described in a revoked license, as well as any use of the materials beyond the scope of an unrevoked license, may constitute copyright infringement and publisher reserves the right to take any and all action to protect its copyright in the materials.
9. Warranties: Publisher makes no representations or warranties with respect to the licensed material.
10. Indemnity: You hereby indemnify and agree to hold harmless publisher and CCC, and their respective officers, directors, employees and agents, from and against any and all claims arising out of your use of the licensed material other than as specifically authorized pursuant to this license.
11. No Transfer of License: This license is personal to you and may not be sublicensed, assigned, or transferred by you to any other person without publisher's written permission.
12. No Amendment Except in Writing: This license may not be amended except in a writing signed by both parties (or, in the case of publisher, by CCC on publisher's behalf).
13. Objection to Contrary Terms: Publisher hereby objects to any terms contained in any purchase order, acknowledgment, check endorsement or other writing prepared by you,

which terms are inconsistent with these terms and conditions or CCC's Billing and Payment terms and conditions. These terms and conditions, together with CCC's Billing and Payment terms and conditions (which are incorporated herein), comprise the entire agreement between you and publisher (and CCC) concerning this licensing transaction. In the event of any conflict between your obligations established by these terms and conditions and those established by CCC's Billing and Payment terms and conditions, these terms and conditions shall control.

14. Revocation: Elsevier or Copyright Clearance Center may deny the permissions described in this License at their sole discretion, for any reason or no reason, with a full refund payable to you. Notice of such denial will be made using the contact information provided by you. Failure to receive such notice will not alter or invalidate the denial. In no event will Elsevier or Copyright Clearance Center be responsible or liable for any costs, expenses or damage incurred by you as a result of a denial of your permission request, other than a refund of the amount(s) paid by you to Elsevier and/or Copyright Clearance Center for denied permissions.

LIMITED LICENSE

The following terms and conditions apply only to specific license types:

15. **Translation**: This permission is granted for non-exclusive world **English** rights only unless your license was granted for translation rights. If you licensed translation rights you may only translate this content into the languages you requested. A professional translator must perform all translations and reproduce the content word for word preserving the integrity of the article.

16. **Posting licensed content on any Website**: The following terms and conditions apply as follows: Licensing material from an Elsevier journal: All content posted to the web site must maintain the copyright information line on the bottom of each image; A hyper-text must be included to the Homepage of the journal from which you are licensing at http://www.sciencedirect.com/science/journal/xxxxx or the Elsevier homepage for books at http://www.elsevier.com; Central Storage: This license does not include permission for a scanned version of the material to be stored in a central repository such as that provided by Heron/XanEdu.

Licensing material from an Elsevier book: A hyper-text link must be included to the Elsevier homepage at http://www.elsevier.com . All content posted to the web site must maintain the copyright information line on the bottom of each image.

Posting licensed content on Electronic reserve: In addition to the above the following clauses are applicable: The web site must be password-protected and made available only to bona fide students registered on a relevant course. This permission is granted for 1 year only. You may obtain a new license for future website posting.

17. **For journal authors:** the following clauses are applicable in addition to the above:

Preprints:

A preprint is an author's own write-up of research results and analysis, it has not been peer-reviewed, nor has it had any other value added to it by a publisher (such as formatting, copyright, technical enhancement etc.).

Authors can share their preprints anywhere at any time. Preprints should not be added to or enhanced in any way in order to appear more like, or to substitute for, the final versions of articles however authors can update their preprints on arXiv or RePEc with their Accepted Author Manuscript (see below).

If accepted for publication, we encourage authors to link from the preprint to their formal publication via its DOI. Millions of researchers have access to the formal publications on ScienceDirect, and so links will help users to find, access, cite and use the best available version. Please note that Cell Press, The Lancet and some society-owned have different preprint policies. Information on these policies is available on the journal homepage.

Accepted Author Manuscripts: An accepted author manuscript is the manuscript of an article that has been accepted for publication and which typically includes author-incorporated changes suggested during submission, peer review and editor-author communications.

Authors can share their accepted author manuscript:

- immediately
  - via their non-commercial person homepage or blog
  - by updating a preprint in arXiv or RePEc with the accepted manuscript
  - via their research institute or institutional repository for internal institutional uses or as part of an invitation-only research collaboration work-group
  - directly by providing copies to their students or to research collaborators for their personal use
  - for private scholarly sharing as part of an invitation-only work group on commercial sites with which Elsevier has an agreement
- After the embargo period
  - via non-commercial hosting platforms such as their institutional repository
  - via commercial sites with which Elsevier has an agreement

In all cases accepted manuscripts should:

- link to the formal publication via its DOI
- bear a CC-BY-NC-ND license - this is easy to do
- if aggregated with other manuscripts, for example in a repository or other site, be shared in alignment with our hosting policy not be added to or enhanced in any way to appear more like, or to substitute for, the published journal article.

Published journal article (JPA): A published journal article (PJA) is the definitive final record of published research that appears or will appear in the journal and embodies all value-adding publishing activities including peer review co-ordination, copy-editing, formatting, (if relevant) pagination and online enrichment.
Policies for sharing publishing journal articles differ for subscription and gold open access articles:
Subscription Articles: If you are an author, please share a link to your article rather than the full-text. Millions of researchers have access to the formal publications on ScienceDirect, and so links will help your users to find, access, cite, and use the best available version.
Theses and dissertations which contain embedded PJAs as part of the formal submission can be posted publicly by the awarding institution with DOI links back to the formal publications on ScienceDirect.
If you are affiliated with a library that subscribes to ScienceDirect you have additional private sharing rights for others' research accessed under that agreement. This includes use for classroom teaching and internal training at the institution (including use in course packs and courseware programs), and inclusion of the article for grant funding purposes.
Gold Open Access Articles: May be shared according to the author-selected end-user license and should contain a CrossMark logo, the end user license, and a DOI link to the formal publication on ScienceDirect.
Please refer to Elsevier's posting policy for further information.
18. **For book authors** the following clauses are applicable in addition to the above: Authors are permitted to place a brief summary of their work online only. You are not allowed to download and post the published electronic version of your chapter, nor may you scan the printed edition to create an electronic version. **Posting to a repository:** Authors are permitted to post a summary of their chapter only in their institution's repository.
19. **Thesis/Dissertation**: If your license is for use in a thesis/dissertation your thesis may be submitted to your institution in either print or electronic form. Should your thesis be published commercially, please reapply for permission. These requirements include permission for the Library and Archives of Canada to supply single copies, on demand, of the complete thesis and include permission for Proquest/UMI to supply single copies, on demand, of the complete thesis. Should your thesis be published commercially, please reapply for permission. Theses and dissertations which contain embedded PJAs as part of the formal submission can be posted publicly by the awarding institution with DOI links back to the formal publications on ScienceDirect.

Elsevier Open Access Terms and Conditions

This page is available in the following languages:

Creative Commons License Deed

Attribution-NonCommercial 3.0 Unported (CC BY-NC 3.0)

This is a human-readable summary of (and not a substitute for) the license.

You are free to:

Share — copy and redistribute the material in any medium or format

Adapt — remix, transform, and build upon the material

The licensor cannot revoke these freedoms as long as you follow the license terms.

Under the following terms:

Attribution — You must give appropriate credit, provide a link to the license, and indicate if changes were made. You may do so in any reasonable manner, but not in any way that suggests the licensor endorses you or your use.

NonCommercial — You may not use the material for commercial purposes.

No additional restrictions — You may not apply legal terms or technological measures that legally restrict others from doing anything the license permits.

Notices:

You do not have to comply with the license for elements of the material in the public domain or where your use is permitted by an applicable exception or limitation.

No warranties are given. The license may not give you all of the permissions necessary for your intended use. For example, other rights such as publicity, privacy, or moral rights may limit how you use the material.